UNIVERSITY OF CALIFORNIA

Santa Barbara

Using End-of-Life Polymers and Bio-Derived Precursors to Synthesize Commodity Chemicals

A dissertation submitted in partial satisfaction of the

requirements for the degree Doctor of Philosophy

in Chemistry

by

Manhao Zeng

Committee in charge:

Professor Mahdi Abu-Omar, Chair

Professor Eric McFarland

Professor Javier Read de Alaniz

Professor Lior Sepunaru

September 2022

The dissertation of Manhao Zeng is approved.

_____

Professor Eric McFarland

_____

Professor Javier Read de Alaniz

_____

Professor Lior Sepunaru

_____

Professor Mahdi Abu-Omar, Committee Chair

July 2022

Using End-of-Life Polymers and Bio-Derived Precursors to Synthesize Commodity Chemicals

Manhao Zeng

Dedicated to those who train every day and go to war with their own weaknesses to become the strongest version of themselves.

No excuses. No complacency.

Discipline = Freedom

Know thyself.

ACKNOWLEDGEMENTS

Six years consist of 72 months, 288 weeks, 2,190 days, or 3,153,600 minutes. During this time, the Earth will have fully rotated 2,190 times and revolved around the sun six times. In the Milky Way galaxy where the Earth is located, 42 new stars will have been born in six years. Given that a jellyfish has a lifespan of 1-3 years, up to six generations of jellyfish will have lived and died. On the other hand, the average dog will have lived about half its life while a perennial daylily flower will have bloomed six times. Furthermore, 110 billion human taste buds will have been replaced and 88 million trees will have been cut to create paper bags. In America, where the typical citizen lives 79 years, 8% of one's life will have passed. Today, a child turns six years old.

All of this is to say that the universe constantly changes from day to day, hour to hour, second to second. In my six years, however, I pursued a graduate degree in chemistry at a somewhat timeless institution where students never seem to get older, but you do. At this training ground, my objectives were to challenge myself, to build the discipline to overcome any tough situation, and to better understand how to not be afraid of fear. Compared to who I was six years ago, I would like to think that I have improved as a human being, even if just slightly, a transformation made possible by the freedom provided in the Abu-Omar lab.

A wise man named David Goggins once said, "From the moment you take your first breath, you become eligible to die." In the brevity of this existence, it's never too late to change.

VITA OF MANHAO ZENG
July 2022

EDUCATION

2022	Doctorate of Philosophy in Chemistry (Materials) University of California, Santa Barbara, CA, USA
2015	Bachelor of Science in Chemistry Gettysburg College, Gettysburg, PA, USA

PUBLICATIONS

1. **Zeng, M.**; Lee, Y.-H.; Strong, G.; LaPointe, A. M.; Kocen, A. L.; Qu, Z.; Coates, G. W.; Scott, S. L.; Abu-Omar, M. M. Chemical Upcycling of Polyethylene to Value-Added α,ω-Divinyl-Functionalized Oligomers. *ACS Sustainable Chem. Eng.* **2021**, *9* (41), 13926–13936. https://doi.org/10.1021/acssuschemeng.1c05272.

2. *Zhang, F.; ***Zeng, M.**; Yappert, R. D.; Sun, J.; Lee, Y.-H.; LaPointe, A. M.; Peters, B.; Abu-Omar, M. M.; Scott, S. L. Polyethylene Upcycling to Long-Chain Alkylaromatics by Tandem Hydrogenolysis/Aromatization. *Science* **2020**, *370* (6515), 437–441. https://doi.org/10.1126/science.abc5441.

   **These authors contributed equally to this work.*

3. Siirila, M. J.; **Zeng, M.**; Woodroffe, J.-D.; Askew, R. L.; Harvey, B. G. Synthesis and Characterization of High-Performance Renewable Diesel Fuel from Bioderived 1-Octen-3-Ol. *Energy Fuels* **2020**, *34* (7), 8325–8331. https://doi.org/10.1021/acs.energyfuels.0c00120.

4. Horváth, V.; Kutner, D. J.; **Zeng, M. D.**; Epstein, I. R. Phase-Frequency Model of Strongly Pulse-Coupled Belousov-Zhabotinsky Oscillators. *Chaos* **2019**, *29* (2), 023128. https://doi.org/10.1063/1.5082161.

5. Fenton, O. S.; Kauffman, K. J.; McClellan, R. L.; Kaczmarek, J. C.; **Zeng, M. D.**; Andresen, J. L.; Rhym, L. H.; Heartlein, M. W.; DeRosa, F.; Anderson, D. G. Customizable Lipid Nanoparticle Materials for the Delivery of SiRNAs and MRNAs. *Angew. Chem. Int. Ed.* **2018**, *57* (41), 13582–13586. https://doi.org/10.1002/anie.201809056.

6. Fenton, O. S.; Kauffman, K. J.; Kaczmarek, J. C.; McClellan, R. L.; Jhunjhunwala, S.; Tibbitt, M. W.; **Zeng, M. D.**; Appel, E. A.; Dorkin, J. R.; Mir, F. F.; Yang, J. H.; Oberli, M. A.; Heartlein, M. W.; DeRosa, F.; Langer, R.; Anderson, D. G. Synthesis and Biological Evaluation of Ionizable Lipid Materials for the In Vivo Delivery of Messenger RNA to B Lymphocytes. *Adv. Mater.* **2017**, *29* (33), 1606944. https://doi.org/10.1002/adma.201606944.

7. Gunasekara, T.; Preston, A. Z.; **Zeng, M.**; Abu-Omar, M. M. Highly Regioselective α-Olefin Dimerization Using Zirconium and Hafnium Amine Bis(Phenolate) Complexes. *Organometallics* **2017**, *36* (15), 2934–2939. https://doi.org/10.1021/acs.organomet.7b00359.

ABSTRACT

Using End-of-Life Polymers and Bio-Derived Precursors to Synthesize Commodity Chemicals

by

Manhao Zeng

The majority of chemicals the world relies on today are derived from petroleum. Since fossil fuels are non-renewable resources that cannot be sustainably relied upon in the long-term, it is of interest to explore new ways to synthesize commodity chemicals using alternative starting materials. Herein, this work will describe how polymer waste and bio-based precursors can be applied to create chemicals typically derived from virgin petroleum feedstock.

In the past century, the world has produced over 7.5 billion metric tonnes of plastics which weigh more than one billion elephants, but 76% of these materials have been discarded into landfills or mismanaged, causing negative externalities such as environmental damage, deleterious health effects, and global economic loss. The research presented demonstrates how multiple types of polyethylene (PE), a frequently used plastic that comprises 36% of all polymers created, can be chemically upgraded using two routes. First, tandem catalytic conversion by platinum supported on γ-alumina under mild conditions (280 °C without solvent or additives) upcycles PE into high yields (up to 80 wt%) of lubricant grade valuable long-chain alkylaromatics and alkylnaphthenes. Second, a simple, three step sequence of bromination, dehydrobromination, and olefin metathesis reactions, each with respectable yields (86-97%), transforms PE into value-added α,ω-divinyl-functionalized oligomers with shorter, tunable chain lengths that can be used in the synthesis of lubricants and new

commodity polymers, with preliminary technoeconomic analyses that demonstrate this three-step process could be economically viable on an industrial scale.

Transitioning to renewable bio-based resources to generate energy can be a sustainable method to counter the negative environmental impacts of extracting non-renewable oil from the Earth. Using 1-octen-3-ol, an alcohol that can be derived from nature, high-performance $C_{16}H_{32}$ diesel was created in three steps with mostly high yields and conversions: (1) dehydration [58% yield], (2) Diels-Alder cyclodimerization [92% conversion], and (3) hydrogenation [95% yield]. With a high gravimetric net heat of combustion of 43.41 MJ/L and a cetane number of 71 which are greater than those for diesel fuel, this high-quality biofuel transcends the performance of diesels used today.

Table of Contents

Chapter 1. Introduction: The Current Management of End-of-Life Polymers

1.1 Motivation

The origin of plastics development begins in the 19th century, during which people regularly slaughtered elephants in India and Africa to capitalize upon the ivory from their tusks and decimated their populations. Since this inhumane approach nearly drove the elephant species to extinction and clearly could not be sustained for the long-term, celluloid was invented in 1863 to replace ivory as the first human-made plastic derived from bio-derived cellulose nitrate and camphor.[1] Over forty years later, the first fully synthetic plastic was invented in 1907 to replace shellac extracted from the East Asian lac bug for use in insulation.[1,2] Known as Bakelite, the plastic was synthesized from formaldehyde and phenol and was found to be a hard substance that did not dissolve in any solvent, the first of its kind.[1] Since its widespread implementation in insulation, infrastructure, and other modern applications in the 20th century, Bakelite also paved the way for the subsequent development of numerous plastics such as cellophane (1913), polyethylene (1933), nylon (1938), polystyrene (1944), and polypropylene (1954), some of which would prove to be essential to the outcome of World War II and the global economic development that followed in 1950 and beyond.[2]

Today, plastics undeniably play significant roles in society because of their durability, malleability, and low manufacturing cost, among other advantages.[3] The most widely manufactured synthetic plastics (Figure 1.1) include polyethylene (PE), polypropylene (PP), polystyrene (PS), polyvinyl chloride (PVC), polyethylene terephthalate (PET), and

polyurethanes (PU), with PE and PP currently accounting for more than 50% of the plastics produced globally.[4]

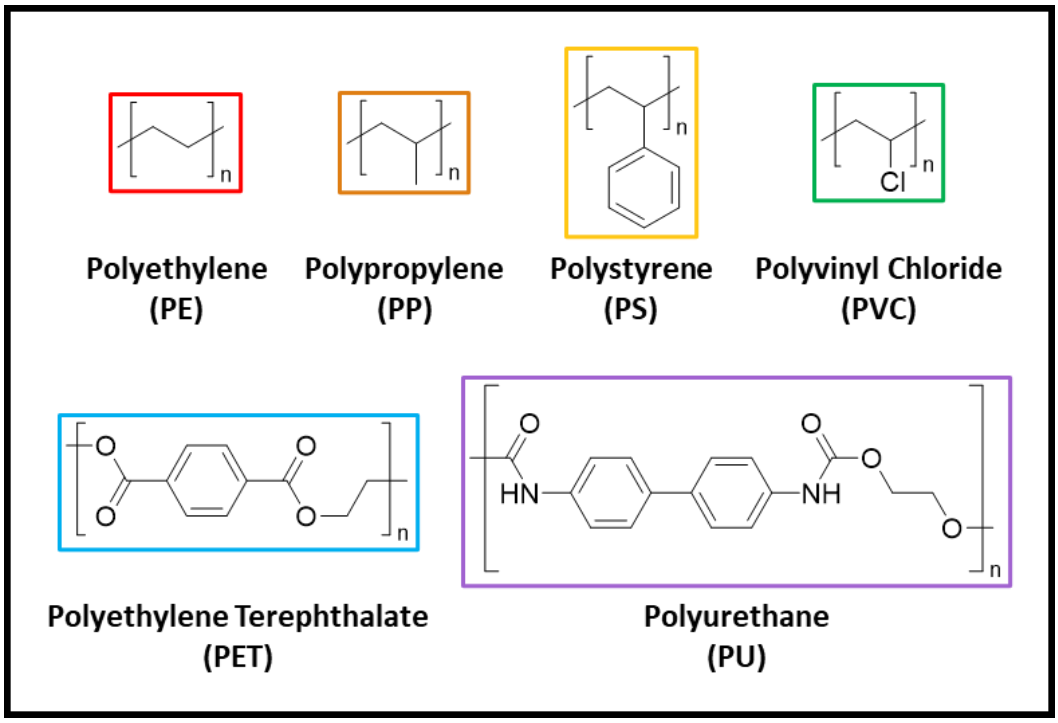

Figure 1.1 Molecular structures of the most commonly produced plastics today.

Given the increasing industrialization of countries all over the world, the quantity of plastics manufactured has drastically risen from under 2 million metric tonnes in 1950 to 367 million metric tonnes in 2020, with a projection to almost double to 660 million metric tonnes by 2036. [3,5] To date, the world has generated over 7.5 billion metric tonnes of plastics which weigh more than one billion elephants or 822,000 Eiffel Towers.[6] Since no practical process has been developed to effectively manage plastics on a global scale and because most of these materials have been designed as single-use goods,[3,6] however, 76% of all plastics created have been discarded into landfills or improperly disposed, thus contributing to environmental

pollution, poisoning anthropogenic food and water resources, and resulting in other negative consequences.[7–11]

While the current state of plastics management can be classified as unsustainable from both environmental and health perspectives, the same conclusion can be reached from an economic point of view as well. For instance, as the most common application of plastics, single-use packaging provides many benefits because of its durability and convenience. After a short life-cycle of less than one day,[3] however, 95% of the material value from these discarded plastics is not recovered, thus generating an economic expenditure of at least $80 billion every year from single-use packaging alone.[12,13] Furthermore, the present and future polymer waste generated from plastics manufactured in just the year of 2019 has been estimated to produce a lifetime cost of $3.7 trillion linked to adverse externalities such as societal health and environmental contamination,[14,15] which remarkably exceeds the gross domestic spending of many countries and greatly transcends the estimated profit share of $26-39 billion that corporations reap from capitalizing upon these materials.[12,13] Because of the serious concerns presented with the mishandled disposal of end-of-life plastics, developing more practical, sustainable techniques to properly manage these pervasive materials has become a worldwide interest.

1.2 Present-Day Challenges with Plastics "Recycling"

Based upon the model of "reduce, reuse, and recycle," reducing and reusing are the more effective routes of managing plastics compared to recycling, the least favorable method which requires large inputs of energy, lacks efficiency, and can generate hazardous waste in the process.[16] While less than 10% of these materials undergo recycling,[3] which mostly

involves shipping end-of-life plastics to low-income countries,[16] plastics are questionably advertised as recyclable, as evidenced by the recycling symbol (Figure 1.2) with labels 1-7 that correlate to chemical composition.[17]

Figure 1.2 Universal recycling symbol commonly stamped on plastics.[17]

In 2020, FRONTLINE and NPR (National Public Radio) reported[18] that the plastics industry has been marketing the alluring promise of plastics recycling to the public since the 1980s with the primary goal of making more profit from selling plastic. Larry Thomas, the former president of the lobby group Society of the Plastics Industry which led the movement to implement the current plastics recycling system by 1988, admitted that "If the public thinks that recycling is working, then they're not going to be as concerned about the environment. I think [the industry] knew that the infrastructure wasn't there to really have recycling amount to a whole lot."[19–21] To avoid proposed bans on plastic, former Dupont manager Ronald Liesemer acknowledged that "Making recycling work was a way to keep their products in the marketplace."[19–21] Internal documents in 1973 originating from within the plastics industry itself also expressed reservations about recycling by remarking on how the process was "costly" and "difficult," with a follow-up memo in 1974 describing how there was "serious doubt" that plastic recycling "can ever be made viable on an economic basis."[19–21]

In this system, the modern means of repurposing waste plastics can be classified into four categories: primary, secondary, tertiary, and quaternary.[22] Primary and secondary methods

involve mechanical recycling, while tertiary and quaternary techniques rely on chemical recycling.[23] Although the idea of plastics "recycling" implies that these materials can be reprocessed repeatedly, modern attempts of doing so on large scales have not been successful.

1.3 Traditional Mechanical Means of "Recycling"

As the most common technique to deal with waste polymers today, mechanical recycling can be performed under primary and secondary methods.[24] Analogous with the idea of "reuse" in the principle of "reduce, reuse, and recycle," primary recycling simply involves further repurposing end-of-life material with minimal modification for additional applications.[25] In secondary recycling, plastics first need to be sorted according to their resin type to ensure compatibility with subsequent steps.[26] Then, these materials are cleaned and dried to remove food, oils, and other physical contamination. Afterwards, the plastic is shredded and sorted by color into pieces that can either be extruded or converted into pellets that are used in product manufacturing.[26]

While the concept of mechanical recycling is simple in theory, the many disadvantages associated with this process hinder its large-scale implementation. As complex polymeric mixtures that also contain toxic pollutants,[27] chemical additives, food scraps, metals, paper, and miscellaneous organic matter, plastic waste can be challenging to differentiate and sort without specialized equipment such as FT-NIR (Fourier Transform Near-Infrared) sensors that identify a material's functional groups or floatation apparatuses for separation by density.[16] Given the diverse variety of chemicals in plastic waste, however, even substantial investments in these advanced technologies have not made widespread progress in effectively addressing the challenges associated with separating these materials in a cost-efficient manner.[28,29] The

select minority of polymers that can undergo recycling also require energy intensive procedures[30] to thoroughly clean for the final product to maintain properties similar to that made of virgin material, as even minor amounts of contamination can ultimately result in physical deterioration and discoloration.[31] Since the extrusion process has been reported to cause chemical degradation via chain scission, chain branching, or crosslinking reactions through radicals formed by shearing in the presence of heat and/or oxygen (Figure 1.3),[22,32,33] the overall product generally contains defects and is downgraded for use in lower quality purposes such as making carpets or insulation and cannot be reprocessed again using this method.[28]

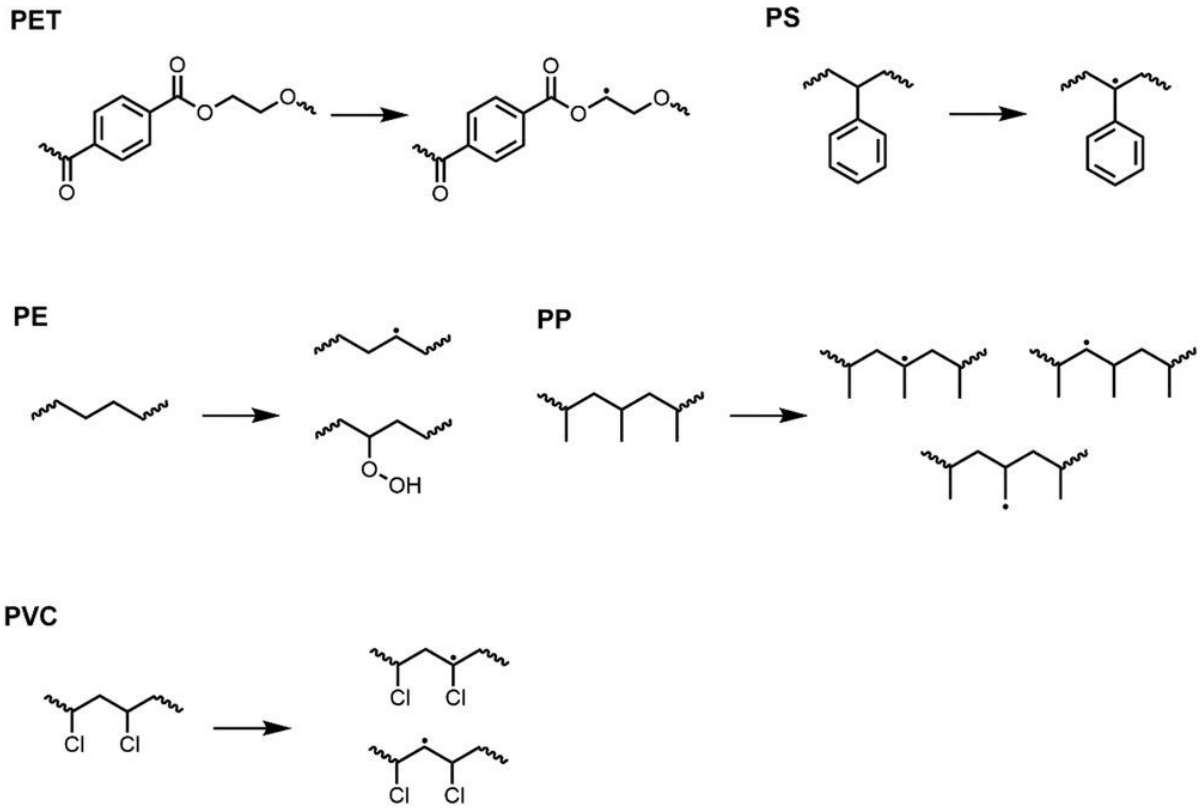

Figure 1.3 Some proposed radical species formed during extrusion.[22,32,33] Figure adapted from Schyns, Z. O. G. and Shaver, M. P.[22]

1.4 Traditional Chemical Means of "Recycling"

Considering the numerous drawbacks of mechanical recycling, greater attention has been given to chemical means of treating plastic waste that can be categorized into tertiary and quaternary technologies. Tertiary recycling involves the chemical degradation of the polymer into subunits that can be transformed into a new product using methods such as solvolysis while quaternary recycling relies on pyrolysis and incineration to recover energy from these discarded materials.[34]

In the process of solvolysis (*solv*- meaning "solvent" and -*lysis* meaning "breaking"), water, alcohol, and other nucleophilic solvents are used to cleave C-X linkages, where X consists of non-carbon or hydrogen atoms that include oxygen or nitrogen.[35] Regarding commercial plastics with heteroatoms such as polyethylene terephthalate (PET) and polyurethane (PU) which contain degradable ester and amide functional groups (Figure 1.1), solvolysis breaks the C-O and C-N bonds[36] to form functionalized monomers and/or oligomers that may then be recycled to synthesize new polymers and other materials or used as a chemical feedstock. As exemplified by the solvolysis of PET using water (Scheme 1.1), also called hydrolysis, the resulting terephthalic acid and ethylene glycol monomers can be used to manufacture PET again.[37]

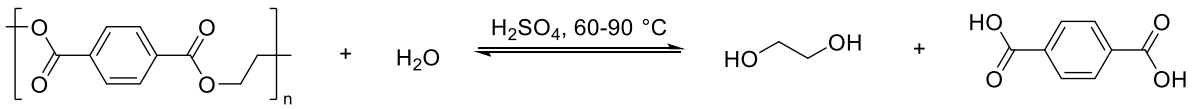

Scheme 1.1 Solvolysis of PET using water to form ethylene glycol and terephthalic acid.[37]

Other forms of solvolysis include but are not limited to aminolysis, alcoholysis, glycolysis, and ammonolysis, which are performed using amines ($-NH_2$), alcohols (-OH), glycols (HO-R-OH), and ammonium (NH_3), respectively.[35,37] While solvolysis can depolymerize heteroatom polymers into their initial monomers, this method to chemically recycle plastics requires specialized infrastructure and additional chemical additives that render the uneconomical and impractical relative to conventional plastic synthesis routes reliant on virgin materials.[38]

Although solvolysis can only be performed on certain types of polymers, thermal treatment methods can use multiple types of plastic to recover energy from and can be advantageously conducted using mixed waste streams. Some heteroatom polymers such as polyvinyl chloride, polyurethanes, and polyethylene terephthalate, however, are deemed less suitable for this process because they also produce HCl, HCN, oxygenated small molecules, and other unfavorable gases which have low energy values and complicate the purification of any desired products.[39–42] During pyrolysis, the starting material is heated at 450 °C or greater under oxygen free conditions to generate complex mixtures of lower molecular weight products including gases, liquids, char, and waxes.[43,44] Because the mechanism of this chemistry involves random radical-induced chain scission, the overall products created from this method lack selectivity, as demonstrated by the pyrolysis of polyethylene (PE) in Scheme 1.2.[45]

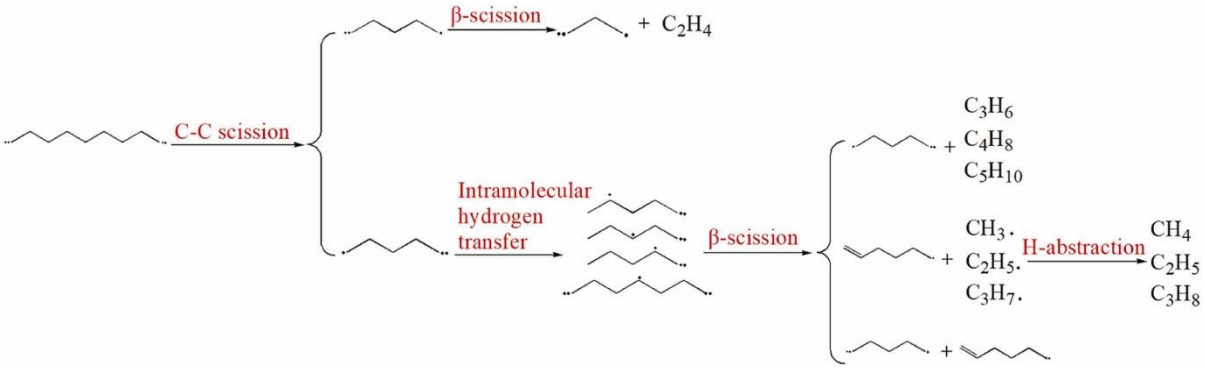

Scheme 1.2 Proposed mechanism of the pyrolysis of polyethylene. Adapted from Jiang, J., *et. al.*[45]

To solve this challenge, catalysts with Lewis acid sites such as the zeolite ZSM-5 [$Na_nAl_nSi_{96-n}O_{192}\cdot 16H_2O$ ($0<n<27$)][46] are used in plastics pyrolysis to perform cracking, isomerization, cyclization, and aromatization reactions that direct some selectivity towards liquid oils and aromatic compounds that have applications in fuels and lubricants.[47–52] In addition to traditional batch reactors, more advanced vessels including fixed bed, fluidized bed, semi-batch, and plasma reactors have been developed to enhance the reaction yields and selectivity of pyrolysis while lowering the reaction temperatures and times.[53,54] While these technological improvements have been shown to result in greater product selectivity and yields compared to standard methods, they do not address the high energy input requirements that currently hinder the large-scale implementation of pyrolysis.[55]

Similarly, incineration can be performed to manage waste plastics by combusting the material at 900-1100 °C under air to generate energy.[56] Given how the operating temperature of incineration may be even greater than that of pyrolysis, this method lacks efficiency and has high costs. Even though energy is generated from the gases in this reaction, toxic by-products

such as SO_x and NO_x gases or heavy metals that may be present in the residual ash complicate the application of this technique as a long-term solution for plastic waste management.[27,56]

1.5 Conclusion

Today's methods of managing plastic waste through conventional mechanical and chemical routes have provided neither sustainable nor practical answers to the growing accumulation of end-of-life polymers in landfills and in the environment. Given the quantifiable impact that this problem has to the global economy and to societal health, more effective responses that valorize plastic waste are imperative. Since most commodity materials currently used are derived from non-renewable fossil fuels, implementing superior techniques to recycle existing petroleum-based plastics into products that can be recirculated into society would provide an avenue to reduce pollution and transition the world away from excessively extracting more oil through unsustainable means.

1.6 References

(1) American Chemical Society National Historic Chemical Landmarks. Bakelite: The World's First Synthetic Plastic. Http://Www.Acs.Org/Content/Acs/En/Education/Whatischemistry/Landmarks/Bakelite.Html (Accessed June 2, 2022).

(2) Chalmin, P. The History of Plastics: From the Capitol to the Tarpeian Rock. *Field Actions Science Reports* **2019**, No. 19, 6–11.

(3) Geyer, R.; Jambeck, J. R.; Law, K. L. Production, Use, and Fate of All Plastics Ever Made. *Sci. Adv.* **2017**, *3* (7), e1700782. https://doi.org/10.1126/sciadv.1700782.

(4) Ali, S. S.; Elsamahy, T.; Koutra, E.; Kornaros, M.; El-Sheekh, M.; Abdelkarim, E. A.; Zhu, D.; Sun, J. Degradation of Conventional Plastic Wastes in the Environment: A Review on Current Status of Knowledge and Future Perspectives of Disposal. *Science of The Total Environment* **2021**, *771*, 144719. https://doi.org/10.1016/j.scitotenv.2020.144719.

(5) Plastics Europe. Plastics - the Facts 2021. Https://Plasticseurope.Org/Wp-Content/Uploads/2021/12/Plastics-the-Facts-2021-Web-Final.Pdf (Accessed June 2, 2022).

(6) Phys.Org. 8.3 Billion Metric Tons: Scientists Calculate Total Amount of Plastics Ever Produced. Https://Phys.Org/News/2017-07-Billion-Metric-Tons-Scientists-Total.Html (Accessed June 2, 2022).

(7) Borrelle, S. B.; Ringma, J.; Law, K. L.; Monnahan, C. C.; Lebreton, L.; McGivern, A.; Murphy, E.; Jambeck, J.; Leonard, G. H.; Hilleary, M. A.; Eriksen, M.; Possingham, H. P.; De Frond, H.; Gerber, L. R.; Polidoro, B.; Tahir, A.; Bernard, M.; Mallos, N.; Barnes, M.; Rochman, C. M. Predicted Growth in Plastic Waste Exceeds Efforts to Mitigate Plastic Pollution. *Science* **2020**, *369* (6510), 1515–1518. https://doi.org/10.1126/science.aba3656.

(8) Law, K. L.; Starr, N.; Siegler, T. R.; Jambeck, J. R.; Mallos, N. J.; Leonard, G. H. The United States' Contribution of Plastic Waste to Land and Ocean. *Sci. Adv.* **2020**, *6* (44), eabd0288. https://doi.org/10.1126/sciadv.abd0288.

(9) Jambeck, J. R.; Geyer, R.; Wilcox, C.; Siegler, T. R.; Perryman, M.; Andrady, A.; Narayan, R.; Law, K. L. Plastic Waste Inputs from Land into the Ocean. *Science* **2015**, *347* (6223), 768–771. https://doi.org/10.1126/science.1260352.

(10) Leslie, H. A.; van Velzen, M. J. M.; Brandsma, S. H.; Vethaak, A. D.; Garcia-Vallejo, J. J.; Lamoree, M. H. Discovery and Quantification of Plastic Particle Pollution in Human Blood. *Environment International* **2022**, *163*, 107199. https://doi.org/10.1016/j.envint.2022.107199.

(11) Evode, N.; Qamar, S. A.; Bilal, M.; Barceló, D.; Iqbal, H. M. N. Plastic Waste and Its Management Strategies for Environmental Sustainability. *Case Studies in Chemical and Environmental Engineering* **2021**, *4*, 100142. https://doi.org/10.1016/j.cscee.2021.100142.

(12) World Economic Forum, Ellen MacArthur Foundation and McKinsey & Company, The New Plastics Economy: Rethinking the Future of Plastics, 2016, Https://Emf.Thirdlight.Com/Link/Faarmdpz93ds-5vmvdf/@/Download/1 (Accessed June 2, 2022).

(13) World Economic Forum, Ellen MacArthur Foundation and McKinsey & Company,The New Plastics Economy: Rethinking the Future of Plastics Background to Key Statistics from the Report, 2016, Https://Emf.Thirdlight.Com/Link/F668rdcezflu-Oxunnl/@/Download/1 (Accessed June 2, 2022).

(14) World Wide Fund For Nature, Plastics: The Cost to Society, Environment and the Economy, 2021, Https://Europe.Nxtbook.Com/Nxteu/Wwfintl/Tcops/Index.Php (Accessed June 2, 2022).

(15) Rhodes, C. J. Plastic Pollution and Potential Solutions. *Science Progress* **2018**, *101* (3), 207–260. https://doi.org/10.3184/003685018X15294876706211.

(16) International Pollutants Elimination Network, Plastic Waste Management Hazards: Waste-to-Energy, Chemical Recycling, and Plastic Fuels, 2021,

Https://Ipen.Org/Sites/Default/Files/Documents/Ipen-Plastic-Waste-Management-Hazards-En.Pdf (Accessed June 3, 2022).

(17) ASTM International, Resin Identification Codes, 2008, Https://Web.Archive.Org/Web/20201125105205/Http://Www.Astm.Org/SNEWS/SO_2008/Wilhelm_so08.Html (Accessed June 3, 2022).

(18) *Frontline, Plastic Wars, 2020, Https://Www.Pbs.Org/Wgbh/Frontline/Film/Plastic-Wars/ (Accessed June 3, 2022).*

(19) Frontline, Plastics Industry Insiders Reveal the Truth About Recycling, 2020, Https://Www.Pbs.Org/Wgbh/Frontline/Article/Plastics-Industry-Insiders-Reveal-the-Truth-about-Recycling/ (Accessed June 3, 2022).

(20) National Public Radio, Plastic Wars: Industry Spent Millions Selling Recycling — To Sell More Plastic, 2020, Https://Www.Npr.Org/2020/03/31/822597631/Plastic-Wars-Three-Takeaways-from-the-Fight-over-the-Future-of-Plastics (Accessed June 3, 2022).

(21) National Public Radio, How Big Oil Misled The Public Into Believing Plastic Would Be Recycled, 2020, Https://Www.Npr.Org/2020/09/11/897692090/How-Big-Oil-Misled-the-Public-into-Believing-Plastic-Would-Be-Recycled (Accessed June 3, 2022).

(22) Schyns, Z. O. G.; Shaver, M. P. Mechanical Recycling of Packaging Plastics: A Review. *Macromol. Rapid Commun.* **2021**, *42* (3), 2000415. https://doi.org/10.1002/marc.202000415.

(23) Ragaert, K.; Delva, L.; Van Geem, K. Mechanical and Chemical Recycling of Solid Plastic Waste. *Waste Management* **2017**, *69*, 24–58. https://doi.org/10.1016/j.wasman.2017.07.044.

(24) Grigore, M. Methods of Recycling, Properties and Applications of Recycled Thermoplastic Polymers. *Recycling* **2017**, *2* (4), 24. https://doi.org/10.3390/recycling2040024.

(25) Perego, C.; Ingallina, P. Recent Advances in the Industrial Alkylation of Aromatics: New Catalysts and New Processes. *Catalysis Today* **2002**, *73* (1–2), 3–22. https://doi.org/10.1016/S0920-5861(01)00511-9.

(26) Al-Salem, S. M.; Lettieri, P.; Baeyens, J. Recycling and Recovery Routes of Plastic Solid Waste (PSW): A Review. *Waste Management* **2009**, *29* (10), 2625–2643. https://doi.org/10.1016/j.wasman.2009.06.004.

(27) Verma, R.; Vinoda, K. S.; Papireddy, M.; Gowda, A. N. S. Toxic Pollutants from Plastic Waste- A Review. *Procedia Environmental Sciences* **2016**, *35*, 701–708. https://doi.org/10.1016/j.proenv.2016.07.069.

(28) Lange, J.-P. Managing Plastic Waste─Sorting, Recycling, Disposal, and Product Redesign. *ACS Sustainable Chem. Eng.* **2021**, *9* (47), 15722–15738. https://doi.org/10.1021/acssuschemeng.1c05013.

(29) Muñoz Meneses, R. A.; Cabrera-Papamija, G.; Machuca-Martínez, F.; Rodríguez, L. A.; Diosa, J. E.; Mosquera-Vargas, E. Plastic Recycling and Their Use as Raw Material for the Synthesis of Carbonaceous Materials. *Heliyon* **2022**, *8* (3), e09028. https://doi.org/10.1016/j.heliyon.2022.e09028.

(30) Roosen, M.; De Somer, T.; Demets, R.; Ügdüler, S.; Meesseman, V.; Van Gorp, B.; Ragaert, K.; Van Geem, K. M.; Walgraeve, C.; Dumoulin, A.; De Meester, S. Towards a Better Understanding of Odor Removal from Post-Consumer Plastic Film Waste: A

Kinetic Study on Deodorization Efficiencies with Different Washing Media. *Waste Management* **2021**, *120*, 564–575. https://doi.org/10.1016/j.wasman.2020.10.021.

(31) Hahladakis, J. N.; Iacovidou, E. Closing the Loop on Plastic Packaging Materials: What Is Quality and How Does It Affect Their Circularity? *Sci Total Environ* **2018**, *630*, 1394–1400. https://doi.org/10.1016/j.scitotenv.2018.02.330.

(32) Gryn'ova, G.; Hodgson, J. L.; Coote, M. L. Revising the Mechanism of Polymer Autooxidation. *Org. Biomol. Chem.* **2011**, *9* (2), 480–490. https://doi.org/10.1039/C0OB00596G.

(33) Ravve, A. Degradation of Polymers. In *Principles of Polymer Chemistry*; Springer US: Boston, MA, 2000; pp 581–616. https://doi.org/10.1007/978-1-4615-4227-8_9.

(34) Beghetto, V.; Sole, R.; Buranello, C.; Al-Abkal, M.; Facchin, M. Recent Advancements in Plastic Packaging Recycling: A Mini-Review. *Materials* **2021**, *14* (17), 4782. https://doi.org/10.3390/ma14174782.

(35) Xanthos, M.; Patel, S. H. Solvolysis. In *Frontiers in the Science and Technology of Polymer Recycling*; Akovali, G., Bernardo, C. A., Leidner, J., Utracki, L. A., Xanthos, M., Eds.; Springer Netherlands: Dordrecht, 1998; pp 425–436. https://doi.org/10.1007/978-94-017-1626-0_20.

(36) Goodship, V. Recycling Issues in Polymer Matrix Composites. In *Failure Mechanisms in Polymer Matrix Composites*; Elsevier, 2012; pp 337–367. https://doi.org/10.1533/9780857095329.2.337.

(37) Al-Sabagh, A. M.; Yehia, F. Z.; Eshaq, Gh.; Rabie, A. M.; ElMetwally, A. E. Greener Routes for Recycling of Polyethylene Terephthalate. *Egyptian Journal of Petroleum* **2016**, *25* (1), 53–64. https://doi.org/10.1016/j.ejpe.2015.03.001.

(38) George, N.; Kurian, T. Recent Developments in the Chemical Recycling of Postconsumer Poly(Ethylene Terephthalate) Waste. *Ind. Eng. Chem. Res.* **2014**, *53* (37), 14185–14198. https://doi.org/10.1021/ie501995m.

(39) Yu, J.; Sun, L.; Ma, C.; Qiao, Y.; Yao, H. Thermal Degradation of PVC: A Review. *Waste Management* **2016**, *48*, 300–314. https://doi.org/10.1016/j.wasman.2015.11.041.

(40) Dimitrov, N.; Kratofil Krehula, L.; Ptiček Siročić, A.; Hrnjak-Murgić, Z. Analysis of Recycled PET Bottles Products by Pyrolysis-Gas Chromatography. *Polymer Degradation and Stability* **2013**, *98* (5), 972–979. https://doi.org/10.1016/j.polymdegradstab.2013.02.013.

(41) Yu, J.; Liu, S.; Cardoso, A.; Han, Y.; Bikane, K.; Sun, L. Catalytic Pyrolysis of Rubbers and Vulcanized Rubbers Using Modified Zeolites and Mesoporous Catalysts with Zn and Cu. *Energy* **2019**, *188*, 116117. https://doi.org/10.1016/j.energy.2019.116117.

(42) Paabo, M.; Levin, B. C. A Review of the Literature on the Gaseous Products and Toxicity Generated from the Pyrolysis and Combustion of Rigid Polyurethane Foams. *Fire Mater.* **1987**, *11* (1), 1–29. https://doi.org/10.1002/fam.810110102.

(43) Miandad, R.; Rehan, M.; Barakat, M. A.; Aburiazaiza, A. S.; Khan, H.; Ismail, I. M. I.; Dhavamani, J.; Gardy, J.; Hassanpour, A.; Nizami, A.-S. Catalytic Pyrolysis of Plastic Waste: Moving Toward Pyrolysis Based Biorefineries. *Front. Energy Res.* **2019**, *7*, 27. https://doi.org/10.3389/fenrg.2019.00027.

(44) Yan, G.; Jing, X.; Wen, H.; Xiang, S. Thermal Cracking of Virgin and Waste Plastics of PP and LDPE in a Semibatch Reactor under Atmospheric Pressure. *Energy Fuels* **2015**, *29* (4), 2289–2298. https://doi.org/10.1021/ef502919f.

(45) Jiang, J.; Shi, K.; Zhang, X.; Yu, K.; Zhang, H.; He, J.; Ju, Y.; Liu, J. From Plastic Waste to Wealth Using Chemical Recycling: A Review. *Journal of Environmental Chemical Engineering* **2022**, *10* (1), 106867. https://doi.org/10.1016/j.jece.2021.106867.

(46) ACS Material, ZSM-5 - Zeolite Socony Mobil–5, 2019, Https://Www.Acsmaterial.Com/Blog-Detail/Zsm-5-Molecular-Seive.Html (Accessed June 5, 2022).

(47) Anuar Sharuddin, S. D.; Abnisa, F.; Wan Daud, W. M. A.; Aroua, M. K. A Review on Pyrolysis of Plastic Wastes. *Energy Conversion and Management* **2016**, *115*, 308–326. https://doi.org/10.1016/j.enconman.2016.02.037.

(48) Sivagami, K.; Kumar, K. V.; Tamizhdurai, P.; Govindarajan, D.; Kumar, M.; Nambi, I. Conversion of Plastic Waste into Fuel Oil Using Zeolite Catalysts in a Bench-Scale Pyrolysis Reactor. *RSC Adv.* **2022**, *12* (13), 7612–7620. https://doi.org/10.1039/D1RA08673A.

(49) Francis, J.; Guillon, E.; Bats, N.; Pichon, C.; Corma, A.; Simon, L. J. Design of Improved Hydrocracking Catalysts by Increasing the Proximity between Acid and Metallic Sites. *Applied Catalysis A: General* **2011**, *409–410*, 140–147. https://doi.org/10.1016/j.apcata.2011.09.040.

(50) Sato, K.; Nishimura, Y.; Honna, K.; Matsubayashi, N.; Shimada, H. Role of HY Zeolite Mesopores in Hydrocracking of Heavy Oils. *Journal of Catalysis* **2001**, *200* (2), 288–297. https://doi.org/10.1006/jcat.2001.3184.

(51) Ravi, M.; Sushkevich, V. L.; van Bokhoven, J. A. Lewis Acidity Inherent to the Framework of Zeolite Mordenite. *J. Phys. Chem. C* **2019**, *123* (24), 15139–15144. https://doi.org/10.1021/acs.jpcc.9b03620.

(52) Matsunaga, Atsushi.; Yagi, Masataro. Separation of Aromatic Compounds in Lubricant Base Oils by High Performance Liquid Chromatography. *Anal. Chem.* **1978**, *50* (6), 753–756. https://doi.org/10.1021/ac50027a022.

(53) Dogu, O.; Pelucchi, M.; Van de Vijver, R.; Van Steenberge, P. H. M.; D'hooge, D. R.; Cuoci, A.; Mehl, M.; Frassoldati, A.; Faravelli, T.; Van Geem, K. M. The Chemistry of Chemical Recycling of Solid Plastic Waste via Pyrolysis and Gasification: State-of-the-Art, Challenges, and Future Directions. *Progress in Energy and Combustion Science* **2021**, *84*, 100901. https://doi.org/10.1016/j.pecs.2020.100901.

(54) Diaz-Silvarrey, L. S.; Zhang, K.; Phan, A. N. Monomer Recovery through Advanced Pyrolysis of Waste High Density Polyethylene (HDPE). *Green Chem.* **2018**, *20* (8), 1813–1823. https://doi.org/10.1039/C7GC03662K.

(55) Qureshi, M. S.; Oasmaa, A.; Pihkola, H.; Deviatkin, I.; Tenhunen, A.; Mannila, J.; Minkkinen, H.; Pohjakallio, M.; Laine-Ylijoki, J. Pyrolysis of Plastic Waste: Opportunities and Challenges. *Journal of Analytical and Applied Pyrolysis* **2020**, *152*, 104804. https://doi.org/10.1016/j.jaap.2020.104804.

(56) Moharir, R. V.; Gautam, P.; Kumar, S. Waste Treatment Processes/Technologies for Energy Recovery. In *Current Developments in Biotechnology and Bioengineering*; Elsevier, 2019; pp 53–77. https://doi.org/10.1016/B978-0-444-64083-3.00004-X.

Chapter 2. Polyethylene Upcycling to Long-Chain Alkylaromatics by Tandem Hydrogenolysis/Aromatization

***** *This chapter was reproduced from the following publication. The author of this Ph. D. thesis, Manhao Zeng, is the leading coauthor of this publication who contributed to all parts relevant to this work.*

*Zhang, F.; ***Zeng, M.**; Yappert, R. D.; Sun, J.; Lee, Y.-H.; LaPointe, A. M.; Peters, B.; Abu-Omar, M. M.; Scott, S. L. Polyethylene Upcycling to Long-Chain Alkylaromatics by Tandem Hydrogenolysis/Aromatization. *Science* **2020**, *370* (6515), 437–441. https://doi.org/10.1126/science.abc5441.

**These authors contributed equally to this work.*

2.1 Abstract

The current scale of plastics production and the accompanying waste disposal problems represent a largely untapped opportunity for chemical upcycling. Tandem catalytic conversion by platinum supported on γ-alumina converts various polyethylene grades in high yields (up to 80 weight percent) to low- molecular-weight liquid/wax products, in the absence of added solvent or molecular hydrogen, with little production of light gases. The major components are valuable long-chain alkylaromatics and alkylnaphthenes (average ~C_{30}, dispersity $Đ$ = 1.1). Coupling exothermic hydrogenolysis with endothermic aromatization renders the overall transformation thermodynamically accessible despite the moderate reaction temperature of

280 °C. This approach demonstrates how waste polyolefins can be a viable feedstock for the generation of molecular hydrocarbon products.

2.2 Introduction

Over the past 70 years, global production of synthetic, petroleum-based plastics has risen sharply, from less than 2 million tonnes in 1950 to 380 million tonnes in 2015.[1] Production is projected to double again within the next 20 years.[2] Plastics have become indispensable in many facets of modern life, enhancing the security of our food and health care systems, the performance of textiles, the versatility of consumer electronics, and the energy efficiency of transportation. About 40% of these plastics are destined for short-term use, and most (>90% in the United States) are not recycled.[1] The vast bulk of this plastic waste ends up in land- fills or is incinerated. However, the embodied energy that can be recovered by combustion is far less than that used in the original manufacturing of the plastic.[3] Furthermore, a substantial fraction of the waste is mismanaged, ending up in rivers and oceans where its chemical inertness leads to extremely slow degradation and visible accumulation in the natural environment.[4,5]

Efforts to develop closed-loop life cycles for synthetic plastics by relying on collection, separation, and mechanical recycling have had limited success. The inferior properties of the recycled materials, relative to virgin plastics, contribute to the economic challenges of the "downcycling" model.[6] New types of polymers that degrade rapidly in the environment are being investigated,[7] although such materials do not currently have either the physical properties or the cost structure to displace existing commodity plastics. Degradable plastics can also contaminate recycling streams and may encourage single-use product design.

Depolymerization (also known as chemical or feedstock recycling) can recover the original monomer subunits, repolymerization of which yields materials with properties identical to those of the original plastic.[8] However, this strategy requires prohibitive amounts of energy for polyolefins such as polyethylene (PE) and polypropylene (PP). Controlled partial depolymerization could convert post-consumer waste plastics directly into more valuable chemicals ("upcycling"), although few such processes have yet been developed.

High- and low-density polyethylenes (HDPE and LDPE) currently represent the largest fraction (36% by mass) of all plastic waste.[1] Their depolymerization by pyrolysis at temperatures above 400 °C, with or without a catalyst, generates complex, low-value mixtures of gas, liquid hydrocarbons, and char.[9,10] Somewhat more selective disassembly can be achieved at lower temperatures via catalytic hydrogenolysis[11, 12] or tandem catalytic alkane metathesis,[13] but the low-value alkane products are unlikely to recoup the costs of recovery, separation, and processing using large amounts of a co-reactant (H_2 or liquid alkanes, respectively).

Aromatics are more attractive target products from partial depolymerization. The conventional process for making aromatics is naphtha reforming. This energy-intensive process generates a mixture known as BTX (benzene-toluene-xylenes) at 500-600 °C.[14] In a subsequent step with a large environmental footprint, BTX is alkylated to give linear alkylbenzenes (LABs, used for making surfactants). The most widely used processes require linear olefins (typically, C_{10} to C_{16}) and liquid HF or $AlCl_3$-HCl as the acid catalyst.[15] Manufacturing the BTX by aromatization of shale gas–derived light alkanes requires harsher reaction conditions (propane, 550-700 °C; ethane, 600-800 °C; methane, 900-1000 °C),[16] and the catalysts tend to deactivate rapidly. New zeolite-based catalysts can transform either

methanol[17] or syngas[18] into BTX aromatics at lower temperatures, 300-400°C. Biomass-based routes include oxidative coupling of ethanol to aromatic alcohols and aldehydes,[19] hydrogenolysis/hydrodeoxygenation of bio-oils or lignin to give propylbenzene,[20] and Diels-Alder reactions of carbohydrate-derived furanics to give *p*-xylene.[21] However, slow rates, low yields, and high H_2 requirements make these processes expensive to operate, and none are practiced commercially. BTX is also formed in the catalytic pyrolysis of PE at 400-600°C, although deactivation of the zeolite catalysts by coking is severe.[22] The yields are moderate (up to 50 wt%), and large amounts of low-value gases (C_1 to C_5, > 50 wt%) are formed. Conventional and proposed routes to BTX and linear alkylaromatics are compared in Fig. 2.1.

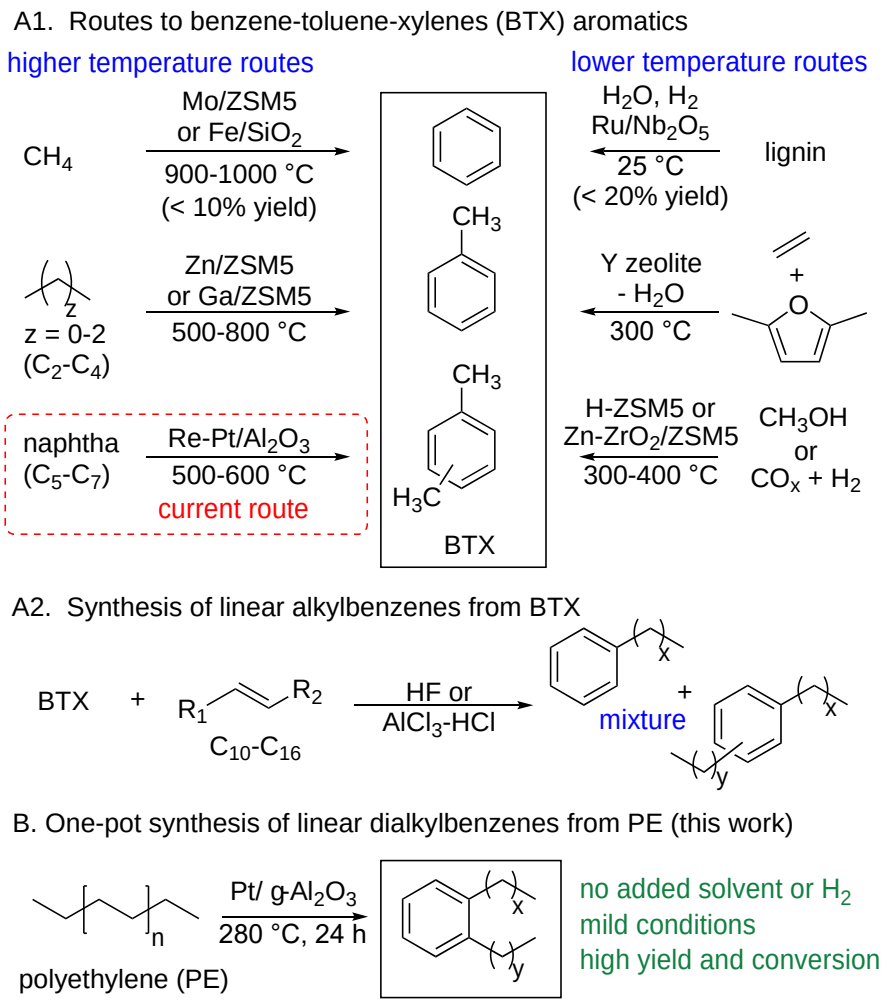

Figure 2.1 Routes to alkylbenzenes. (A to C) Current and proposed routes to BTX (A) and the current downstream transformation of BTX to linear alkylbenzenes (B) are compared to the one-pot tandem process from polyethylene (C) reported here.

2.3 Results and Discussion

Here, we report a one-pot, low-temperature catalytic method to convert various grades of PE directly to liquid alkylaromatics over a simple heterogeneous catalyst. In a proof-of-concept experiment, a low-molecular-weight PE (0.118 g, M_w = 3.5 × 10^3 g/mol, $Đ$ = 1.90) was combined with Pt/γ-Al_2O_3 (0.200 g, containing 1.5 wt% Pt dispersed as ~1-nm

nanoparticles; fig. A.1A and A.1B) in an unstirred mini-autoclave (internal volume 10 ml) without solvent or added H_2 (Fig. 2.2A). After 24 hours at 280 ± 5 °C, the liquid/wax products (80% by mass) were recovered for characterization by dissolving in hot $CHCl_3$ (Fig. 2.2B, experiment 1).

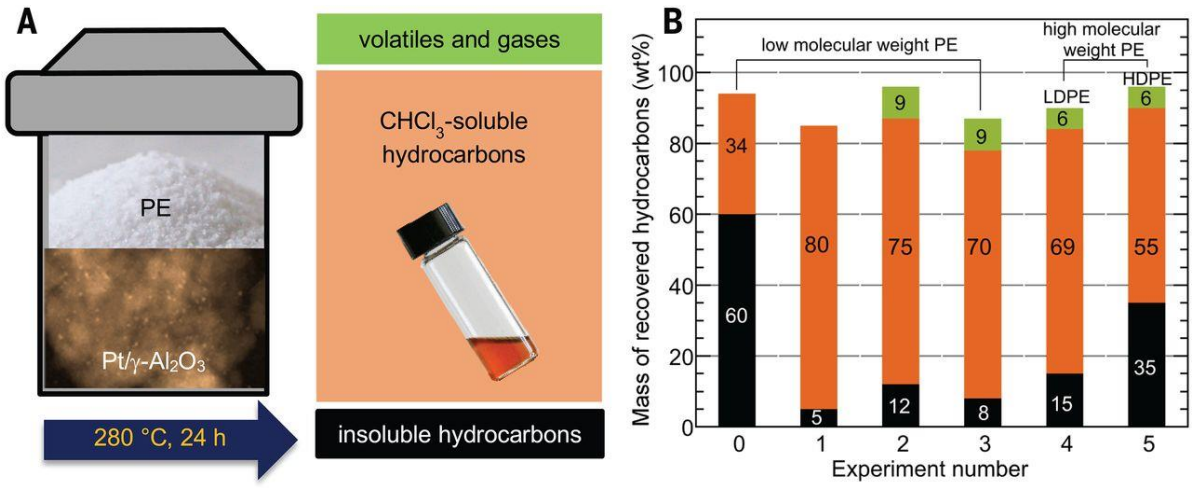

Figure 2.2 Solvent-free conversion of various types of polyethylene. (A) Schematic of reactor and product fractions, with photographs of the powdered polymer and liquid products, as well as a transmission electron micrograph of the catalyst. (B) Hydrocarbon distributions after 24 hours at 280°C. Reactions of a low-molecular-weight PE (M_w = 3.52 × 10^3 g/mol, $Đ$ = 1.90) in an unstirred mini-autoclave reactor: (0) catalyzed by γ-Al_2O_3 (no gas recovery); (1) catalyzed by Pt/γ-Al_2O_3 (no gas recovery); (2) catalyzed by Pt/γ-Al_2O_3 (with gas recovery). Reactions catalyzed by Pt/γ-Al_2O_3 in a stirred autoclave reactor with gas recovery: (3) low-molecular-weight PE; (4) LDPE bag (M_w = 9.45 × 10^4 g/mol, $Đ$ = 7.37); (5) HDPE bottle cap (M_w = 5.35 × 10^4 g/mol, $Đ$ = 3.61).

According to gel permeation chromatography with refractive index detection (GPC-RI), most of the PE underwent a decrease in M_w by nearly a factor of 10, to 430 g/mol, as well as the expected[23] decrease in dispersity (to $Đ$ = 1.31). On the basis of their orange color and the appearance of ^{1}H nuclear magnetic resonance (NMR) signals in the region 6.5 to 9.0 ppm (Fig. A.2), these hydrocarbons appear to have substantial aromatic content. The $CHCl_3$-insoluble solids include a small amount of organic residue (~5 wt%) in addition to the catalyst. The former includes unreacted polymer and large oligomers (including less soluble alkylaromatics), as judged by infrared and ^{1}H NMR spectroscopy (Figs. A.3 and A.4). The missing mass (~15 wt%) is presumably volatile hydrocarbons and gases, which were not collected in this exploratory experiment. In a control experiment conducted without the catalyst under the same reaction conditions, the PE showed no appreciable decrease in M_w. A second control experiment using the same amount of γ–Al_2O_3 but without Pt resulted mostly in a $CHCl_3$-insoluble residue (~60 wt%) and a much lower yield of soluble hydrocarbon products (34 wt%), with a smaller decrease in molecular weight (M_w = 1421 g/mol, $Đ$ = 1.85) and negligible aromatic content (Fig. 2.2B, experiment 0).

To obtain a more complete mass balance and to characterize the volatile reaction products, the exploratory experiment was repeated in a mini-autoclave equipped with a gas port. The recovered gases represent a small fraction of the original polymer mass (9 wt%). They include H_2 (0.2 mg, quantified by GC-TCD) and light hydrocarbons (C_1 to C_8, 9.8 mg, quantified by GC-FID) (Figs. A.5 and A.6). The latter were primarily methane, ethane and propane, with minor amounts of *n*-hexane, cyclohexane, methylcyclopentane, benzene, and *n*-heptane. Additional volatile hydrocarbons (C_7 to C_{11}, 1.5 mg) were recovered by distillation from the autoclave at 150 °C. Their major component was toluene 47 wt%). Together, the light

hydrocarbons, the $CHCl_3$-soluble liquids/waxes (89 mg) and the insoluble organic residue (14 mg) represent an overall mass balance of 96% (Fig. 2.2B, experiment 2).

When the reaction was conducted in a larger, stirred autoclave (internal volume 90 ml), most of the PE (70 wt%) was converted at 280 °C to high-boiling liquids/waxes (Fig. 2.2B, experiment 3). In this case, the waxes (24 wt%, M_w = 723 g/mol, $Đ$ = 1.34) separated spontaneously from the liquids (46 wt%, M_w = 520 g/mol, $Đ$ = 1.12) inside the reactor. GPC analysis of the liquid fraction using both RI and ultra-violet (UV) detection gave similar results (Fig. 2.3A), demonstrating that the UV-active (i.e., aromatic) chromophores were evenly distributed across the molecular weight range. The ^{13}C NMR spectrum contains signals in the aromatic region (120 to 150 ppm), most corresponding to unsubstituted ring carbons (Fig. 2.3B). The ^{1}H NMR spectrum shows that most aromatic protons are associated with benzene rings (6.5 to 7.4 ppm), with fewer bonded to fused aromatic rings such as naphthalenes (7.4 to 9.0 ppm).[24] There is no evidence for olefins or dienes (4.5 to 6.5 ppm; fig. A.8A).

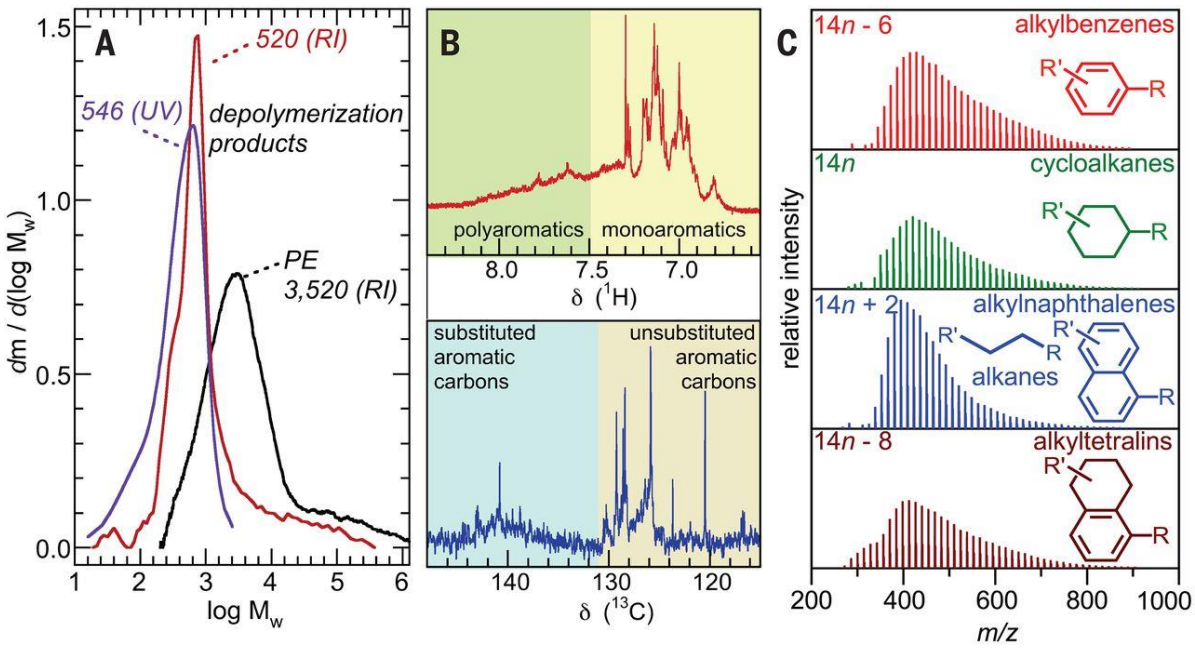

Figure 2.3 Analysis of the liquid hydrocarbon fraction from the solvent-free catalytic conversion of polyethylene. Sample had M_w = 3.52 × 10^3 g/mol and was heated for 24 hours at 280°C (Fig. 2.2B, experiment 3). (A) GPC analysis, conducted using both RI and UV detectors. (B) ^{1}H and ^{13}C NMR spectra, recorded in deuterated TCE. (C) FD-MS analysis.

The high yield of liquid alkylaromatics was particularly promising; such compounds find widespread application as surfactants, lubricants, refrigeration fluids, and insulating oils,[25] and their manufacture from waste polyethylene could displace fossil fuel–based routes. The ^{1}H NMR spectrum reveals more information about the alkyl substituents (Fig. A.8A). Protons associated with an aliphatic carbon directly bonded to an aromatic ring (C_α) resonate in the region 2 to 4 ppm. The overall ratio $H_\alpha/H_{aromatic}$ = 1.1 indicates that the major species are, on average, dialkylaromatics (figs. A.7 and A.8A). This finding is consistent with a previous report in which dialkylbenzenes were the major products of catalytic aromatization of lighter

n-alkanes (C_6 to C_{12}),[26] and with their proposed mechanism of formation by dehydrocyclization of polyethylene (Fig. 2.4).

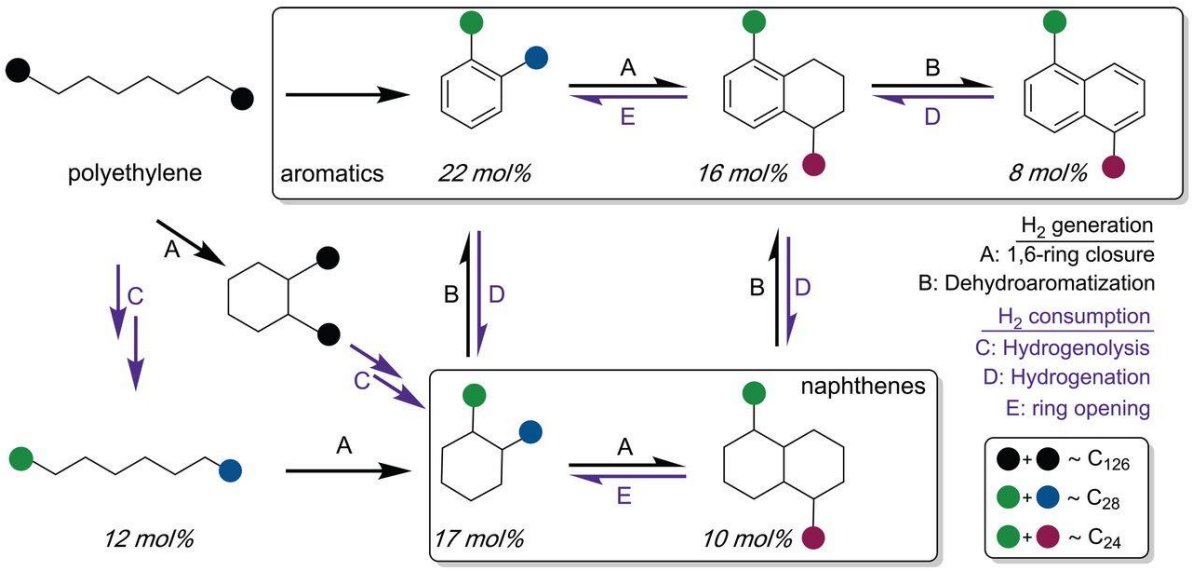

Figure 2.4 Overall PE conversion to alkylaromatics and alkylnaphthenes, and proposed mechanism of tandem polyethylene hydrogenolysis/aromatization via dehydrocyclization. Yields of each product were estimated using a combination of ^{1}H NMR and FD-MS analysis (see supplementary materials and tables A.2 and A.4).

Combining this information with the overall fraction of aromatic protons (0.037) and the average carbon number (C_{34} for this experiment, based on the M_n value determined by GPC), we estimate the overall alkylaromatic selectivity in the liquid fraction to be 57 ± 5 mol%, of which ~40 mol% is monoaromatic (Table A.3, experiment 3). Using the aromatic carbon fraction (0.10 according to ^{13}C NMR; fig. A.8B) instead results in a similar estimate for the alkylaromatic selectivity, 52 ± 4 mol%. Furthermore, many of the alkyl substituents are unbranched at the C_α position, judging by the intense ^{1}H signals at 2.35 to 2.85 ppm. The

paraffinic -CH_2-/-CH_3 ratio, 7.5, suggests that each alkyl substituent possesses, on average, < 1 branch point.

Individual molecular components in the liquid fraction were identified using field desorption–mass spectrometry (FD-MS; fig. A.9). Each mass series shows a log-normal distribution with a maximum intensity at ~C_{30} (fig. A.10). The most abundant products are the alkylbenzene series (14n – 6, ~22 mol %), as shown in Fig. 2.3C. Saturated alkanes and alkylnaphthalenes share the same mass profile (14n + 2, 20 mol%) and are the next most abundant group, with smaller amounts of alkyltetralins (14n – 8, 16 mol%) and alkylnaphthenes (i.e., alkylcycloalkanes; 14n, 17 mol%). Alkylnaphthalenes presumably arise by further dehydrocyclization of alkylbenzenes (Fig. 2.4).[27] Minor aromatic products include polyaromatics such as alkylanthracenes and alkylphenanthrenes (14n – 4, 7 mol%) and their partially hydrogenated analogs (14n – 10, 8 mol%). According to FD-MS, the selectivity for mono- aromatic products (including both alkylbenzenes and alkyltetralins) is ~40 mol%, consistent with the ^{1}H NMR analysis described above. The alkylnaphthene products, which have intrinsic value as solvents and hydrogen donors,[28] could be further dehydrogenated to alkylaromatics by active control of the partial pressure of H_2 in the reactor. The total yield of cyclic products (both alkylaromatics and alkylnaphthenes) in the liquid products is 88 mol% (Table A.4).

When the reaction time was extended from 24 to 36 hours at 280 °C, similar products were formed (Table A.3, experiment S1), although the molecular weight distributions of both liquid and wax fractions shifted to slightly lower values (Fig. A.11) and the dispersity decreased further (to $Đ$ = 1.06). At the same time, the alkylaromatic selectivity increased (24 hours, 52 and 71 mol%, respectively, in the liquid and wax fractions; 36 hours, 70 and 88

mol%, respectively) (Table A.3). Alkylaromatic yields were also strongly temperature-dependent. After 24 hours at a lower temperature (250 °C), the $CHCl_3$-soluble hydrocarbons (13 wt%) showed a smaller extent of depolymerization (M_w = 1.8 × 10^3 g/mol, $Đ$ = 2.11) and negligible aromatic content; most PE was simply not converted. At a higher reaction temperature (330 °C), the polymer was largely converted in 24 hours; however, the major products (77 wt%) were gases and volatile hydrocarbons. The yield of $CHCl_3$-soluble hydrocarbons was low (~10 wt%), although the overall yield of aromatics was higher ($H_{aromatic}/H_{total}$ = 0.38), with more polyaromatics (H_{mono}/H_{poly} = 0.25). The optimum temperature for alkylbenzene formation is therefore 250 °C < T < 330 °C.

The time course of PE depolymerization was studied at 280 °C (Table A.5, experiments 1a to 1g). A short induction period, lasting about 1 hour, corresponds in large part to the time required for thermal equilibration of the reactor (~0.75 hours). After this time, the liquid hydrocarbon fraction increased (Fig. 2.5A) as M_n decreased, eventually approaching a plateau at 315 g/mol after ~6 hours (Fig. 2.5B). The dispersity $Đ$ increased initially from 1.94 to 2.36, then decreased to stabilize at 1.31. The alkylaromatic yield also changed appreciably over the course of the reaction. After 3 hours, aromatic protons represented <1% of all protons, mainly associated with alkyl- benzenes (Fig. 2.5, C and D). At longer reaction times, the aromatic fraction and the yield of alkylnaphthalenes increased (Table A.5).

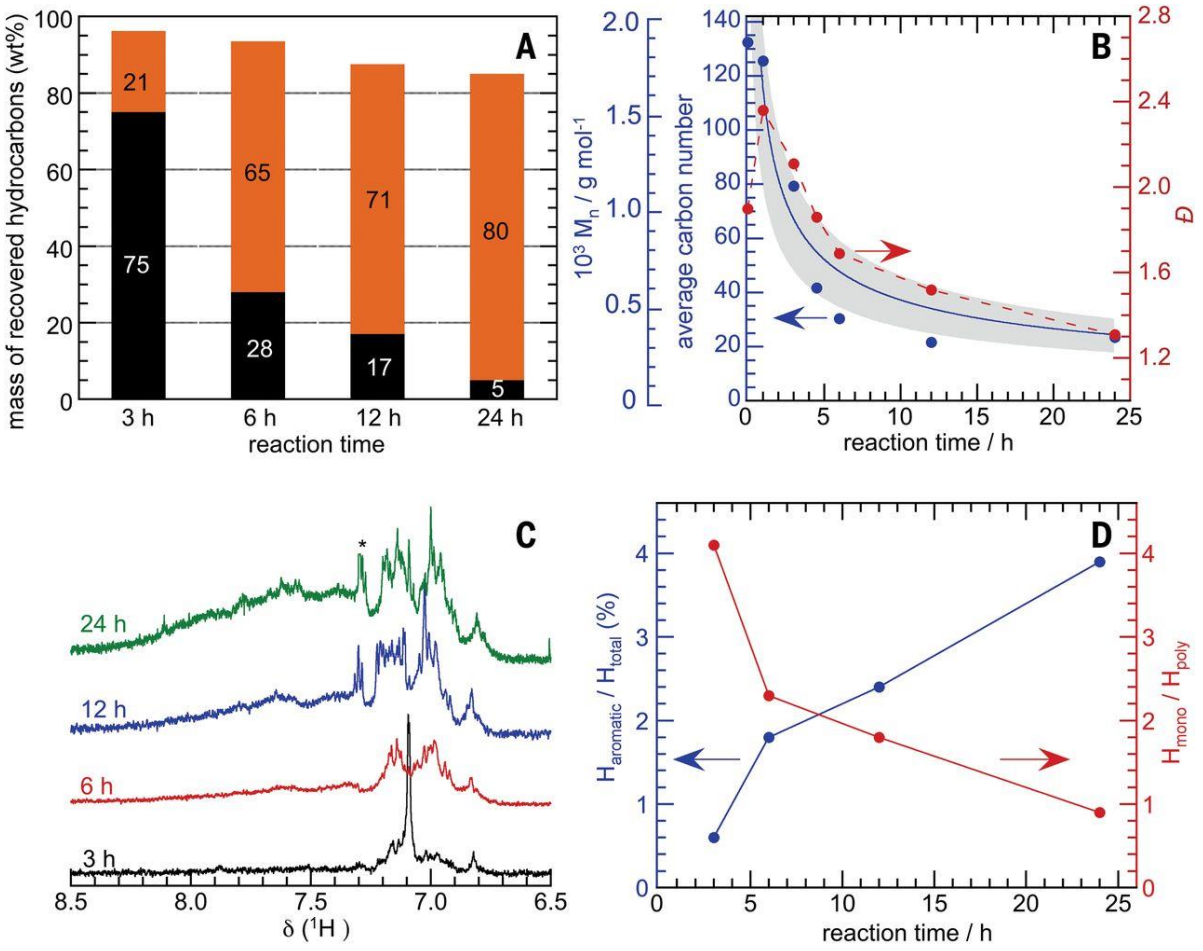

Figure 2.5 Time course of the solvent-free disassembly of polyethylene (M_n = 1.85 × 10^3 g/mol; $Đ$ = 1.90) catalyzed by Pt/γ-Al_2O_3 in an unstirred mini-autoclave reactor at 280°C. (A) Evolution of major product fractions (orange, $CHCl_3$-soluble liquids/waxes; black, insoluble hydrocarbons). (B) Overall molecular weight (M_n, blue) and dispersity ($Đ$, red) for all non-gas hydrocarbons. The red dashed line is present only to guide the eye. The curve fit (solid blue line) shows the refinement of Eq. 2.3 to the M_n data. Initial conditions: total carbon n_C = 8.4 mmol; number of polymer chains N_0 = 68 μmol; total Pt m_{Pt} = 3 × 10^{-3} g; selectivity for aromatization versus hydrogenolysis, s = 1/2 (eq. A.22). The shaded region indicates the 95% confidence bands for the model fit. Each independent measurement, which may diverge from the fit because of measurement error, has a 95% confidence interval that represents the mean

of many measurements. The set of confidence intervals at all reaction times represents the confidence bands in which the true fit, given the form in Eq. 2.3, lies. Because the fit and its confidence bands predict the mean of many measurements at a given reaction time, individual measurements can lie outside these bands. (C) Time course of the ^{1}H NMR spectra of the liquid/wax fraction in the aromatic region. The asterisk indicates a truncated residual solvent signal. (D) The fraction of aromatic protons and the ratio of mono- to polyaromatic protons.

We also assessed the thermodynamics of *n*-alkane aromatization. The temperature needed to achieve appreciable aromatic yields for this endothermic reaction (Eq. 2.1) decreases as the molecular weight increases.[29]

$$C_mH_{2m+2} \rightarrow C_mH_{2m-6} + 4\ H_2 \qquad \text{(eq 2.1)}$$

Nonetheless, direct PE conversion to aromatics appears to require particularly mild conditions relative to the much higher operating temperatures generally required for making BTX from molecular *n*-alkanes (Fig. 2.1). Thermodynamic values for converting linear PE chains to alkylaromatics at 280 °C in 1 atm H_2, estimated using Benson group contributions for long-chain *n*-alkanes,[30] are $\Delta H_1° = 246$ kJ/mol and $\Delta G_1° = 31$ kJ/mol. Thus, aromatization alone is indeed disfavored. However, the reaction occurs in tandem with hydrogenation of a suitable hydrogen acceptor. In solvent-less PE depolymerization, the PE chains themselves serve as an internal hydrogen sink (Fig. 2.4). Using Benson group contributions again, the estimated thermodynamic values for C-C bond hydrogenolysis (Eq. 2.2) are $\Delta H_2^o = -49$ kJ/mol and $\Delta G_2^o = -74$ kJ/mol.

$$C_{m+n}H_{2(m+n)+2} + H_2 \rightarrow C_mH_{2m+2} + C_nH_{2n+2} \quad \text{(eq 2.2)}$$

Consequently, aromatization becomes favorable at 280 °C ($\Delta G° = 0$) when even 10% of the H_2 generated is consumed in PE hydrogenolysis. On the basis of alkylaromatic yield, the aromatization in experiment 2 of Fig. 2.2B generated 0.50 mmol H_2. More than 90% of this H_2 (0.47 mmol) was consumed in reducing the molecular weight of the polymer via hydrogenolysis, making the tandem process thermo-dynamically favorable. However, the residual H_2 found in the reactor headspace at the end of the reaction (0.11 mmol) exceeds the expected value (0.03 mmol). Therefore, a significant amount of H_2 is generated in other reactions, such as PE dehydrocyclization to give cycloalkanes and tetralins. Both were observed by FD-MS (see above). Indeed, their yields are higher than the thermodynamic predictions, which favor aromatics. We observed that some of these more saturated compounds condense outside the autoclave's heated zone where the catalyst is located, thereby preventing their further dehydrogenation.

To explore whether polyethylene is necessary to produce long-chain alkylaromatics by tandem catalytic hydrogenolysis/aromatization, we investigated the reaction of *n*-$C_{30}H_{62}$ under the same conditions (Table A.6, experiments S2 and S3). Compared to PE, the *n*-$C_{30}H_{62}$ chains experience only half as much hydrogenolysis (consuming just 0.25 mmol H_2 according to Fig. A.12), as expected on the basis of the chain length dependence of hydrogenolysis kinetics.[31] Molecules in the liquid products have an average chain length of C_{20}, with low alkylaromatic content (~10 mol%). Because hydrogenolysis and aromatization occur in tandem, they must occur together. Consequently, the formation of alkylaromatics is greatly enhanced by the use of polyethylene as a feedstock.

Although there are far too many individual reactions and products to formulate a precise kinetic model, a simplified model captures the main features of the tandem reaction. We assume that the Pt surface is covered with molten PE and/or PE-derived hydrocarbons at all times, and that the hydrogenolysis turnover frequency is constant on sites not occupied by aromatic hydrocarbons. As the latter form, they adsorb more strongly than alkanes,[32] occupying active sites and reducing the hydrogenolysis rate accordingly. We also assume that hydrogenolysis is random (i.e., all aliphatic C-C bonds are equally likely to be cleaved).[33] The sole adjustable parameter, *k/K*, is the ratio of the rate constant for hydrogenolysis (*k*) and the equilibrium constant for competitive adsorption of aromatics and aliphatic chains (*K*) (eq. A.14). Equation 2.3 predicts the evolution of the average chain length as a function of the reaction time, initial total carbon amount n_C, and total platinum mass m_{Pt}.

$$\ln\left(1-\frac{3}{M_n(t)}+\frac{3}{M_n(0)}\right)+\left(\frac{3}{M_n(t)}-\frac{3}{M_n(0)}\right)=-\frac{k}{K}\frac{m_{Pt}}{n_C}t \qquad \text{(eq 2.3)}$$

The curve fit of Eq. 3 to an experimental dataset is shown in Fig. 2.5B, starting with the data point at t = 1 hour (i.e., after the induction period caused by reactor heating). Assuming a preferential binding for aromatics of $K = 3.2 \times 10^6$,[32] the hydrogenolysis rate constant k is estimated to be 6.4×10^2 $mol_{C\text{-}C}$ bonds h^{-1} per g_{Pt} at 280 °C.

The stability of the Pt/γ–Al_2O_3 catalyst was investigated by conducting three consecutive 6-hour reactions (to ensure much less than full conversion), with regeneration of the recovered catalyst between each experiment (see Appendix A). The liquid/wax yield decreased by 15 wt% in the second run but stabilized in the third run (Table A.6, experiments S4 to S6, and Fig. A.13). The activity decrease between the first and second runs was

comparable to the decrease in the active Pt surface area measured by CO chemisorption, with no notable change between the second and third runs (Table A6, experiments S4 to S6). Thus, the intrinsic activity of the catalyst (turnover frequency) appears to be unchanged. The average carbon number of the liquid/wax product increased between the first and second 6-hour runs (as expected because of the lower extent of depolymerization), then stabilized in the third run. Transmission electron microscopy analysis of a catalyst used for 24 hours and regenerated by calcination showed that the Pt nano- particles increased in size slightly, from 0.8 to 1.2 nm (Fig. A.1, C and D). In a preliminary scale-up attempt, the amount of PE was increased by nearly a factor of 10 (to 1.1 g) while maintaining the same PE:Pt ratio and reaction conditions. After 24 hours, 0.56 g of a liquid product (M_w = 483 g/mol, $Đ$ = 1.29) with 27 mol% aromatic content was obtained (Table A.6, experiment S7).

To investigate how a tandem catalytic process could be deployed to convert waste polyethylene without large energy input, we also performed solvent-free depolymerization of two different commercial grades of PE: an LDPE plastic bag ($M_w = 9.45 \times 10^4$ g/mol, $Đ$ = 7.37) and an HDPE water-bottle cap ($M_w = 5.35 \times 10^4$ g/mol, $Đ = 3.61$). These higher molecular weight polymers behaved similarly to the lower molecular weight polyethylene, giving liquid/wax products with an average carbon number of ~C_{30}. After 24 hours at 280 °C, the overall liquid yields were 69 and 55 wt% for LDPE and HDPE, respectively (Fig. 2.2B, experiments 4 and 5), with alkylaromatic selectivities of ~44 and 50 mol% (Table A3, experiments 4 and 5). Thus, the extent of depolymerization is slightly lower in the same reaction time. For these higher-molecular-weight polyethylenes, the batch process generates its own highly viscous solvent as depolymerization proceeds. Recycling some of the alkylaromatic liquids to serve as solvent for the next batch may accelerate the reaction by

facilitating mass and heat transport. The similar results for three very different plastics (including two commercial- grade samples of LDPE and HDPE) suggest that density, degree of branching, and common processing impurities are not major issues.

2.4 Conclusion

Shorter residence times should also improve the selectivity for monoaromatic hydrocarbons relative to naphthalenes, etc., and suppress the already low gas yields even further. Alkylbenzene selectivity may be further improved by active control of the partial pressure of H_2, which must be high enough to promote PE hydrogenolysis but low enough to suppress aromatic hydrogenation. Catalyst improvements in these directions will be necessary to make the tandem reaction compatible with continuous processing and, ultimately, economically viable. The alkylbenzenes with their linear side chains could be sulfonated to produce biodegradable surfactants, which are interesting as higher-value chemical products. This type of commodity polymer upcycling can result in displacement of fossil carbon–based feedstocks, while simultaneously incentivizing better management of plastic waste and recovering considerable material value that can be recirculated into the global economy.

2.5 Acknowledgements

Funding: Supported by award DE-AC-02-07CH11358 from the U.S. Department of Energy, Office of Basic Energy Sciences, Division of Chemical Sciences, Geosciences, and Biosciences, as a subcontract from Ames Laboratory. Some experiments were performed using the MRL Shared Experimental Facilities, supported by the MRSEC Program of the NSF under

award DMR 1720256, a member of the NSF-funded Materials Research Facilities Network (www.mrfn.org).

2.6 References

(1) Geyer, R.; Jambeck, J. R.; Law, K. L. Production, Use, and Fate of All Plastics Ever Made. *Sci. Adv.* **2017**, *3* (7), e1700782. https://doi.org/10.1126/sciadv.1700782.

(2) Lebreton, L.; Andrady, A. Future Scenarios of Global Plastic Waste Generation and Disposal. *Palgrave Commun* **2019**, *5* (1), 6. https://doi.org/10.1057/s41599-018-0212-7.

(3) Eriksson, O.; Finnveden, G. Plastic Waste as a Fuel - CO2-Neutral or Not? *Energy Environ. Sci.* **2009**, *2* (9), 907. https://doi.org/10.1039/b908135f.

(4) Jambeck, J. R.; Geyer, R.; Wilcox, C.; Siegler, T. R.; Perryman, M.; Andrady, A.; Narayan, R.; Law, K. L. Plastic Waste Inputs from Land into the Ocean. *Science* **2015**, *347* (6223), 768–771. https://doi.org/10.1126/science.1260352.

(5) Chamas, A.; Moon, H.; Zheng, J.; Qiu, Y.; Tabassum, T.; Jang, J. H.; Abu-Omar, M.; Scott, S. L.; Suh, S. Degradation Rates of Plastics in the Environment. *ACS Sustainable Chem. Eng.* **2020**, *8* (9), 3494–3511. https://doi.org/10.1021/acssuschemeng.9b06635.

(6) Rahimi, A.; García, J. M. Chemical Recycling of Waste Plastics for New Materials Production. *Nat Rev Chem* **2017**, *1* (6), 0046. https://doi.org/10.1038/s41570-017-0046.

(7) Zhu, Y.; Romain, C.; Williams, C. K. Sustainable Polymers from Renewable Resources. *Nature* **2016**, *540* (7633), 354–362. https://doi.org/10.1038/nature21001.

(8) Vollmer, I.; Jenks, M. J. F.; Roelands, M. C. P.; White, R. J.; Harmelen, T.; Wild, P.; Laan, G. P.; Meirer, F.; Keurentjes, J. T. F.; Weckhuysen, B. M. Beyond Mechanical

Recycling: Giving New Life to Plastic Waste. *Angew. Chem. Int. Ed.* **2020**, *59* (36), 15402–15423. https://doi.org/10.1002/anie.201915651.

(9) Ignatyev, I. A.; Thielemans, W.; Vander Beke, B. Recycling of Polymers: A Review. *ChemSusChem* **2014**, *7* (6), 1579–1593. https://doi.org/10.1002/cssc.201300898.

(10) Anuar Sharuddin, S. D.; Abnisa, F.; Wan Daud, W. M. A.; Aroua, M. K. A Review on Pyrolysis of Plastic Wastes. *Energy Conversion and Management* **2016**, *115*, 308–326. https://doi.org/10.1016/j.enconman.2016.02.037.

(11) Dufaud, V.; Basset, J.-M. Catalytic Hydrogenolysis at Low Temperature and Pressure of Polyethylene and Polypropylene to Diesels or Lower Alkanes by a Zirconium Hydride Supported on Silica-Alumina: A Step Toward Polyolefin Degradation by the Microscopic Reverse of Ziegler-Natta Polymerization. *Angew Chem Int Ed Engl* **1998**, *37* (6), 806–810. https://doi.org/10.1002/(SICI)1521-3773(19980403)37:6<806::AID-ANIE806>3.0.CO;2-6.

(12) Celik, G.; Kennedy, R. M.; Hackler, R. A.; Ferrandon, M.; Tennakoon, A.; Patnaik, S.; LaPointe, A. M.; Ammal, S. C.; Heyden, A.; Perras, F. A.; Pruski, M.; Scott, S. L.; Poeppelmeier, K. R.; Sadow, A. D.; Delferro, M. Upcycling Single-Use Polyethylene into High-Quality Liquid Products. *ACS Cent. Sci.* **2019**, *5* (11), 1795–1803. https://doi.org/10.1021/acscentsci.9b00722.

(13) Jia, X.; Qin, C.; Friedberger, T.; Guan, Z.; Huang, Z. Efficient and Selective Degradation of Polyethylenes into Liquid Fuels and Waxes under Mild Conditions. *Sci. Adv.* **2016**, *2* (6), e1501591. https://doi.org/10.1126/sciadv.1501591.

(14) Rahimpour, M. R.; Jafari, M.; Iranshahi, D. Progress in Catalytic Naphtha Reforming Process: A Review. *Applied Energy* **2013**, *109*, 79–93. https://doi.org/10.1016/j.apenergy.2013.03.080.

(15) Perego, C.; Ingallina, P. Recent Advances in the Industrial Alkylation of Aromatics: New Catalysts and New Processes. *Catalysis Today* **2002**, *73* (1–2), 3–22. https://doi.org/10.1016/S0920-5861(01)00511-9.

(16) *Natural Gas Processing from Midstream to Downstream*, First edition.; Elbashir, N. O. M., El-Halwagi, M. M., Economou, I. G., Hall, K. R., Eds.; John Wiley & Sons: Hoboken, NJ, 2019.

(17) Yarulina, I.; Chowdhury, A. D.; Meirer, F.; Weckhuysen, B. M.; Gascon, J. Recent Trends and Fundamental Insights in the Methanol-to-Hydrocarbons Process. *Nat Catal* **2018**, *1* (6), 398–411. https://doi.org/10.1038/s41929-018-0078-5.

(18) Cheng, K.; Zhou, W.; Kang, J.; He, S.; Shi, S.; Zhang, Q.; Pan, Y.; Wen, W.; Wang, Y. Bifunctional Catalysts for One-Step Conversion of Syngas into Aromatics with Excellent Selectivity and Stability. *Chem* **2017**, *3* (2), 334–347. https://doi.org/10.1016/j.chempr.2017.05.007.

(19) Wang, Q.-N.; Weng, X.-F.; Zhou, B.-C.; Lv, S.-P.; Miao, S.; Zhang, D.; Han, Y.; Scott, S. L.; Schüth, F.; Lu, A.-H. Direct, Selective Production of Aromatic Alcohols from Ethanol Using a Tailored Bifunctional Cobalt–Hydroxyapatite Catalyst. *ACS Catal.* **2019**, *9* (8), 7204–7216. https://doi.org/10.1021/acscatal.9b02566.

(20) Maneffa, A.; Priecel, P.; Lopez-Sanchez, J. A. Biomass-Derived Renewable Aromatics: Selective Routes and Outlook for *p* -Xylene Commercialisation. *ChemSusChem* **2016**, *9* (19), 2736–2748. https://doi.org/10.1002/cssc.201600605.

(21) Williams, C. L.; Chang, C.-C.; Do, P.; Nikbin, N.; Caratzoulas, S.; Vlachos, D. G.; Lobo, R. F.; Fan, W.; Dauenhauer, P. J. Cycloaddition of Biomass-Derived Furans for Catalytic Production of Renewable *p* -Xylene. *ACS Catal.* **2012**, *2* (6), 935–939. https://doi.org/10.1021/cs300011a.

(22) Lopez, G.; Artetxe, M.; Amutio, M.; Bilbao, J.; Olazar, M. Thermochemical Routes for the Valorization of Waste Polyolefinic Plastics to Produce Fuels and Chemicals. A Review. *Renewable and Sustainable Energy Reviews* **2017**, *73*, 346–368. https://doi.org/10.1016/j.rser.2017.01.142.

(23) Inaba, A.; Kashiwagi, T. A Calculation of Thermal Degradation Initiated by Random Scission. 1. Steady-State Radical Concentration. *Macromolecules* **1986**, *19* (9), 2412–2419. https://doi.org/10.1021/ma00163a014.

(24) Occelli, M. L. *Fluid Catalytic Cracking VII: Materials, Methods and Process Innovations.*; Elsevier Science: Amsterdam, 2011.

(25) *Synthetics, Mineral Oils, and Bio-Based Lubricants: Chemistry and Technology*, Third edition.; Rudnick, L. R., Ed.; Chemical industries; CRC Press, Taylor & Francis Group: Boca Raton London New York, 2020.

(26) Ahuja, R.; Punji, B.; Findlater, M.; Supplee, C.; Schinski, W.; Brookhart, M.; Goldman, A. S. Catalytic Dehydroaromatization of N-Alkanes by Pincer-Ligated Iridium Complexes. *Nature Chem* **2011**, *3* (2), 167–171. https://doi.org/10.1038/nchem.946.

(27) Mostad, H. B.; Riis, T. U.; Ellestad, O. H. Catalytic Cracking of Naphthenes and Naphtheno-Aromatics in Fixed Bed Micro Reactors. *Applied Catalysis* **1990**, *63* (1), 345–364. https://doi.org/10.1016/S0166-9834(00)81724-8.

(28) Zhu, Q.-L.; Xu, Q. Liquid Organic and Inorganic Chemical Hydrides for High-Capacity Hydrogen Storage. *Energy Environ. Sci.* **2015**, *8* (2), 478–512. https://doi.org/10.1039/C4EE03690E.

(29) Pradhan, S.; Lloyd, R.; Bartley, J. K.; Bethell, D.; Golunski, S.; Jenkins, R. L.; Hutchings, G. J. Multi-Functionality of Ga/ZSM-5 Catalysts during Anaerobic and Aerobic Aromatisation of n-Decane. *Chem. Sci.* **2012**, *3* (10), 2958. https://doi.org/10.1039/c2sc20683h.

(30) Linstrom, P. NIST Chemistry WebBook, NIST Standard Reference Database 69, 1997. https://doi.org/10.18434/T4D303.

(31) Flaherty, D. W.; Iglesia, E. Transition-State Enthalpy and Entropy Effects on Reactivity and Selectivity in Hydrogenolysis of *n* -Alkanes. *J. Am. Chem. Soc.* **2013**, *135* (49), 18586–18599. https://doi.org/10.1021/ja4093743.

(32) Xu, C.; Tsai, Y. L.; Koel, B. E. Adsorption of Cyclohexane and Benzene on Ordered Tin/Platinum (111) Surface Alloys. *J. Phys. Chem.* **1994**, *98* (2), 585–593. https://doi.org/10.1021/j100053a038.

(33) Carter, J. Hydrogenolysis of N-Heptane over Unsupported Metals. *Journal of Catalysis* **1971**, *20* (2), 223–229. https://doi.org/10.1016/0021-9517(71)90083-2.

Chapter 3. Chemical Upcycling of Polyethylene to Value-Added α,ω-Divinyl-Functionalized Oligomers

***** *This chapter was reproduced from the following publication. The author of this Ph. D. thesis, Manhao Zeng, is the leading author of this publication who contributed to all parts relevant to this work.*

Zeng, M.; Lee, Y.-H.; Strong, G.; LaPointe, A. M.; Kocen, A. L.; Qu, Z.; Coates, G. W.; Scott, S. L.; Abu-Omar, M. M. Chemical Upcycling of Polyethylene to Value-Added α,ω-Divinyl-Functionalized Oligomers. *ACS Sustainable Chem. Eng.* **2021**, *9* (41), 13926–13936. https://doi.org/10.1021/acssuschemeng.1c05272.

3.1 Abstract

Today, only 9% of plastic waste is recycled worldwide, with polyethylene being one of the most frequently discarded plastics. In this work, a new route to chemically recycle polyethylene is demonstrated. Polyethylenes of two different molecular weights (M_n=1.5 kg/mol and M_n=6.6 kg/mol) were upgraded to value-added α,ω-divinyl-functionalized oligomers with shorter, tunable chain lengths via a sequence of bromination, dehydrobromination, and olefin metathesis reactions. Brominated polyethylene (BPE) was isolated in good yields (up to 86 wt%, based on PE) by direct bromination of polyethylene in air, without oxidative cleavage side-reactions. Elimination of bromide resulted in complete conversion of BPE to vinylene polyethylene (VPE) in high yields (up to 91 wt%, based on BPE). Ethenolysis of VPE afforded α,ω-divinyl-functionalized oligomers, also in high yields

(up to 97 wt%, based on VPE), with carbon numbers significantly lower than those of the starting PE. Preliminary technoeconomic analyses demonstrate that this three-step process could be economically viable on an industrial scale for upcycling PE into value-added chemicals that can be used in the synthesis of lubricants, as well as transformed into new commodity polymers such as polyolefins, polyethers, polyesters, and polyamides.

3.2 Introduction

Since the invention of synthetic plastics in the early 20th century, their use has become prevalent in diverse applications such as packaging, electronics, and textiles. Consequently, plastic production has risen dramatically, from 2 million metric tons in 1950 to 380 million metric tons in 2015.[1] The latter quantity is projected to double by 2034.[2] As the most common application of plastics, single-use packaging provides many benefits to society because of its durability and low weight, but after a short life-cycle (on average, less than one year), most of these materials end up in landfills.[1] Since only 9% of plastic waste undergoes recycling worldwide,[1] the discarded materials contribute to persistent environmental pollution[3,4] and leach contaminants that poison wildlife.[5] Recycling is an alternative to the single use of these materials. Because of the rising demand for plastic, developing effective recycling methods has become a worldwide concern. Mechanical recycling is a simple approach,[2] but there is little economic incentive for it because it results in downcycling.[6] Generally, mechanically recycled plastics have inferior physical properties relative to virgin materials, thus restricting their use to lower-value applications.[2,7,8]

Thermal and catalytic pyrolysis are alternatives that allow for chemical recycling of plastics, by deconstructing the organic materials at elevated temperatures (> 400 °C) in an

oxygen-free environment. Thermal pyrolysis is unselective, producing a low-value mixture of liquid and gas hydrocarbons of varying chain length as well as non-volatile char.[9] The addition of a catalyst such as HZSM-5 zeolite decreases the temperature required for pyrolysis,[10] but the coke generated from this process quickly reduces catalyst efficiency and increases cost.[9] Milder, more selective alternatives to pyrolysis have been reported to convert polyethylene to saturated liquid hydrocarbons,[11] which are suitable for use as fuels or lubricants.[12,13] Oxidative conversion of PE is reported to give small molecule dicarboxylic acids, although the yields of these functionalized products were low.[14] Nevertheless, chemical recycling presents a unique opportunity to extract value from post-consumer plastic waste.

Previously, we demonstrated that polyethylene can be upgraded to valuable alkylaromatics that can be precursors to detergents.[15] In this work, we report on the chemical upcycling of PE via a three-step process involving bromination, dehydrobromination, and olefin metathesis (Scheme 3.1). The resulting α,ω-divinyl-functionalized oligomers have a variety of potential value-added uses, including serving as monomers in the syntheses of poly-α-olefin lubricants, polyolefins, polyethers, polyesters, and polyamides.[16-17] By tuning the degree of bromination, we demonstrate that PE can be converted selectively to α,ω-divinyl-functionalized oligomers of various chain lengths. The HBr (and, if necessary, KBr) by-products can, in principle, be recycled by oxidation to regenerate Br_2,[18–25] in processes that have already been demonstrated at scale.[24,25] A preliminary techno-economic assessment (TEA) suggests that the process in Scheme 3.1 could be profitable on an industrial scale.

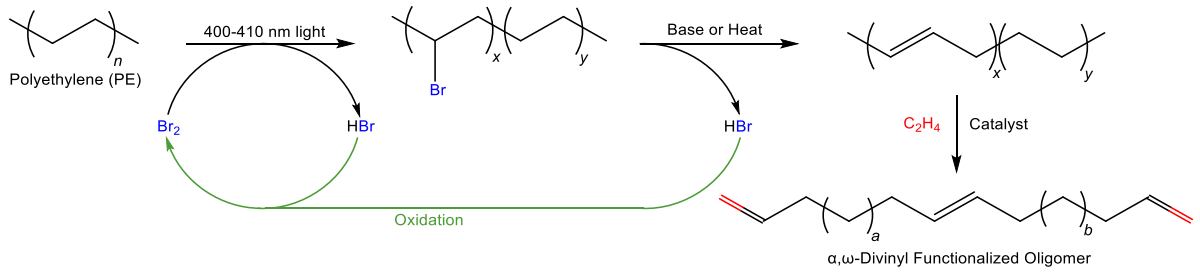

Scheme 3.1 Strategy for PE upcycling to value-added α,ω-divinyl-functionalized oligomers, as described in this work.

3.3 Results and Discussion

Bromination of Polyethylene (PE). Alkane C-H bonds are readily halogenated via free-radical substitution.[26–28] PE, a saturated polymer with a -CH_2CH_2- repeat group, can be brominated using 400-410 nm light to initiate the reaction with Br_2, in the presence of a solvent such as benzene which dissolves the PE but which does not undergo free-radical substitution itself under these conditions. Here, two different samples of PE with M_n = 1.5 kg/mol ($Đ$ = 2.2) and M_n = 6.6 kg/mol ($Đ$ = 3.8) were used to incorporate different quantities of bromine by varying the amounts of Br_2 added. The brominated PEs (BPE) were subsequently isolated by precipitation with methanol.

All BPEs made by this route have lower C, H contents by weight and display higher M_n values in comparison to the starting PE (Figs. A.1 and A.2), as expected due to the incorporation of bromine (Table 3.1). The reaction efficiencies (defined as [non-C+H wt% / expected Br wt%, based on the quantity of Br_2 added] × 100%) are high (up to 94 mol%), indicating that most of the added Br_2 reacts with the polymer. The higher molecular weight PE (i.e., with fewer polymer chains on molar basis) shows a lower bromination efficiency than the lower molecular weight PE. This observation suggests that PE bromination becomes

increasingly difficult as the degree of bromination increases and is consistent with a previous report that free-radical bromination of short-chain alkanes is more selective for mono- vs. polybromination.[29]

Table 3.1 Efficiency of PE bromination to give BPE

Starting PE				BPE Product						
Entry[a]	M_n (kg/mol)	$Đ$	(C+H)[b] (wt%)	Entry[a]	mol Br_2 : mol C_2H_4[c]	M_n (kg/mol)	$Đ$	(C+H)[d] (wt%)	Efficiency[e] (%)	Isolated Yield (%)
PE-1	1.5	2.2	99	BPE-1	1 : 5	4.4	2.1	68	88	83
				BPE-2	1 : 10	3.8	2.0	79	94	85
PE-2	6.6	3.8	98	BPE-3	1 : 5	15	4.2	72	77	86

[a] Starting polymer: PE-1 for BPE-1 and BPE-2; PE-2 for BPE-3. [b] Determined by elemental analysis to show starting polymer composition is C+H exclusively. [c] Ratio of Br_2 added per ethylene monomer. [d] Determined by elemental analysis. [e] Calculated as [(100 – [C+H wt%]) / Expected Br wt%] × 100 %. Expected Br content is based on the quantity of Br_2 added.

BPE-3 has a bromine content of 28 wt%, and an organic (C+H) content of 72 wt%, indicating that PE bromination in air occurred without significant oxidative side-reactions. This is an advantage of our procedure relative to previous work, in which oxygen-containing functional groups such as alcohols and carboxylic acids were reported to form during bromination of PE.[26,30,31] The HBr produced during the synthesis of BPE-3 was recovered as AgBr by bubbling through a solution of $AgNO_3$. The AgBr mass accounts for 91% of the expected HBr yield. Thus HBr can be recovered in high yield for the purpose of regenerating Br_2.[25]

Compared to ^{1}H NMR spectrum of the starting PE (Fig. A.3), the spectrum of BPE contains new signals at 3.6-5.2 ppm and 1.8 ppm (Fig. 3.1a) corresponding to protons located α and β to brominated carbons, respectively. The ^{13}C NMR spectrum contains characteristic signals at 59 and 39 ppm (Fig. 3.1b) that represent the α and β carbons, respectively.[27] These spectra provide clear evidence of successful bromination. According to 2D ^{1}H-^{13}C HSQC analysis of BPE (Fig. A.4), the α signals correspond to an odd number of protons, most likely -CHBr- (since CH_3Br, a volatile molecule, would have been removed during workup). While free-radical reactions may result in polymer chain scission,[32] the absence of -CH_2Br end groups suggests that the structural integrity of the polymer is retained during the synthesis of BPE, which is important for controlled modification of PE. Solution bromination as performed here therefore also has an advantage over previous reports in which bromination of the surfaces of PE films by Br_2 gas under UV light resulted in significant C-C bond cleavage.[26,30] In comparison to the IR spectra of PE, the BPE polymers also show new IR bands at 537 and 613 cm^{-1} that represent C-Br stretching modes (Figs. A.5 and A.6),[26,28] further confirming the incorporation of Br directly into the structure of BPE.

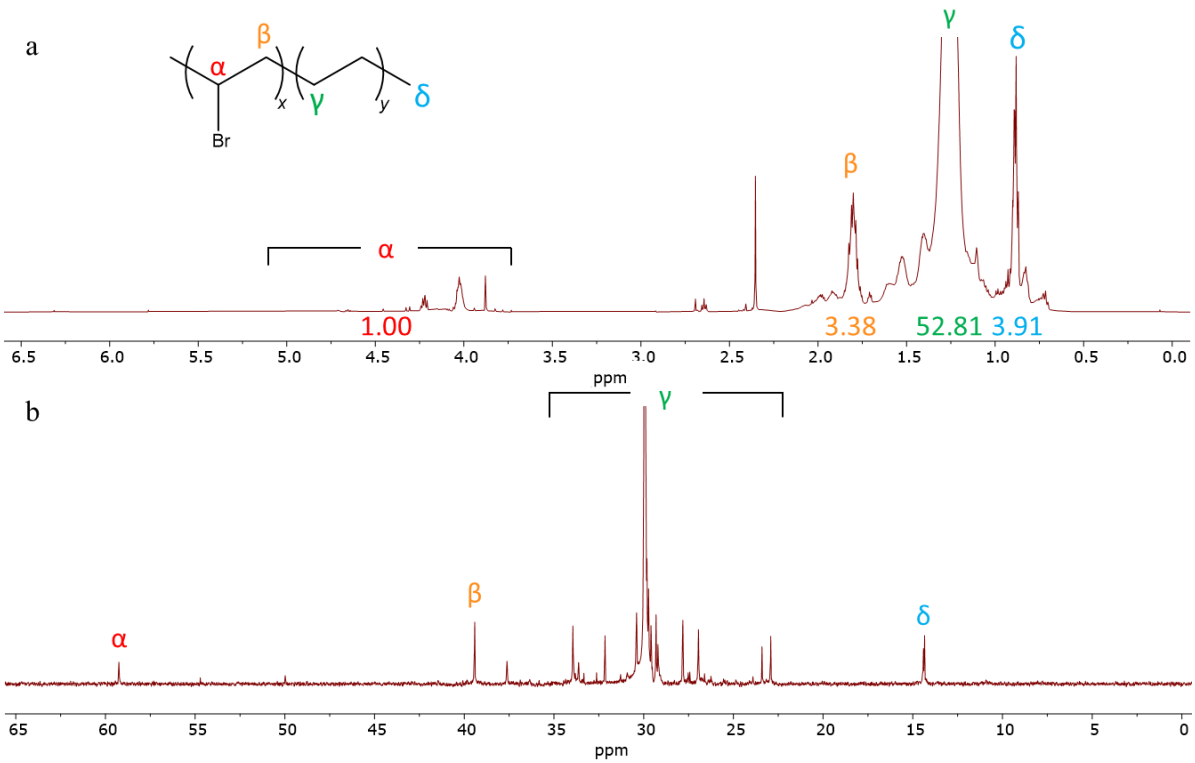

Figure 3.1 NMR spectra of BPE-2: (a) ^{1}H NMR, and (b) ^{13}C NMR, both recorded in $CDCl_3$.

Dehydrobromination of BPE. The strong, sterically hindered base *t*-BuOK was chosen to perform dehydrohalogenation of BPE (Scheme 3.2), in order to obtain vinylene polyethylene (VPE) exclusively, and to avoid substitution reactions.[33] The reaction conditions and order of addition are critical. Adding all reagents at once, at room temperature, and/or using a stoichiometric amount of base relative to the number of C-Br bonds in BPE, gave a polymer product that was insoluble in organic solvents (chloroform, toluene, and trichlorobenzene) even at temperatures as high as 150 °C. This observation indicates significant cross-linking; the mechanism of this phenomenon is currently under investigation. In contrast, adding a heated solution of BPE dropwise to a hot solution of *t*-BuOK ensured that the polymer was always dilute. The solubility of the products in solvents such as toluene and chloroform suggests that cross-linking was minimal.

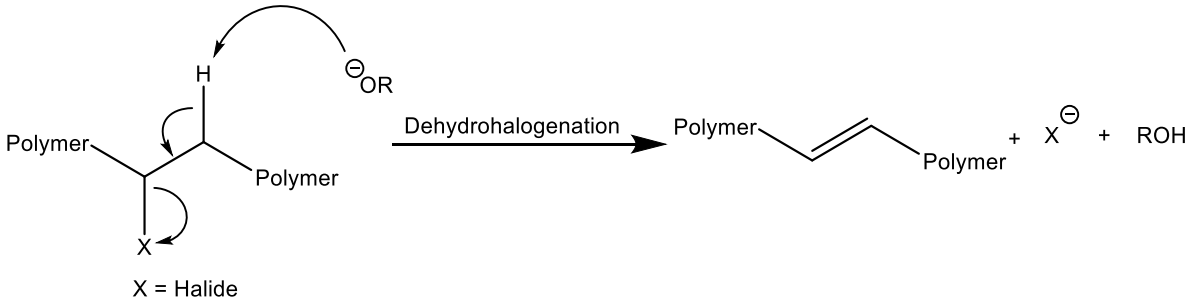

Scheme 3.2 General mechanism of dehydrohalogenation to form vinylene polyethylene (VPE).

In the absence of cross-linking, the VPE should have a carbon-to-vinylene molar ratio similar to the original C/Br ratio of BPE. However, quantification of the vinylene groups by ^{1}H NMR indicated higher carbon-to-vinylene molar ratios than expected (Table 3.2). This finding suggests some cross-linking did occur to reduce the vinylene content. More cross-linking occurred in VPE derived from the BPE with higher bromine content (see Table 3.2, VPE-1 vs. VPE-2). The molecular weight of VPE-2 appears to be higher than that of VPE-1 (Fig. A7), possibly because some of the more highly cross-linked polymer in VPE-1 is not soluble enough for analysis by GPC. Notably, the VPE derived from PE with M_n = 6.6 kg/mol (VPE-3) was fully dissolved in toluene only after stirring at 95 °C for 15 h. Since this starting PE has approximately 4 times more monomer units per chain than the lower molecular weight PE (M_n = 1.5 kg/mol), even a low degree of cross-linking would result in substantially longer polymer chains that are challenging to dissolve.

Table 3.2 Analysis of vinylene polyethylenes (VPEs), in comparison to their BPE precursors.

Starting BPE			VPE Product				
Entry	M_n (kg/mol)	C / Br [a]	Entry	M_n (kg/mol)	$Đ$	C / Vinylene [b]	Isolated Yield (%)
BPE-1	4.4	12	VPE-1	1.4	2.0	42	88
BPE-2	3.8	22	VPE-2	2.1	2.5	61	91
BPE-3	15	15	VPE-3	-	-	228 [c]	69

[a] Calculated from elemental analysis. [b] Calculated based on ^{1}H NMR, using an internal standard. See the supporting information for sample calculations of C/Br and C/vinylene molar ratios. [c] Approximate value, because the polymer did not dissolve fully prior to NMR analysis.

The absence of ^{1}H signals at 3.6-5.2 ppm (C*H*Br) and ^{13}C signals at 59 ppm (*C*HBr) (Fig. 3.2) in VPE indicates that BPE was completely debrominated. The pair of peaks at (5.39, 5.35) ppm in the ^{1}H NMR spectrum, and at (131, 130) ppm in the ^{13}C NMR spectrum, are characteristic of internal alkenes (vinylenes), and provide decisive evidence for the formation of both *cis* and *trans* isomers. The more stable *trans* isomer, represented by the downfield peaks,[34] is the major product. Furthermore, no double bond oxidation occurred, as evidenced by the absence of ^{1}H signals at 3.3-4.0 ppm (C*H*$_2$OR) and ^{13}C signals at 150-210 ppm (*C*=O).[33] IR analysis of VPE confirms the disappearance of the peaks corresponding to C-Br stretching at 537 and 613 cm^{-1} (Fig. A.8). A new broad peak at 1560 cm^{-1} represents C=C stretching, while the sharp signal at 965 cm^{-1} is characteristic of the =C-H bending mode of *trans*-alkenes.[35]

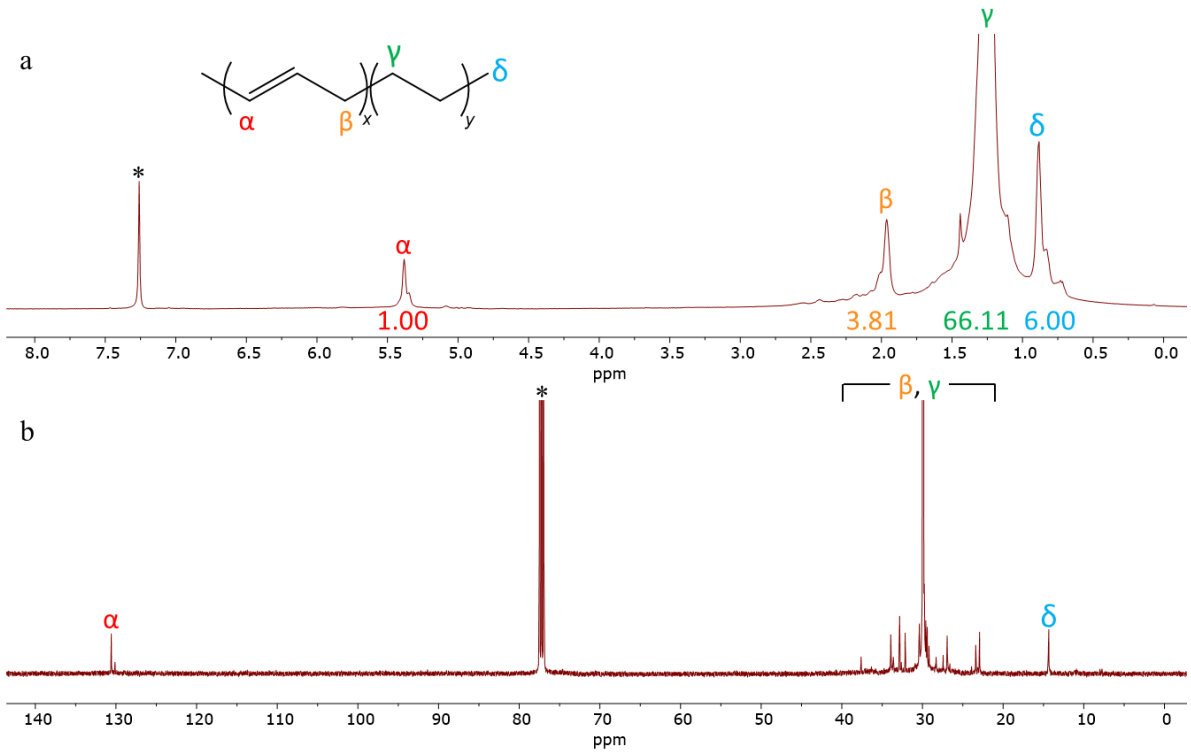

Figure 3.2 NMR spectra of VPE (Table 3.2, VPE-2): (a) ^{1}H NMR, and (b) ^{13}C NMR. *From $CDCl_3$ solvent.

Ethenolysis of Vinylene Polyethylene (VPE). The long-chain vinylene polymers were converted to shorter-chain α,ω-divinyl-functionalized oligomers via ethenolysis, using a commercially-available ruthenium metathesis catalyst, Grubbs Catalyst® M202. It was chosen for its thermal stability and high reported conversion of vinylenes to vinyl groups, with minimal isomerization side-reactions.[36,37] In optimization experiments, polybutadiene (PBD) was used as a model unsaturated polymer, in order to assess the frequency of side-reactions under the ethenolysis conditions. PBD has one vinylene group per four carbons, and should yield exclusively 1,5-hexadiene and propylene (through cleavage of the polymer end-groups) as the ultimate products of ethenolysis.

While the GC-FID and GC-MS analyses of the gases in the headspace did indicate the formation of 1,5-hexadiene and propylene (Figs. A.9 and A.10), other isomers including 2,4-hexadiene were detected as well, demonstrating isomerization of vinyl groups to vinylenes under the experimental conditions. Secondary cross-metathesis (CM) reactions also take place, as evidenced by the presence of pentadiene and 2-butene which can only form through such side-reactions. ^{1}H NMR analysis of the reaction mixture (Fig. A.11) revealed more signals in the olefinic region than expected if only 1,5-hexadiene and propylene were formed. According to a previous report, PBD homo-metathesis is favored over ethenolysis at lower ethylene pressures (ca. 2 bar), since cyclization can occur via a back-biting mechanism to form stable five- or six-membered rings.[38] Such rings may explain the extra peaks observed in the ^{1}H NMR spectra.

The catalyst loading, reaction time, and ethylene pressure that maximize conversion of VPE were investigated (Table 3.3). In a control experiment involving VPE-1 homo-metathesis conducted without ethylene (Table 3.3, Entry 0), the average molecular weight of the recovered polymer was unchanged. No vinyl signals were observed by ^{1}H NMR, indicating that ethylene is required to form them. Higher catalyst loadings (Entry 1-3) and ethenolysis times longer than 1 h (Entries 5-7 and 9-10) did not result in higher vinylene conversion to vinyl groups. However, ruthenium hydrides which form upon alkylidene decomposition are reported to isomerize vinyl groups to more stable vinylenes.[38–40] The effect of ethylene pressure was investigated using VPE-2 (Entries 4-5, 8). While ethylene is obviously required to achieve ethenolysis, performing reactions with ethylene pressures > 2.7 bar resulted in lower vinyl yields. In previous work, ethylene has been proposed to cause catalyst deactivation through mechanisms involving the formation of unstable ruthenium methylidenes, thus inhibiting

ethenolysis.[40,41] Higher ethylene pressures are also reported to favor unproductive metathesis reactions with ethylene that compete with productive ethenolysis.[16,38]

Table 3.3 ^{1}H NMR Analysis of Reaction Mixtures[a] Resulting from Ethenolysis of VPE at 100 °C

Entry	Substrate	Ru (mol%)	C_2H_4 Pressure (bar)	Time (h)	Vinyl (% Yield)[b]	Vinylene (% Remaining)[b]	Recovered C=C (%)[c]
0	VPE-1	2.5	0	1	0	80	80
1		1.0	2.7	1	10	49	59
2		2.5	2.7	1	48	28	76
3		5.0	2.7	1	45	25	70
4	VPE-2	2.5	2.7	1	57	14	71
5		2.5	4.4	1	32	34	66
6		2.5	4.4	4	25	29	54
7		2.5	4.4	20	15	38	53
8		2.5	8.0	1	22	43	65
9	VPE-3	2.5	2.7	1	52	44	96
10		2.5	2.7	2	48	46	94

[a] Quantification of vinylenes and vinyl groups in the reaction mixture is based on analysis by ^{1}H NMR with an internal standard. [b] Values are calculated relative to the quantity of initial vinylene groups present in the starting VPE. [c] Values are calculated as vinyl (% yield) + vinylene (% remaining).

Based on these experiments, the highest conversion of vinylene to vinyl groups (86%, Table 3.3, Entry 4) was obtained under optimal conditions of 2.5 mol% Ru catalyst and 2.7 bar C_2H_4 in a reaction time of 1 h. Analysis of the gases in the vessel headspace by GC-FID (Fig. A.12) showed that most of the volatiles are propylene and *cis*- and *trans*-2-butenes, with minor unidentified species with carbon numbers greater than C4. It should be noted that

volatiles dissolved in the reaction mixture were not analyzed. When all volatiles were removed from the reaction mixture, the α,ω-divinyl-functionalized oligomers were isolated in high yields (Table 3.4, see sample calculation in Appendix A). Based on the mass balance, the minor quantity not recovered is attributed to volatiles, and/or product losses during workup.

Table 3.4 Characterization of the α,ω-divinyl-functionalized oligomers isolated from ethenolysis of VPE [a]

Substrate	Entry	M_n (g/mol)	$Đ$	Vinyl (%)	Vinylene (%)	Recovered C=C (%)	Isolated Yield (%) [b]
VPE-1	Divinyl-1	671	2.0	24	41	65	97
VPE-2	Divinyl-2	854	2.1	46	12	58	92
VPE-3	Divinyl-3[c]	-	-	45	47	92	94

[a] Reaction conditions: 50 mg polymer, 2.5 mol% catalyst, 2.7 bar C_2H_4 for 1 hr. [b] Calculated from recovered mass / [(100% - % remaining vinylene in reaction mixture) × moles of starting vinylene × C_2H_4 molar mass + mass of starting VPE]. [c] No data were acquired due to the very low solubility of the product.

According to ^{1}H NMR analysis of the isolated α,ω-divinyl functionalized oligomers (Fig. 3.3a, conducted in the absence of toluene), residual vinylenes appear at 5.4 ppm while a pair of signals corresponding to vinyl groups are observed as a doublet of doublets at 5.8 ppm (-*H*C=CH_2) and as a multiplet at 5.0 ppm (H_2C=CH-). Vinyl formation was further confirmed via ^{13}C NMR (Fig. 3.3b), by the presence of two peaks at 140 ppm (-*C*H=CH_2) and at 114 ppm (*C*H_2=CH-). The vinylene signals at 130 and at 131 ppm are significantly attenuated, providing further evidence for the conversion of vinylene. Use of dichloroethane as an internal standard to quantify the olefinic groups present in the α,ω-divinyl-functionalized oligomers revealed

that the isolated oligomers contain fewer such groups than were present in the reaction mixture (Fig. A.13). This is most likely a consequence of the loss of volatile olefins during workup. Notably, the α,ω-divinyl-functionalized oligomer with the higher olefinic content (divinyl-1) experienced more ruthenium hydride-catalyzed isomerization than the oligomer with the lower olefinic content (divinyl-2), as shown by the decrease in the vinyl yield and increase in the vinylene yield in the isolated oligomer (Table 3.4), relative to the corresponding reaction mixtures (Table 3.3, Entries 2, 4, and 9).

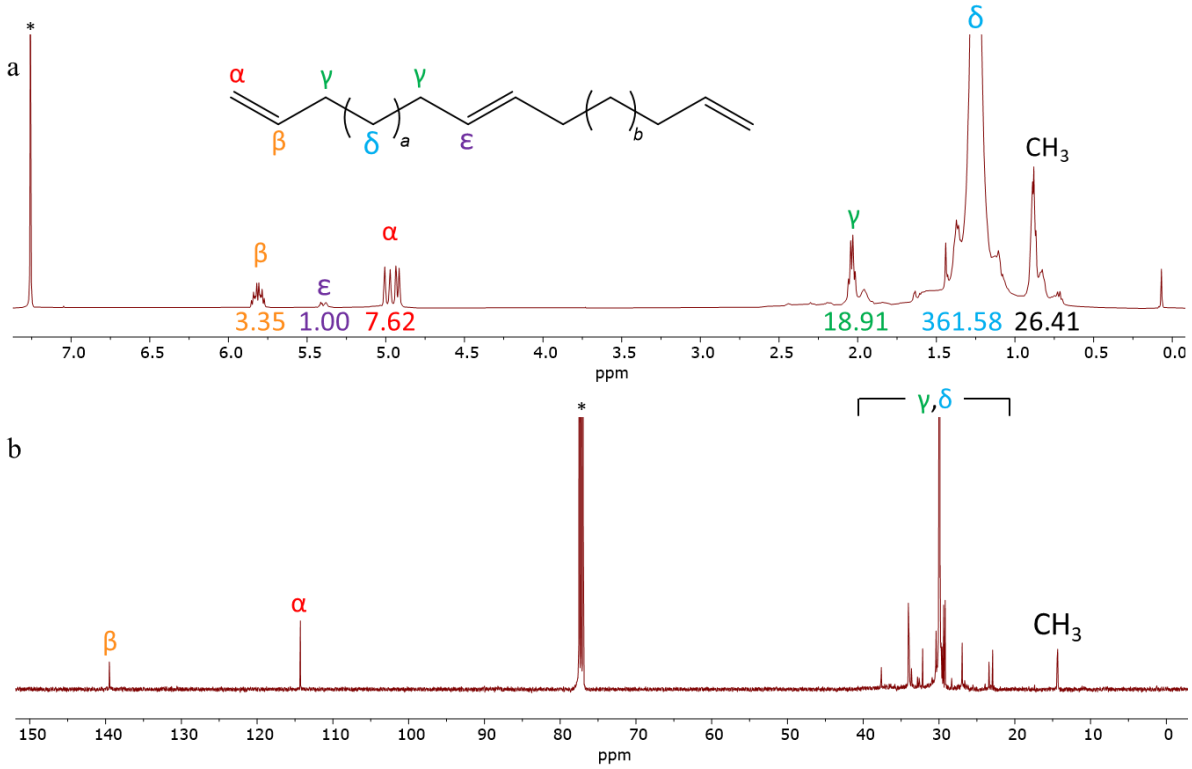

Figure 3.3 NMR spectra of isolated α,ω-divinyl functionalized oligomers formed by ethenolysis (Table 3.4, divinyl-2): (a) ^{1}H NMR, and (b) ^{13}C NMR. *From $CDCl_3$ solvent.

According to GPC (Fig. A.14), divinyl-1 and divinyl-2 underwent a reduction in molecular weight relative to the starting VPE, confirming that ethylene successfully cleaved the C-C double bonds in the unsaturated polymer. Whereas the starting PE (M_n =1.5 kg/mol) has on average 108 carbon atoms, divinyl-1 has on average just 48 carbon atoms, while divinyl-2 has on average 61 carbon atoms. Complete conversion of the internal double bonds of VPE-1 and VPE-2 to vinyl groups during ethenolysis would give α,ω-divinyl-functionalized oligomers with carbon numbers of 44 and 63, respectively. These values are close to the experimental values obtained by GPC, demonstrating that PE can be depolymerized in this way to α,ω-divinyl-functionalized oligomers with targeted chain lengths. Characterization of the α,ω-divinyl-functionalized oligomer derived from PE with M_n = 6.6 kg/mol (divinyl-3) was not possible because of its limited solubility in chloroform, toluene, trichlorobenzene, and all other organic solvents, even at temperatures as high as 150 °C.

Preliminary Techno-Economic Assessment (TEA). The economics of chemical upcycling of PE to α,ω-divinyl-functionalized oligomers on an industrial scale were evaluated. The simulated process converts 300 kta (kilotons per annum) PE to α,ω-divinyl-functionalized oligomers, following Scheme 3.1. For safety reasons as well as economics, Br_2 and solvent are recycled. The HBr side-product of bromination is converted to Br_2 over a RuO_2/TiO_2 catalyst, then recycled into the bromination reactor.[24] The assessment assumes 99% recovery of both Br_2 and solvent, a Br_2 : PE mass ratio 50% lower in the simulated process relative to the laboratory scale demonstration, and a solvent : PE mass ratio of 5:1. Complete conversion of Br_2, *t*-BuOK, and HBr are also assumed. Based on this base case scenario, the fixed capital investment (FCI) is estimated to be 157 MM USD, with annual utility costs of 8 MM USD (see Appendix A).

A discounted cash flow analysis was conducted to estimate the net present value (NPV) and internal rate of return (IRR), based on a reported method[42] (see Appendix A). The analysis assumes a selling price for α,ω-divinyl-functionalized oligomers of $1.45/kg, estimated based on a typical selling price of poly-α-olefin.[43] Waste PE was assumed to have no cost.[44] Annual revenue was initially calculated based on selling the α,ω-divinyl-functionalized oligomers as well as the two co-products of the laboratory-scale process (KBr and *t*-BuOH). For this base case scenario, the process revenue is 706 MM USD, with most of the revenue coming from sales of α,ω-divinyl-functionalized oligomer (63%) and KBr (31%). NPV is 308 MM USD with an IRR of 50%, indicating likely process profitability using the assumptions described above.

The effect of selling price and cost variability on NPV was assessed through a sensitivity analysis. Eleven economic parameters were independently varied by ±5% from their reference values (Br_2 and solvent recovery were varied from 100 % to 98.5% and 99.5%, respectively). The results in Fig. 3.4 indicate that Br_2/solvent recovery and α,ω-divinyl-functionalized oligomer selling price greatly impact NPV, highlighting the need for robust recovery systems and accurate α,ω-divinyl-functionalized oligomer market value data. Process design improvements to ensure high Br_2 and solvent recoveries would incur increased capital and utility costs above the base case considered here, but the sensitivity analysis suggests that such increases will have little influence on NPV. Based on this analysis, the process is likely to be profitable regardless of economic parameter variability. However, a negative NPV was obtained when coproduct sale was not included, suggesting that this scenario carries considerable risk.

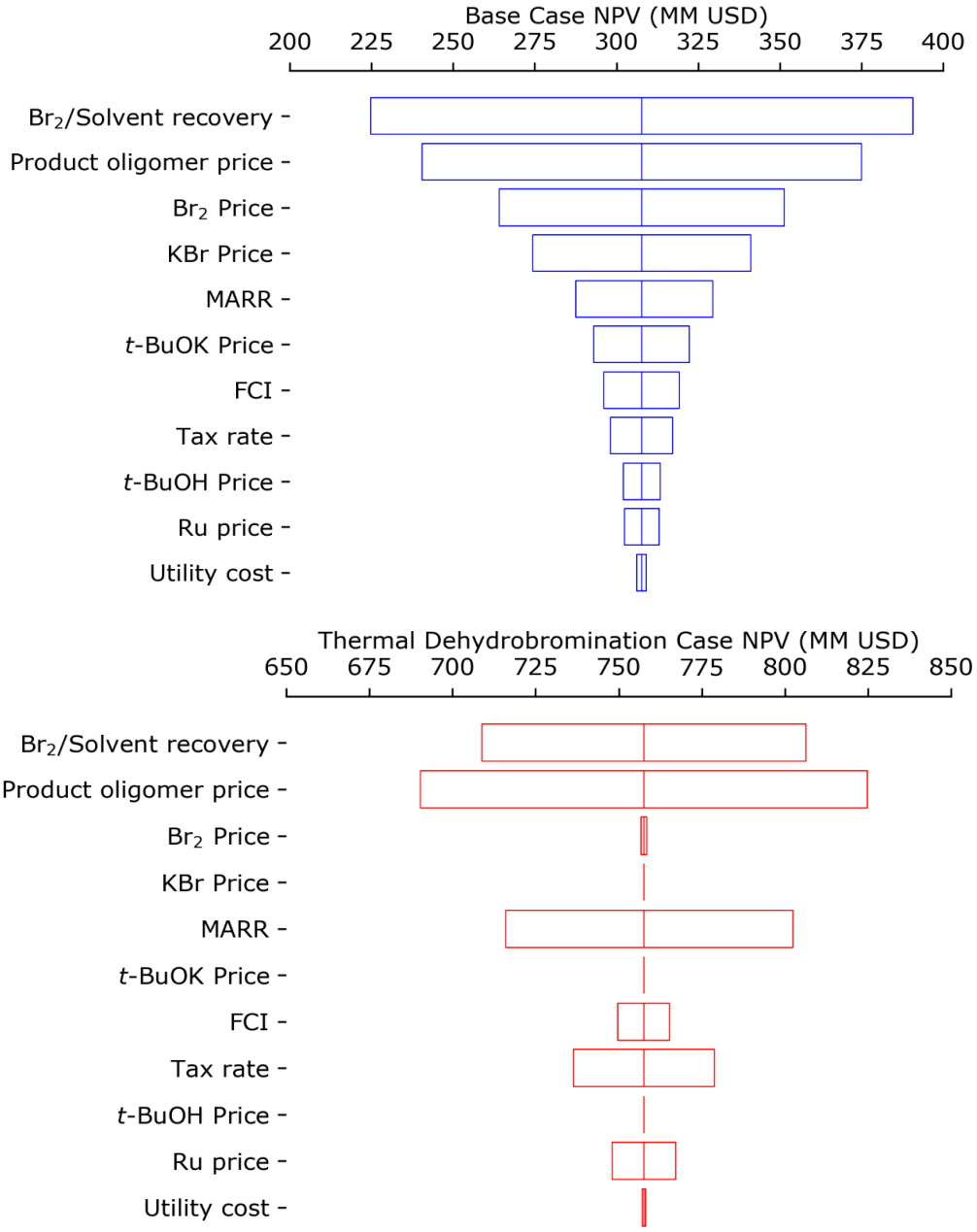

Figure 3.4 Sensitivity analysis of the TEA for two scenarios in the PE-to-α,ω-divinyl-functionalized oligomers process: the base case (with coproduct sales, top) and the thermal dehydrobromination case (no coproduct sales, bottom). Solvents include benzene, THF, and toluene. MARR = Minimum Acceptable Rate of Return. FCI = Fixed Capital Investment.

Prices for Br_2, KBr, *t*-BuOK, and *t*-BuOH impact NPV in ways that can be mitigated and/or eliminated by process design adjustment. The result is an improved industrial-scale process design for converting PE to α,ω-divinyl-functionalized oligomers which yields a positive NPV with revenue derived only from the sale of α,ω-divinyl-functionalized oligomers. Specifically, thermal dehydrobromination can produce the desired olefin and HBr without the need for an expensive base (e.g., *t*-BuOK) or generation of other coproducts (i.e., KBr and *t*-BuOH).[45] The HBr formed in dehydrobromination can be recycled oxidatively to Br_2, as in the base case considered above.

Therefore, a process was designed to convert PE to α,ω-divinyl-functionalized oligomers following Scheme 3.1, except with thermal dehydrobromination replacing *t*-BuOK-mediated dehydrobromination (see Appendix A). Annual revenue was calculated from sale of only α,ω-divinyl-functionalized oligomers. For this process, NPV is more than double the base case (758 MM USD) and IRR is 113%, indicating that such a process should be more profitable. A new sensitivity analysis was conducted (Fig. 3.4). Relative to the base case, the influence of Br_2 price on NPV is reduced by 1.5 orders of magnitude when thermal dehydrobromination is used. All of the Br_2 is recycled, compared to only 50% in the base case. The effects of KBr, *t*-BuOK, and *t*-BuOH prices on NPV are eliminated. More RuO_2/TiO_2 is needed to recycle the additional HBr produced by thermal dehydrobromination and is reflected in a small increased impact of Ru price on NPV. The larger cash flows involved in the thermal dehydrobromination case increase the influence of MARR and tax rate on NPV. Nevertheless, thermal dehydrobromination would vastly improve the economic feasibility of producing α,ω-divinyl-functionalized oligomers from PE.

3.4 Conclusion

The idea to convert end-of-life plastics into valuable chemicals has the potential to reshape the way the world perceives its plastic waste. Innovative approaches such as chemical upcycling and recycling of plastics in a circular carbon economy that generates minimal waste could provide sustainable, long-term solutions to the problem. The work described here demonstrates how PE can be upgraded into value-added α,ω-divinyl-functionalized oligomers in three high-yield steps, involving (1) controlled bromination, whereby precise quantities of Br can be incorporated into PE in air without side-reactions, with the potential to collect and recycle the HBr to regenerate the reagent Br_2, (2) complete elimination of bromide to synthesize vinylenes, and (3) ethenolysis of the vinylenes to yield α,ω-divinyl-functionalized oligomers whose chain lengths can be tuned based on the initial quantity of Br_2 added.

Preliminary techno-economic assessment (TEA) demonstrates that conversion of waste PE to α,ω-divinyl-functionalized oligomers could be profitable on an industrial scale. The intermediate BPE also possesses value, since brominated polymers find use as additives in fire retardants[46] and as ion-exchange materials,[47] for example. Given that alkyl bromides undergo nucleophilic substitution,[33] BPE can also serve as a versatile precursor in the synthesis of other functionalized polyethylenes. In addition, the vinylene double bonds in VPE can be cleaved oxidatively via processes such as ozonolysis,[48–50] to form shorter, more biodegradable chains with carboxylic acid, ketone, and aldehyde functional groups.[32] Overall, this work describes how PE can be upcycled into value-added molecules, including intermediates and polymers, for further use in a circular carbon economy.

3.5 Acknowledgements

This work was supported through a subcontract from the Ames Laboratory with funding from the U.S. Department of Energy (DOE), Office of Science, Office of Basic Energy Sciences, under Contract No. DE-AC02-07CH11358 as part of the Energy Frontier Research Center titled the Institute for Cooperative Upcycling of Plastics (iCOUP). The MRL Shared Experimental Facilities are supported by the MRSEC Program of the NSF under Award No. DMR 1720256; a member of the NSF-funded Materials Research Facilities Network (www.mrfn.org).

3.6 References

(1) Geyer, R.; Jambeck, J. R.; Law, K. L. Production, Use, and Fate of All Plastics Ever Made. *Sci. Adv.* **2017**, *3* (7), e1700782. https://doi.org/10.1126/sciadv.1700782.

(2) Ellen MacArthur Foundation. The New Plastics Economy: Rethinking the Future of Plastics & Catalysing Action, 2017.

(3) Jambeck, J. R.; Geyer, R.; Wilcox, C.; Siegler, T. R.; Perryman, M.; Andrady, A.; Narayan, R.; Law, K. L. Plastic Waste Inputs from Land into the Ocean. *Science* **2015**, *347* (6223), 768–771. https://doi.org/10.1126/science.1260352.

(4) Karami, A.; Golieskardi, A.; Keong Choo, C.; Larat, V.; Galloway, T. S.; Salamatinia, B. The Presence of Microplastics in Commercial Salts from Different Countries. *Sci Rep* **2017**, *7* (1), 46173. https://doi.org/10.1038/srep46173.

(5) Teuten, E. L.; Saquing, J. M.; Knappe, D. R. U.; Barlaz, M. A.; Jonsson, S.; Björn, A.; Rowland, S. J.; Thompson, R. C.; Galloway, T. S.; Yamashita, R.; Ochi, D.; Watanuki, Y.; Moore, C.; Viet, P. H.; Tana, T. S.; Prudente, M.; Boonyatumanond, R.; Zakaria, M.

P.; Akkhavong, K.; Ogata, Y.; Hirai, H.; Iwasa, S.; Mizukawa, K.; Hagino, Y.; Imamura, A.; Saha, M.; Takada, H. Transport and Release of Chemicals from Plastics to the Environment and to Wildlife. *Phil. Trans. R. Soc. B* **2009**, *364* (1526), 2027–2045. https://doi.org/10.1098/rstb.2008.0284.

(6) Rahimi, A.; García, J. M. Chemical Recycling of Waste Plastics for New Materials Production. *Nat Rev Chem* **2017**, *1* (6), 0046. https://doi.org/10.1038/s41570-017-0046.

(7) *Plastics and the Environment*; Harrison, R. M., Hester, R. E., Eds.; Issues in Environmental Science and Technology; Royal Society of Chemistry: Cambridge, 2018. https://doi.org/10.1039/9781788013314.

(8) Ragaert, K.; Delva, L.; Van Geem, K. Mechanical and Chemical Recycling of Solid Plastic Waste. *Waste Management* **2017**, *69*, 24–58. https://doi.org/10.1016/j.wasman.2017.07.044.

(9) Anuar Sharuddin, S. D.; Abnisa, F.; Wan Daud, W. M. A.; Aroua, M. K. A Review on Pyrolysis of Plastic Wastes. *Energy Conversion and Management* **2016**, *115*, 308–326. https://doi.org/10.1016/j.enconman.2016.02.037.

(10) Santos, B. P. S.; Almeida, D. D.; Marques, M. de F. V.; Henriques, C. A. Degradation of Polypropylene and Polyethylene Wastes Over HZSM-5 and USY Zeolites. *Catal Lett* **2019**, *149* (3), 798–812. https://doi.org/10.1007/s10562-019-02677-y.

(11) Jia, X.; Qin, C.; Friedberger, T.; Guan, Z.; Huang, Z. Efficient and Selective Degradation of Polyethylenes into Liquid Fuels and Waxes under Mild Conditions. *Sci. Adv.* **2016**, *2* (6), e1501591. https://doi.org/10.1126/sciadv.1501591.

(12) Celik, G.; Kennedy, R. M.; Hackler, R. A.; Ferrandon, M.; Tennakoon, A.; Patnaik, S.; LaPointe, A. M.; Ammal, S. C.; Heyden, A.; Perras, F. A.; Pruski, M.; Scott, S. L.;

Poeppelmeier, K. R.; Sadow, A. D.; Delferro, M. Upcycling Single-Use Polyethylene into High-Quality Liquid Products. *ACS Cent. Sci.* **2019**, *5* (11), 1795–1803. https://doi.org/10.1021/acscentsci.9b00722.

(13) Tennakoon, A.; Wu, X.; Paterson, A. L.; Patnaik, S.; Pei, Y.; LaPointe, A. M.; Ammal, S. C.; Hackler, R. A.; Heyden, A.; Slowing, I. I.; Coates, G. W.; Delferro, M.; Peters, B.; Huang, W.; Sadow, A. D.; Perras, F. A. Catalytic Upcycling of High-Density Polyethylene via a Processive Mechanism. *Nat Catal* **2020**, *3* (11), 893–901. https://doi.org/10.1038/s41929-020-00519-4.

(14) Bäckström, E.; Odelius, K.; Hakkarainen, M. Trash to Treasure: Microwave-Assisted Conversion of Polyethylene to Functional Chemicals. *Ind. Eng. Chem. Res.* **2017**, *56* (50), 14814–14821. https://doi.org/10.1021/acs.iecr.7b04091.

(15) Zhang, F.; Zeng, M.; Yappert, R. D.; Sun, J.; Lee, Y.-H.; LaPointe, A. M.; Peters, B.; Abu-Omar, M. M.; Scott, S. L. Polyethylene Upcycling to Long-Chain Alkylaromatics by Tandem Hydrogenolysis/Aromatization. *Science* **2020**, *370* (6515), 437–441. https://doi.org/10.1126/science.abc5441.

(16) Bidange, J.; Fischmeister, C.; Bruneau, C. Ethenolysis: A Green Catalytic Tool to Cleave Carbon-Carbon Double Bonds. *Chem. Eur. J.* **2016**, *22* (35), 12226–12244. https://doi.org/10.1002/chem.201601052.

(17) Ray, S.; Rao, P. V. C.; Choudary, N. V. Poly-α-Olefin-Based Synthetic Lubricants: A Short Review on Various Synthetic Routes: PAO SYNTHESIS: A SHORT REVIEW. *Lubr. Sci.* **2012**, *24* (1), 23–44. https://doi.org/10.1002/ls.166.

(18) Sun, M.; Lowry, G. V.; Gregory, K. B. Selective Oxidation of Bromide in Wastewater Brines from Hydraulic Fracturing. *Water Research* **2013**, *47* (11), 3723–3731. https://doi.org/10.1016/j.watres.2013.04.041.

(19) Ding, K.; Metiu, H.; Stucky, G. D. Interplay Between Bromine and Iodine in Oxidative Dehydrogenation. *ChemCatChem* **2013**, *5* (7), 1906–1910. https://doi.org/10.1002/cctc.201200913.

(20) Breed, A.; Doherty, M. F.; Gadewar, S.; Grosso, P.; Lorkovic, I. M.; McFarland, E. W.; Weiss, M. J. Natural Gas Conversion to Liquid Fuels in a Zone Reactor. *Catalysis Today* **2005**, *106* (1–4), 301–304. https://doi.org/10.1016/j.cattod.2005.08.001.

(21) Zhou, X.-P.; Yilmaz, A.; Yilmaz, G. A.; Lorkovic, I. M.; Laverman, L. E.; Weiss, M.; Sherman, J. H.; McFarland, E. W.; Stucky, G. D.; Ford, P. C. An Integrated Process for Partial Oxidation of Alkanes. *Chem. Commun.* **2003**, No. 18, 2294. https://doi.org/10.1039/b307235e.

(22) Tsai, K. Y.-D.; Chang, I.-J. Photocatalytic Oxidation of Bromide to Bromine. *Inorg. Chem.* **2017**, *56* (2), 693–696. https://doi.org/10.1021/acs.inorgchem.6b01652.

(23) Zhao, M.; Lu, W. Catalytic Bromination of Alkyl Sp3C–H Bonds with KBr/Air under Visible Light. *Org. Lett.* **2018**, *20* (17), 5264–5267. https://doi.org/10.1021/acs.orglett.8b02208.

(24) Moser, M.; Rodríguez-García, L.; Amrute, A. P.; Pérez-Ramírez, J. Catalytic Bromine Recovery: An Enabling Technology for Emerging Alkane Functionalization Processes. *ChemCatChem* **2013**, *5* (12), 3520–3523. https://doi.org/10.1002/cctc.201300609.

(25) John J. Waycuilis; William J. Turner. Process for Converting Gaseous Alkanes to Liquid Hydrocarbons. US 8,232,441 B2.

(26) Balamurugan, S.; Mandale, A. B.; Badrinarayanan, S.; Vernekar, S. P. Photochemical Bromination of Polyolefin Surfaces. *Polymer* **2001**, *42* (6), 2501–2512. https://doi.org/10.1016/S0032-3861(00)00632-7.

(27) Plummer, C. M.; Zhou, H.; Zhu, W.; Huang, H.; Liu, L.; Chen, Y. Mild Halogenation of Polyolefins Using an N-Haloamide Reagent. *Polym. Chem.* **2018**, *9* (11), 1309–1317. https://doi.org/10.1039/C8PY00013A.

(28) Arroyo, N. A.; Hiltner, A. Suspension Bromination of High-Density Polyethylene. *J. Appl. Polym. Sci.* **1979**, *23* (5), 1473–1485. https://doi.org/10.1002/app.1979.070230518.

(29) Li, Y.; Ju, J.; Jia, J.; Sheng, W.; Han, L.; Gao, J. Highly Efficient Oxidative Bromination of Alkanes with the HBr-H2O2 System in the Presence of Catalyst. *Chin. J. Chem.* **2010**, *28* (12), 2428–2432. https://doi.org/10.1002/cjoc.201190016.

(30) Vaisman, L.; Fernanda González, M.; Marom, G. Transcrystallinity in Brominated UHMWPE Fiber Reinforced HDPE Composites: Morphology and Dielectric Properties. *Polymer* **2003**, *44* (4), 1229–1235. https://doi.org/10.1016/S0032-3861(02)00848-0.

(31) Chanunpanich, N.; Ulman, A.; Strzhemechny, Y. M.; Schwarz, S. A.; Janke, A.; Braun, H. G.; Kraztmuller, T. Surface Modification of Polyethylene through Bromination. *Langmuir* **1999**, *15* (6), 2089–2094. https://doi.org/10.1021/la980996f.

(32) Gewert, B.; Plassmann, M. M.; MacLeod, M. Pathways for Degradation of Plastic Polymers Floating in the Marine Environment. *Environ. Sci.: Processes Impacts* **2015**, *17* (9), 1513–1521. https://doi.org/10.1039/C5EM00207A.

(33) Vollhardt, K. P. C.; Schore, N. E. *Organic Chemistry: Structure and Function*, 7th edition.; W.H. Freeman and Company: New York, 2014.

(34) Smarun, A. V.; Duzhin, F.; Petković, M.; Vidović, D. Alkene-Assisted Cis-to-Trans Isomerization of Non-Conjugated Polyunsaturated Alkenes. *Dalton Trans.* **2017**, *46* (41), 14244–14250. https://doi.org/10.1039/C7DT03041J.

(35) Coates, J. Interpretation of Infrared Spectra, A Practical Approach. In *Encyclopedia of Analytical Chemistry*; Meyers, R. A., Ed.; John Wiley & Sons, Ltd: Chichester, UK, 2006; p a5606. https://doi.org/10.1002/9780470027318.a5606.

(36) Behr, A.; Krema, S.; Kämper, A. Ethenolysis of Ricinoleic Acid Methyl Ester – an Efficient Way to the Oleochemical Key Substance Methyl Dec-9-Enoate. *RSC Adv.* **2012**, *2* (33), 12775. https://doi.org/10.1039/c2ra22499b.

(37) Patil, V. B.; Saliu, K. O.; Jenkins, R. M.; Carnahan, E. M.; Kramer, E. J.; Fredrickson, G. H.; Bazan, G. C. Efficient Synthesis of α,ω-Divinyl-Functionalized Polyolefins. *Macromol. Chem. Phys.* **2014**, *215* (11), 1140–1145. https://doi.org/10.1002/macp.201400139.

(38) Watson, Mark D.; Wagener, Kenneth B. Acyclic Diene Metathesis (ADMET) Depolymerization: Ethenolysis of 1,4-polybutadiene Using a Ruthenium Complex. *Journal of Polymer Science: Part A: Polymer Chemistry* **1999**, *37*, 1857–1861. https://doi.org/10.1002/(SICI)1099-0518(19990615)37:12%3C1857::AID-POLA15%3E3.0.CO;2-C.

(39) Kadyrov, R.; Azap, C.; Weidlich, S.; Wolf, D. Robust and Selective Metathesis Catalysts for Oleochemical Applications. *Top Catal* **2012**, *55* (7–10), 538–542. https://doi.org/10.1007/s11244-012-9832-0.

(40) Spekreijse, J.; Sanders, J. P. M.; Bitter, J. H.; Scott, E. L. The Future of Ethenolysis in Biobased Chemistry. *ChemSusChem* **2017**, *10* (3), 470–482. https://doi.org/10.1002/cssc.201601256.

(41) Marx, V. M.; Sullivan, A. H.; Melaimi, M.; Virgil, S. C.; Keitz, B. K.; Weinberger, D. S.; Bertrand, G.; Grubbs, R. H. Cyclic Alkyl Amino Carbene (CAAC) Ruthenium Complexes as Remarkably Active Catalysts for Ethenolysis. *Angew. Chem. Int. Ed.* **2015**, *54* (6), 1919–1923. https://doi.org/10.1002/anie.201410797.

(42) *Analysis, Synthesis, and Design of Chemical Processes*, 4th ed.; Turton, R., Ed.; Prentice Hall: Upper Saddle River, NJ, 2012.

(43) *Polyalphaolefin-Polyalphaolefin Manufacturers, Suppliers and Exporters on Alibaba.comLubricant*. https://www.alibaba.com/trade/search?fsb=y&IndexArea=product_en&CatId=&SearchText=polyalphaolefin (accessed 2021-07-31).

(44) Gracida-Alvarez, U. R.; Winjobi, O.; Sacramento-Rivero, J. C.; Shonnard, D. R. System Analyses of High-Value Chemicals and Fuels from a Waste High-Density Polyethylene Refinery. Part 1: Conceptual Design and Techno-Economic Assessment. *ACS Sustainable Chem. Eng.* **2019**, *7* (22), 18254–18266. https://doi.org/10.1021/acssuschemeng.9b04763.

(45) Wang, X.; Liu, R.-F.; Cork, J.; Gu, Y.; Upham, D. C.; Laycock, B.; McFarland, E. W. Investigation of the Bromination/Dehydrobromination of Long Chain Alkanes. *Ind. Eng. Chem. Res.* **2017**, *56* (34), 9411–9418. https://doi.org/10.1021/acs.iecr.7b01039.

(46) Lukác, I.; Chmela, S.; Pilichowski, J. F.; Lacoste, J. Brominated Polyethylene. Synthesis, Photooxidation and Use as the Intermediate for the Preparation of New

Polymeric Stabilizers. *Journal of Macromolecular Science, Part A* **1998**, *35* (7), 1337–1348. https://doi.org/10.1080/10601329808002123.

(47) Brian A. Cooke; George Guorlay. Ion-Exchange Material from Halogenated Polyethylene. US 3,433,755 A.

(48) Fisher, T. J.; Dussault, P. H. Alkene Ozonolysis. *Tetrahedron* **2017**, *73* (30), 4233–4258. https://doi.org/10.1016/j.tet.2017.03.039.

(49) Henne, A. L.; Hill, P. The Preparation of Aldehydes, Ketones, and Acids by Ozone Oxidation. *J. Am. Chem. Soc.* **1943**, *65* (5), 752–754. https://doi.org/10.1021/ja01245a003.

(50) Moorthy, J. N.; Parida, K. N. Oxidative Cleavage of Olefins by In Situ-Generated Catalytic 3,4,5,6-Tetramethyl-2-Iodoxybenzoic Acid/Oxone. *J. Org. Chem.* **2014**, *79* (23), 11431–11439. https://doi.org/10.1021/jo502002w.

Chapter 4. Introduction: Using Bio-Derived Precursors to Make Petroleum-Based Chemicals

4.1 Motivation

Because of expanding industrialization and growing populations of people, the global demand for energy has increased every year from 1965 to 2019. In 2019, 84% of the primary energy generated originated from nonrenewable fossil fuels,[1] which are associated with negative externalities such as environmental pollution and deleterious effects to anthropogenic health upon their extraction from within the Earth's crust.[2] While the world's energy usage decreased by 4.5% in 2020 because of widespread lockdowns during the coronavirus pandemic, this reduction in energy consumption is projected to be short-lived.[1] To diminish reliance on petroleum, researchers have employed new strategies to apply renewable, non-petroleum based precursors to synthesize commodity chemicals traditionally derived from fossil fuels.[3]

Renewable energy can be generated from biological feedstocks commonly referred to as biomass to yield biofuels that can be combusted in the same way that petroleum-based fossil fuels are.[4] The energy in biomass originates from photosynthesis (eq. 4.1)[5] where solar energy is transformed into chemical energy stored within the plant.[6,7]

$$6\ H_2O\ +\ \text{light}\ +\ 6\ CO_2 \longrightarrow C_6H_{12}O_6\ +\ 6\ O_2 \qquad \text{(eq 4.1)}$$

Today, biofuels consist of 10% of the world's primary energy resources, with a projection to reach 28% by 2026[8] and can be classified as first, second, third, and fourth generations according to their original feedstock source and their method of conversion (Figure 4.1).[9]

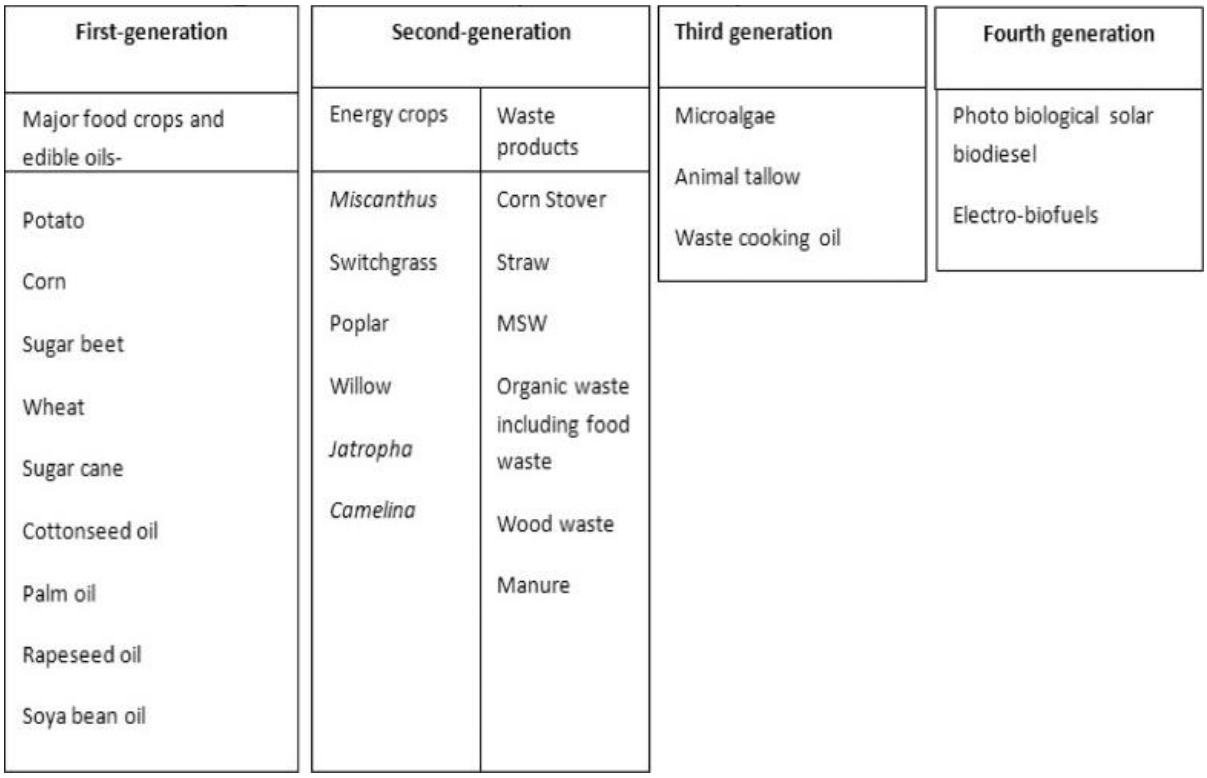

Figure 4.1 The four classifications of biofuels. Figure adapted from Mahapatra, S., *et. al*.[9]

4.2 First Generation Biofuels

First generation biofuels such as ethanol, butanol, and propanol are derived from sugar cane, corn, potatoes, and other edible crops with high sugar or starch content through fermentation processes.[10] Glucose, for example, can be converted to ethanol using yeast (*Saccharomyces cerevisiae*) under anaerobic conditions (eq 4.2).[11,12]

$$C_6H_{12}O_6 \xrightarrow{\text{Yeast Enzyme}} 2\,C_2H_5OH + 2\,CO_2 \qquad \text{(eq 4.2)}$$

Similarly, peanuts, soybeans, and other oil crops can be used to produce biodiesels. Since the triglycerides extracted from these plants have high viscosities which limit their application as liquid fuel, they are converted via transesterification with alcohols using acidic

or basic catalysts to yield biodiesels such as fatty acid methyl esters (FAMEs) that have similar viscosities as petroleum-based diesels (Scheme 4.1).[12,13]

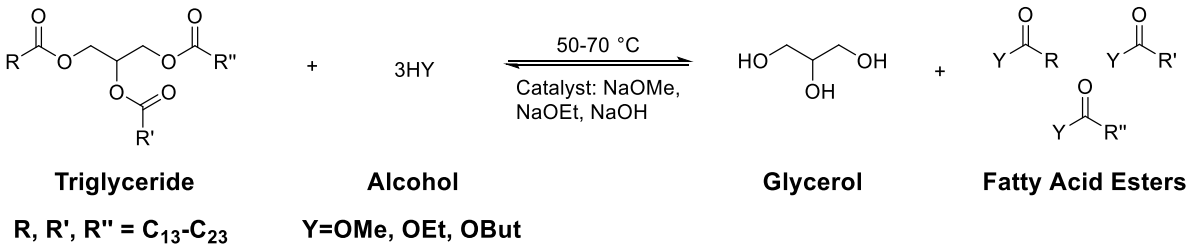

Scheme 4.1 Standard transesterification of triglycerides to yield biodiesels. Scheme adapted from Luque, R., *et. al.*[12]

According to the overall life cycle analysis of traditional diesels which originate from fossil fuels versus plant-based FAME biodiesels, FAMEs have been documented to emit 22% less carbon dioxide. Furthermore, even blending conventional diesel with 20% biodiesel results in a 16% net reduction in carbon emissions.[13]

While the methods to develop these chemicals from food crops have been well-developed, the generation of energy through these methods competes with the need to produce food, thus hindering first generation biofuels to be sustainable long-term alternatives to fossil fuels.[14] In addition, overdependence on a select set of crops results in the development of monocultures that require large quantities of agricultural land, water, and resources to support.[10] The lack of biodiversity from growing only a handful of crop varieties reduces the versatility of the species to adapt to possible changes in the environment caused by climate change, disease, and other events.[15] Given how first generation biofuels would also require subsidies from governments to support,[16] this source of energy would not be reliable for prolonged, large-scale, ubiquitous use.

4.3 Second Generation Biofuels

As a more practical alternative to first generation biofuels which rely on food-related crops, second generation biofuels are derived from nonedible biomass such as lignocellulose, which consists of 10-25 wt% lignin, 40-60 wt% cellulose, and 20-40 wt% hemicellulose (Figure 4.2).[12,17–19]

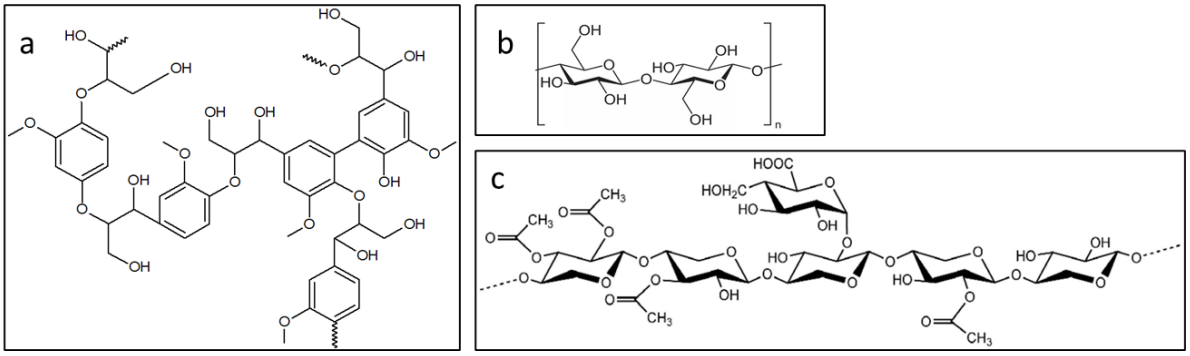

Figure 4.2 Representative structures of the components that lignocellulose consists of:[19] (a) lignin, (b) cellulose, (c) hemicellulose.

Consequently, chemically recycling lignocellulose to produce biofuels would serve as an effective method to meet the world's demand for energy while not compromising anthropogenic food resources. Two methodologies to convert lignocellulose to biofuels involve using either (1) thermochemical or (2) biochemical routes (Figure 4.3).[20]

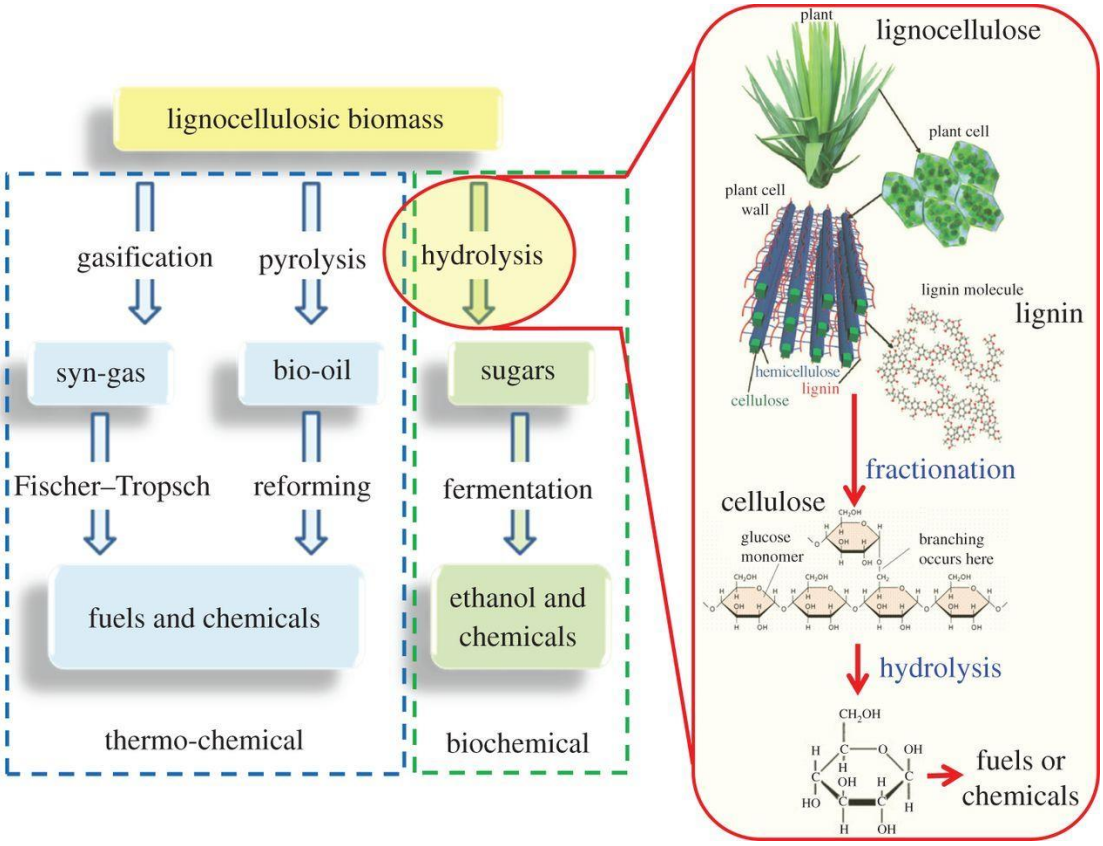

Figure 4.3 Thermochemical and biochemical routes to upgrade lignocellulose. Figure adapted from Wilson, K., *et. al*.[21]

Thermochemical conversion of lignocellulose typically occurs under elevated temperatures and oxygen-free conditions to yield multiple chemical fractions. Lower temperatures between 250 to 350 °C predominantly produce biochar while pyrolysis of lignocellulose under reaction temperatures from 550 to 750 °C results in the formation of bio-oils.[20] These liquid fuels, however, have notable disadvantages that stem from their high oxygen and water content, which reduce their heating value and result in immiscibility with traditional fuels and inadequate molecular stability.[21] These challenges, which limit the performance of these liquid fuels, can be overcome by performing deoxygenation protocols such as decarboxylation and hydrodeoxygenation to pretreat the biomass where oxygen is

chemically released as carbon dioxide and water, respectively.[22,23] Gasification of lignocellulose between 750-1,200 °C generates carbon monoxide and hydrogen gas,[24] otherwise known as synthesis gas (syngas) which can be directly used for fuel[25] or upgraded into liquid fuels, olefins, and other value-added chemicals via the Fischer Tropsch Synthesis (eq 4.3) using elevated temperatures between 200-400 °C and pressures between 15-40 bar in the presence of an iron or cobalt catalyst.[26–30]

$$(2n + 1)\ H_2 + n\ CO \rightarrow C_nH_{2n+2} + n\ H_2O \qquad \text{(eq 4.3)}$$

Under biochemical conversion, lignocellulose must initially undergo milling, thermal, and chemical pre-treatment steps[31] to remove lignin and hemicellulose and to extract cellulose, which is composed of fermentable glucose building blocks that can be biochemically converted to biofuels.[32] Afterwards, cellulose is hydrolyzed using enzymes or acid to yield glucose monomers.[33] Notable factors that affect the effectiveness of hydrolysis include porosity, surface area, crystallinity, and purity of the starting cellulose.[34] Finally, the sugar products from hydrolysis are converted into bioethanol under anaerobic conditions at 30 to 65 °C using enzymes, bacteria, and yeast as biocatalysts.[21,35] Interestingly, the direct fermentation of cellulose into biofuel has also been reported using *Neurospora*, *Monilia*, *Paecilomyces*, and *Fusarium* microbes that perform saccharification and fermentation at the same time in one consolidated reaction.[36]

In a similar way, the sugars that comprise hemicellulose can also be biochemically converted into bioethanol. However, in addition to glucose and other C_6 sugars, hemicellulose

also contains C_5 sugars such as xylose which complicate the fermentation process to produce bioethanol.[34]

Since lignin is a polymer that consists of three primary monolignol monomers[37] (*p*-coumaryl alcohol, coniferyl alcohol, and sinapyl alcohol) and does not contain sugars, fermentation does not effectively degrade lignin. Using alternative methods, however, lignin can be biodegraded into valuable chemicals using H_2O_2 in the presence of a peroxidase enzyme, for instance.[34,38]

While second generation biofuels do not rely on food crops for their production, second generation biofuels require supplemental procedural steps to create in comparison to first generation biofuels, thus restricting the scale at which these energy sources can be implemented.[39]

4.4 Third Generation Biofuels

Both first and second generation biofuels require the use of extensive areas of agricultural territory to produce, thus causing concerns related to competing interests in the usage or development of land.[40] Third generation biofuels provide solutions to this problem by using microbes and microalgae such as cyanobacteria (*Chloroxybacteria*) and green algae (*Chlorophyta*) which do not require large amounts to land to maintain and can be cultivated using agricultural scraps, waste waters, and non-arable soil.[41] Other significant advantages to using microoganisms for chemical development include the ability to produce biofuels year-round without needing to depend on crops that can only be harvested at certain times in a year, exponential rates of growth where some microalgae species can double their biomass as

quickly as 3.5 hours, and higher yields of biofuels and a lower water expenditure relative to land crops.[42–46]

As photosynthetic organisms known as autotrophs, microalgae contain chlorophyll which enables them to capture energy from sunlight in the form of chemical energy using carbon dioxide as their central supply of carbon (eq 4.2).[47] They can also inhibit the formation of toxic nitrogen oxide compounds in the environments they are cultivated in and absorb phosphorus, nitrogen, inorganic salts, and other toxins which may be used as nutrients from wastewater, thus serving to bioremediate their surroundings in the process of producing renewable bio-derived chemicals.[47,48] The chemical precursors to biofuels which microorganisms generate can be formed either through biochemical or thermochemical conversion processes that utilize similar techniques similar to those discussed in section 4.2 regarding second generation biofuels.

Classified as a biochemical conversion, transesterification (Scheme 4.1) can be performed on the triglycerides extracted from microalgae, which can be engineered to accrue up to 73% of their mass as lipids that predominantly consist of these compounds, to yield biodiesel-grade FAMEs.[49,50] Interestingly, the glycerol by-product can be recycled as feed to develop future microalgae cultures, thus contributing to the sustainability of the process.[51] Since the biomass derived from microalgae usually contains 70-72% by mass of sugar, starch, and cellulose by mass, with cellulose comprising up to 60% by mass, these carbohydrates can be isolated and then fermented into ethanol.[52]

Thermochemical methods to convert microalgal biomass into biooils used as fuel include fast or slow pyrolysis routes that occur at temperatures between 200-700 °C under air-free conditions.[50] In addition to producing char, fast pyrolysis also forms aromatic and aliphatic

hydrocarbons, phenols, and other liquid products with yields up to 59%.[53,54] Slow pyrolysis, on the other hand, creates volatiles such as carbon dioxide and methane that can compose as much as 76% of the products formed.[55] Also known as natural gas, methane is considered a source of renewable energy and the cleanest burning hydrocarbon fuel.[56,57] Furthermore, the products of pyrolysis can be combusted in the presence of oxygen to generate methanol, hydrogen gas, and other high-value chemicals.[50]

4.6 Conclusion

Petroleum-based fuels and chemicals can be derived from renewable biological sources using methodologies characterized as first, second, and third generation technologies which play crucial roles in the transition away from dependence on nonrenewable fossil fuels. While first generation biochemicals rely on food crops to produce, second generation technologies address this challenge by using nonedible biomass instead. The difficulties with using terrestrial biomass for chemical synthesis, however, is that these starting materials grow seasonally and require substantial quantities of land and water to develop. Third generation technologies that use microorganisms provide answers to the limitations of the previous two generations, as microorganisms do not require extensive resources to grow and can be cultivated using anthropogenic waste. Although the worldwide implementation of these technologies to create chemicals is hindered by their high cost of production, advances have been made to explore fourth generation biochemical development involving the genetic modification of microorganisms to obtain higher yields at shorter time scales to ensure that the production of bio-based chemicals is economically competitive with those derived using traditional methods.[24]

4.7 References

(1) Bp. Statistical Review of World Energy 2021 | 70th Edition, 2021. Https://Www.Bp.Com/Content/Dam/Bp/Business-Sites/En/Global/Corporate/Pdfs/Energy-Economics/Statistical-Review/Bp-Stats-Review-2021-Full-Report.Pdf.

(2) TENORM, Oil and Gas Production Wastes. Https://Www.Epa.Gov/Radiation/Tenorm-Oil-and-Gas-Production-Wastes (Accessed May 24, 2022).

(3) Moodley, P. Sustainable Biofuels: Opportunities and Challenges. In *Sustainable Biofuels*; Elsevier, 2021; pp 1–20. https://doi.org/10.1016/B978-0-12-820297-5.00003-7.

(4) Sánchez, J.; Curt, M. D.; Robert, N.; Fernández, J. Biomass Resources. In *The Role of Bioenergy in the Bioeconomy*; Elsevier, 2019; pp 25–111. https://doi.org/10.1016/B978-0-12-813056-8.00002-9.

(5) Johnson, M. P. Photosynthesis. *Essays in Biochemistry* **2016**, *60* (3), 255–273. https://doi.org/10.1042/EBC20160016.

(6) Potters, Geert; Van Goethem, Davina; Schutte, Frances. Promising Biofuel Resources: Lignocellulose and Algae. *Nature Education* **2010**, *3* (9), 14.

(7) Demirel, Y. Sugar versus Lipid for Sustainable Biofuels. *Int J Energy Res* **2018**, *42* (3), 881–884. https://doi.org/10.1002/er.3914.

(8) International Energy Agency. Biofuels-Energy and Technologies-IEA. Https://Www.Iea.Org/Fuels-and-Technologies/Bioenergy (Accessed May 25, 2022).

(9) Mahapatra, S.; Kumar, D.; Singh, B.; Sachan, P. K. Biofuels and Their Sources of Production: A Review on Cleaner Sustainable Alternative against Conventional Fuel, in

the Framework of the Food and Energy Nexus. *Energy Nexus* **2021**, *4*, 100036. https://doi.org/10.1016/j.nexus.2021.100036.

(10) Dahman, Y.; Syed, K.; Begum, S.; Roy, P.; Mohtasebi, B. Biofuels. In *Biomass, Biopolymer-Based Materials, and Bioenergy*; Elsevier, 2019; pp 277–325. https://doi.org/10.1016/B978-0-08-102426-3.00014-X.

(11) Singh, R.; Prakash, A.; Balagurumurthy, B.; Bhaskar, T. Hydrothermal Liquefaction of Biomass. In *Recent Advances in Thermo-Chemical Conversion of Biomass*; Elsevier, 2015; pp 269–291. https://doi.org/10.1016/B978-0-444-63289-0.00010-7.

(12) Luque, R.; Herrero-Davila, L.; Campelo, J. M.; Clark, J. H.; Hidalgo, J. M.; Luna, D.; Marinas, J. M.; Romero, A. A. Biofuels: A Technological Perspective. *Energy Environ. Sci.* **2008**, *1* (5), 542. https://doi.org/10.1039/b807094f.

(13) Fukuda, H.; Kondo, A.; Noda, H. Biodiesel Fuel Production by Transesterification of Oils. *Journal of Bioscience and Bioengineering* **2001**, *92* (5), 405–416. https://doi.org/10.1016/S1389-1723(01)80288-7.

(14) Alam, Md. S.; Tanveer, Md. S. Conversion of Biomass into Biofuel: A Cutting-Edge Technology. In *Bioreactors*; Elsevier, 2020; pp 55–74. https://doi.org/10.1016/B978-0-12-821264-6.00005-X.

(15) Correa, D. F.; Beyer, H. L.; Possingham, H. P.; Thomas-Hall, S. R.; Schenk, P. M. Biodiversity Impacts of Bioenergy Production: Microalgae vs. First Generation Biofuels. *Renewable and Sustainable Energy Reviews* **2017**, *74*, 1131–1146. https://doi.org/10.1016/j.rser.2017.02.068.

(16) R. Doornbusch, R. Steenblik. Biofuels: Is the Cure Worse than the Disease? 2007. Paper Prepared for the Round Table on Sustainable Development, Organisation for Economic

Co-Operation and Development (OECD), Paris. 11–12 September, SG/SO/RT(2007)3/REV1. Http://Www.Oecd.Org/Dataoecd/9/3/39411732.Pdf.

(17) Sarika, P. R.; Nancarrow, P.; Khansaheb, A.; Ibrahim, T. Bio-Based Alternatives to Phenol and Formaldehyde for the Production of Resins. *Polymers* **2020**, *12* (10), 2237. https://doi.org/10.3390/polym12102237.

(18) Katahira, R.; Elder, T. J.; Beckham, G. T. Chapter 1. A Brief Introduction to Lignin Structure. In *Energy and Environment Series*; Beckham, G. T., Ed.; Royal Society of Chemistry: Cambridge, 2018; pp 1–20. https://doi.org/10.1039/9781788010351-00001.

(19) Yang, H.; Yan, R.; Chen, H.; Lee, D. H.; Zheng, C. Characteristics of Hemicellulose, Cellulose and Lignin Pyrolysis. *Fuel* **2007**, *86* (12–13), 1781–1788. https://doi.org/10.1016/j.fuel.2006.12.013.

(20) Lee, R. A.; Lavoie, J.-M. From First- to Third-Generation Biofuels: Challenges of Producing a Commodity from a Biomass of Increasing Complexity. *Animal Frontiers* **2013**, *3* (2), 6–11. https://doi.org/10.2527/af.2013-0010.

(21) Wilson, K.; Lee, A. F. Catalyst Design for Biorefining. *Phil. Trans. R. Soc. A.* **2016**, *374* (2061), 20150081. https://doi.org/10.1098/rsta.2015.0081.

(22) Kaewpengkrow, P.; Atong, D.; Sricharoenchaikul, V. Catalytic Upgrading of Pyrolysis Vapors from Jatropha Wastes Using Alumina, Zirconia and Titania Based Catalysts. *Bioresource Technology* **2014**, *163*, 262–269. https://doi.org/10.1016/j.biortech.2014.04.035.

(23) Keller, T. C.; Rodrigues, E. G.; Pérez-Ramírez, J. Generation of Basic Centers in High-Silica Zeolites and Their Application in Gas-Phase Upgrading of Bio-Oil. *ChemSusChem* **2014**, *7* (6), 1729–1738. https://doi.org/10.1002/cssc.201301382.

(24) Mat Aron, N. S.; Khoo, K. S.; Chew, K. W.; Show, P. L.; Chen, W.; Nguyen, T. H. P. Sustainability of the Four Generations of Biofuels – A Review. *Int J Energy Res* **2020**, *44* (12), 9266–9282. https://doi.org/10.1002/er.5557.

(25) da Rosa, A. V.; Ordóñez, J. C. Hydrogen Production. In *Fundamentals of Renewable Energy Processes*; Elsevier, 2022; pp 419–470. https://doi.org/10.1016/B978-0-12-816036-7.00021-X.

(26) Cheng, K.; Kang, J.; King, D. L.; Subramanian, V.; Zhou, C.; Zhang, Q.; Wang, Y. Advances in Catalysis for Syngas Conversion to Hydrocarbons. In *Advances in Catalysis*; Elsevier, 2017; Vol. 60, pp 125–208. https://doi.org/10.1016/bs.acat.2017.09.003.

(27) Wu, C.; Tu, X. Biological and Fermentative Conversion of Syngas. In *Handbook of Biofuels Production*; Elsevier, 2016; pp 335–357. https://doi.org/10.1016/B978-0-08-100455-5.00012-6.

(28) Dry, M. E. Practical and Theoretical Aspects of the Catalytic Fischer-Tropsch Process. *Applied Catalysis A: General* **1996**, *138* (2), 319–344. https://doi.org/10.1016/0926-860X(95)00306-1.

(29) Dry, M. E. High Quality Diesel via the Fischer-Tropsch Process - a Review. *J. Chem. Technol. Biotechnol.* **2002**, *77* (1), 43–50. https://doi.org/10.1002/jctb.527.

(30) Demirbas, A. Progress and Recent Trends in Biofuels. *Progress in Energy and Combustion Science* **2007**, *33* (1), 1–18. https://doi.org/10.1016/j.pecs.2006.06.001.

(31) Hamawand, I.; Seneweera, S.; Kumarasinghe, P.; Bundschuh, J. Nanoparticle Technology for Separation of Cellulose, Hemicellulose and Lignin Nanoparticles from

Lignocellulose Biomass: A Short Review. *Nano-Structures & Nano-Objects* **2020**, *24*, 100601. https://doi.org/10.1016/j.nanoso.2020.100601.

(32) Brautaset, T.; Ellingsen, T. E. Lysine. In *Comprehensive Biotechnology*; Elsevier, 2011; pp 541–554. https://doi.org/10.1016/B978-0-08-088504-9.00220-8.

(33) Sun, Y.; Cheng, J. Hydrolysis of Lignocellulosic Materials for Ethanol Production: A Review. *Bioresource Technology* **2002**, *83* (1), 1–11. https://doi.org/10.1016/S0960-8524(01)00212-7.

(34) Chakraborty, S.; Aggarwal, V.; Mukherjee, D.; Andras, K. Biomass to Biofuel: A Review on Production Technology: BIOMASS TO BIOFUEL. *Asia-Pac. J. Chem. Eng.* **2012**, *7*, S254–S262. https://doi.org/10.1002/apj.1642.

(35) Hamelinck, C. N.; Hooijdonk, G. van; Faaij, A. P. Ethanol from Lignocellulosic Biomass: Techno-Economic Performance in Short-, Middle- and Long-Term. *Biomass and Bioenergy* **2005**, *28* (4), 384–410. https://doi.org/10.1016/j.biombioe.2004.09.002.

(36) Lynd, L.; Zyl, W.; Mcbride, J.; Laser, M. Consolidated Bioprocessing of Cellulosic Biomass: An Update. *Current Opinion in Biotechnology* **2005**, *16* (5), 577–583. https://doi.org/10.1016/j.copbio.2005.08.009.

(37) del Río, J. C.; Rencoret, J.; Gutiérrez, A.; Elder, T.; Kim, H.; Ralph, J. Lignin Monomers from beyond the Canonical Monolignol Biosynthetic Pathway: Another Brick in the Wall. *ACS Sustainable Chem. Eng.* **2020**, *8* (13), 4997–5012. https://doi.org/10.1021/acssuschemeng.0c01109.

(38) Vélez-Mercado, M. I.; Talavera-Caro, A. G.; Escobedo-Uribe, K. M.; Sánchez-Muñoz, S.; Luévanos-Escareño, M. P.; Hernández-Terán, F.; Alvarado, A.; Balagurusamy, N. Bioconversion of Lignocellulosic Biomass into Value Added Products under Anaerobic

Conditions: Insight into Proteomic Studies. *IJMS* **2021**, *22* (22), 12249. https://doi.org/10.3390/ijms222212249.

(39) Magda, R.; Szlovák, S.; Tóth, J. The Role of Using Bioalcohol Fuels in Sustainable Development. In *Bio-Economy and Agri-production*; Elsevier, 2021; pp 133–146. https://doi.org/10.1016/B978-0-12-819774-5.00007-2.

(40) Brennan, L.; Owende, P. Biofuels from Microalgae—A Review of Technologies for Production, Processing, and Extractions of Biofuels and Co-Products. *Renewable and Sustainable Energy Reviews* **2010**, *14* (2), 557–577. https://doi.org/10.1016/j.rser.2009.10.009.

(41) Searchinger, T.; Heimlich, R.; Houghton, R. A.; Dong, F.; Elobeid, A.; Fabiosa, J.; Tokgoz, S.; Hayes, D.; Yu, T.-H. Use of U.S. Croplands for Biofuels Increases Greenhouse Gases Through Emissions from Land-Use Change. *Science* **2008**, *319* (5867), 1238–1240. https://doi.org/10.1126/science.1151861.

(42) Chisti, Y. Biodiesel from Microalgae. *Biotechnology Advances* **2007**, *25* (3), 294–306. https://doi.org/10.1016/j.biotechadv.2007.02.001.

(43) Metting, F. B. Biodiversity and Application of Microalgae. *Journal of Industrial Microbiology & Biotechnology* **1996**, *17* (5–6), 477–489. https://doi.org/10.1007/BF01574779.

(44) Spolaore, P.; Joannis-Cassan, C.; Duran, E.; Isambert, A. Commercial Applications of Microalgae. *Journal of Bioscience and Bioengineering* **2006**, *101* (2), 87–96. https://doi.org/10.1263/jbb.101.87.

(45) Dismukes, G. C.; Carrieri, D.; Bennette, N.; Ananyev, G. M.; Posewitz, M. C. Aquatic Phototrophs: Efficient Alternatives to Land-Based Crops for Biofuels. *Current Opinion in Biotechnology* **2008**, *19* (3), 235–240. https://doi.org/10.1016/j.copbio.2008.05.007.

(46) Saha, S.; Sharma, A.; Purkayastha, S.; Pandey, K.; Dhingra, S. Bio-Plastics and Biofuel. In *Plastics to Energy*; Elsevier, 2019; pp 365–376. https://doi.org/10.1016/B978-0-12-813140-4.00014-5.

(47) Hussian, A. E. M. The Role of Microalgae in Renewable Energy Production: Challenges and Opportunities. In *Marine Ecology - Biotic and Abiotic Interactions*; Türkoğlu, M., Önal, U., Ismen, A., Eds.; InTech, 2018. https://doi.org/10.5772/intechopen.73573.

(48) Molazadeh, M.; Ahmadzadeh, H.; Pourianfar, H. R.; Lyon, S.; Rampelotto, P. H. The Use of Microalgae for Coupling Wastewater Treatment With CO2 Biofixation. *Front. Bioeng. Biotechnol.* **2019**, *7*, 42. https://doi.org/10.3389/fbioe.2019.00042.

(49) Liang, Y.; Sarkany, N.; Cui, Y.; Yesuf, J.; Trushenski, J.; Blackburn, J. W. Use of Sweet Sorghum Juice for Lipid Production by Schizochytrium Limacinum SR21. *Bioresource Technology* **2010**, *101* (10), 3623–3627. https://doi.org/10.1016/j.biortech.2009.12.087.

(50) Suali, E.; Sarbatly, R. Conversion of Microalgae to Biofuel. *Renewable and Sustainable Energy Reviews* **2012**, *16* (6), 4316–4342. https://doi.org/10.1016/j.rser.2012.03.047.

(51) Rana, M. S.; Prajapati, S. K. Stimulating Effects of Glycerol on the Growth, Phycoremediation and Biofuel Potential of Chlorella Pyrenoidosa Cultivated in Wastewater. *Environmental Technology & Innovation* **2021**, *24*, 102082. https://doi.org/10.1016/j.eti.2021.102082.

(52) Nahak, S.; Nahak, G.; Pradhan, I.; Sahu, R. K. Bioethanol from Marine Algae: A Solution to Global Warming Problem. *Journal of Applied Environmental and Biological Sciences* **2011**, *1* (4), 74–80.

(53) Miao, X.; Wu, Q. High Yield Bio-Oil Production from Fast Pyrolysis by Metabolic Controlling of Chlorella Protothecoides. *Journal of Biotechnology* **2004**, *110* (1), 85–93. https://doi.org/10.1016/j.jbiotec.2004.01.013.

(54) Du, Z.; Li, Y.; Wang, X.; Wan, Y.; Chen, Q.; Wang, C.; Lin, X.; Liu, Y.; Chen, P.; Ruan, R. Microwave-Assisted Pyrolysis of Microalgae for Biofuel Production. *Bioresource Technology* **2011**, *102* (7), 4890–4896. https://doi.org/10.1016/j.biortech.2011.01.055.

(55) Grierson, S.; Strezov, V.; Ellem, G.; Mcgregor, R.; Herbertson, J. Thermal Characterisation of Microalgae under Slow Pyrolysis Conditions. *Journal of Analytical and Applied Pyrolysis* **2009**, *85* (1–2), 118–123. https://doi.org/10.1016/j.jaap.2008.10.003.

(56) Abanades, S.; Abbaspour, H.; Ahmadi, A.; Das, B.; Ehyaei, M. A.; Esmaeilion, F.; El Haj Assad, M.; Hajilounezhad, T.; Jamali, D. H.; Hmida, A.; Ozgoli, H. A.; Safari, S.; AlShabi, M.; Bani-Hani, E. H. A Critical Review of Biogas Production and Usage with Legislations Framework across the Globe. *Int. J. Environ. Sci. Technol.* **2022**, *19* (4), 3377–3400. https://doi.org/10.1007/s13762-021-03301-6.

(57) Chong, Z. R.; Yang, S. H. B.; Babu, P.; Linga, P.; Li, X.-S. Review of Natural Gas Hydrates as an Energy Resource: Prospects and Challenges. *Applied Energy* **2016**, *162*, 1633–1652. https://doi.org/10.1016/j.apenergy.2014.12.061.

Chapter 5. Synthesis and Characterization of High-Performance Renewable Diesel Fuel from Bioderived 1-Octen-3-ol

***** *Sections of this chapter were reproduced from the following publication with permission from Dr. Benjamin Harvey, the principal investigator of the project at the Naval Air Weapons Station China Lake (Ridgecrest, CA). The author of this Ph. D. thesis, Manhao Zeng, is a coauthor of this publication who contributed to experimental design, performed reactions, and analyzed research data relevant to this work.*

Siirila, M. J.; **Zeng, M.**; Woodroffe, J.-D.; Askew, R. L.; Harvey, B. G. Synthesis and Characterization of High-Performance Renewable Diesel Fuel from Bioderived 1-Octen-3-ol. *Energy Fuels* **2020**, *34* (7), 8325–8331. https://doi.org/10.1021/acs.energyfuels.0c00120.

5.1 Abstract

Because the extraction of fossil fuels contributes to climate change, environmental pollution, and deleterious health effects, efforts have been made to develop alternative strategies to derive energy from renewable, nonpetroleum-based resources. Herein, 1-octen-3-ol, a bioavailable alcohol, was converted to a high-performance $C_{16}H_{32}$ biodiesel using a straightforward three-step protocol with mostly high yields and conversions: (1) dehydration [58% yield], (2) Diels-Alder cyclodimerization [92% conversion], and (3) hydrogenation [95% yield]. With a high gravimetric net heat of combustion of 43.41 MJ/L (17% greater than that of traditional diesel) and a cetane number of 71 (more than 30 units greater than that of the

minimum for diesel fuel), this exceptional, renewable biofuel surpasses the performance of conventional diesels.

5.2 Introduction

Today, 84% of the world's energy comes from combusting fossil fuels.[1] The methods to extract these materials from within the Earth, however, results in environmental pollution, societal exposure to toxic heavy metals, contamination of drinking water, and other negative externalities.[2–4] While there is growing interest in developing more sustainable alternatives using biomass to overcome the challenges presented with petroleum, a minority of the world's energy comes from bio-based sources (only 12% in 2019).[5]

To enhance the viability of using biomass to create energy, researchers have developed four generations of biofuels with each subsequent generation being more advantageous than the previous.[6] While the first and second generation technologies are mostly based upon plant and animal matter, the chemicals developed using third and fourth generation technologies rely on microorganisms.[6–8] Using these renewable methods, triglycerides and alcohols can be extracted from biomass and transesterified (Scheme 4.1) to produce bio-diesel grade fatty acid methyl esters (FAMEs, Figure 5.1).[9–11]

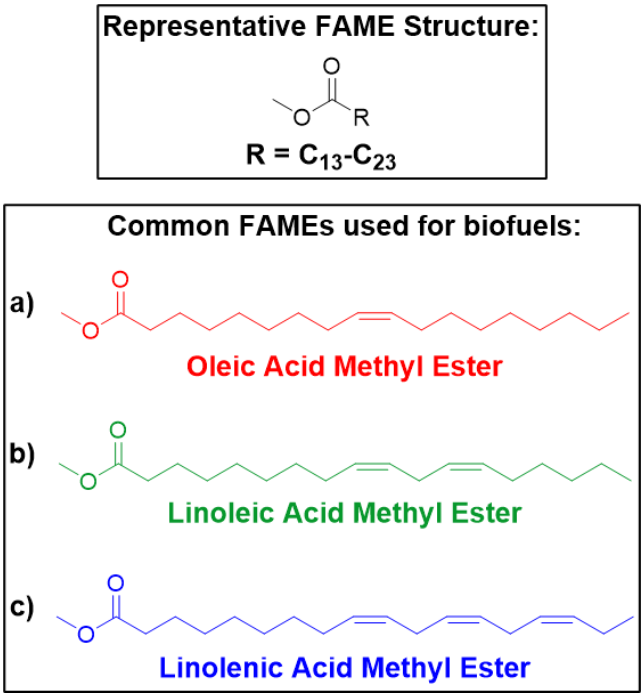

Figure 5.1 Representative chemical composition of fatty acid methyl esters (FAMEs) and examples of common FAMEs (unsaturated C_{18} methyl esters) used for biofuels.[10]

As the most prevalent source of biodiesel, FAMEs improve the performance of the combustion engine, among other advantages.[12] Compared to conventional diesel fuels from petroleum, FAMEs also emit less carbon monoxide and fewer hazardous particulates such as sulfur dioxide when burned and have greater cetane numbers, a notable characteristic which pertains to the combustion quality attributable to diesel fuels.[13–15] In practice, the advantages of FAMEs are maximized when they are used as formulations with commercial diesel fuels at 20-50% ratios.[10] Because the oxygen content in the ester functional group of FAMEs limits the net heat of combustion from these biodiesels by 10%, these biodiesels are normally mixed with other sources.[16,17] Other disadvantages to using these chemicals for biofuel include undesired transesterification reactions with the ambient moisture in air that degrade FAMEs into acids which may cause corrosion while oxidation of the unsaturated hydrocarbons present

in the backbone of some FAMEs (Figure 5.1) also reduces their combustion properties.[18] To address the molecular instability of renewable biodiesels, research has been performed to catalytically hydrogenate alkenes and deoxygenate fatty acids using processes such as hydrodeoxygenation where oxygen is released in the form of water to generate aliphatic hydrocarbons[19] with linear structures that have average volumetric densities and net heats of combustion. Incorporating alkanes with cyclic structures, however, has been demonstrated to provide superior biofuels with higher volumetric densities and net heats of combustion.[20–23]

In this work, high-performance biodiesel grade compounds were synthesized from 1-octen-3-ol, a renewable alcohol that can be derived from bioavailable linoleic acid[24–27] under a simple three-step process (Scheme 5.1) involving (1) dehydration, (2) Diels-Alder cyclodimerzation, and (3) hydrogenation to yield $C_{16}H_{32}$ isomers with cyclic and aliphatic components. Afterwards, the fuel properties of these chemicals are investigated and compared to those from both traditional and alternative renewable fuels.

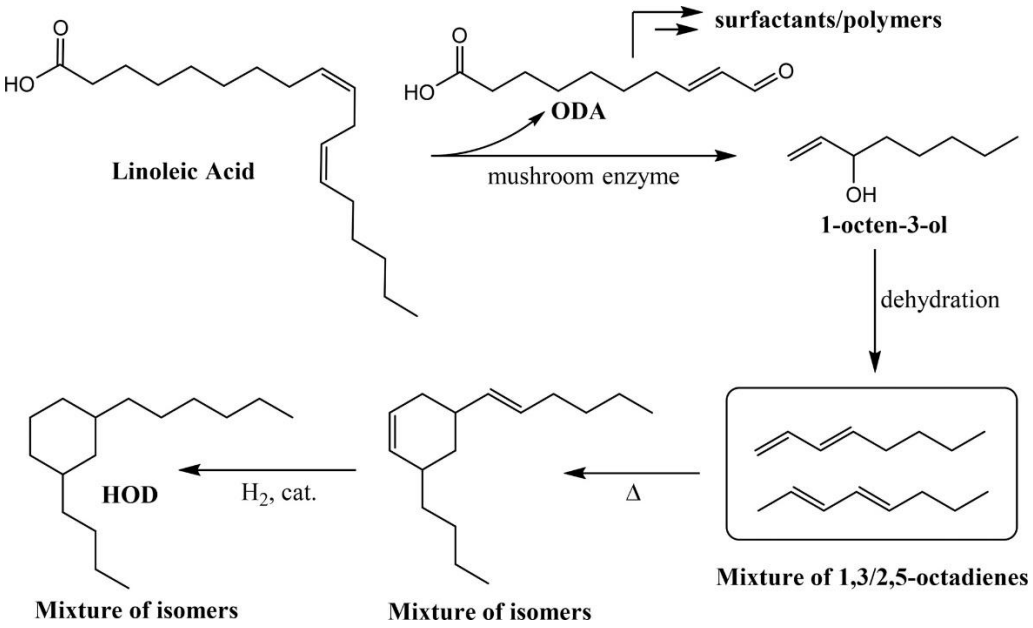

Scheme 5.1 Synthesis of high-performance $C_{16}H_{32}$ diesel fuel from bio-based chemicals.

5.3 Results and Discussion

1-Octen-3-ol was dehydrated using *p*-toluenesulfonic acid as the catalyst. The oil bath temperature was maintained at about 140–150 °C to allow for efficient distillation of water and dienes, while limiting the distillation of the starting material, which has a boiling point of 175 °C. Simple dehydration would be expected to yield cis- and trans-1,3-octadiene, but acid catalyzed isomerization also generated various geometric isomers of 2,4-octadiene. A gas chromatogram of the dienes (Figure 5.2) revealed six isomers. The two geometric isomers of 1,3-octadiene were found to elute first and represented 45% of the total chromatogram area. Four geometric isomers of 2,4-octadiene were also observed, representing 53% of the chromatogram area. A small amount of the starting material was present in the distillate but typically only accounted for about 2% of the chromatogram area. As expected, the NMR spectra were quite complicated (Figures C.1 and C.2) due to the presence of several different species.

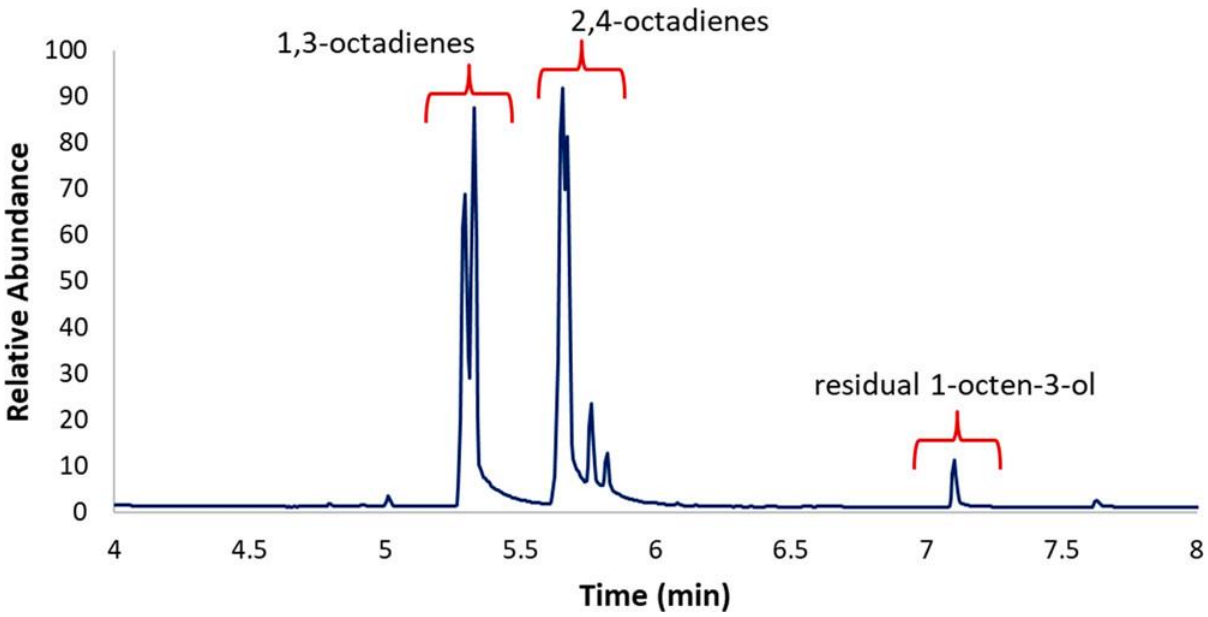

Figure 5.2 Gas chromatogram of octadiene dimers prepared via dehydration of 1-octen-3-ol.

With significant quantities of octadienes available for study, conditions were explored for the efficient conversion of these mixtures to blends of monocyclic C_{16} compounds. Some initial catalytic studies were conducted with $LFe(NO)_2Cl$ (L = triphenylphosphine oxide)[28] and $[Fe(NO)_2Cl]_2$ at temperatures ranging from ambient up to 100 °C,[29,30] but in contrast to successful cycloaddition results with isoprene,[28,31] only modest amounts of dimers were observed. Using previous thermal dimerization studies of isoprene and 1,3-pentadiene,[32-34] we transitioned to a catalyst-free method. The octadiene mixture was dimerized in an autoclave at 240 °C under a nitrogen atmosphere. This approach allowed for elimination of both a reaction solvent and catalyst, reducing chemical waste and the need for additional purification steps. This procedure resulted in an octadiene conversion of >90% and a dimer:trimer ratio of 7.8 (Figure 5.3). The product mixture was simply decanted from the autoclave and then subjected to hydrogenation. Although the hydrogenation step could likely have been conducted without additional solvent, to enhance the reaction rate and allow for a complete reaction under modest conditions, hexanes and acetic acid were added to the hydrocarbon mixture. After hydrogenation, the acetic acid was readily removed by a water/dilute base wash and the C_{16} fraction was then isolated by fractional vacuum distillation. The ^{1}H NMR spectrum of the hydrogenated octadiene dimers (HOD**)** revealed complete conversion to saturated cycloalkanes (Figure C.4), while GC–MS analysis demonstrated the effective removal of heavier oligomers (Figure C.5).

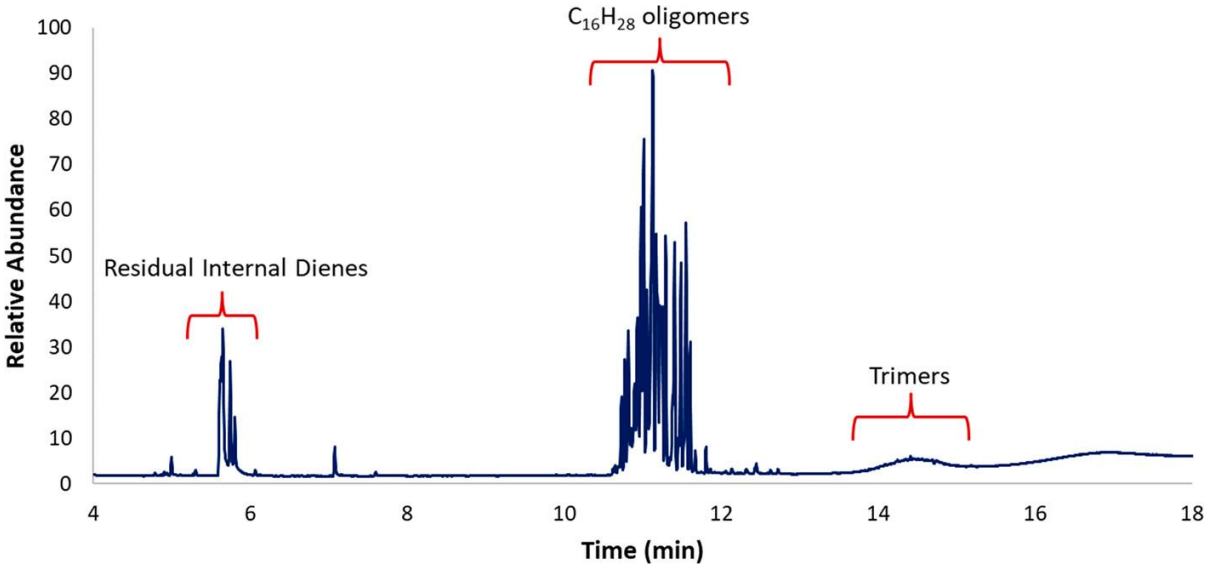

Figure 5.3 Gas chromatogram of crude octadiene oligomers.

The elemental analysis results strongly supported a molecular formula of $C_{16}H_{32}$, consistent with monocyclic products. In addition, the density of HOD was 0.835 g/mL, substantially higher than that of the acyclic $C_{16}H_{34}$ compound hexadecane (ρ = 0.773 g/mL). The higher density of HOD can be attributed to the confinement of six carbons from each isomer to a cyclohexane ring. Due to the generation of multiple isomers, the NMR spectra were quite complicated and not diagnostic of the fuel composition. However, the gas chromatogram exhibited 14 significant peaks, consistent with the expected number of constitutional isomers (Figure 5.4). Isomers **1**–**4** were generated by homodimerization of 1,3-octadiene, while isomers **5**–**7** resulted from the cross-dimerization of 1,3-octadiene and 2,4-octadiene. Finally, isomers **8**–**14** were generated by homodimerization of 2,4-octadiene. Steric effects suggested that **1**, **5**, and **13** were the most abundant isomers. In addition to the constitutional isomers, numerous diastereomers are also present, but the overlap of peaks in the GC precluded a more detailed treatment.

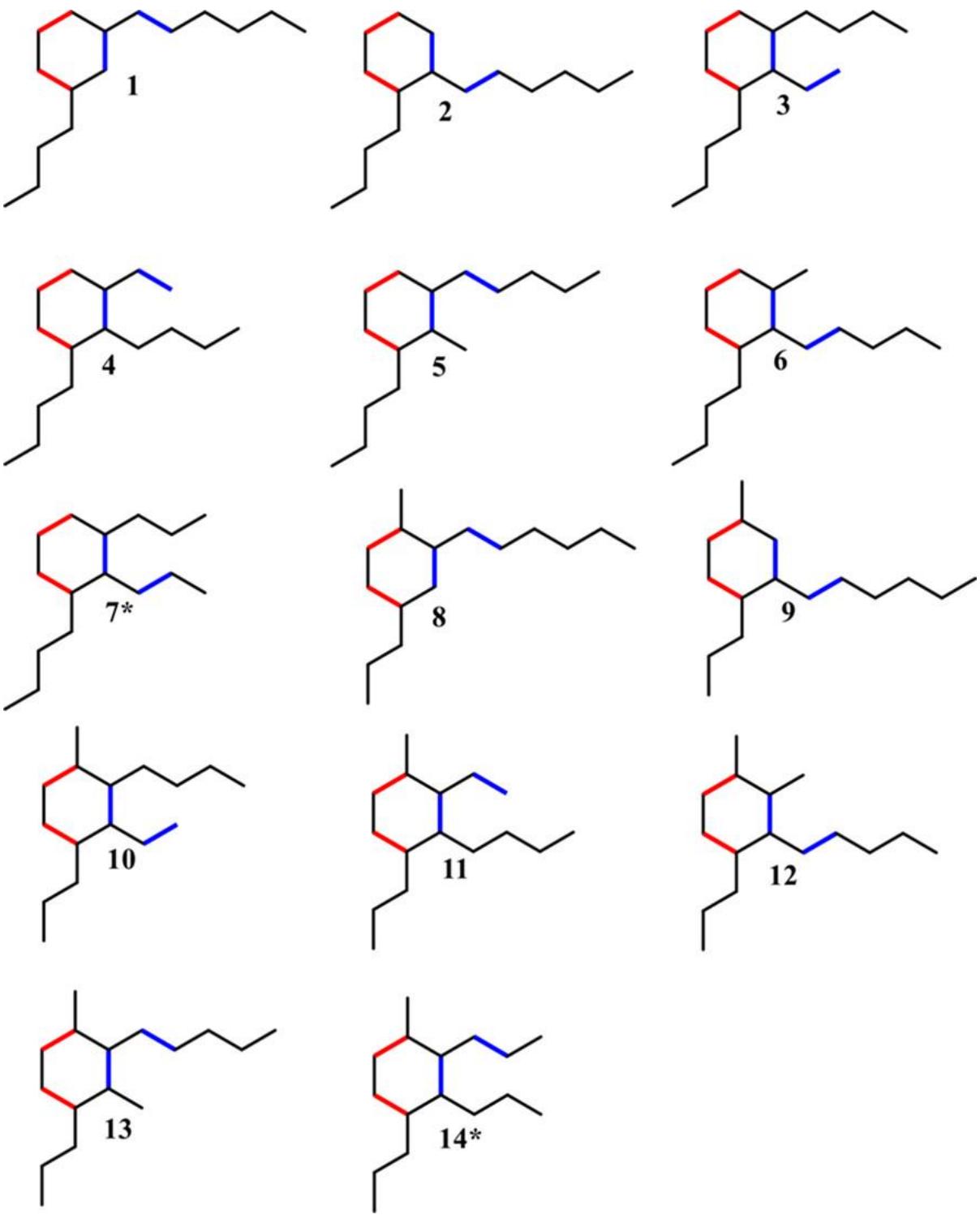

Figure 5.4 Constitutional isomers present in HOD**.** The red and blue lines denote the location of the original dienes. An asterisk (*) next to a compound number indicates that the saturated compound could have been isolated from either of two different alkene regioisomers.

Fuel Properties

To evaluate HOD as a potential diesel fuel surrogate, the density, flashpoint, heat of combustion, low temperature thermomechanical properties, and kinematic viscosity of the dimer mixture were measured (Table 5.1). As mentioned above, the density of HOD was 0.835 g/mL, which is ~8% higher than that of Jet-A (>0.775 g/mL), 11% higher than that of typical synthetic paraffinic kerosenes like hydrotreated fatty acids and esters (e.g. HEFA-Jet, $d \sim 0.75$ g/mL), 7% higher than that of hydrotreated renewable diesel (HRD), and comparable to that of petroleum-derived diesel fuel (~0.826–0.859 g/mL).[35] The flashpoint of HOD was 106 °C. This value is significantly higher than that required for Diesel #2 (>50 °C), but quite comparable to soy biodiesel, which has a reported flashpoint of 104 °C.[36] The volumetric net heat of combustion was 36.25 MJ/L, approximately 11% higher than that of biodiesel, 5–7% higher than that of HRD, and comparable to that of petroleum-derived diesel fuel. The gravimetric NHOC of HOD was 43.41 MJ/kg, which is 1.3% higher than that of conventional diesel fuel and 17% higher than that of soy biodiesel.[37] This increase in gravimetric NHOC can be attributed to the lack of ester groups present in biodiesel, and aromatic compounds, which comprise up to 40% of petroleum-derived diesel fuel. The reported gravimetric NHOC of HRD is 1.6% higher than that of HOD due to its higher hydrogen content.

Table 5.1 Fuel Properties of Conventional Fuels, Biodiesel, and HOD

fuel	density (g/mL)	NHOC (MJ/L)	NHOC (MJ/kg)	η[a] (40 °C, mm^2/s)	cetane number	flash point (°C)
Jet-A	>0.775	>33.17	>42.8	N/A		>38
Diesel #2	0.826−0.859	~35.95	~42.8	2.1−4.1	>40	>50
soy biodiesel[b]	0.882	32.64	37.01	4.26	51	104[c]
HRD (NExBTL)[d]	0.775−0.785	~34	~44	2.9−3.5	84−99[e]	
HOD	0.835	36.25	43.41	3.69	71[f]	106

[a] η refers to kinematic viscosity. [b] Values taken from reference (37). [c] Reference (36). [d] Neste Oil hydrotreated/isomerized vegetable oil.[38] [e] Blending cetane number. [f] Derived cetane number measured by IQT.

The cetane number of a diesel fuel is critical for suitable performance under compression ignition conditions. The cetane number is inversely proportional to ignition delay, with long alkyl chains resulting in short ignition delays (high cetane numbers) and highly branched molecules, aromatics, and most multicyclic compounds having low cetane numbers.[21,39,40] Given the monocyclic structure of the molecules in the HOD mixture and the significant chain branching resulting from the 2,4-octadienes, it was not clear if the cetane number of HOD would be high enough (>40) for efficient combustion in a conventional diesel engine. The derived cetane number of HOD was measured by IQT and found to be 71.2, more than 30 units higher than the lower limit for petroleum diesel, and 20 units higher than soy biodiesel.[37] This remarkable DCN suggests that HOD can be used as a significant component of commercial diesel fuel, or as an additive to upgrade lower cetane fuels.

Although the HOD mixture is complex, and the origins of the high DCN are not completely understood, consideration of the major components of HOD, including 1-butyl-3-hexylcylohexane (**1**), 1-butyl-2,3-dipropylcyclohexane (**7**), and 1,3-dimethyl-2-pentyl-4-propylcyclohexane (**13**) can provide some insight. Neglecting the cyclic nature of the isomers, **1** has a continuous 15-carbon chain with branch sites at the 5- and 9-positions. Similarly, **7** has

a continuous 12-carbon chain with branch sites at the 4- and 8-positions, while **13** has a 13-carbon chain with branch sites at the 4-, 7-, and 8-positions. As a comparison, tridecane, has a reported cetane number of approximately 80,[41] while 7-butyltridecane and farnesane (2,6,10-trimethyldodecane) have reported cetane numbers of 70 and 59, respectively.[39] These examples demonstrate that increasing the number of branch sites decreases the cetane number of the hydrocarbon. However, in the case of HOD, the impact of multiple branch sites is minor, leading to a DCN decrease of only a few units compared to the analogous linear hydrocarbons. A more direct comparison with representative C_{16} cycloalkanes is not currently viable, given the lack of literature data. However, recent work has shown that C_{12}-C_{15} alkyl diamondoids (highly branched multicyclic alkanes with fused cyclohexane ring systems and short alkyl chains) have reported DCNs ranging from 43 to 49,[20,22,23] suggesting that cyclohexane ring systems do not have a significant negative impact on the DCN of parent hydrocarbons.

In addition to high cetane numbers, good cold flow properties are critical for the use of diesel fuels at subambient temperatures. HOD exhibited excellent low temperature properties with no freezing point observed by differential scanning calorimetry (DSC) and a glass transition temperature of −90 °C via thermomechanical analysis. In contrast, soy biodiesel has a freezing point of around 0 °C,[37] while Diesel #2 has a required pour point of less than −3 °C.

The kinematic viscosity of HOD over the temperature range of −20 to 40 °C is shown in Figure 5.5. The kinematic viscosity of HOD at 40 °C was 3.69 mm^2/s, which is within the acceptable range for Diesel #2 (2.1–4.1 mm^2/s), and 13% lower than that of soy biodiesel. In addition, although the kinematic viscosity of HOD at −20 °C was nearly 50 mm^2/s, recent studies with C_{15} multicyclic sesquiterpanes having similar viscosities suggested that significant quantities of HOD could be blended with low viscosity synthetic paraffinic kerosenes (SPKs),

or petroleum-derived jet fuel, while maintaining the −20 °C viscosity requirements for Jet-A (8.0 mm^2/s).[21,42] To determine the maximum amount of HOD that could be blended in conventional jet fuel while still meeting the viscosity specification, a series of blends were prepared ranging from 10 to 40% HOD in Jet-A (Table C.1-C.5). The −20 °C kinematic viscosities for the blends ranged from 4.86–8.59 mm^2/s (Figure 5.6), with the 30% blend exhibiting a kinematic viscosity of 6.96 mm^2/s at −20 °C, well within the specification for Jet-A (<8.0 mm^2/s). Although not included in the specification for Jet-A, fuels with viscosities above 12.0 mm^2/s at −40 °C can be problematic due to potential difficulties in the ability to relight engines at altitude.[43] The −40 °C kinematic viscosity of the 15% HOD blend was 12.27 mm^2/s, while the 20% blend had a −40 °C kinematic viscosity of 13.25 mm^2/s. Using the more stringent viscosity limit at −40 °C, the maximum amount of HOD that can be safely blended with Jet-A is around 15%.

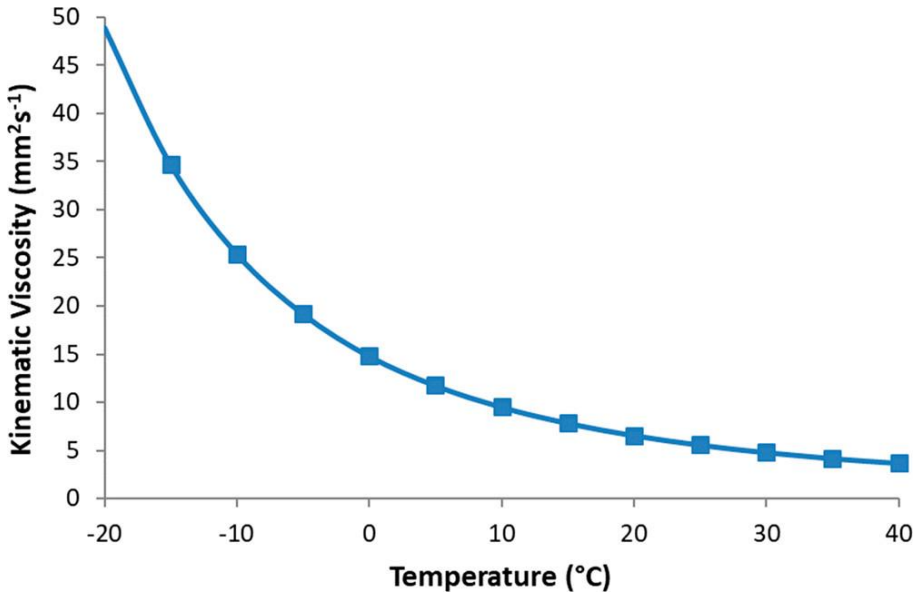

Figure 5.5 Kinematic viscosity of HOD between −20 and 40 °C.

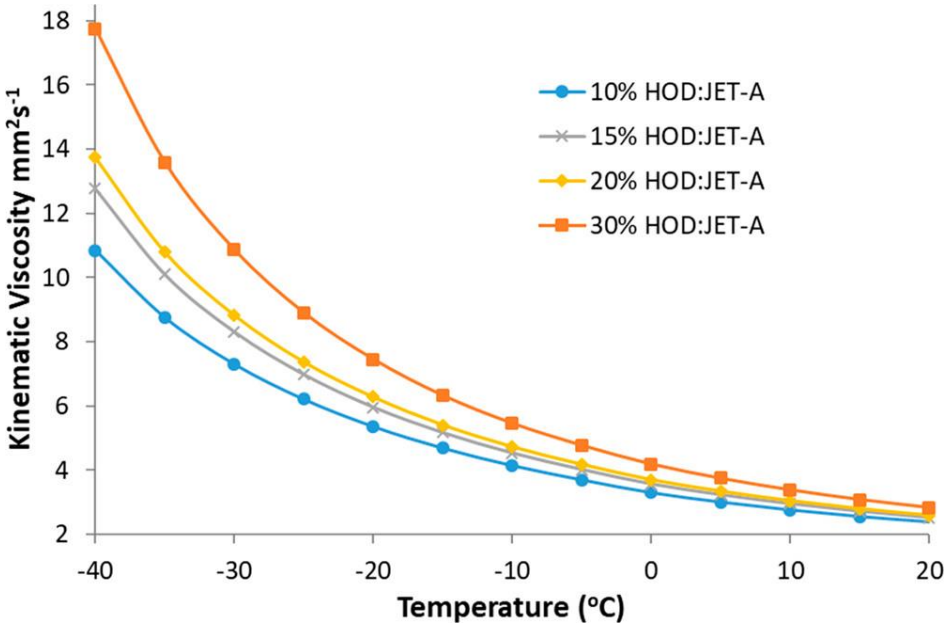

Figure 5.6 Kinematic viscosity of HOD/Jet-A blends from −40 to 20 °C.

Several other methods have recently been explored for the synthesis of cycloalkanes with intermediate length alkyl chains. For example, Huber synthesized a mixture of butylcyclopentane and 1,3-dibutylcyclopentane from bio-based butanal and cyclopentanone. The mixture of these components had a density of 0.82 g/mL and a freezing point of −93.8 °C.[44] Zhang et al. synthesized 1,1-dipentylcyclohexane through alkylation of 2-methylfuran with cyclohexanone, followed by hydrodeoxygenation.[45] The resulting fuel blendstock exhibited a density of 0.825 g/mL and a freezing point of −26.4 °C. Similarly, 1,1-dipentylcyclopentane was prepared from cyclopentanone and 2-methylfuran to obtain a fuel product with a density of 0.819 g/mL and a freezing point of −33.6 °C.[46] Zou et al. explored a series of 1,3-disubstituted cyclopentanes and cyclohexanes with pentyl or hexyl substituents.[47] These fuel mixtures exhibited densities ranging from 0.815–0.826 g/mL and freezing points ranging from −24.6 to −9.5 °C. In comparison to these examples, HOD exhibited a higher density and lower freezing point when molecules having similar molecular weights were

considered. More in-depth comparisons of key fuel properties, including cetane numbers and NHOCs, were not possible due to the lack of information in the literature.

Perhaps most relevant to the current discussion, Staples *et al.* recently reported the synthesis of C_{20} cycloalkanes by Diels–Alder cyclodimerization of the acyclic monoterpene myrcene followed by hydrogenation.[48] The resulting mixture, designated as camphorane, exhibited a density of 0.826 g/mL, a 40 °C kinematic viscosity of 9.32 mm^2/s, a gravimetric NHOC of 43.23 MJ/kg, and a derived cetane number of 57.6. In comparison, HOD has a 1.1% higher density, 60% lower kinematic viscosity at 40 °C, 0.4% higher gravimetric NHOC, and 23% higher DCN than that of camphorane.

5.4 Conclusion

Starting with 1-octen-3-ol, a renewable starting material, an effective three-step process with mostly high yields and conversions involving (1) dehydration [58% yield], (2) Diels-Alder cyclodimerization [92% conversion], and (3) hydrogenation [95% crude yield] was conducted to obtain high performance $C_{16}H_{32}$ diesels with cyclic and aliphatic components that contributed to their robust properties. Notably, these renewable biofuels had net heats of combustions that were 11% and 1.3% greater than those of soy and petroleum-based diesels, respectively. While mediocre cetane numbers of 50 are considered favorable for traditional and renewable biodiesels, HOD outperforms both with an exceptional cetane number of 71, thus demonstrating its potential to replace conventional biodiesels in the future.

5.5 Acknowledgements

Funding for this research was provided in part by the Naval Air Warfare Center, Weapons Division PL-219 program.

5.6 References

(1) Bp. Statistical Review of World Energy 2021 | 70th Edition, 2021. Https://Www.Bp.Com/Content/Dam/Bp/Business-Sites/En/Global/Corporate/Pdfs/Energy-Economics/Statistical-Review/Bp-Stats-Review-2021-Full-Report.Pdf.

(2) TENORM, Oil and Gas Production Wastes. Https://Www.Epa.Gov/Radiation/Tenorm-Oil-and-Gas-Production-Wastes (Accessed May 24, 2022).

(3) U.S. EPA. Plan to Study the Potential Impacts of Hydraulic Fracturing on Drinking Water Resources (EPA/600/R-11/122A), 2011, Https://Data.Globalchange.Gov/Report/Epa-600-r-11-122#.

(4) Colborn, T.; Kwiatkowski, C.; Schultz, K.; Bachran, M. Natural Gas Operations from a Public Health Perspective. *Human and Ecological Risk Assessment: An International Journal* **2011**, *17* (5), 1039–1056. https://doi.org/10.1080/10807039.2011.605662.

(5) C2ES, Renewable Energy, Https://Www.C2es.Org/Content/Renewable-Energy/ (Accessed June 1, 2022).

(6) Mat Aron, N. S.; Khoo, K. S.; Chew, K. W.; Show, P. L.; Chen, W.; Nguyen, T. H. P. Sustainability of the Four Generations of Biofuels – A Review. *Int J Energy Res* **2020**, *44* (12), 9266–9282. https://doi.org/10.1002/er.5557.

(7) Moodley, P. Sustainable Biofuels: Opportunities and Challenges. In *Sustainable Biofuels*; Elsevier, 2021; pp 1–20. https://doi.org/10.1016/B978-0-12-820297-5.00003-7.

(8) Correa, D. F.; Beyer, H. L.; Possingham, H. P.; Thomas-Hall, S. R.; Schenk, P. M. Biodiversity Impacts of Bioenergy Production: Microalgae vs. First Generation Biofuels. *Renewable and Sustainable Energy Reviews* **2017**, *74*, 1131–1146. https://doi.org/10.1016/j.rser.2017.02.068.

(9) Fukuda, H.; Kondo, A.; Noda, H. Biodiesel Fuel Production by Transesterification of Oils. *Journal of Bioscience and Bioengineering* **2001**, *92* (5), 405–416. https://doi.org/10.1016/S1389-1723(01)80288-7.

(10) Kim, J.-K.; Jeon, C.-H.; Lee, H.; Park, Y.-K.; Min, K.; Hwang, I.; Kim, Y.-M. Effect of Accelerated High Temperature on Oxidation and Polymerization of Biodiesel from Vegetable Oils. *Energies* **2018**, *11* (12), 3514. https://doi.org/10.3390/en11123514.

(11) Yaakob, Z.; Mohammad, M.; Alherbawi, M.; Alam, Z.; Sopian, K. Overview of the Production of Biodiesel from Waste Cooking Oil. *Renewable and Sustainable Energy Reviews* **2013**, *18*, 184–193. https://doi.org/10.1016/j.rser.2012.10.016.

(12) Awogbemi, O.; Inambao, F.; Onuh, E. I. Optimization of FAME Composition for Improved Engine Performance and Emissions Reduction. *International Journal of Low-Carbon Technologies* **2020**, *15* (4), 583–593. https://doi.org/10.1093/ijlct/ctaa027.

(13) Miraboutalebi, S. M.; Kazemi, P.; Bahrami, P. Fatty Acid Methyl Ester (FAME) Composition Used for Estimation of Biodiesel Cetane Number Employing Random Forest and Artificial Neural Networks: A New Approach. *Fuel* **2016**, *166*, 143–151. https://doi.org/10.1016/j.fuel.2015.10.118.

(14) Piloto-Rodríguez, R.; Sánchez-Borroto, Y.; Lapuerta, M.; Goyos-Pérez, L.; Verhelst, S. Prediction of the Cetane Number of Biodiesel Using Artificial Neural Networks and Multiple Linear Regression. *Energy Conversion and Management* **2013**, *65*, 255–261. https://doi.org/10.1016/j.enconman.2012.07.023.

(15) Bai, A.; Jobbágy, P.; Popp, J.; Farkas, F.; Grasselli, G.; Szendrei, J.; Balogh, P. Technical and Environmental Effects of Biodiesel Use in Local Public Transport. *Transportation Research Part D: Transport and Environment* **2016**, *47*, 323–335. https://doi.org/10.1016/j.trd.2016.06.009.

(16) Etim, A. O.; Jisieike, C. F.; Ibrahim, T. H.; Betiku, E. Biodiesel and Its Properties. In *Production of Biodiesel from Non-Edible Sources*; Elsevier, 2022; pp 39–79. https://doi.org/10.1016/B978-0-12-824295-7.00004-8.

(17) Lopes, S. M.; Furey, R.; Geng, P. Calculation of Heating Value for Diesel Fuels Containing Biodiesel. *SAE Int. J. Fuels Lubr.* **2013**, *6* (2), 407–418. https://doi.org/10.4271/2013-01-1139.

(18) Sugiyama, G.; Maeda, A.; Nagai, K. Oxidation Degradation and Acid Generation in Diesel Fuel Containing 5% FAME; 2007; pp 2007-01–2027. https://doi.org/10.4271/2007-01-2027.

(19) Ameen, M.; Azizan, M. T.; Yusup, S.; Ramli, A.; Yasir, M. Catalytic Hydrodeoxygenation of Triglycerides: An Approach to Clean Diesel Fuel Production. *Renewable and Sustainable Energy Reviews* **2017**, *80*, 1072–1088. https://doi.org/10.1016/j.rser.2017.05.268.

(20) Harrison, K. W.; Harvey, B. G. Renewable High Density Fuels Containing Tricyclic Sesquiterpanes and Alkyl Diamondoids. *Sustainable Energy Fuels* **2017**, *1* (3), 467–473. https://doi.org/10.1039/C6SE00108D.

(21) Harvey, B. G.; Merriman, W. W.; Koontz, T. A. High-Density Renewable Diesel and Jet Fuels Prepared from Multicyclic Sesquiterpanes and a 1-Hexene-Derived Synthetic Paraffinic Kerosene. *Energy Fuels* **2015**, *29* (4), 2431–2436. https://doi.org/10.1021/ef5027746.

(22) Harrison, K. W.; Rosenkoetter, K. E.; Harvey, B. G. High Density Alkyl Diamondoid Fuels Synthesized by Catalytic Cracking of Alkanes in the Presence of Adamantane. *Energy Fuels* **2018**, *32* (7), 7786–7791. https://doi.org/10.1021/acs.energyfuels.8b00792.

(23) Harvey, B. G.; Harrison, K. W.; Davis, M. C.; Chafin, A. P.; Baca, J.; Merriman, W. W. Molecular Design and Characterization of High-Cetane Alkyl Diamondoid Fuels. *Energy Fuels* **2016**, *30* (12), 10171–10178. https://doi.org/10.1021/acs.energyfuels.6b01865.

(24) Assaf, S.; Hadar, Y.; Dosoretz, C. G. Biosynthesis of 13-Hydroperoxylinoleate, 10-Oxo-8-Decenoic Acid and 1-Octen-3-Ol from Linoleic Acid by a Mycelial-Pellet Homogenate of Pleurotus Pulmonarius. *J. Agric. Food Chem.* **1995**, *43* (8), 2173–2178. https://doi.org/10.1021/jf00056a040.

(25) Morawicki, R. O.; Beelman, R. B. Study of the Biosynthesis of 1-Octen-3-Ol Using a Crude Homogenate of Agaricus Bisporus in a Bioreactor. *J Food Science* **2008**, *73* (3), C135–C139. https://doi.org/10.1111/j.1750-3841.2007.00660.x.

(26) Morawicki, R. O.; Beelman, R. B.; Peterson, D.; Ziegler, G. Biosynthesis of 1-Octen-3-Ol and 10-Oxo-Trans-8-Decenoic Acid Using a Crude Homogenate of Agaricus Bisporus. *Process Biochemistry* **2005**, *40* (1), 131–137. https://doi.org/10.1016/j.procbio.2003.11.037.

(27) Ahmed, M. U.; Dunn, J. A.; Walla, M. D.; Thorpe, S. R.; Baynes, J. W. Oxidative Degradation of Glucose Adducts to Protein. Formation of 3-(N Epsilon-Lysino)-Lactic Acid from Model Compounds and Glycated Proteins. *Journal of Biological Chemistry* **1988**, *263* (18), 8816–8821. https://doi.org/10.1016/S0021-9258(18)68379-6.

(28) Strope, D. J. Phillips Petroleum Company, Bartlesville, OK. US Patent 4144278, 1979.

(29) Ligabue, R. A.; Dupont, J.; de Souza, R. F. Liquid–Liquid Two-Phase Cyclodimerization of 1,3-Dienes by Iron-Nitrosyl Dissolved in Ionic Liquids. *Journal of Molecular Catalysis A: Chemical* **2001**, *169* (1–2), 11–17. https://doi.org/10.1016/S1381-1169(00)00550-1.

(30) Ballivet-Tkatchenko, D.; Billard, C.; Revillon, A. Cationic Metal Nitrosyl Complexes. IV. Polymerization of Olefins with Dinitrosyl Iron Complexes. *J. Polym. Sci. Polym. Chem. Ed.* **1981**, *19* (7), 1697–1706. https://doi.org/10.1002/pol.1981.170190710.

(31) Maxfield, P. L. Phillips Petroleum Company, US Patent 3481710, 1969.

(32) Krupka, J.; Kolena, J. Gas Chromatographic Data and Identification of Isomeric Products of Cycloaddition Reactions of Conjugated C5 Dienes. *Petroleum and Coal* **2012**, *54* (4), 385–396.

(33) Krupka, J.; Pašek, J.; Lederer, J.; Bílková, D. KINETICS OF CYCLOADDITION REACTIONS OF CONJUGATED C5 DIENES. *Petroleum & Coal* **2014**, *56* (4), 428–441.

(34) Nazarov, I. N.; Kuznetsova, A. I.; Kuznetsov, N. V.; Titov, Yu. A. Diene Condensation of 1,3-Dimethylbutadiene with Unsymmetric Dienophiles. *Russ Chem Bull* **1959**, *8* (4), 634–638. https://doi.org/10.1007/BF00915857.

(35) Infineum International, Ltd. Worldwide Winter Diesel Fuel Quality Survey, 2018, Https://Www.Infineuminsight.Com/Media/2228/Infineum-Wdfqs-2018-V10-14112018.Pdf (Accessed June 1, 2022).

(36) Mattos, R. A. de; Bastos, F. A.; Tubino, M. Correlation Between the Composition and Flash Point of Diesel-Biodiesel Blends. *Journal of the Brazilian Chemical Society* **2014**. https://doi.org/10.5935/0103-5053.20140262.

(37) Hoekman, S. K.; Broch, A.; Robbins, C.; Ceniceros, E.; Natarajan, M. Review of Biodiesel Composition, Properties, and Specifications. *Renewable and Sustainable Energy Reviews* **2012**, *16* (1), 143–169. https://doi.org/10.1016/j.rser.2011.07.143.

(38) Rantanen, L.; Linnaila, R.; Aakko, P.; Harju, T. NExBTL - Biodiesel Fuel of the Second Generation; 2005; pp 2005-01–3771. https://doi.org/10.4271/2005-01-3771.

(39) Yanowitz, J.; Ratcliff, M.; McCormick, R.; Taylor, J.; Murphy, M. *Compendium of Experimental Cetane Numbers*; NREL/TP-5400-61693, 1150177; 2014; p NREL/TP-5400-61693, 1150177. https://doi.org/10.2172/1150177.

(40) Ghosh, P.; Jaffe, S. B. Detailed Composition-Based Model for Predicting the Cetane Number of Diesel Fuels. *Ind. Eng. Chem. Res.* **2006**, *45* (1), 346–351. https://doi.org/10.1021/ie0508132.

(41) Harrison, K. W.; Harvey, B. G. High Cetane Renewable Diesel Fuels Prepared from Bio-Based Methyl Ketones and Diols. *Sustainable Energy Fuels* **2018**, *2* (2), 367–371. https://doi.org/10.1039/C7SE00415J.

(42) Meylemans, H. A.; Baldwin, L. C.; Harvey, B. G. Low-Temperature Properties of Renewable High-Density Fuel Blends. *Energy Fuels* **2013**, *27* (2), 883–888. https://doi.org/10.1021/ef301608z.

(43) Wilson, G. R.; Edwards, T.; Corporan, E.; Freerks, R. L. Certification of Alternative Aviation Fuels and Blend Components. *Energy Fuels* **2013**, *27* (2), 962–966. https://doi.org/10.1021/ef301888b.

(44) Yang, J.; Li, S.; Li, N.; Wang, W.; Wang, A.; Zhang, T.; Cong, Y.; Wang, X.; Huber, G. W. Synthesis of Jet-Fuel Range Cycloalkanes from the Mixtures of Cyclopentanone and Butanal. *Ind. Eng. Chem. Res.* **2015**, *54* (47), 11825–11837. https://doi.org/10.1021/acs.iecr.5b03379.

(45) Zhang, X.; Deng, Q.; Han, P.; Xu, J.; Pan, L.; Wang, L.; Zou, J.-J. Hydrophobic Mesoporous Acidic Resin for Hydroxyalkylation/Alkylation of 2-Methylfuran and Ketone to High-Density Biofuel. *AIChE J.* **2017**, *63* (2), 680–688. https://doi.org/10.1002/aic.15410.

(46) Li, G.; Li, N.; Wang, X.; Sheng, X.; Li, S.; Wang, A.; Cong, Y.; Wang, X.; Zhang, T. Synthesis of Diesel or Jet Fuel Range Cycloalkanes with 2-Methylfuran and Cyclopentanone from Lignocellulose. *Energy Fuels* **2014**, *28* (8), 5112–5118. https://doi.org/10.1021/ef500676z.

(47) Deng, Q.; Xu, J.; Han, P.; Pan, L.; Wang, L.; Zhang, X.; Zou, J.-J. Efficient Synthesis of High-Density Aviation Biofuel via Solvent-Free Aldol Condensation of Cyclic Ketones and Furanic Aldehydes. *Fuel Processing Technology* **2016**, *148*, 361–366. https://doi.org/10.1016/j.fuproc.2016.03.016.

(48) Staples, O.; Leal, J. H.; Cherry, P. A.; McEnally, C. S.; Pfefferle, L. D.; Semelsberger, T. A.; Sutton, A. D.; Moore, C. M. Camphorane as a Renewable Diesel Blendstock Produced by Cyclodimerization of Myrcene. *Energy Fuels* **2019**, *33* (10), 9949–9955. https://doi.org/10.1021/acs.energyfuels.9b02557.

Appendix A

Appendix to Chapter 2

***** *This chapter was reproduced from the following publication. The author of this Ph. D. thesis, Manhao Zeng, is the leading coauthor of this publication who contributed to all parts relevant to this work.*

*Zhang, F.; ***Zeng, M.**; Yappert, R. D.; Sun, J.; Lee, Y.-H.; LaPointe, A. M.; Peters, B.; Abu-Omar, M. M.; Scott, S. L. Polyethylene Upcycling to Long-Chain Alkylaromatics by Tandem Hydrogenolysis/Aromatization. *Science* **2020**, *370* (6515), 437–441. https://doi.org/10.1126/science.abc5441.

**These authors contributed equally to this work.*

Materials

Trimethyl(cyclopentadienyl)platinum ($CpPtMe_3$, 99%) and γ-alumina (Lot 29481900, 186m^2/g, pore volume 0.50 cm^3/g) were both purchased from Strem. Chloroform (HPLC, OmniSolv®, CX1054-6) was obtained from EMD Millipore Corp. HPLC-grade water, dichloromethane (≥99.9%, GC Resolv™), triethylamine (HPLC-grade) and 1,2,4-trichlorobenzene (HPLC-grade) were obtained from Fisher Chemicals. H_2 (4.0% in Ar, Airgas) was purified by passage through 13X molecular sieves and BTS catalyst (Sigma Aldrich) before use. H_2 (10.0% in Ar, Airgas) was used for calibration of the TCD response. CO (9.890% in He, Airgas) was used for CO pulse chemisorption. Propene (99.8%) was obtained

from PRAXAir. 1,1,2,2-Tetrachloroethane-d_2 (TCE-d_2, ≥99.5 atom % D), KBr (FT-IR grade), triacontane (*n*- $C_{30}H_{62}$, 98%), dodecylbenzene (97%) 1,4-didodecylbenzene (95%), di-*tert*-butylhydroxytoluene (>99%), and chloroplatinic acid hexahydrate (≥ 37.5 wt% Pt) were all purchased from Sigma Aldrich and used as received. Dichloromethane-d_2 (99.8 atom % D) and bromobenzene-d_5 (99 atom %D) was purchased from Cambridge Isotope Laboratories. A standard mixture of saturated alkanes(C_7 - C_{40}, certified reference material, 1000 μg/mL each component in hexane) and a standard Pt solution containing (976 ± 2) mg Pt/kg in 5% HCl and high-purity water were obtained from SigmaAldrich. A low molecular weight polyethylene (Lot SKU-427772) was purchased from Sigma Aldrich. Low density polyethylene (LDPE) was obtained from a discarded plastic packaging bag and cut into mm-size pieces before use. High density polyethylene (HDPE) was the cap of a disposable PET water bottle. It was cut into mm-size pieces, frozen in liquid N_2, and the particle size was further reduced in a coffee-grinder before use. Polymer properties are summarized in Table A.1.

Catalyst synthesis and characterization

γ-Alumina was calcined in flowing air at 500 °C for 4 h, followed by evacuation (10^{-4} Torr) at 450 °C for 12 h. Volatile trimethyl(cyclopentadienyl)platinum (32 ± 1 mg) was deposited onto the dry alumina (1.000 ± 0.020 g) by vacuum sublimation (ca. 10^{-4} Torr) at room temperature.[1] The reactor was shaken vigorously during the procedure to promote uniform deposition, then was evacuated at room temperature for 1 h to remove physiosorbed $PtCp(CH_3)_3$. The resulting solid was reduced in flowing H_2 (4.0% in Ar, 30 mL/min) as the temperature was ramped to 250 °C at a rate of 2 °C/min. The reactor was held at this

temperature for 2 h, then cooled to room temperature and evacuated for 15 min. The reduced catalyst was stored in an Ar-filled glovebox until use to avoid re-oxidation in air.

TEM images of the catalyst were obtained on either a FEI Titan 80-300 kV S/TEM or ThermoFisher Talos F200X. Pt particle sizes were measured from the high angle annular dark field(HAADF) images. The fresh catalyst contains particles with an average size of (0.9 ± 0.2) nm (Fig.A.1A and A.1B). After the catalytic disassembly of PE at 280 °C for 24 h, the average size increased slightly, to (1.2 ± 0.3) nm (Fig. A.1C and A.1D).

Metal analyses were performed by Inductively-Coupled Plasma (ICP) – Optical Emission Spectrometry (ICP-OES) on a Thermo iCAP 6300. A calibration curve was constructed using standard Pt solutions, prepared using a commercial Pt standard with a mixture of aqua regia in HPLC-grade water (4% v:v). Pt was extracted from solid catalyst samples at 75 °C in aqua regia under magnetic stirring for 30 min, based on a slight modification of a previously described procedure.[2] The resulting suspensions were allowed to stand at room temperature for 24 h, then filtered. The solid residue was washed three times with HPLC-grade H_2O. The combined filtrates were diluted with aqua regia (4% v:v in water) and analyzed by ICP-OES, using the spectral lines at 214.423 and 203.646 nm. The fresh catalyst contains 1.5 wt% Pt.

The accessible Pt surface area, dispersion and particle size of fresh and recycled Pt catalystswere also determined by CO chemisorption, using a Micrometrics Autochem ii 2920 equipped with a TCD detector. A U-shaped quartz reactor was packed with a plug of quartz wool which supported a catalyst bed of ca. 35 mg. A thermocouple was attached to the outside of the reactor, at the level of the middle of the bed. The catalyst was first activated by heating in H_2/Ar (10 vol%) to 200 °C at a ramp rate of 5 °C/min and held at 200 °C for 2 h before

cooling to room temperature under flowing He. Next, the catalyst was subjected to 20 pulses of CO (9.890 vol% in He). Each pulse had a volume of 124 microliter at 1 atm. The amount of CO not adsorbed in each pulse was measured.

The metal surface area, SA_{Pt} (m^2 g^{-1}), estimated nanoparticle size (nm), and Pt dispersion D (%), were calculated using eq A.1-A.3, assuming hemispherical Pt nanoparticles.

$$SA_{Pt} = \frac{S_f N_A SA_{cross} V_{ad}}{mWV_m} \quad \text{(eq A.1)}$$

$$\text{Pt } nanoparticle\ size\ (nm) = \frac{6}{d_{Pt} SA_{Pt}} \quad \text{(eq A.2)}$$

$$D\ (\%) = \frac{S_f M V_{ad}}{mWV_n} \times 100 \quad \text{(eq A.3)}$$

Here, S_f = stoichiometry factor (Pt/CO molar ratio) = 1, N_A is Avogadro's number, SA_{cross} = Pt atom cross-sectional area (8.0×10^{-20} m^2), d_{Pt} = Pt density (2.145×10^{-20} g/nm^3), V_{ad} = volume ofchemisorbed CO under STP conditions (mL), m = sample mass (g), W = weight fraction of Pt in the sample, as determined by ICP-OES (0.015 g_{Pt}/g sample), V_m = molar volume of CO (2.24×10^4 mL/mol) at STP, and the number 6 is based on the assumption of hemispherical geometry. The fresh catalyst containing 1.5 wt% Pt has an active metal surface area of 215 m^2/g (Table A.4), corresponding to 1.3 nm particles, with ca. 87 % dispersion based on total Pt content. The small particle size is consistent with the TEM observation (Fig. A.1A and A.1B). After the 1st recycle, the active Pt surface area and dispersion decreased to 154 m^2/g and 62%, respectively. The particlesize increased to 1.8 nm, consistent with the slight increase observed in the TEM images (Fig. A.1C and A.1D). The active Pt surface area and dispersion of the recycled catalyst after the 3rd run stabilized at 145 m^2/g and 59%, confirming no significant change between the 2nd and 3rd recycles.

Catalytic conversion of polyethylene

Initial screening reactions and time-resolved experiments were conducted in unstirred stainless-steel mini-autoclaves made from Swagelok junctions,[3] each with an internal volume of ca. 10 mL. In a typical procedure, the reduced catalyst (1.5 wt% Pt/γ–Al_2O_3, 0.200 g) and a sample of the appropriate PE material (0.118 g) were loaded into an autoclave reactor inside an Ar-filled glove-box. The reactor was sealed, removed from the glove-box and placed in a temperature-controlled muffle furnace (Thermo Scientific Lindberg/Blue M BF51848C) that waspre-heated to the desired temperature. When the furnace door was opened to insert the autoclave,the temperature decreased by 20-30 °C, but returned to the desired temperature within ca. 5 min. Reaction timing started when the temperature stabilized. During the 24 h reaction time, the furnacetemperature fluctuated by ± 5 °C. After the specified reaction time, the reactor was removed fromthe oven and cooled rapidly in a jet of compressed air to quench the reaction.

At the end of the reaction, the reactor was opened inside a fume hood and the gases were vented. The remaining material was transferred onto a fine glass frit (4.0-5.5 μm), washed with hot (50 °C) chloroform, and filtered to remove insolubles. Soluble hydrocarbons were recovered by evaporating the chloroform under reduced pressure (0.1 Torr) overnight. The insoluble material,including the catalyst and hydrocarbons insoluble in hot chloroform, was recovered from the frit.After removing the chloroform residue by evacuating under reduced pressure (0.1 Torr) overnight,the insoluble material was weighed. The yield of insoluble hydrocarbons was calculated as the difference between the total mass of recovered solid and the initial mass of the catalyst. Since volatiles were not recovered in these experiments, their

yield was calculated as the difference between the initial mass of PE and that of the recovered soluble and insoluble hydrocarbons.

To characterize volatile reaction products, a mini-autoclave was modified with a gas outletmade from a Swagelok hose connector sealed with a hexagon socket head screw cap containing aCu O-ring. The total internal volume of the reactor and the gas outlet, 13 mL, was measured by filling with water. The mini-autoclave and a Schlenk flask capped with a white rubber septum were connected via Tygon tubing to a glass vacuum line equipped with a pressure gauge and a port forgas sampling. The Schlenk flask and the lines were evacuated under reduced pressure (10^{-4} Torr),then isolated from the pumping system. The gases in the autoclave were expanded into the line byloosening the screw cap, and the pressure was measured. The volatiles yield was estimated using the total volume of the gas line and the Schlenk flask as measured by gas expansion (152 mL), andthe ideal gas law. An aliquot of gas (400 μL) was removed via the sampling port for analysis of H_2 by GC-TCD, using a gas-tight syringe. The Ar present in the autoclave at the start of the reaction (1 atm) was used as the internal standard. Propene, which is not a reaction product, was injected into the Schlenk tube as an internal standard for hydrocarbon analysis by GC-FID. An aliquot (0.2 mL) was then removed for analysis. The total GC yields of H_2 and light hydrocarbons are consistent with the total yield of gases based on pressure measurement, with a precision of ± 10%.

To analyze volatile hydrocarbons that may have been lost during solvent removal from the chloroform-soluble fraction, the reactor contents were transferred with the aid of chloroform (5 mL) into a Schlenk flask. The contents were distilled at 150 °C, while condensing volatile productsand chloroform in a receiving flask cooled in a dry ice/acetone bath. The clear, colorless distillatewas transferred to a 10 mL volumetric flask, 2 mg mesitylene was added as

an internal standard, and the flask was filled to the 10 mL mark with chloroform. The solution was analyzed on an Agilent 6890N Network Gas Chromatograph equipped with a DB-5 column and an FID detector,using response factors measured for toluene and light *n*-alkanes (C_7-C_{11}) relative to mesitylene. The total mass of recovered volatile products from distillation is small (ca. 1.5 mg, measured by GC-FID), with toluene being the major product.

Some reactions were conducted in a larger autoclave reactor (Parr Series 5000 Multiple Reactor System, internal volume ca. 100 mL, stainless steel). The contents were stirred at 678 rpm,using a magnetic stir bar encapsulated in Pyrex. Timing of the reaction began when the internal temperature reached the set temperature, 250 °C; reported reaction times do not include the time (ca. 30 min) needed to heat the reactor from room temperature. Since the internal thermocouple islocated above the solids in the reactor, it reads the temperature of the gas phase rather than the solid/liquid phase. The temperature of the autoclave wall was also measured externally with a thermometer and stabilized at (280 ± 5) °C during the reaction time.

The autoclave was cooled to room temperature prior to opening, by immersing the bottomof the vessel in 25 °C water for 15 min. Gases were collected as described above. When the autoclave lid was removed, an oily liquid was observed to have adhered on the lid and separated from the catalyst at the bottom of the vessel. It was recovered by dissolving in hot chloroform, then evaporating the solvent under reduced pressure overnight. The solid products were transferredonto a fine glass frit, then washed with hot chloroform. The solvent was removed from the filtrate by evaporation overnight at 0.1 Torr. The insoluble material remaining on the frit, including the catalyst and insoluble hydrocarbons, was recovered and weighed. The mass of insoluble hydrocarbons was calculated by subtracting the initial mass of

the catalyst. Some hydrocarbons were not recovered during workup, due to the difficulty in washing the dead volumes in the connectors and valves of the autoclave.

Catalytic conversion of *n*-$C_{30}H_{62}$

A mixture of 0.120 g *n*-$C_{30}H_{62}$ and 0.200 g Pt/γ-Al_2O_3 was heated at (280 ± 5) °C under Ar for 24 h in mini-autoclaves. After the reaction, the gas products were analyzed by GC-TCD and GC-FID as described above. The remaining material was extracted with $CHCl_3$ at room temperature, separated from the insoluble catalyst as a yellow liquid, then, mesitylene (2.0 mg) was added as an internal standard. The solution was analyzed on an Agilent 6890N gas chromatograph equipped with a DB-5 column and an FID detector.

Peak assignments were made by comparing retention times to a standard mixture of n-alkanes(C_7 - C_{40}), standard mesitylene, as well as by matching to peaks identified by GC-MS with the aid of a mass spectral library (NIST 107). Among the liquid products, the major species are n-alkanes (C_7 - C_{30}). The minor products are mostly branched alkanes, with smaller contributions from cycloalkanes and alkylbenzenes. The presence of multiple isomers with overlapping peaks hindered more complete analysis. Nevertheless, hydrocarbons that elute together have the same carbon number and very similar response factors (within 3%). Therefore, based on the mass of mesitylene, the peak areas and response factors for each species, the absolute amount of each species could be obtained. Since there is a negligible amount of insoluble hydrocarbon in the solid phase (less than 0.1% by mass), the species detected in both gas and liquid phases (89% yield) were combined to obtain a total distribution (see Fig. A.12). C_5, C_6, and C_7 compounds were not fully accounted for because their signals overlapped with that of $CHCl_3$.

For ^{1}H NMR analysis, undeuterated $CHCl_3$ was removed by evaporation overnight at 0.1 Torr,resulting in a ca. 70 wt% yield of liquid products consisting only of molecules larger than C_9. Mesitylene was also mostly removed (< 0.1 mol% remaining) as evidenced by GC-FID analysis.

Catalyst recycling

For the catalyst recycling test, the freshly reduced catalyst (1.5 wt% Pt/γ–Al_2O_3, 0.300 g) and a low molecular weight PE (M_n = 1.85 x 10^3 g/mol, $Đ$ = 1.90, 0.177 g) were loaded into 2x 10 mLmini-autoclave reactors inside an Ar-filled glove-box. Two PE depolymerization reactions were conducted in parallel at 280 °C for 6 h. The catalyst was recovered from both reactors, combined and calcined in flowing O_2 (50 mL/min) at 400 °C for 2 h to remove organic residue. The absence of hydrocarbons was verified by the complete disappearance of the C-H stretching modes in the IR spectrum (Fig. A.14). The calcined catalyst was re-reduced in flowing H_2 (4 vol% in Ar, 50 mL/min) at 250 °C for 3 h to give 0.520 g once-recycled catalyst. This once-recycled catalyst (0.200 g) was loaded with low molecular weight PE (0.118 g) into 2x 10 mL mini-autoclave reactors inside an Ar-filled glove box and the reaction was conducted again at 280 °C for 6 h. A similar catalyst recovery/regeneration procedure gave 340 mg twice-recycled catalyst. This twice-recycled catalyst (275 mg) was loaded with PE (163 mg) in a 10 mL mini-autoclave and the reaction was conducted a third time at 280 °C for 6 h. Note that for each experiment, the mass ratio of PE (M_n = 1.85 x 10^3 g/mol, $Đ$ = 1.90) and catalyst (Pt/γ-Al_2O_3, 1.5 wt% Pt) was constant at 0.60.

Analysis of starting materials and products

Gas chromatography. Hydrocarbons in the gas fraction (C_1-C_9) were analyzed quantitatively on a Shimadzu GC-2010 gas chromatograph equipped with a capillary column (Supelco Alumina Sulfate plot, 30 m x 0.32 mm) and a flame ionization detector (FID). Propene was added as an internal standard. Relative carbon response factors were assumed to be 1.0. The injector and detector temperatures were 200 °C. The temperature ramp program was: 90 °C (hold3 min), ramp 10 °C /min to 150 °C (hold 20 min).

Hydrocarbons in the gas fraction (C_1-C_9) were analyzed qualitatively on a Shimadzu GC- 2010 gas chromatograph equipped with an Agilent DB-1 capillary column (dimethylpolysiloxane,30 m x 0.25 mm x 0.25 μm) coupled to a QP2010 Mass Spectrometer. The injector and detector temperatures were 250 °C. The temperature ramp program was: 40 °C (hold 3 min), ramp 25 °C per min to 250 °C (hold 10 min).

H_2 was quantified on a Shimadzu GC-8AIT gas chromatograph equipped with a packed column (ShinCarbon ST 80/100, 2 m x 2 mm) and a thermal conductivity detector (TCD), using Ar as the internal standard. The linear response of the TCD signal to the injected volume of H_2 andAr was confirmed using standard H_2/Ar gas mixtures. The response factors for H_2 (f_{H_2}) and Ar (f_{Ar}) were obtained as the slopes of fitted lines. The column, injector and detector temperatures were 130 °C. The TCD current: 70 mA and the head pressure were 300 kPa (N_2).

Hydrocarbons in the liquid fraction (C_6-C_{30}) were quantitatively analyzed on an Agilent 6890N Network gas chromatograph equipped with an Agilent DB-5 capillary column (fused silica,30 m x 0.25 mm x 0.25 μm) and FID. The inlet and detector temperatures were 300 and 280 °C, respectively. The temperature ramp program was: 40 °C (hold 3 min), ramp 25 °C /min to 320 °C(hold 10 min). The flow rate was 1.0 mL/min (He) with a split ratio of 5:1.

Gel permeation chromatography. Molecular weight distributions of the starting PE or the hydrocarbon products were analyzed on an Agilent PL-GPC 220 gel permeation chromatograph, equipped with a PL-Gel Mixed B guard column, three PL-Gel Mixed B columns, and a refractive index (RI) detector. Samples were dissolved in 1,2,4-trichlorobenzene (TCB) containing di-*tert*- butylhydroxytoluene (BHT, 0.01 wt%), by heating at 150 °C for at least 1 h. Elution was achievedusing TCB (with BHT) at 150 °C and 1.0 mL min^{-1}. The molecular weight response was calibratedwith monomodal, linear polyethylene standards (Varian). To ensure accurate measurement of lowmolecular weight materials (M_w <1000 g/mol), PE standards with peak molecular weights M_p of507 and 1180 g/mol (Polymer Standards Services) were included in the calibration.

To examine the distribution of chromophores, selected product mixtures were also analyzed by GPC with UV detection. Analysis was conducted on a Waters 2690 HPLC equipped with two Agilent Columns (PLgel, 5μm MiniMIX-D, 250×4.6 mm) and a guard column (MW linear range 200 - 400,000 g/mol), a Waters 2410 refractive index (RI) detector and a Waters 2998 photodiode array detector (PDA). Chloroform with 0.25 vol% triethylamine was used as the mobile phase at room temperature and 0.35 mL/min. Calibration was achieved using polystyrene standards (Agilent EasiVial kit, linear response for the range 200 < molecular weight < 400,000 g/mol).

NMR spectroscopy. ^{1}H NMR spectra of the starting PE were recorded in bromobenzene-$d_5$at 80 °C using a Varian Unity Inova 500 MHz spectrometer. Spectra of the products were recordedin 1,1,2,2-tetrachloroethane-d_2.^{1}H NMR spectra were acquired at 600 MHz on a Varian Unity Inova AS600 spectrometer, and were analyzed using MestReNova (v11.0.1, Mestrelab Research S. L.). ^{13}C NMR spectra were acquired on a Bruker AVANCE III

Ultrashield Plus 800 MHz (18.8T) spectrometer, and were analyzed using Topspin (v4.0.6, Bruker Biospin). A Bruker TXI HCNcryoprobe was used to enhance sensitivity for direct ^{13}C detection. ^{13}C spectra were recorded usinga long relaxation delay (10 s) to ensure quantitative intensities. Chemical shifts (δ, ppm) were calibrated using the residual proton signals of the solvent and referenced to tetramethylsilane (TMS).

IR spectroscopy. Spectra were recorded on a Shimadzu Prestige-21 spectrometer. Samples(2 mg) were ground with a mortar and pestle, mixed with KBr (100 mg), and pressed into 15 mmdiameter pellets using a force of 4 tons. IR spectra were measured with a resolution of 1.0 cm^{-1} over the range 400–4000 cm^{-1}. A background spectrum of a KBr pellet was subtracted from eachsample spectrum.

Field Desorption Mass Spectroscopy (FD-MS). Spectra were obtained on a Waters Micromass GCT Premier Time of Flight mass spectrometer, operating with an extraction rod voltage of 12 kV. Samples were dissolved in dichloromethane and loaded directly onto a CARBOTEC FD emitter, consisting of a 10 µm tungsten wire carrying a pyrocarbon coating of microneedles (ca. 120 µm diameter). Nominal mass data were acquired while employing a data- dependent ramp of the emitter current from 0-90 mA, pausing the ramp when more than 30 countsper scan were observed in the base peak ion. The extraction rods were cleaned between acquisitionsby slowly raising the extraction rod current to 3 A while maintaining a 12 kV charge. The emitterwas cleaned between acquisitions by raising the emitter current to 95 mA for 5 s. The calibration range is $400 < m/z < 1200$, with a maximum mass error of 0.2 *m/z*. A mixture of triacontane ($C_{30}H_{62}$), and 1,4-didodecylbenzene ($C_{30}H_{54}$) in a molar ratio of 1:1.02 was analyzed to assess sensitivity and accuracy for detecting and quantifying different types of hydrocarbons. Each compound gave its molecular ion as the major peak. The similar peak

heights confirm that this data is suitable for the semi-quantitative analysis of their relative abundance.

Differential Scanning Calorimetry (DSC). DSC measurements were performed on a Mettler Toledo Polymer DSC instrument and analyzed using the STARe software. Each polymer sample (approx. 5 mg) was placed in a crimped aluminum pan. Using a heating/cooling rate of 10 °C/min, the samples were heated from -70 to 200 °C under a flow of N_2, cooled to -70 °C, then heated to -200 °C. The crystallization temperature (T_c) and the melting temperature (T_m) were obtained from the first cooling and second heating cycles, respectively.

Estimated branching frequency in PE

The average number of methyl groups per 1000 carbons was estimated using the formula $(I_{CH3}/3)/[(I_{CH} + I_{CH2} + I_{CH3})/2] \times 1000$, where I_{CH3}, I_{CH2}, and I_{CH} are the ^{1}H NMR integrations for the methyl, methylene, and methine signals, respectively.[4] For the commercial HDPE material, the value could not be determined because the polymer did not dissolve completely.

Assessment of selectivity

1. NMR method

Although the ^{1}H and ^{13}C NMR spectra are complex due to the presence of multiple isomers, they can be integrated for various functional group regions. The sample calculations below correspond to analysis for the $CHCl_3$-soluble liquid hydrocarbon fractions recovered from the autoclave after depolymerization of 0.118 g PE (M_w = 3.52 x 10^3 g/mol, $Đ$ = 1.9) with

0.200 g Pt/γ–Al_2O_3 (1.5 wt% Pt) at 280 °C for 24 h. Results for other product fractions and reaction conditions are summarized in Table A.2.

To estimate selectivities for each type of aromatic products, we begin by assuming that the major aromatic products are dialkylbenzenes and dialkylnaphthalenes. Integration of the aromatic line region gives a ratio of monoaromatic protons to polyaromatic protons, H_{mono}/H_{poly}, of 1.6 (Fig. A.8A). Thus, the molar ratio of dialkylbenzenes (each with 4 H) to dialkylnaphthalenes (each with 6 H) is 2.4. Consequently, if dialkylnaphthalenes represent *x* mol% of all products, then dialkylbenzenes represent 2.4*x* mol%, and the selectivity to alkylaromatics (S_{Ar}) is the combination of the two fractions, 3.4x mol%. The remainder, (1-3.4*x*) mol%, corresponds to saturated alkanes (since olefins were not detected in significant amounts by ^{1}H NMR).

According to GPC analysis, the liquid hydrocarbon products have an M_n value of 466 g/mol (corresponding to an averaged carbon number C_{34}, in good agreement with the FD-MS result), with a narrow dispersity ($Đ$ = 1.12). The aromatic protons (H_{Ar}) in the products are distributed as dialkylnaphthalenes (6*x* mol%) and dialkylbenzenes (4 × 2.4*x* mol%). Furthermore, the total protons (H_{total}) are distributed as dialkylnaphthalenes ($C_{34}H_{56}$, 56*x* mol%), dialkylbenzenes ($C_{34}H_{62}$, 62 × 2.4*x* mol%), and saturated alkanes ($C_{34}H_{70}$, 70 × (100 - 3.4*x*) mol%). The ratio H_{Ar}/H_{total} (0.037 observed in Fig. A.8A) is given by eq A.4:

$$\frac{H_{Ar}}{H_{total}} = \frac{6x + 4\times2.4x}{56x + 62\times2.4x + 70(100-3.4x)} = 0.037 \qquad \text{(eq A.4)}$$

The resulting dialkylnaphthalene mole fraction is x = 15.4, while the dialkylbenzene mole fraction is 2.4x = 36.9. The total selectivity to aromatics in the $CHCl_3$-soluble hydrocarbons is therefore 52.3 mol%.

A similar assessment was undertaken by integrating the aromatic region (120 – 150 ppm) and the aliphatic region (10 – 40 ppm) of the corresponding ^{13}C NMR spectrum (Fig. A.8B). The fraction of aromatic carbons is (0.10 ± 0.01). Since carbon atoms associated with naphthalene and benzene rings are difficult to distinguish by ^{13}C NMR, we used the ratio from the ^{1}H NMR analysis (1:3.5). In addition, the average total carbon number in the hydrocarbon products is C_{34} according to GPC. Since dialkylnaphthalenes contribute 10x mol% C_{Ar}, while dialkylbenzenes contribute 6×(2.4x) mol% C_{Ar}, the ratio C_{Ar}/C_{total} is given by eq A.5:

$$\frac{C_{Ar}}{C_{total}} = \frac{10x+6\times2.4x}{34} = 0.10 \qquad \text{(eq A.5)}$$

The resulting dialkylnaphthalene mole fraction, x, is 0.139, similar to the value obtained by analysis of the ^{1}H NMR spectrum (0.155). The dialkylbenzene mole fraction is 0.334, for a total aromatic selectivity of 47 mol%. This value is slightly smaller than the value estimated by ^{1}H NMR (52 mol%), presumably due to experimental uncertainty.

We note that these estimated aromatic selectivities depend on the average carbon number. Due to differences in the hydrodynamic radii of dialkylaromatics compared to linear PE, the experimental values for M_n are lower than the actual M_n values. For example, a dodecylbenzene standard (246 g/mol) gave a measured M_n of 166 g/mol, and a di-dodecylbenzene standard (414 g/mol) gave a measured M_n of 345 g/mol. Therefore, the GPC method underestimates the mass by ca. 17%. Using an average carbon number 16% higher (C_{40}) instead of C_{34} to assess the alkylaromatic selectivity would result in a slightly higher total aromatic selectivity, 61 mol% by ^{1}H NMR and 56 mol% by ^{13}C NMR. Thus, considering the

uncertainty in the average carbon number derived from M_n, we estimate the overall alkylaromatic selectivity in the liquid fraction to be (57 ± 5) mol% by ^{1}H NMR, and (52 ± 4) mol% by ^{13}C NMR.

The ^{1}H NMR analysis described above was applied to the liquid hydrocarbons recovered after 24 h reaction of n-$C_{30}H_{62}$ in a mini-autoclave reactor at (280 ± 5) °C, yielding the values for H_{mono}/H_{poly} and H_{Ar}/H_{total} shown in Table A.6. However, due to the lower molecular weights involved, the average carbon number in the liquid products was obtained by GC-FID (instead of GPC). Based on the peak areas and response factors for each species, the product distribution for the liquid products was obtained. The average carbon number (20, on a molar basis) was calculated using on the following formula:

$$average\ carbon\ number = \sum_{C10}^{C30} mole\ fraction * carbon\ number \qquad \text{(eq A.6)}$$

The alkylbenzene selectivity was determined by combining this number with the ^{1}H NMR results.

2. FD-MS method

Peaks were separated into several series based on mass and carbon number (n), as shown in Table A.2. The paraffin yield includes alkanes, cycloalkanes, and dicycloparaffins. The yield of monoaromatics includes alkylbenzenes, benzocycloparaffins, and benzodicycloparaffins. In the benzocycloparaffins, it is most likely to be alkyltetralins. The yield of polyaromatics includes alkylnaphthalenes, alkylanthracenes, and alkylphenanthrenes. In order to compute selectivities, the FD-MS signal was filtered to assign each peak to one of these series. The filtered signal (peak height) was then interpolated and integrated to compute

the relative total response of each series. The results are shown in Fig. 2.3C and Table A.4. An alternative analysis using total peak areas for each series yielded similar results.

H_2 Balance

The conversion of PE (0.064 mmol, M_n = 1.85 x 10^3 g/mol, average C_{132}) into gas-phase hydrocarbons ($C_{1\text{-}9}$, 0.34 mmol) and liquid-phase molecules (average C_{30}, 0.19 mmol) in Exp. 2 requires 0.47 mmol H_2, assuming that each H_2 cleaves one C-C bond and generates two alkanefragments ($n_{H2} = n_{C1-9} + n_{C30} - n_{C132}$). The amount of free H_2 remaining in the gas phase after reaction is 0.11 mmol, for a total of 0.58 mmol H_2. According to ^{1}H NMR of the liquid products (0.21 mmol, average C_{30}), the mole fractions of alkylbenzene and alkylnaphthalene are 0.33 and 0.19, respectively. The alkylbenzene yield is 0.063 mmol, while the alkylnaphthalene yield is 0.036 mmol. Since each alkylbenzene or alkylnaphthalene molecule generates 4 or 7 H_2 molecules,respectively, the total H_2 generated is 0.50 mmol. This value is similar to the value obtained by mass balance (0.58 mmol).

Conversion of *n*-$C_{30}H_{62}$ (0.23 mmol) in Exp. S3 gives hydrocarbons ranging from C_1 to C_{29} (0.47 mmol), requiring 0.24 mmol H_2 (Table A.6). Including the remaining H_2 in the reactor (0.064mmol) gives a total of 0.30 mmol H_2. According to ^{1}H NMR, the mole fractions of alkylbenzene and alkylnaphthalene are 0.11 and 0.035, respectively. The alkylbenzene yield is 0.045 mmol, while the alkylnaphthalene yield is 0.011 mmol. The total H_2 generated is 0.26 mmol. This value is similar to the value obtained by mass balance (0.30 mmol).

Thermodynamic analysis of tandem hydrogenolysis/aromatization

The thermodynamic feasibility of the tandem reaction was assessed using data computed using Benson group increment theory for gas phase alkanes and alkylbenzenes (*40*). Increment values are compiled in Table A.7. The thermodynamic contributions to a linear alkane C_nH_{2n+2} are:

$$g_{A,n} = (n-2)g_1 + 2g_2 \qquad \text{(eq A.7)}$$

The thermodynamic contributions for the alkane hydrogenolysis reaction (eq A.8) are:

$$C_{m+n}H_{2m+2n+2} + H_2 \rightarrow C_mH_{2m+2} + C_nH_{2n+2} \qquad \text{(eq A.8)}$$

$$g_{Hy} = g_{A,n} + g_{A,m} - g_{A,n+m} - g_H = -2g_1 + 2g_2 - g_H \qquad \text{(eq A.9)}$$

Note that the linearity of the Benson group contributions eliminates the chain length dependence according to eq A.9, since changes in the number of methylene carbons ($-2g_1$) and the number of methyl chain ends ($+2g_2$) are independent of the initial chain length. The thermodynamic contributions to an *ortho*-dialkylbenzene C_nH_{2n-6} are:

$$g_{B,n} = (n-10)g_1 + 2g_2 + 2g_3 + 4g_4 + 2g_5 + g_6 \qquad \text{(eq A.10)}$$

The thermodynamic contributions to the aromatization reaction (eq A.11) are given in eq A.12:

$$C_mH_{2m+2} \rightarrow C_mH_{2m-6} + 4H_2 \qquad \text{(eq A.11)}$$

$$g_{Ar} = g_{B,n} + 4g_H - g_{A,n} = -8g_1 + 2g_3 + 4g_4 + 2g_5 + g_6 + 4g_H \qquad \text{(eq A.12)}$$

Note that the linearity of the Benson group contributions also removes the chain length dependence from eq A.12, since the change in the number of methylene carbons ($-8g_1$) is independent of the initial chain length.

Derivation of rate model for tandem hydrogenolysis/aromatization

In our simplified kinetic model, we assume that the hydrocarbon products contain only two types of carbon: aliphatic, and aromatic. Furthermore, the kinetic model is comprised of only two reactions, hydrogenolysis (eq A.8) and aromatization (eq A.11). Once an aromatic ring is formed, we assume it does not undergo further reaction. However, the aliphatic substituents on an aromatic ring can continue to undergo hydrogenolysis and aromatization.

Since there is no solvent in the reactor, each surface Pt atom is always in contact with either an aliphatic carbon (i.e., methyl or methylene) *A*, or an aromatic carbon *B*. We assume the two types of carbon compete for adsorption sites according to eq A.13, where A_{ads} and B_{ads} are adsorbed aliphatic and aromatic carbons, respectively.

$$A_{ads} + B \rightleftharpoons A + B_{ads} \qquad \text{(eq A.13)}$$

Adsorption is governed by the equilibrium expression, eq A.14, where θ_A and θ_B are the surface coverages of *A* and *B*, respectively:

$$K = \frac{[A]\theta_B}{[B]\theta_A} \qquad \text{(eq A.14)}$$

The site balance and mass balance require:

$$\theta_A + \theta_B = 1 \qquad \text{(eq A.15)}$$

$$n_A + n_B = n_C \qquad \text{(eq A.16)}$$

where n_A and n_B are the number of aliphatic and aromatic carbons at any time, and n_C is the total number of carbons in the system. If the amounts of adsorbed *A* and *B* are small relative to the total amounts of *A* and *B* (true except in the earliest stages of reaction, when n_B is very small), then we can solve the equilibrium expression for θ_A as follows:

$$\frac{[A]}{[B]} = \frac{n_A}{n_B} \qquad \text{(eq A.17)}$$

$$\theta_A = \frac{n_A}{n_A + K(n_C - n_A)} \quad \text{(eq A.18)}$$

Since one aromatization reaction (eq A.8) forms 6 aromatic carbons and removes 6 aliphatic carbons, the rate of aromatization is:

$$r_{Ar} = \frac{1}{6}\frac{dn_B}{dt} = -\frac{1}{6}\frac{dn_A}{dt} \quad \text{(eq A.19)}$$

The rate of aromatization, relative to the rate of hydrogenolysis, is constrained by two factors: the observed mass balance on hydrogen and the observed aromatic product fraction. The model cannot simultaneously satisfy both constraints, as the mass balance on hydrogen is distorted by contributions of significant non-aromatic, nonlinear molecules, and the aromatic fraction is distorted by the presence of large amounts of light hydrocarbon gases. These gases represent a large portion of the scission products on a molar basis, even if they account for a relatively small portion of the mass in the system. To avoid introducing additional complexity to the model, we ignore the light hydrocarbons and hydrogen balance, and focus solely on the liquid products.

The experimental ^{1}H NMR, ^{13}C NMR and GPC results indicate an overall selectivity for aromatic molecules in the liquid product of ca. 50%. Let us denote the number of molecules consisting only of aliphatic carbons as N_A, and the number of molecules with at least one aromatic carbon as N_B. Each hydrogenolysis (eq A.8) reaction results in a net increase of one solely aliphatic molecule, and each aromatization (eq A.11) reaction converts one aliphatic molecule to one aromatic molecule. Assuming the number of initial molecules is small and the reaction rates are approximately constant over a short period of time, the number of molecules of each time evolve with time *t* as

$$N_A = r_{Hy}t - r_{Ar}t \quad \text{(eq A.20)}$$

$$N_B = r_{Ar}t \quad \text{(eq A.21)}$$

We may then write the molar selectivity among the products *s* as

$$\frac{1}{2} = s = \frac{N_B}{N_A+N_B} = \frac{r_{Ar}}{r_{Hy}} \qquad \text{(eq A.22)}$$

This implies that the rate of aromatization (eq A.11) is half that of the rate of hydrogenolysis (eq A.8). Therefore, the rate of hydrogenolysis can be written in terms of the rates of formation of either aromatic or aliphatic carbons:

$$r_{Hy} = \frac{1}{s} r_{Ar} = \frac{1}{6s}\frac{dn_B}{dt} = -\frac{1}{6s}\frac{dn_A}{dt} \qquad \text{(eq A.23)}$$

We assume the rate law for hydrogenolysis is first-order in both the mass of catalytic Pt, m_{Pt}, and the coverage of active Pt sites by aliphatic carbons, θ_A, with a second-order rate constant *k* (dimensions $g_{Pt}^{-1}\ s^{-1}$):

$$r_{Hy} = k n_{Pt} \theta_A = \frac{k m_{Pt} n_A}{n_A + K(n_C - n_A)} \qquad \text{(eq A.24)}$$

$$\frac{dn_A}{dt} = \frac{-6sk m_{Pt} n_A}{n_A + K(n_C - n_A)} \qquad \text{(eq A.25)}$$

Integration of eq A.22 leads to the following expressions:

$$\int_{n_{A,0}=n_C}^{n_A} \frac{n_A + K(n_C - n_A)}{n_A} dn_A = -6sk m_{Pt} \int_0^t dt \qquad \text{(eq A.26)}$$

$$K n_C ln\frac{n_A}{n_C} + (K-1)(n_C - n_A) = -6sk m_{Pt} t \qquad \text{(eq A.27)}$$

For K >> 1, the integrated rate law simplifies to:

$$ln\frac{n_A}{n_C} + \left(1 - \frac{n_A}{n_C}\right) = \frac{-6sk m_{Pt} t}{K n_C} \equiv -\tau \qquad \text{(eq A.28)}$$

where τ is a dimensionless time. This equation can be solved for the fraction of aliphatic carbon, n_A/n_C, using the Lambert W function:

$$\frac{n_A}{n_C} = -W\left(e^{-(\tau+1)}\right) \qquad \text{(eq A.29)}$$

The shape of this function is shown in Fig. A.15.

We can also use eq A.28 to predict the evolution of the number-average chain length of all chains, M_n. We assume that the loss of mass to light hydrocarbons is negligible. First, note that the number of aromatic carbons is given by $n_B = n_C - n_A$, and that six aromatic carbons correspond to one aromatization event. The number of hydrogenolysis events is $n_B / (6s)$, or $n_B /3$ for $s = 1/2$. Each hydrogenolysis event results in a new chain, therefore the total number of chains present at time t, N_t, is:

$$N_t = N_0 + \frac{1}{6s} n_B = N_0 + \frac{1}{6s}(n_C - n_A) \qquad \text{(eq A.30)}$$

where N_0 is the initial number of polymer chains in the system. The number-average chain length, M_n, evolves in time as:

$$M_n(t) = \frac{n_C}{N_t} = \frac{n_C}{N_0 + \frac{1}{6s}(n_C - n_A)} \qquad \text{(eq A.31)}$$

Thus

$$\frac{1}{M_n(t)} = \frac{N_0}{n_C} + \frac{n_C - n_A}{6s n_C} = \frac{1}{M_n(0)} + \frac{1}{6s}\left(1 - \frac{n_A}{n_C}\right) \qquad \text{(eq A.32)}$$

Rearranging eq A.32 for n_A/n_C and substituting into eq A.28 yields the relationship between M_n and reaction time:

$$1 - \frac{n_A}{n_C} = \frac{6s}{M_n(t)} - \frac{6s}{M_n(0)} \qquad \text{(eq A.33)}$$

$$ln\left(1 - \frac{6s}{M_n(t)} + \frac{6s}{M_n(0)}\right) + \left(\frac{6s}{M_n(t)} - \frac{6s}{M_n(0)}\right) = -\tau \qquad \text{(eq A.34)}$$

Plotting the inverse number average molecular weight in terms of dimensionless time yields Fig. A.15 inverted in the y-axis, shown in Fig. A.16.

The example above pertains to a system with no aromatic carbons initially present, $n_B(0) = 0$. If this is not the case, the algebra becomes more complicated, but an expression for the evolution of the average chain length may still be found. As aromatic carbons occupy catalytic sites without participating in hydrogenolysis, their presence slows down

hydrogenolysis. When $n_B(0)$ is large relative to m_{Pt}, no aliphatic carbons adsorb, and no hydrogenolysis takes place.

An additional effect not included in the model is the ability of aromatics to consume hydrogen for their own hydrogenation. This may become significant at sufficiently high aromatic concentrations.

Finally, we consider a model in which aromatization (eq A.8) does not occur. This is the case when the H_2 partial pressure is very large, and the reaction equilibrium disfavors further H_2 production via aromatization. Thus, assuming no initial aromatics ($n_B(0) = 0$) and no aromatization ($r_{Ar} = 0$), we write the rate of formation of new aliphatic chains as:

$$\frac{dN}{dt} = r_{Hy} = km_{Pt} \qquad \text{(eq A.35)}$$

Integration of eq A.35 leads to

$$N_t = N_0 + km_{Pt}t \qquad \text{(eq A.36)}$$

Analogous to eq A.31, the number-average chain length evolves in time as:

$$M_n(t) = \frac{n_C}{N_t} = \frac{n_C}{N_0 + km_{Pt}t} \qquad \text{(eq A.37)}$$

Rearranging and noting that $n_C/N_0 = M_n(0)$ yields an expression similar to eq A.34:

$$\frac{1}{M_n(t)} - \frac{1}{M_n(0)} = \frac{km_{Pt}}{n_C} \equiv \tau_H \qquad \text{(eq A.38)}$$

where τ_H is an alternative dimensionless time for the case of hydrogenolysis without aromatization.

We note that both models (i.e., with and without the contribution of the aromatization reaction) display similar behaviors. In both, the evolution in average chain length slows and appears to halt, due to the constant rate of new chain production. Since the number of chains increases at a constant pace, chains made later in the reaction have a smaller impact on the average chain length. When aromatization is possible, the kinetics of chain cleavage are slowed

even more, because the active sites become progressively occupied by strongly adsorbed aromatics. This has a more severe effect on the leveling of the average chain length, relative to the model without aromatic formation.

Uncertainty assessment

The model in eq 2.3 was fit to the experimental data (time dependence of the number-average chain length) using Mathematica's NonlinearModelFit routine. This process assumes that the observed number-average chain lengths from any given experiment are independent and normallydistributed with a common standard deviation, estimated to be ±15 carbons, regardless of reactiontime. The first assumption is satisfied, because each sample was reacted only once. The second assumption has not been verified here, but is common in statistical inference, and difficult to proveor disprove with the amount of data presented here. We expect that repeating the process with individually assigned weights and errors would only change the reported fit parameters slightly. Confidence intervals were computed from the fit residuals and the covariance of the fit parametersby the delta method.

Supplementary Figures and Tables

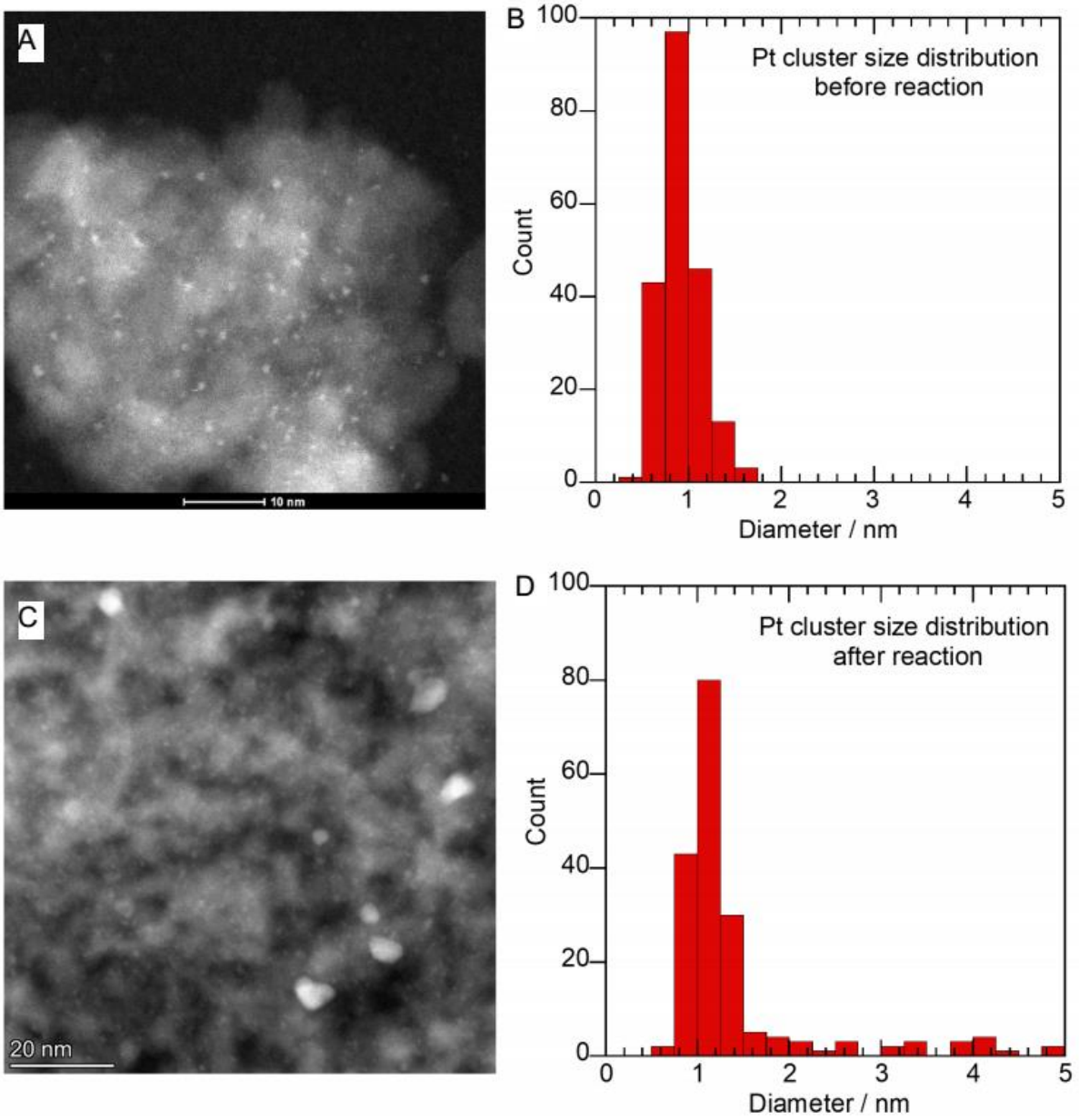

Figure A.1 (A-B) HAADF-STEM images of fresh Pt/ γ -Al_2O_3, and (C-D) histograms showing Pt cluster size distribution.

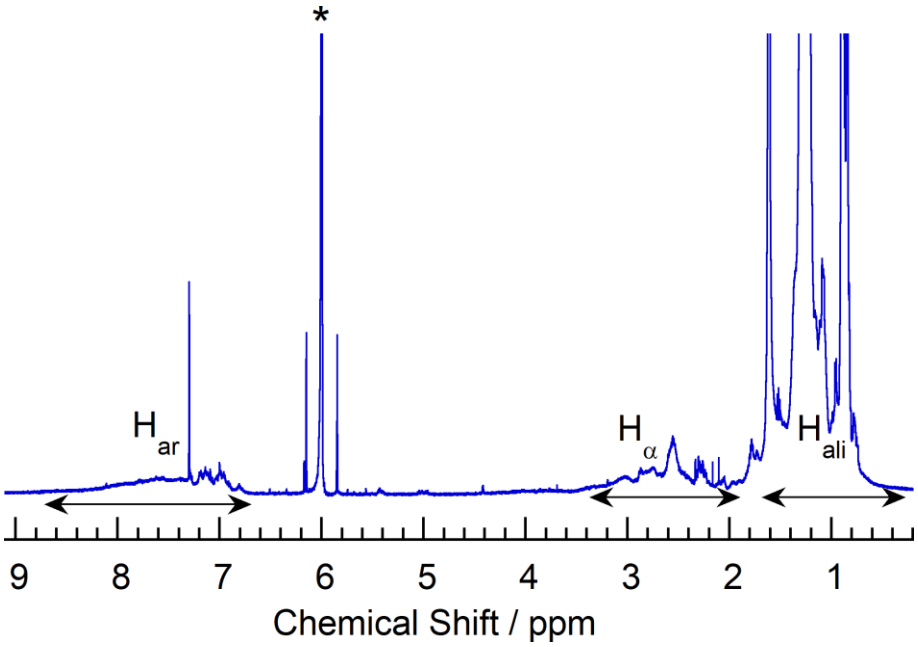

Figure A.2 ^{1}H NMR spectrum of liquid/wax product after heating PE (M_w = 3.52 x 10^3 g/mol, M_n = 1.85 x 10^3 g/mol, $Đ$ = 1.9, average C_{132}) with Pt/γ-Al_2O_3 (1.5 wt% Pt) for 24 h at 280 °C in a mini-autoclave. * indicates residual protons in the solvent (TCE-d_2).

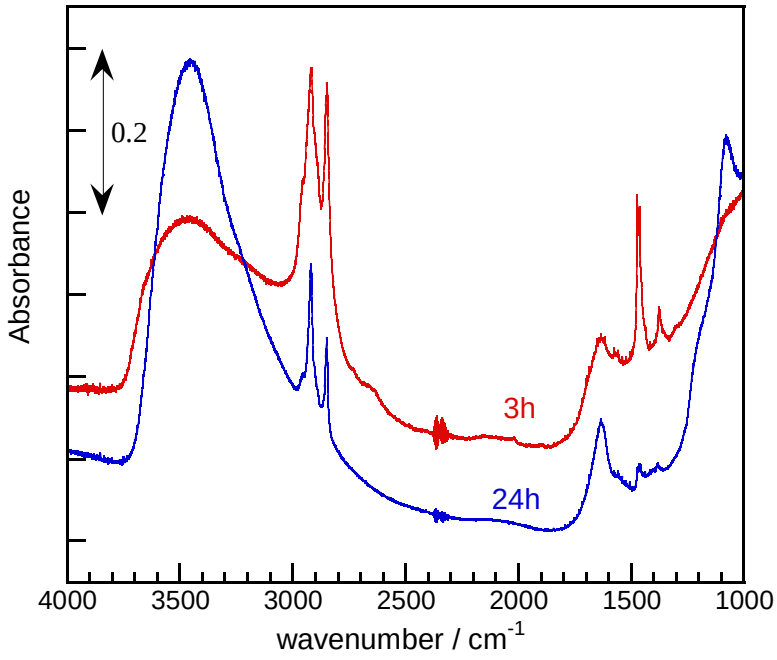

Figure A.3 IR spectra of solid residue (including the catalyst and KBr) recovered after PE reaction for 3 h (red) and 24 h (blue).

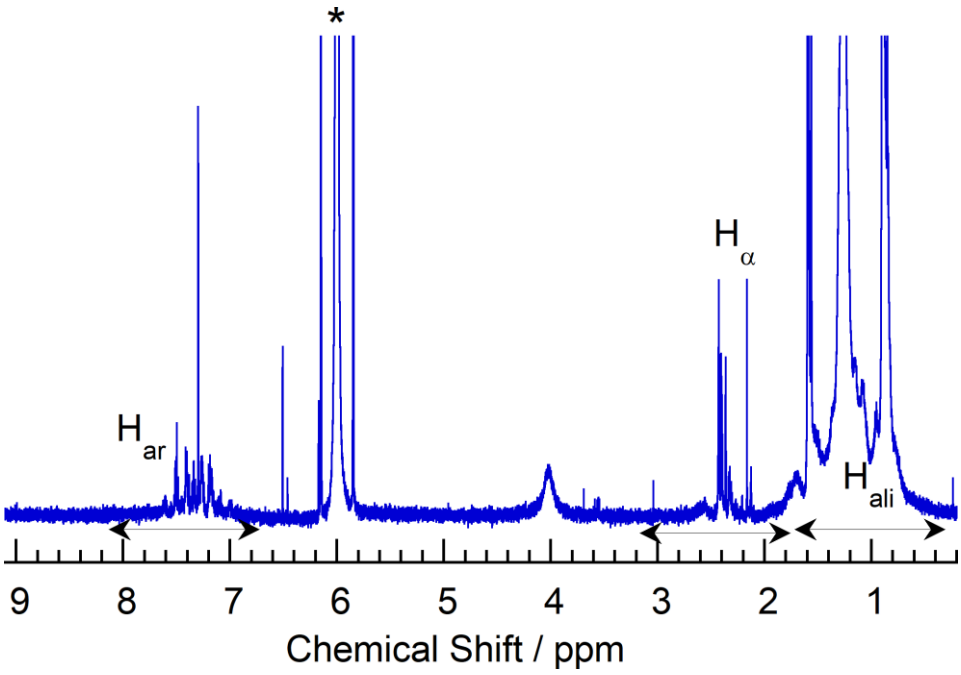

Figure A.4 ^{1}H NMR spectrum (recorded at room temperature) of the soluble component recovered from the solid residue after stirring in TCE-d_2 at 150 °C for 21 h. PE (M_w = 3.52 x 10^3 g/mol, M_n = 1.85 x 10^3 g/mol, $Đ$ = 1.9, average C_{132}) was heated with Pt/γ-Al_2O_3 (1.5 wt% Pt) in a mini- autoclave at 280 °C for 24 h. * indicates residual protons in the solvent (TCE-d_2).

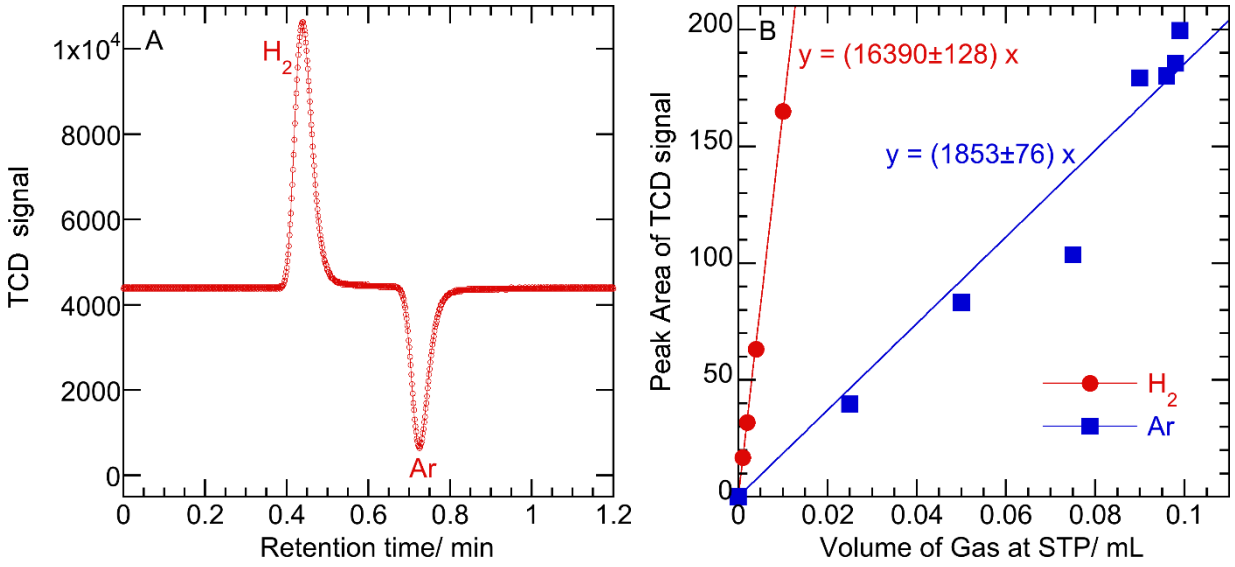

Figure A.5 (A) GC-TCD of gases collected after the catalytic disassembly of PE (M_w = 3.52 x 10^3 g/mol), by heating with 1.5 wt% Pt/γ-Al_2O_3 for 24 h at 280 °C in a 13 mL mini-autoclave, with Ar(12.8 mL, 1 atm) present as internal standard; (B) TCD calibration curve for H_2 and Ar. The molarratio of H_2 to Ar was determined from the peak areas and response factors.

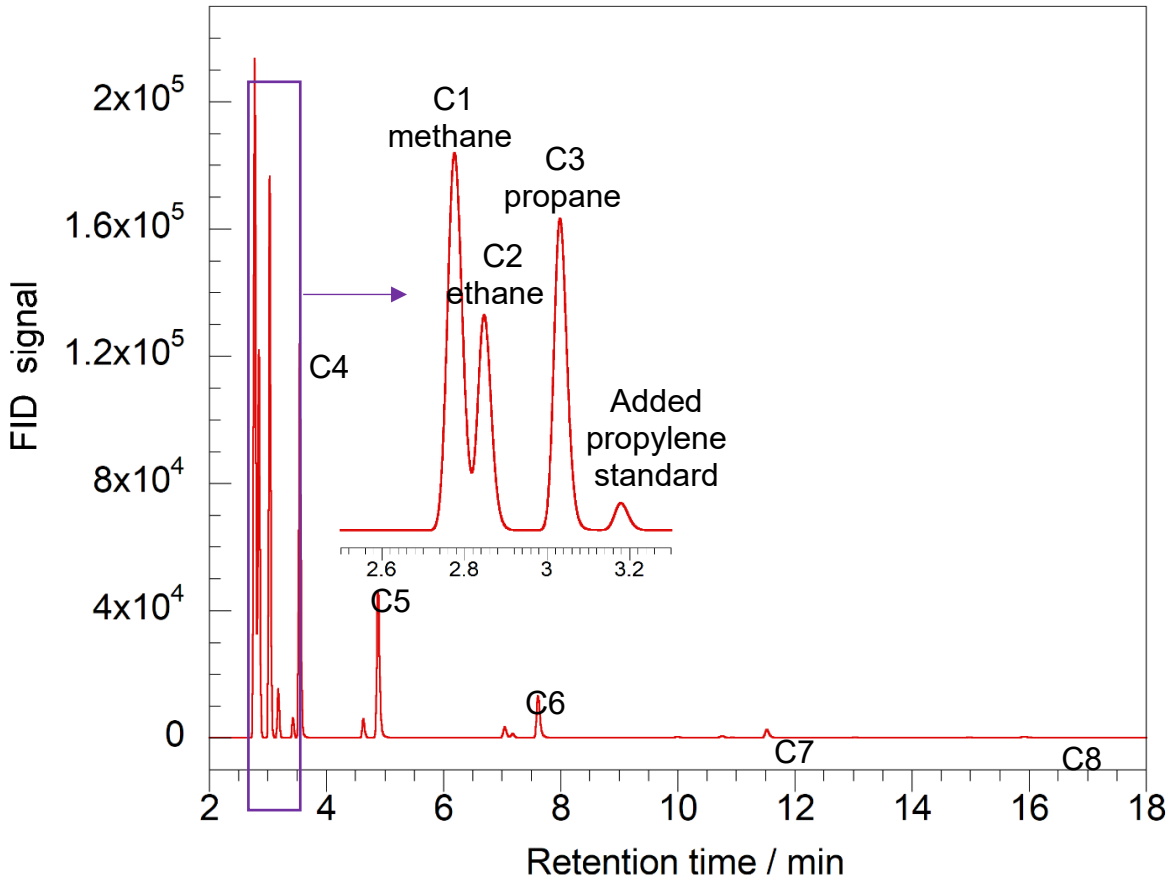

Figure A.6 GC-FID of gases collected after catalytic disassembly of PE (M_w = 3.52 x 10^3 g/mol),by heating with 1.5 wt% Pt/γ-Al_2O_3 for 24 h at 280 °C in a 13 mL mini-autoclave. Propene was added as an internal standard. Relative carbon response factors were assumed to be 1.0.

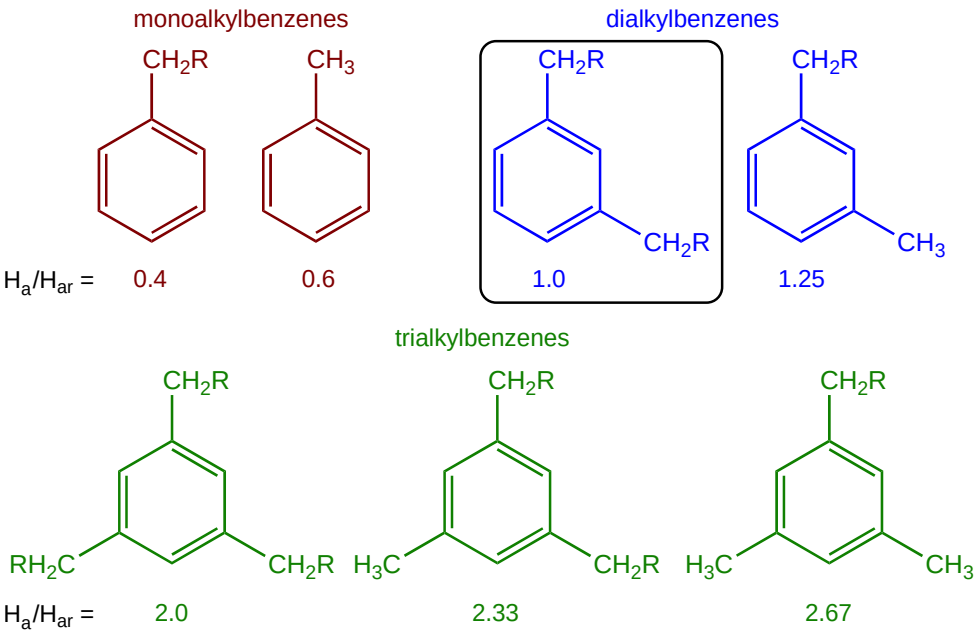

Figure A.7 Possible structures for mono-, di- and tri-substituted alkylbenzenes, and their corresponding H_{α}/H_{ar} ratios. Products with $-C_{\alpha}H_2R$ and $-C_{\alpha}H_3$ substituents are considered to be the major products, because the most intense ^1H NMR signals are observed at 2.35-2.85 ppm.

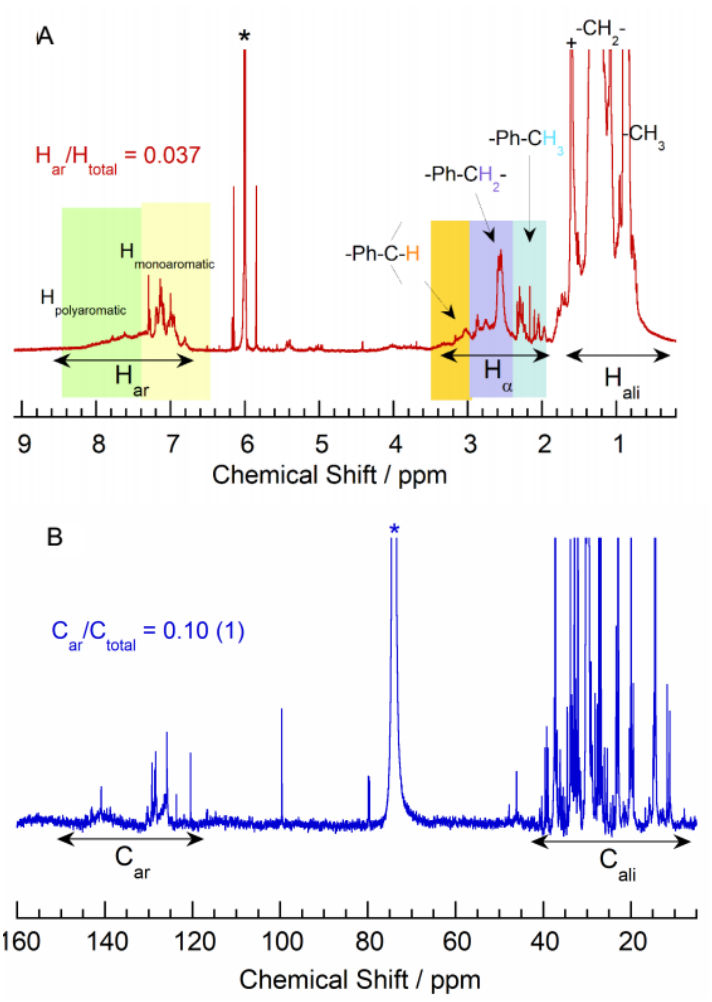

Figure A.8 NMR spectra of the chloroform-soluble wax product obtained from the solvent-free depolymerization of PE (M_n = 1.85 x 10^3 g/mol, $Đ$ = 1.9, average C_{132}) in a Parr autoclave reactor,after 24 h at 280 °C: (A) ^{1}H NMR spectrum; and (B) ^{13}C NMR spectrum. * indicates the solvent (TCE-d_2).

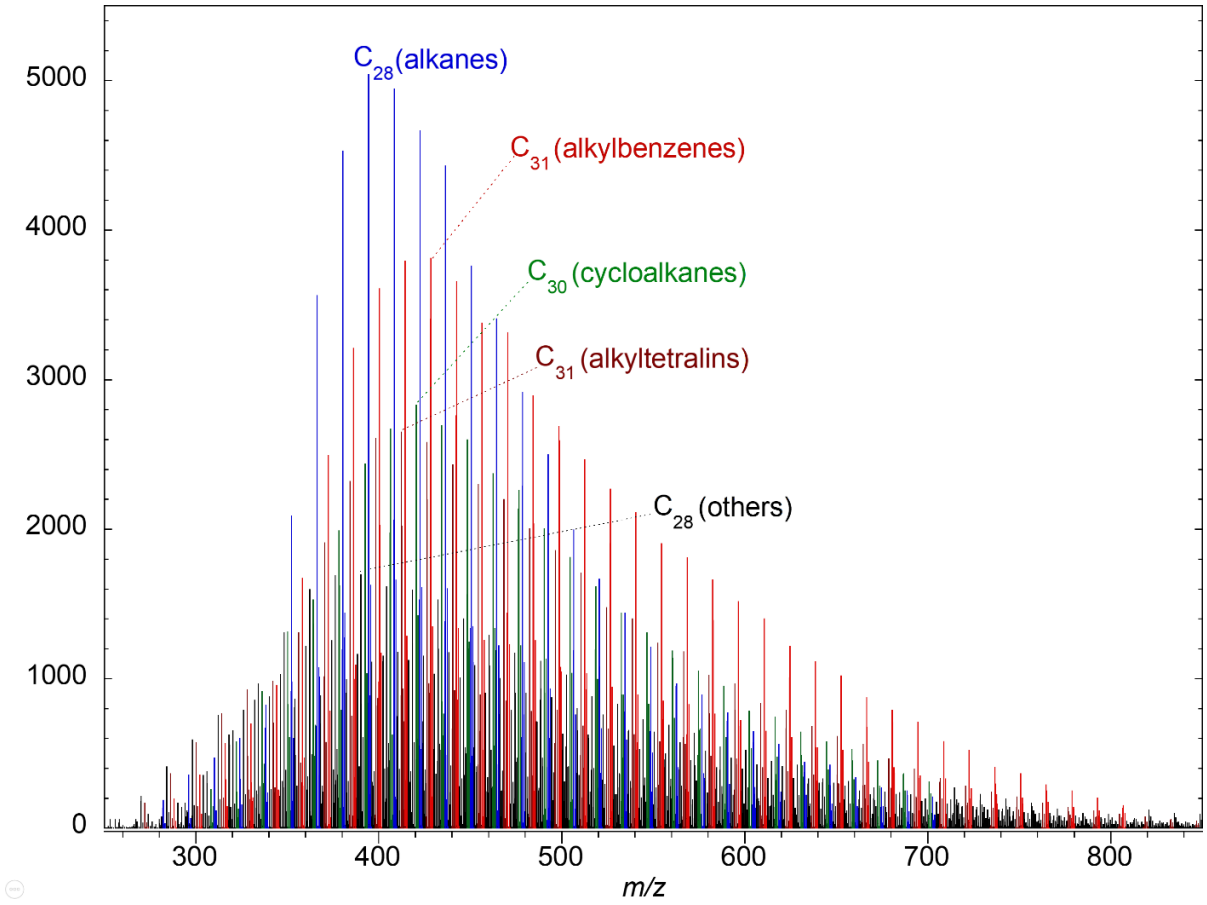

Figure A.9 Full-range FD-MS analysis of lighter hydrocarbons from the solvent-free conversion of PE (M_w = 3.52 x 10^3 g/mol, M_n = 1.85 x 10^3 g/mol, $Đ$ = 1.9, average C_{132}), catalyzed by 1.5 wt%Pt/γ-Al_2O_3 at 280 °C in Parr reactor for 24 h. The carbon number labels indicate the highest peak intensity within each color-coded mass series. The black series includes dicycloparaffins (14n-2),alkylanthracenes (14n-4) and benzodicycloparaffins (14n-10).

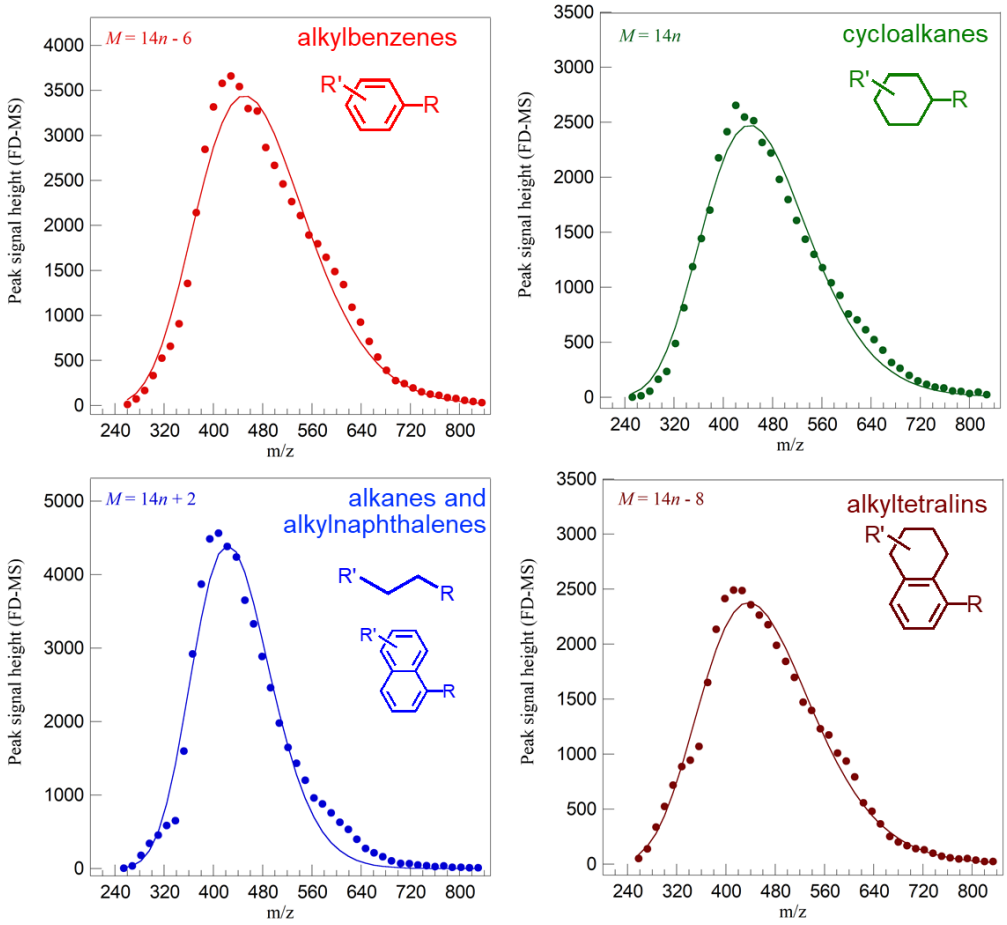

Figure A.10 Log-normal distribution fit of the major hydrocarbon mass series observed by FD-MS.

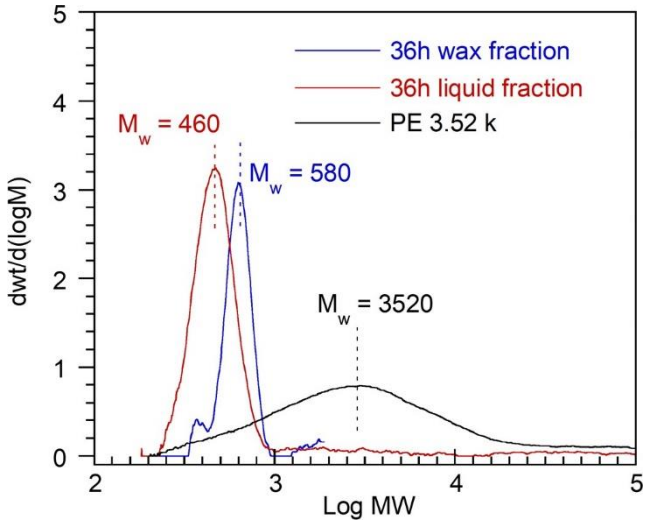

Figure A.11 GPC and molecular weight distribution of lighter and heavier fractions of liquid/wax products from the catalytic disassembly of PE (M_w = 3.52 x 10^3 g/mol, $Đ$ = 1.9, average C_{132}), after heating with 1.5 wt% Pt/γ-Al_2O_3 for 36 h at 280 °C in Parr reactor.

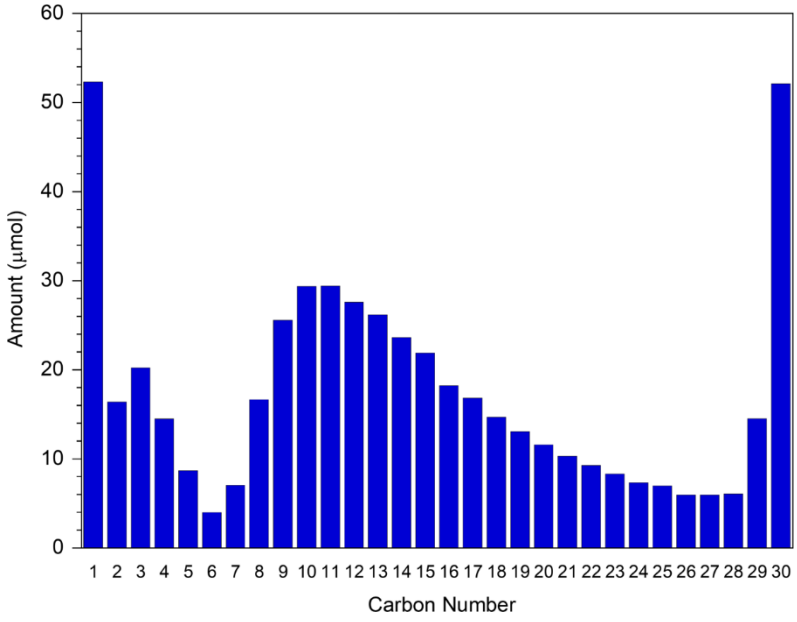

Figure A.12 Distribution of products and unreacted starting material from the catalytic reaction of $C_{30}H_{62}$ with 1.5 wt% Pt/γ-Al_2O_3 in a 12.8 mL mini-autoclave at 280 °C for 24 h.

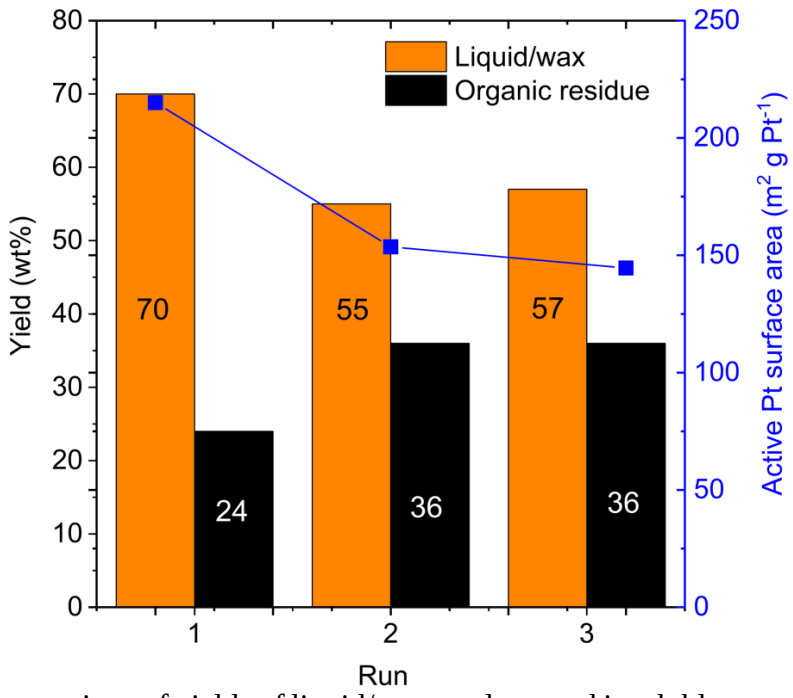

Figure A.13 Comparison of yields of liquid/wax products and insoluble organics, as well as the active Pt surface area (m^2 g_{Pt}) of fresh and recycled catalyst measured by CO chemisorption prior to reaction, in three consecutive catalytic reactions of PE catalyzed by Pt/γ-Al_2O_3 (Table A.6, Exp. S4-6). The yields in the first and second runs are the averages of two duplicate reactions. Reaction conditions: PE (M_n = 1.85 x 10^3 g/mol, $Đ$ = 1.90) and catalyst (Pt/γ-Al_2O_3, 1.5 wt% Pt) were added in a fixed mass ratio of 0.60 (see details on p. 115). Each reaction was conducted at 280 °C for 6 h, in a 10 mL mini-autoclave.

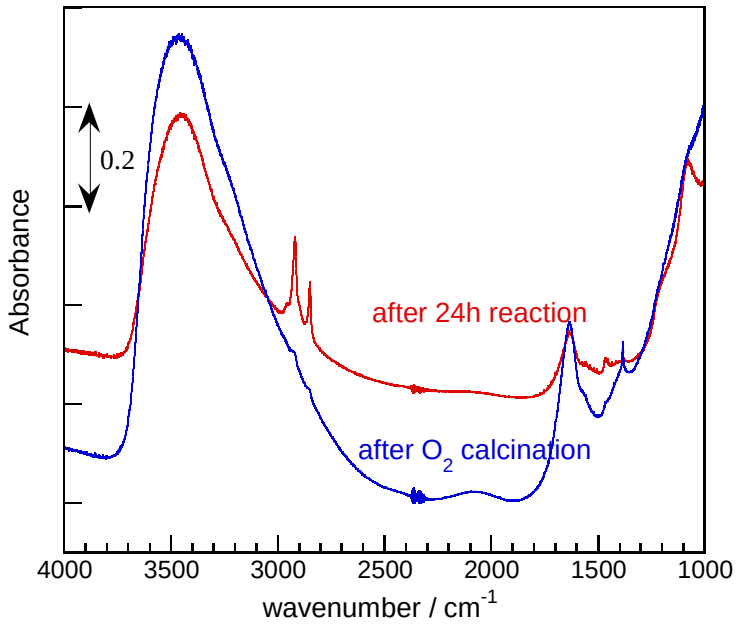

Figure A.14 IR spectra in the wavenumber range of 1000-4000 cm^{-1} of solid residue (containing thecatalyst and diluted with KBr) after PE upgrading reaction at 280 °C for 24h (red) and further calcination in O_2 at 400 °C (blue), respectively.

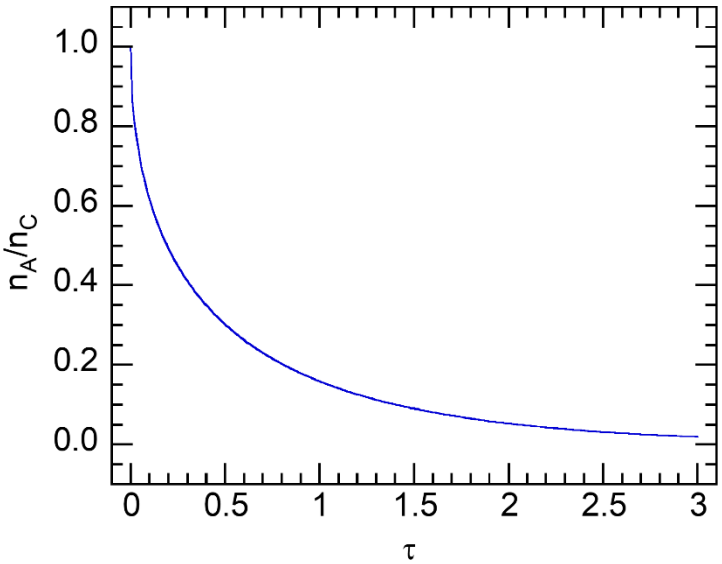

Figure A.15 Fraction of aliphatic carbon, n_A/n_C, as a function of the dimensionless time $= 6\ s\ k\ m_{Pt} t\ /\ K\ n_C$, assuming $K >> 1$ and no aromatics initially present in the reactor, given by eq A.26.

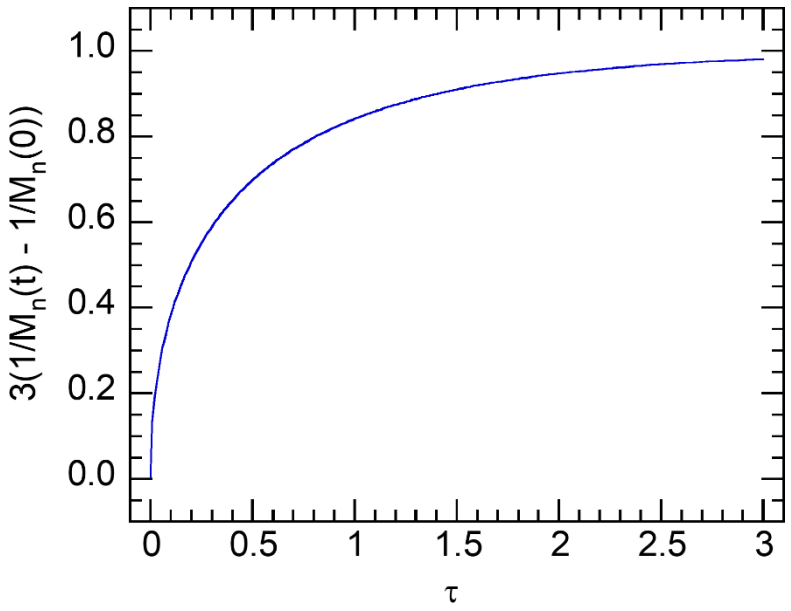

Figure A.16 Relationship between inverse molecular weight and dimensionless time $\tau = 6\ s\ k\ m_{Pt}\ t\ /\ K\ n_C$, given by eq A.31, when $s = 0.5$.

Table A.1 Characterization of polymer starting materials

Starting Material	T_m (°C)	M_n (g/mol)	M_w (g/mol)	$Đ$	Methyl Groups/1000 Carbons
PE (Sigma Lot SKU-427772)	104	1.85×10^3	3.52×10^3	1.9	45.9
LDPE	110, 121	12.8×10^3	94.5×10^3	7.4	23.1
HDPE	130	14.8×10^3	53.5×10^3	3.6	N/A

Table A.2 Mass series of hydrocarbon products observed by FD-MS

m/z	Alternate m/z	Most probable assignment	Alternate assignments
14n		cycloalkanes	diphenylparaffins, naphthocycloparaffins
14n + 2	14n-12	alkanes, alkylnaphthalenes	
14n + 4	14n-10	benzodicycloparaffins	
14n + 6	14-8	benzocycloparaffins	
14n + 8	14n-6	alkylbenzenes	
14n + 10	14n-4	alkylanthracenes/phenanthrenes	tricycloparaffins
14n + 12	14n-2	dicycloparaffins	alkylphenalenes, alkylfluorenes

Table A.3 GPC and ^{1}H NMR characterization of liquid/wax hydrocarbons recovered from the tandem conversion of various PEs [*]

Exp.	PE		Reactor Volume	Time	Products									Total Yield	Total S_{Ar}
	M_n g mol^{-1}	$Đ$	mL	h	Yield %	M_n g mol^{-1}	$Đ$	C_{avg} [†]	$\frac{H_{Ar}}{H_{total}}$	$\frac{H_{mono}}{H_{poly}}$	S_{Ar} [‡] mol%	$\frac{C_{Ar}}{C_{total}}$	S_{Ar} [§] mol%	%	mol%
0[¶]	1.85 x10^3	1.90	10	24	34	768	1.85	55	-	-	-				
1			10	24	80	328	1.31	24	0.039	0.9	40(3)				
2			13	24	75	414	1.24	30	0.040	1.1	52(4)				
3			90	24	46	466	1.12	34	0.037	1.6	57(5)	0.10	52(4)	70	64(5)
					24	538	1.34	39	0.047	1.0	77(6)	0.11	61(5)		
S1			90	36	42	431	1.06	31	0.054	2.3	75(5)	0.13	64(5)	55	81(6)
					13	551	1.06	39	0.058	1.0	92(7)	0.16	91(7)		
4	12.8 x10^3	7.37	90	24	39	366	1.10	27	0.031	1.8	39(3)	0.09	37(3)	69	44(4)
					30	355	1.12	26	0.045	1.1	50(4)	0.10	39(4)		
5	14.8 x10^3	3.61	90	24	20	347	1.09	25	0.041	1.8	46(4)			55	50(4)
					35	353	1.32	26	0.047	1.0	52(4)				

[*] Reaction conditions: 118 mg reactant, 200 mg catalyst (Pt/γ-Al_2O_3, 1.5 wt%), 280 °C. [†] Calculated as M_n/14. Where two entries are present for the same experiment, the liquid/wax hydrocarbon products were collected and analyzed separately. [‡] Selectivity to alkylaromatics (S_{Ar}) calculated based on analysis of ^{1}H NMR spectrum. [§] Selectivity to alkylaromatics (S_{Ar}), as defined on p. 123, calculated based on analysis of ^{13}C NMR spectrum. Uncertainties are propagated from the uncertainty in the average carbon number. [¶] Reaction with γ-Al_2O_3 support only.

Table A.4 FD-MS selectivities for various mass series in the liquid hydrocarbons recovered from tandem PE conversion [*]

Mass series	Major assignment	Method 1 [†] area	%	Method 2 [‡] area	%
14n	cycloparaffins	63270	17	5282	19
14n+2	alkanes, alkylnaphthalenes	77706	20	5914	21
14n+4	benzodicycloparaffins	31089	8	2200	8
14n+6	benzocycloparaffins	60489	16	3714	14
14n+8	alkylbenzenes	85390	22	5229	19
14n+10	alkylanthracenes, etc.	27776	7	2117	8
14n+12	dicycloparaffins	37993	10	3047	11
Total		383713	100	27504	100
monoaromatics		22+16+8 =	46	19 +14 + 8 =	41
Polyaromatics [§]		7 + 8 (of 20) =	15	8 + 6 (of 21) =	14
paraffins		17 + 10 + 12 (of 20) =	39	19 + 11 + 15 (of 21) =	45

* Exp. 3 (see main text). [†] Based on peak heights. [‡] Based on peak areas. [§] The ratio $^1H_{mono}/^1H_{poly}$ = 1.6 was used to calculate the fractional contribution of alkylnaphthalenes in the (14n+2) mass species.

Table A.5 GPC and ^{1}H NMR of liquid/wax hydrocarbons recovered from tandem PE conversion, as a function of reaction time*

Exp.	Time	Products						
	h	Yield %	M_w g mol^{-1}	M_n g mol^{-1}	$Đ$	C_{avg} †	$\frac{H_{Ar}}{H_{total}}$	$\frac{H_{mono}}{H_{poly}}$
1a	1.0 ‡	-	4156	1758	2.36	126	-	-
1b	3.0 ‡	-	2350	1110	2.11	79	-	-
1c	3.0	21	1177	789	1.49	56	0.004	3.8
1d	4.5 ‡	-	1084	584	1.86	42	-	-
1e	6.0	66	716	424	1.69	30	0.018	2.0
1f	12.0	70	460	302	1.52	22	0.024	1.8
1g §	24.0	80	430	328	1.31	23	0.039	0.9

* Reaction conditions: 118 mg PE (M_n = 1.85 x 10^3 g/mol, $Đ$ = 1.90), 200 mg catalyst (Pt/γ-Al_2O_3, 1.5 wt% Pt), 280 °C, 10 mL mini-autoclave. Each experiment was performed independently (not as continuous sampling from one experiment). † Calculated as M_n/14. ‡ GPC analysis was performed on the crude reaction mixture. § This experiment is the same as Exp. 1 in Fig. 2.2B and Table A.3.

Table A.6 GPC and ^{1}H NMR characterization of liquid/wax hydrocarbons recovered from the tandem conversion of triacontane and PE*

Exp.	Reactant	Reactor volume	Products							Active Pt surface area §
			Yield	M_n	$Đ$	C_{avg} †	$\frac{H_{Ar}}{H_{total}}$	$\frac{H_{mono}}{H_{poly}}$	S_{Ar} ‡	
		mL	%	g mol^{-1}					%	m^2 g$_{Pt}^{-1}$
S2	$C_{30}H_{62}$	10	70	-	-	17 ‡‡	0.012	2.2	9	-
S3		13	72	-	-	20 ‡‡	0.016	2.1	14	-
S4	PE	10 §	70(2) ¶	328	1.89	23	0.017	2.0	18	215.2
S5		10 #	55(2) ¶	628	2.21	45	0.013	3.4	27	153.6
S6		10 **	57	694	2.56	50	0.008	2.8	18	144.6
S7		90 ††	4	234	1.08	17	0.017	1.1	14	-
			46	373	1.29	27	0.021	1.8	27	

* Reaction conditions: 118 mg reactant (triacontane or PE, M_n = 1.85 x 10^3 g/mol, $Đ$ = 1.90), 200 mg reduced catalyst (Pt/γ-Al_2O_3, 1.5 wt% Pt), 280 °C for 24 h except where noted. † Calculated as M_n/14. ‡ Selectivity for alkylaromatics (S_{Ar}), as defined on p. 122, calculated based on analysis of ^{1}H NMR spectrum. § Calculated based on CO chemisorption using eq A.1. § Two parallel reactionsin two 10 mL mini-autoclaves at 280 °C for 6 h using fresh catalyst. ¶ The yield of liquid/wax in Exps. S4 and S5 is the average of two duplicate reactions, with the variance in parentheses. # Two parallel reactions in two 10 mL mini-autoclaves at 280 °C for 6 h using once-recycled catalyst. ** Reaction in 10 mL mini-autoclave at 280 °C for 6 h using twice-recycled catalyst. Details for the three consecutive recycling experiments are shown on p. 116. †† Reaction with 1.1 g PE reactant and 1.8 g catalyst at 280 °C. Liquid/wax hydrocarbon products were collected and analyzed separately. ‡‡ Calculated based on GC-FID analysis using eq A.6.

Table A.7 Benson group increments[5] for sub-groups found in linear polyethylene and ortho-substituted dialkylaromatics

Group label	Chemical identity	$\Delta_f H°_{gas,est}$ kJ/mol	$S°_{gas,est}$ J/mol K	Estimated gas-phase increments C_p J/mol K						
				temperature (K)						
				300	400	500	600	800	1000	1500
g_1	$-CH_2-$	-21.0	39.4	23.0	29.1	34.5	39.1	46.3	51.6	59.4
g_2	$-CH_3$	-42.7	127.2	25.9	32.8	39.3	45.2	54.5	61.8	73.6
g_3	C_{Ar}-C	23.0	-32.1	11.2	13.1	15.4	17.4	20.8	22.8	25.0
g_4	C_{Ar}-H	14.0	48.2	13.6	18.6	22.8	26.4	31.5	35.2	40.7
g_5	Ar-$C_\alpha H_2$-	-20.0	39.1	24.4	31.8	37.6	41.9	48.1	52.5	57.6
g_6	Ring strain correction	3.0	-25.0	4.6	6.3	5.4	5.0	3.8	2.9	-0.4
g_H	H_2	0.0	130.7	28.9	29.2	29.2	29.3	29.6	30.2	32.3

References

(1) Gozum, J. E.; Pollina, D. M.; Jensen, J. A.; Girolami, G. S. "Tailored" Organometallics as Precursors for the Chemical Vapor Deposition of High-Purity Palladium and Platinum Thin Films. *J. Am. Chem. Soc.* **1988**, *110* (8), 2688–2689. https://doi.org/10.1021/ja00216a073.

(2) Garcia, J. R. V.; Goto, T. Chemical Vapor Deposition of Iridium, Platinum, Rhodium and Palladium. *Mater. Trans.* **2003**, *44* (9), 1717–1728. https://doi.org/10.2320/matertrans.44.1717.

(3) Marinho, R. S.; Silva, C. N. da; Afonso, J. C.; Cunha, J. W. S. D. da. Recovery of Platinum, Tin and Indium from Spent Catalysts in Chloride Medium Using Strong Basic Anion Exchange Resins. *Journal of Hazardous Materials* **2011**, *192* (3), 1155–1160. https://doi.org/10.1016/j.jhazmat.2011.06.021.

(4) Macala, G. S.; Matson, T. D.; Johnson, C. L.; Lewis, R. S.; Iretskii, A. V.; Ford, P. C. Hydrogen Transfer from Supercritical Methanol over a Solid Base Catalyst: A Model

for Lignin Depolymerization. *ChemSusChem* **2009**, *2* (3), 215–217. https://doi.org/10.1002/cssc.200900033.

(5) Linstrom, P. NIST Chemistry WebBook, NIST Standard Reference Database 69, 1997. https://doi.org/10.18434/T4D303.

Appendix B

Appendix to Chapter 3

***** *This chapter was reproduced from the following publication. The author of this Ph. D. thesis, Manhao Zeng, is the leading author of this publication who contributed to all parts relevant to this work.*

Zeng, M.; Lee, Y.-H.; Strong, G.; LaPointe, A. M.; Kocen, A. L.; Qu, Z.; Coates, G. W.; Scott, S. L.; Abu-Omar, M. M. Chemical Upcycling of Polyethylene to Value-Added α,ω-Divinyl-Functionalized Oligomers. *ACS Sustainable Chem. Eng.* **2021**, *9* (41), 13926–13936. https://doi.org/10.1021/acssuschemeng.1c05272.

Experimental Section

Materials. Polyethylene of two different molecular weights (Lot SKU 427772, M_n=1.5 kg/mol, $Đ$=2.2; and Lot SKU 427799, M_n=6.6 kg/mol, $Đ$=3.8), Br_2 (≥99.99%, trace metals basis), potassium *tert*-butoxide (≥98%), Grubbs Catalyst® M202 (Lot SKU 775258, Umicore), polybutadiene (Lot SKU 434779, M_n=1,530-2,070 g/mol), tetrahydrofuran (THF, anhydrous, ≥99.9%), toluene (HPLC grade, 99.9%), 1,2-dichloroethane (ACS, ≥99.0%), and silica gel (high purity, average pore size 60 Å, 70-230 mesh) were purchased from Sigma Aldrich. Silver nitrate solution (0.100 N, aqueous) was purchased from Ricca Chemical Company. Chloroform (OmniSolv®, 99.9%) and benzene (OmniSolv®, 99.7%) were obtained from EMD Millipore Corp. Methanol (≥99.8%), sodium bisulfite (≥58.5% SO_2), and Fisherbrand™ Plastic pH Strips were purchased from Thermo Fisher Scientific. Chloroform-*d* (D, 99.8%),

toluene-d_8 (D, 99.5%), and bromobenzene-d_5 (D, 99.5%) were obtained from Cambridge Isotope Laboratories. Ethylene (99.999%) was obtained from Matheson. Sodium bicarbonate (≥99.7%) was obtained from Avantor. Celite™ 545, molecular sieves (3 Å, 8 to 12 mesh), and diphenylmethane (99%) were obtained from Acros Organics. Ethyl vinyl ether (99%, stab.) was purchased from Alfa Aesar.

The THF solvent was degassed, dried over molecular sieves, and stored under an inert atmosphere before its use in dehydrohalogenation experiments. Before use, *t*-BuOK was purified in an Ar-filled glovebox by dissolving the solid in THF, filtering the solution through Celite to remove insoluble particles, and evaporating the solvent from the filtrate at 10^{-4} Torr and 40 °C for 15 h to isolate purified *t*-BuOK, which was stored under an inert atmosphere prior to use. All other chemicals were used as received. A 400-410 nm (150 W) UV LED floodlamp from KUKUPPO was used as the light source for bromination experiments. Ethenolysis reactions were performed in an autoclave vessel (Parr Series 5000 Multiple Reactor System, ~100 mL internal volume) stirred at 678 rpm. Reaction times were recorded after the internal temperature stabilized at the reported value, and do not account for the time required for the temperature to stabilize (~10 min).

Bromination of polyethylene. Polyethylene (5.00 g, 179 mmol C_2H_4) was dissolved in 200 mL benzene at 60 °C. Next, the appropriate quantity of Br_2 was added. *Safety note: bromine (Br_2) is a toxic and corrosive fuming dark red liquid at room temperature and must be handled in a properly ventilated fume hood while wearing appropriate PPE*. The dark red solution was irradiated with a 400-410 nm light source placed ~5 cm from the reaction vessel while stirring at reflux (80 °C) until acid was no longer detected in the headspace by the pH test strips. The reaction flask and the light source were enclosed together with aluminum foil

to maximize exposure of the solution to light. The gaseous HBr formed during the reaction was quantified by bubbling through a 500 mL solution of 0.1 M $AgNO_3$ and recovery through filtration as solid AgBr. After reaction, excess $NaHSO_3$ and $NaHCO_3$ were added to the solution to quench residual Br_2 and neutralize any remaining HBr, respectively. The solution was filtered to remove precipitates and the solvent was evaporated, leaving a residue that was subsequently dissolved in 70 mL benzene at 30 °C and added dropwise to 700 mL methanol to precipitate the brominated polyethylene (BPE) product. The mixture was filtered and the solid was rinsed with methanol. The isolated BPE was dried under reduced pressure (10^{-4} Torr) and characterized by ^{1}H and ^{13}C NMR, IR, elemental analysis (C, H, N, Br), and GPC.

Dehydrobromination of BPE. Under an inert atmosphere, *t*-BuOK (4.34 g, 38.7 mmol) was dissolved in 154 mL THF. A separate solution of BPE (9.12 mmol -CHBr-) was dissolved in 240 mL THF at 65 °C and added dropwise (1 drop every 2 s) to the *t*-BuOK solution at 65 °C. After combining the solutions, the mixture was stirred at reflux (66 °C) for 1 h, then the solvent was evaporated under reduced pressure (1 Torr) to recover vinylene PE (VPE). In the synthesis of VPE from PE with M_n = 6.6 kg/mol, the solid product was isolated without purification and washed with deionized water and methanol. In the synthesis of VPE from PE with M_n = 1.5 kg/mol, the residue was dissolved in 100 mL toluene at 30 °C, and the solution was filtered to remove insoluble particles. The solvent was evaporated under reduced pressure (1 Torr) from the filtrate, leaving behind a residue that was redissolved in 20 mL toluene at 30 °C and added dropwise to 200 mL methanol to precipitate the VPE product. The mixture was filtered, and the precipitate was rinsed with deionized water and methanol. The isolated VPE was dried under reduced pressure (10^{-4} Torr). The molar yields of soluble VPE from PEs with M_n = 1.5 and 6.6 kg/mol were determined by ^{1}H NMR using dichloroethane and

diphenylmethane, respectively, as internal standards. The VPE products were also characterized by ^{13}C NMR, IR, and GPC.

Ethenolysis of polybutadiene (PBD). In a Parr vessel, PBD (50 mg) and Grubbs Catalyst® M202 (22.1 mg, 2.5 mol% relative to vinylene) were dissolved in 5 mL toluene. The atmosphere was replaced with 2.7 bar ethylene via 4 pressurize-vent cycles. The vessel was heated at (100 ± 5) °C for 1 h, then cooled in a dry ice/acetone bath. Volatile compounds in the headspace were analyzed by GC-FID and GC-MS. Air was bubbled through the contents in the vessel for 30 min to remove unreacted ethylene. Dichloroethane was added as internal standard and the solution was filtered through a silica plug to remove the catalyst. The vinylene and vinyl functional groups in the reaction mixture were quantified via ^{1}H NMR.

Ethenolysis of vinylene polyethylene (VPE). In a Parr vessel, VPE (50 mg) and Grubbs Catalyst® M202 (2.5 mol% relative to alkene) were dissolved in 5 mL toluene. In the ethenolysis of VPE derived from PE with M_n = 6.6 kg/mol, an additional 4 mL toluene was used, and the mixture was stirred at 95 °C for 15 h to dissolve the polymer prior to adding the catalyst. Then, the atmosphere was replaced with 2.7 bar ethylene via 4 pressurize-vent cycles. The vessel was heated at (100 ± 5) °C for 1 h, then cooled in a dry ice/acetone bath. Volatile compounds in the headspace were analyzed by GC-FID and GC-MS. After bubbling air through the contents in the vessel for 30 min to remove ethylene, 1.0 µL ethyl vinyl ether was added and the reaction mixture was stirred overnight to quench the catalyst. The vinylene and vinyl functional groups in the reaction mixture were quantified via ^{1}H NMR using dichloroethane or diphenylmethane as internal standards. Volatiles were evaporated under reduced pressure (10^{-4} Torr) at 35 °C for 15 h to recover the product oligomers as a precipitate. The vinylene and vinyl functional groups in the isolated α,ω-divinyl-functionalized oligomers

were quantified via ^{1}H NMR using dichloroethane or diphenylmethane as internal standards, while the molecular weights were characterized by GPC.

Nuclear Magnetic Resonance (NMR). ^{1}H NMR spectra were acquired using either a Varian Unity Inova 500 MHz or AS600 600 MHz spectrometer. The 2D ^{1}H-^{13}C HSQC spectrum was obtained using a Varian AS600 600 MHz spectrometer. ^{13}C NMR spectra and all spectra above room temperature were obtained on a Varian Unity Inova 500 MHz spectrometer. ^{1}H and ^{13}C NMR analyses of unreacted PE were performed at 80 °C in bromobenzene-d_5. The vinylene derived from brominated PE with a Br:C ratio of 1:22 was analyzed by ^{1}H NMR at 45 °C in $CDCl_3$. VPE from PE with M_n = 6.6 kg/mol was analyzed via ^{1}H NMR at 92 °C in toluene-d_8. ^{1}H NMR analysis of α,ω-divinyl-functionalized oligomers made from VPE derived from PE with M_n = 6.6 kg/mol was performed at room temperature in toluene-d_8. All other NMR analyses were performed in $CDCl_3$ at room temperature. Chemical shifts (ppm) were referenced to tetramethylsilane (0 ppm).

Gel Permeation Chromatography (GPC). Molecular weights of unreacted PE, VPE, and α,ω-divinyl-functionalized oligomers were analyzed on an Agilent PL-GPC 220 gel permeation chromatograph, equipped with a PL-Gel Mixed B guard column, three PL-Gel Mixed B columns, and a refractive index (RI) detector. Samples were dissolved in 1,2,4-trichlorobenzene (TCB) containing di(*tert*-butyl)hydroxytoluene (BHT, 0.01 wt%) at a loading of approx. 1 mg/mL and were eluted at 150 °C using TCB at a flow rate of 1.0 mL/min. Molecular weight responses were calibrated with monomodal, linear polyethylene standards (Varian and PSS).

The molecular weights of the BPE products were analyzed relative to polystyrene standards on a Waters Alliance e2695 HPLC Separations Module equipped with a Waters 2410

refractive index (RI) detector and a Waters 2998 photodiode array detector (PDA), at a flow rate of 0.3 mL/min using 2 Tosoh Super HZM-N 4.6 mm ID x 150 mm columns and a guard column (MW linear range 200 - 700,000 g/mol). Chloroform containing 0.25 vol% triethylamine was used as the mobile phase at room temperature.

GC-FID. An aliquot of gas from the reaction mixture (0.10 mL) was removed from the Parr reactor for qualitative analysis of light hydrocarbons by GC-FID. The analysis was conducted on a Shimadzu GC-2010 gas chromatograph equipped with a capillary column (Supelco Alumina Sulfate plot, 30 m x 0.32 mm) and a flame ionization detector (FID). The injector and detector temperatures were 200 °C. The temperature ramp program was as follows: hold at 90 °C for 3 min, ramp 20 °C/min to 180 °C, and hold for 10 min.

GC-MS. An aliquot of gas from the reaction mixture (1.00 mL) was removed from the sampling port on the Parr reactor for qualitative analysis of light hydrocarbons by GC-MS. The analysis was conducted on a Shimadzu GC-2010 gas chromatograph equipped with an Agilent DB-1 capillary column (dimethylpolysiloxane, 30 m x 0.25 mm x 0.25 μm) coupled to a QP2010 Mass Spectrometer. The injector and detector temperatures were 250 °C. The temperature ramp program was as follows: hold at 50 °C for 5 min, ramp 10 °C/min to 180 °C, and hold for 10 min.

Infrared Spectroscopy. IR spectra were measured in air using a Nicolet Magna 850 FTIR Spectrometer in the range 500–4000 cm^{-1}.

Elemental Analysis. CHN contents were obtained by a combustion method, using a CEC 440HA Elemental Analyzer in an O_2-enriched He atmosphere. Br analysis was performed by Atlantic Microlabs, Inc. (Norcross, GA, USA).

Techno-Economic Assessment. A process to convert 300 kta (kilotons per annum) PE to α,ω-divinyl-functionalized oligomers was designed using HYSYS V10 (Aspen Technology, Inc.) to size unit operations and estimate utility costs (see Appendix B). Total process equipment cost (TPEC) was estimated using the open-source file CAPCOST_2017_rev2 (Microsoft Excel).[1] Net present value (NPV) was calculated using an established method.[1]

Sample Calculations

Carbon / Br (Table 3.2, BPE-1)

C+H wt% in BPE-1 = 68%

Br wt% in BPE-1 = 100 – (C+H wt%) = 100 - 68 = 32%

$$\text{Molar Ratio of Br : } CH_2 \text{ in BPE-1} = \frac{\text{Br wt\% / Molar Mass of Br}}{CH_2 \text{ wt\% / Molar Mass of } CH_2}$$

$$= (32\% / 79.90 \text{ g/mol Br}) / (68\% / 14.03 \text{ g/mol } CH_2)$$

$$= 1 : 12 \text{ mol Br : mol } CH_2$$

Carbon / Vinylene Group (Table 3.2, VPE-1)

^{1}H NMR was performed on a mixture of 5.4 mg VPE-1 and 1.0 µL DCE in $CDCl_3$.

Ratio of integration of vinylene (4.5-6.4 ppm) to DCE (3.4-4.1 ppm) = 1 : 2.78

1.0 µL DCE = 5.078×10^{-5} mol H (1.826×10^{-5} mol H / integration)

$$\text{Mol of vinylene} = 1.00 \text{ integration} \times \frac{1.826 \times 10^{-5} \text{ mol H}}{\text{integration}} \times \frac{1 \text{ mol vinylene}}{2 \text{ mol H}}$$

$$= 9.131 \times 10^{-6} \text{ mol}$$

Molar mass of vinylene = $\frac{0.0054\ g}{9.131\ x\ 10^{-6}\ mol} = 591.4\ g/mol$

Approximate # of carbon atoms / vinylene group = (591.4 g/mol vinylene) / (14.03 g/mol CH_2) = 42 carbon atoms / vinylene group

<u>% Yields of Isolated α,ω-Divinyl-Functionalized Oligomers (Table 3.4, Entry 1)</u>

Isolated mass of α,ω-divinyl-functionalized oligomers = 50.4 mg

Conversion to vinyl functional group based on remaining vinylene in reaction mixture (Table 3.3, Entry 2) = 100 - 28 = 72%

Expected mass of α,ω-divinyl-functionalized oligomers based on observed vinylene conversion = (initial mol alkene) × (conversion to vinyl functional group) × (C_2H_4 molar mass) + (mass of starting alkene) = (8.455 x 10^{-5} mol) × 0.72 × (28.06 g/mol) + 0.050 g = 0.0517 g

% Yield = $\frac{Recovered\ Yield}{Expected\ Yield} \times 100 = \frac{50.4\ mg}{51.7\ mg} \times 100 = 97\%$

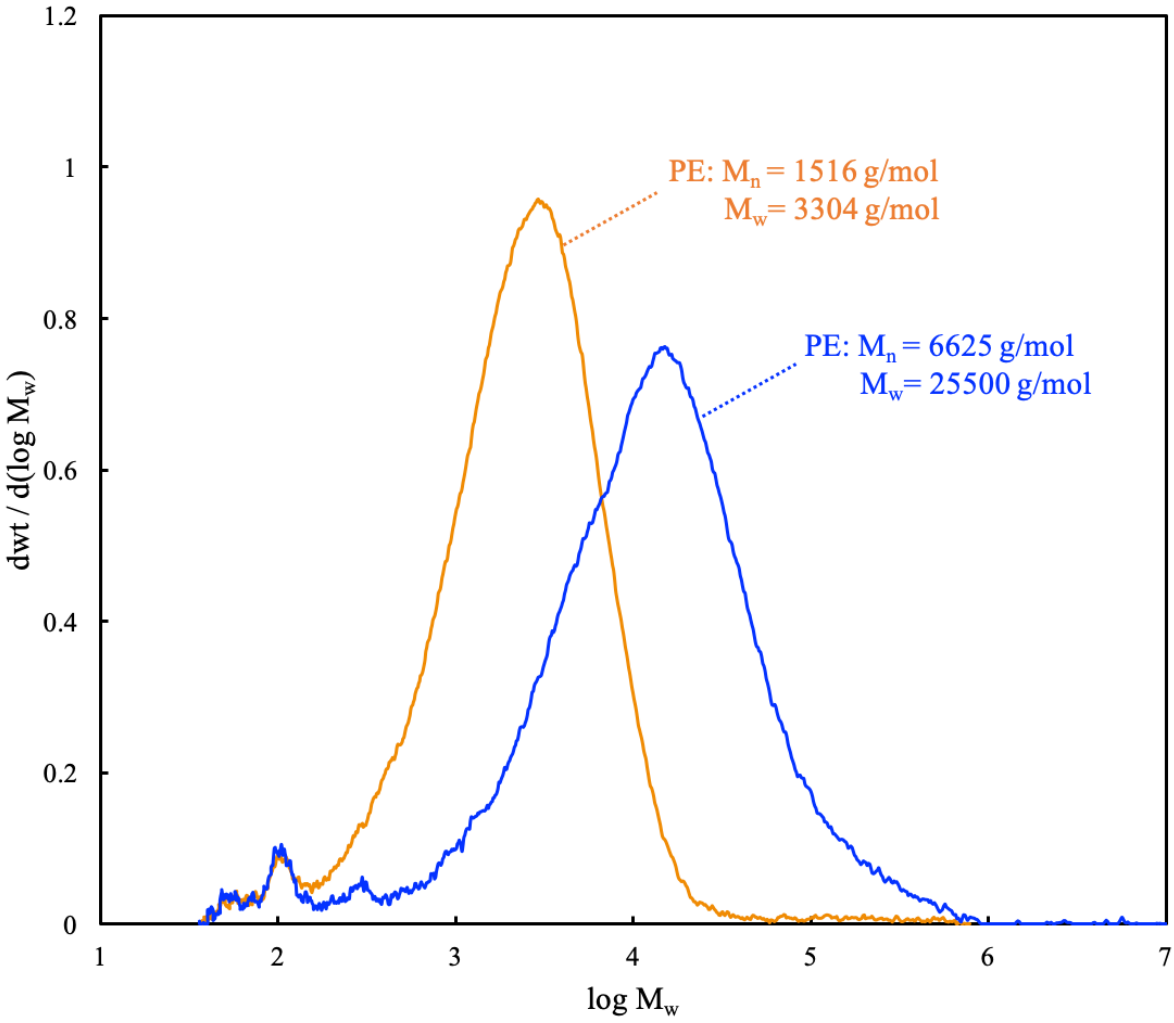

Figure B.1 GPC chromatograms of polyethylenes (PE) used in this work, performed in 1,2,4-trichlorobenzene at 150 °C.

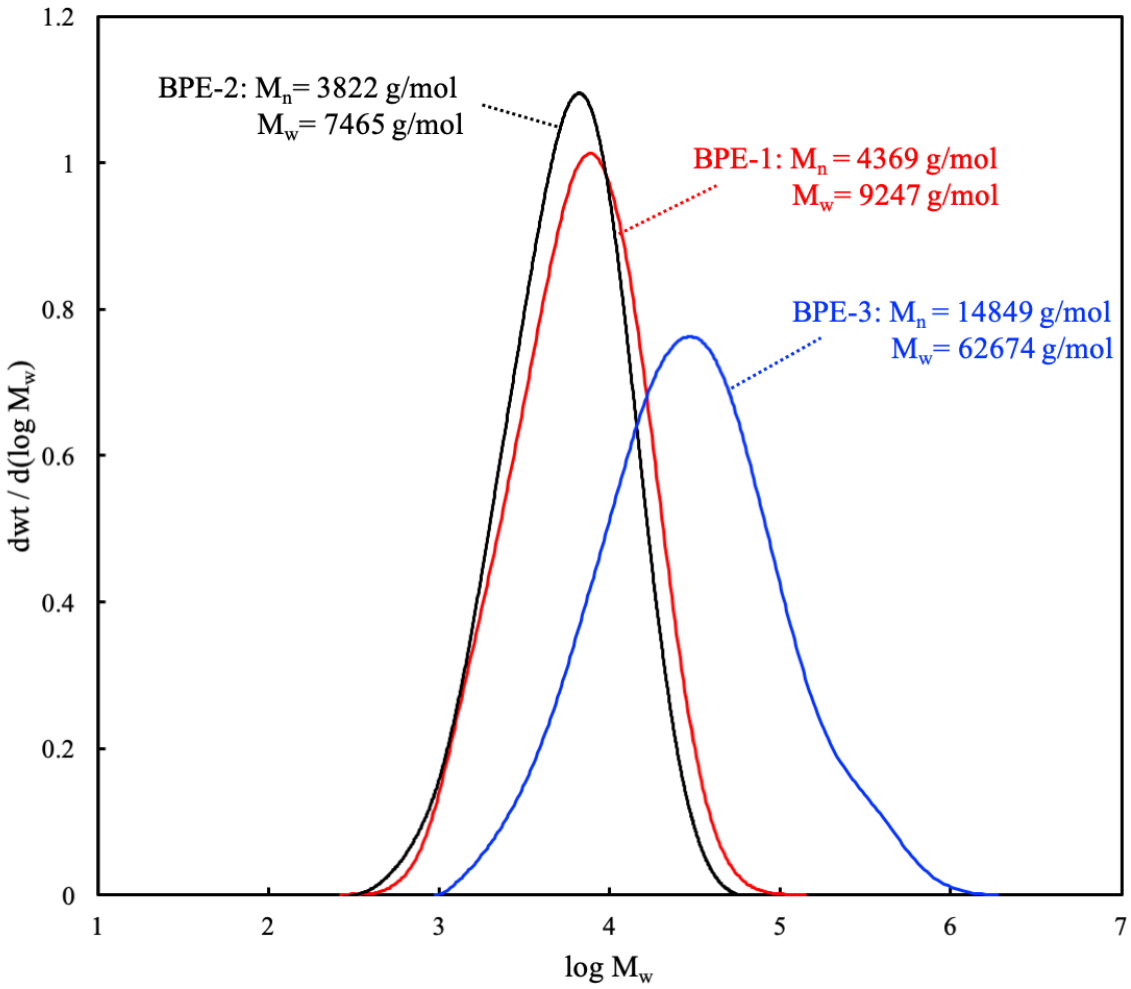

Figure B.2 GPC chromatograms of brominated polyethylenes (BPE) generated in this work, performed in chloroform at room temperature.

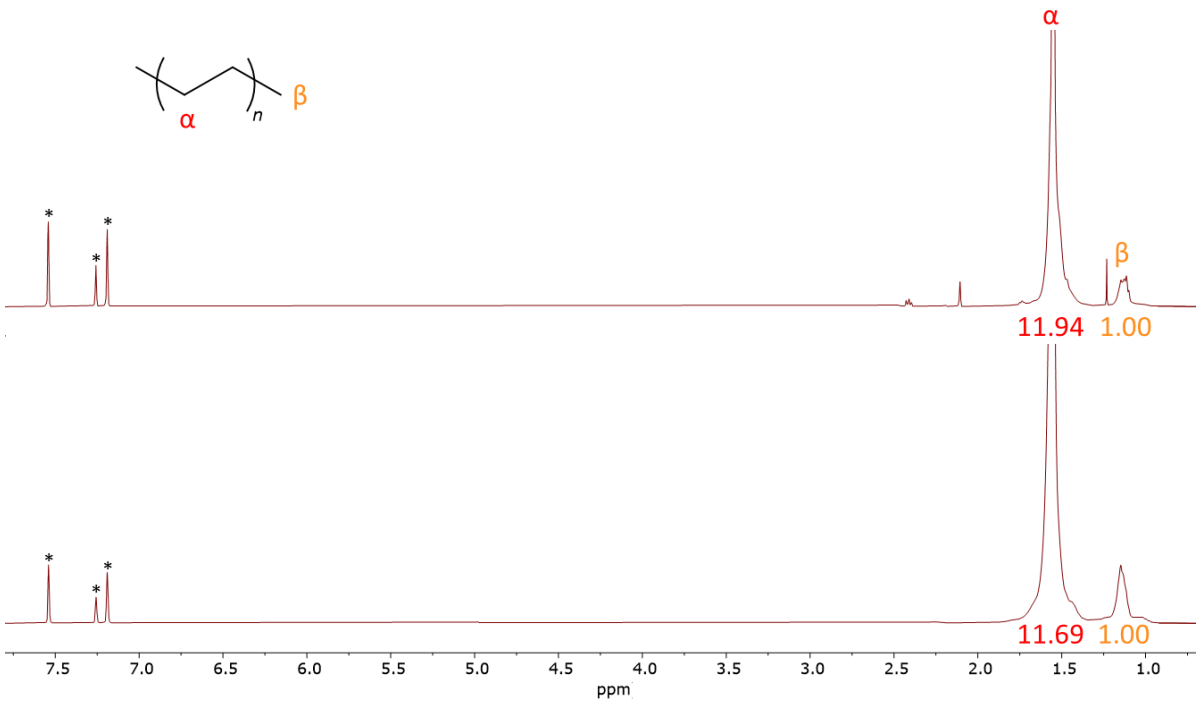

Figure B.3 ^{1}H NMR spectra of unmodified PEs (top: M_n=1.5 kg/mol, bottom: M_n=6.6 kg/mol) in bromobenzene-d_5. *Solvent.

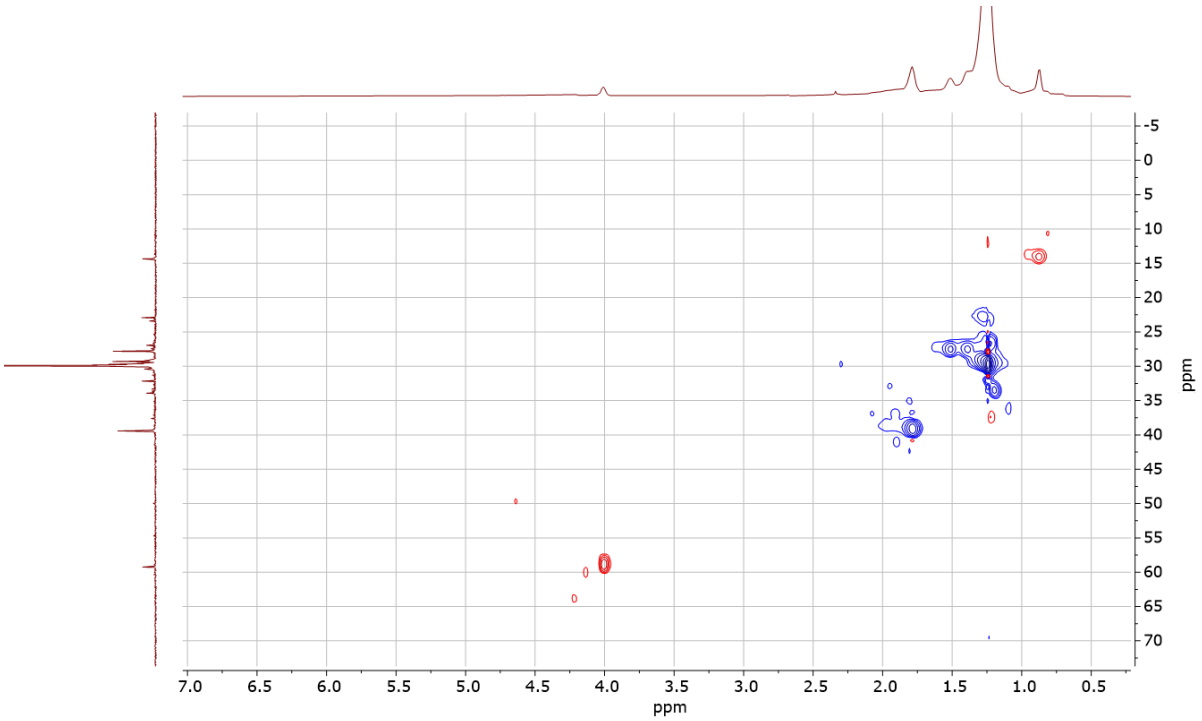

Figure B.4 2D ^{1}H-^{13}C HSQC spectra of BPE (Table 3.1, BPE-1), recorded in $CDCl_3$. Horizontal axis: ^{1}H NMR; vertical axis: ^{13}C NMR; red cross-signals: odd number of protons; blue cross-signals: even number of protons.

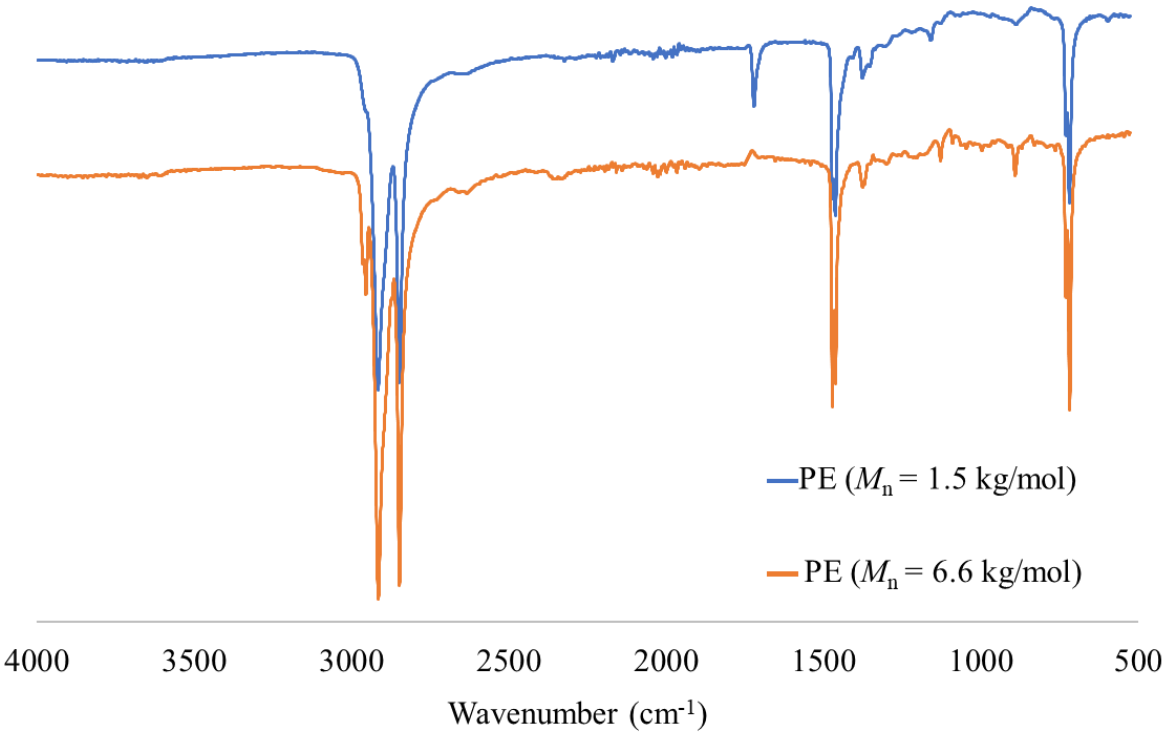

Figure B.5 IR spectra of PE used in this work.

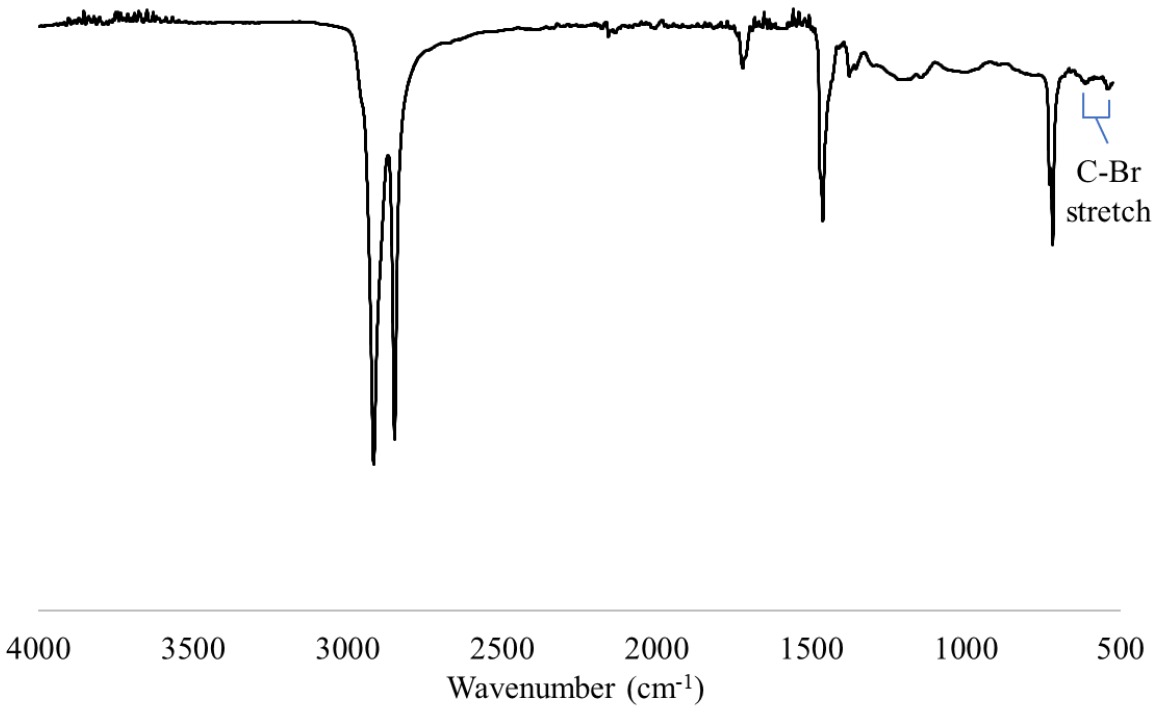

Figure B.6 IR spectrum of BPE (Table 3.1, BPE-1).

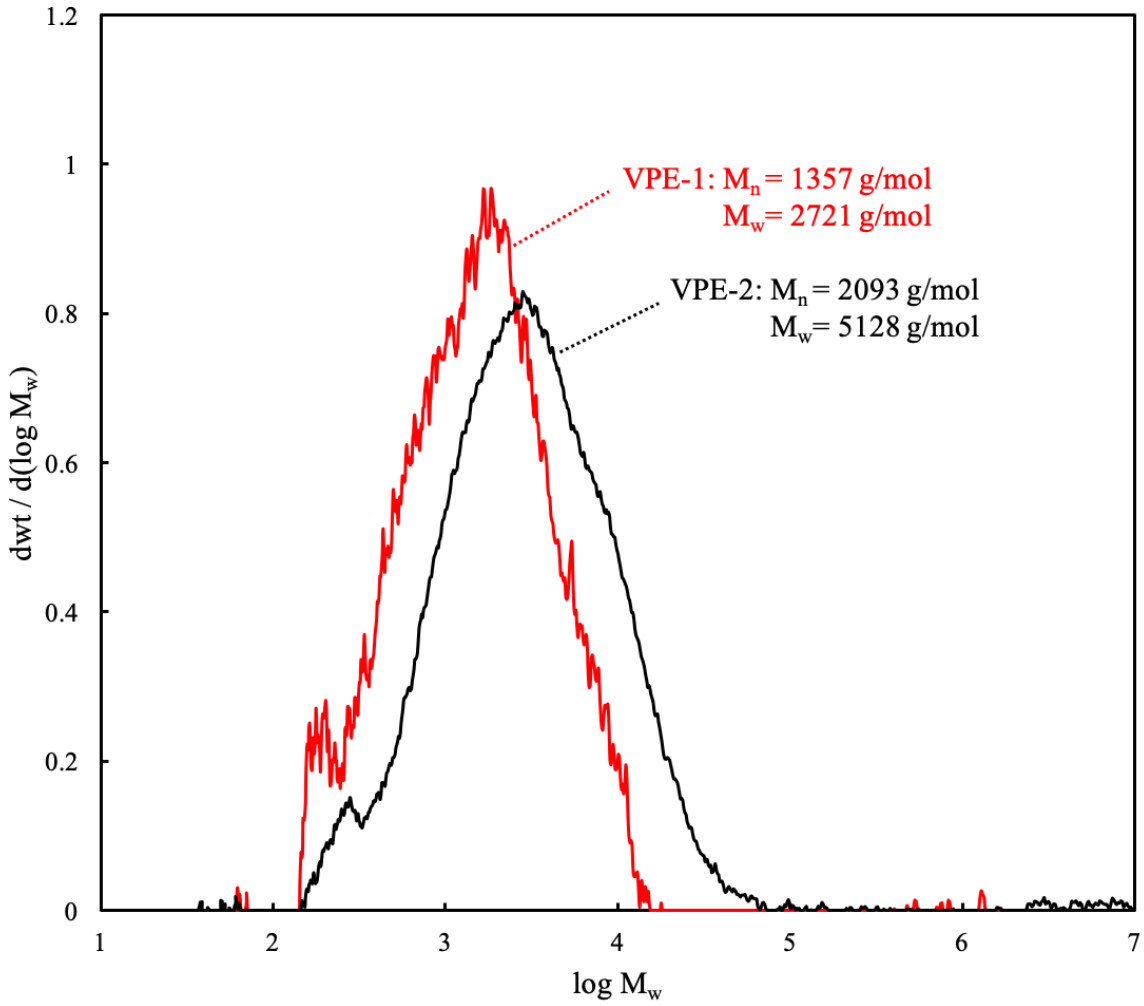

Figure B.7 GPC chromatograms of vinylene polyethylenes (VPE) made in this work, performed in 1,2,4-trichlorobenzene at 150 °C.

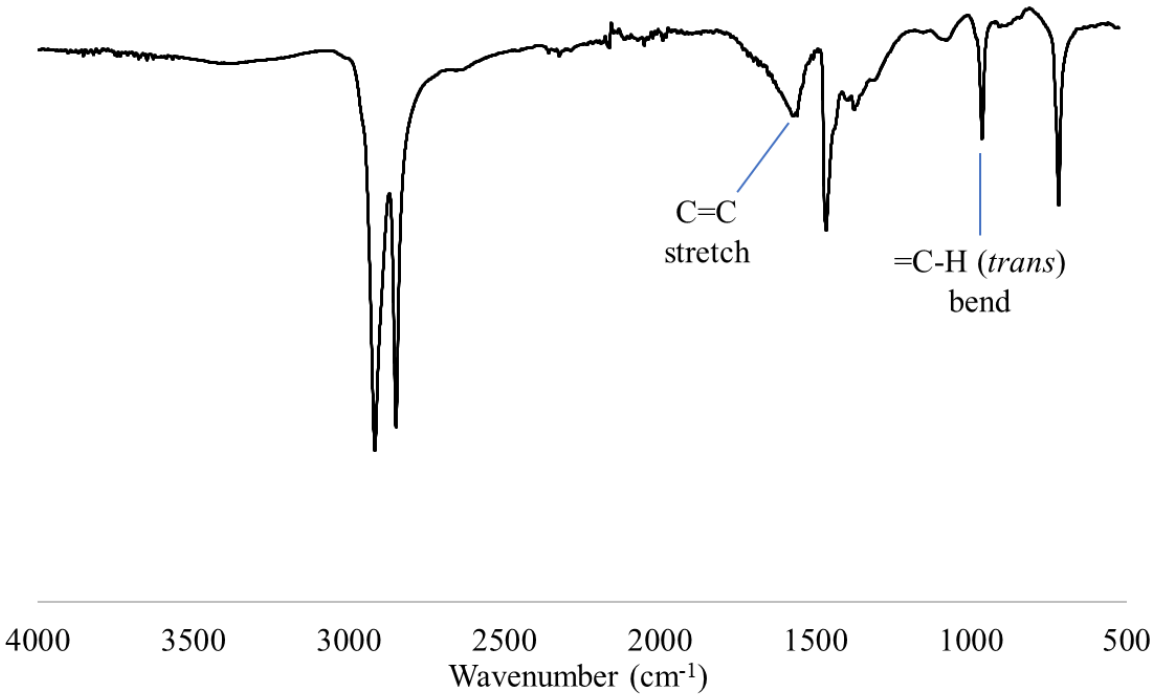

Figure B.8 IR spectrum of VPE (Table 3.2, VPE-1).

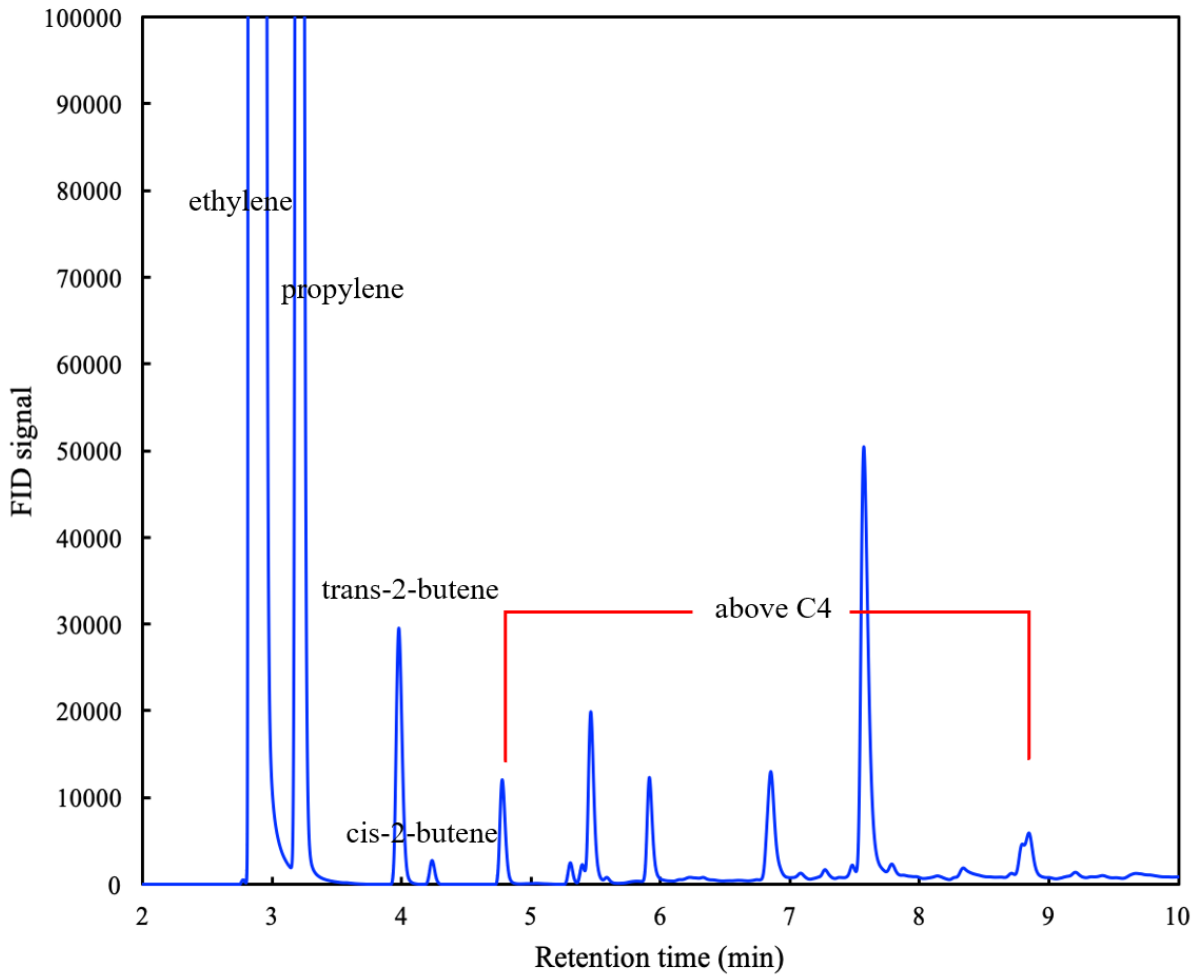

Figure B.9. GC-FID chromatogram of gas phase products detected in headspace after ethenolysis of polybutadiene.

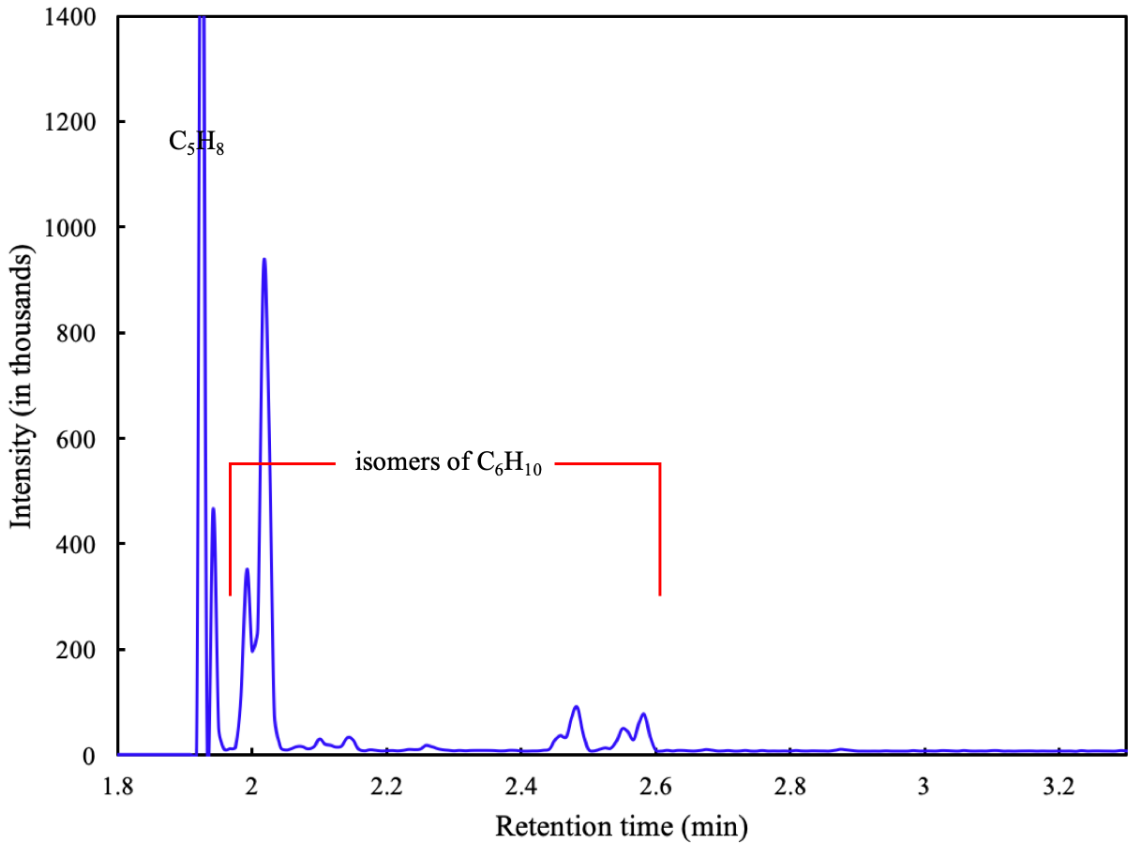

Figure B.10 GC-MS chromatogram of gas phase products with carbon numbers greater than C4 detected in headspace after ethenolysis of polybutadiene.

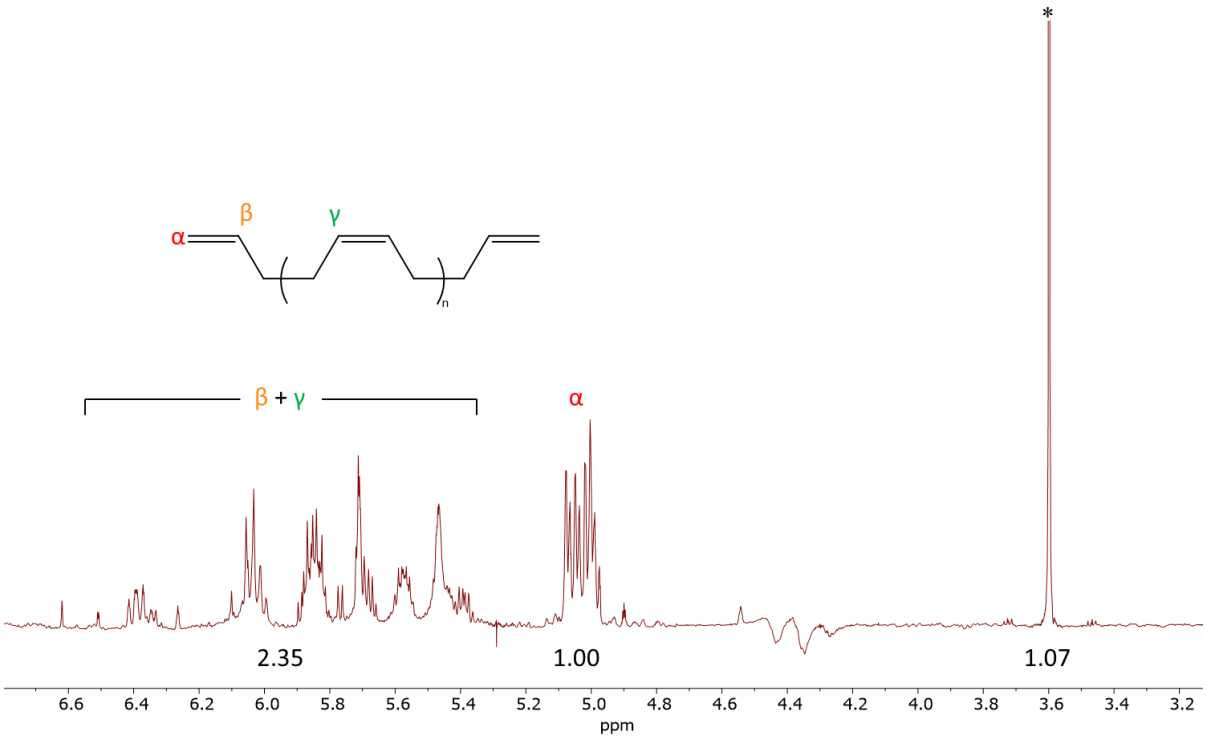

Figure B.11 ^{1}H NMR spectrum of olefins present in the reaction mixture after ethenolysis of polybutadiene, recorded in $CDCl_3$. *Dichloroethane internal standard.

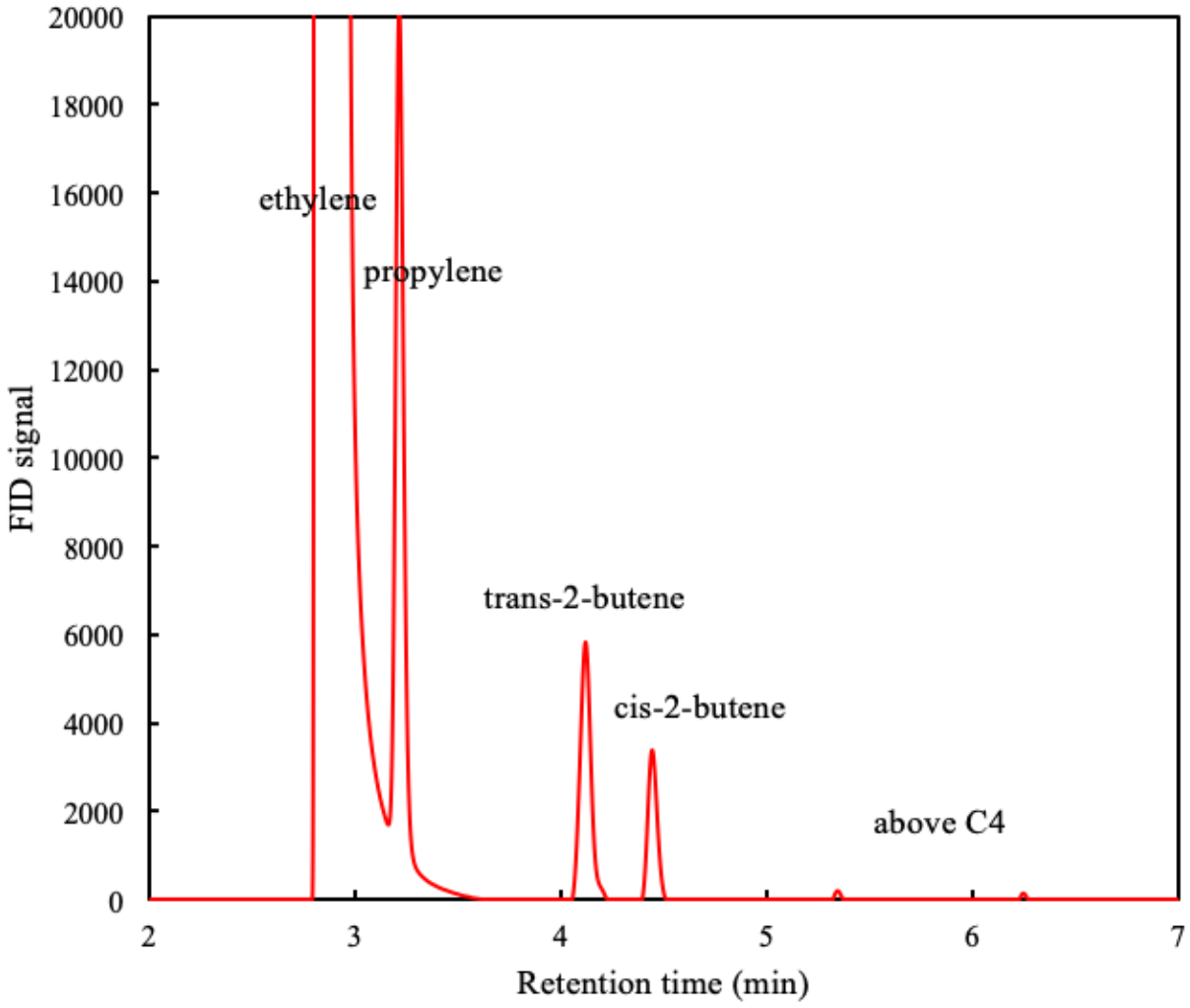

Figure B.12 GC-FID chromatogram of volatile species detected in vessel headspace after ethenolysis of VPE (Table 3.3, Entry 4).

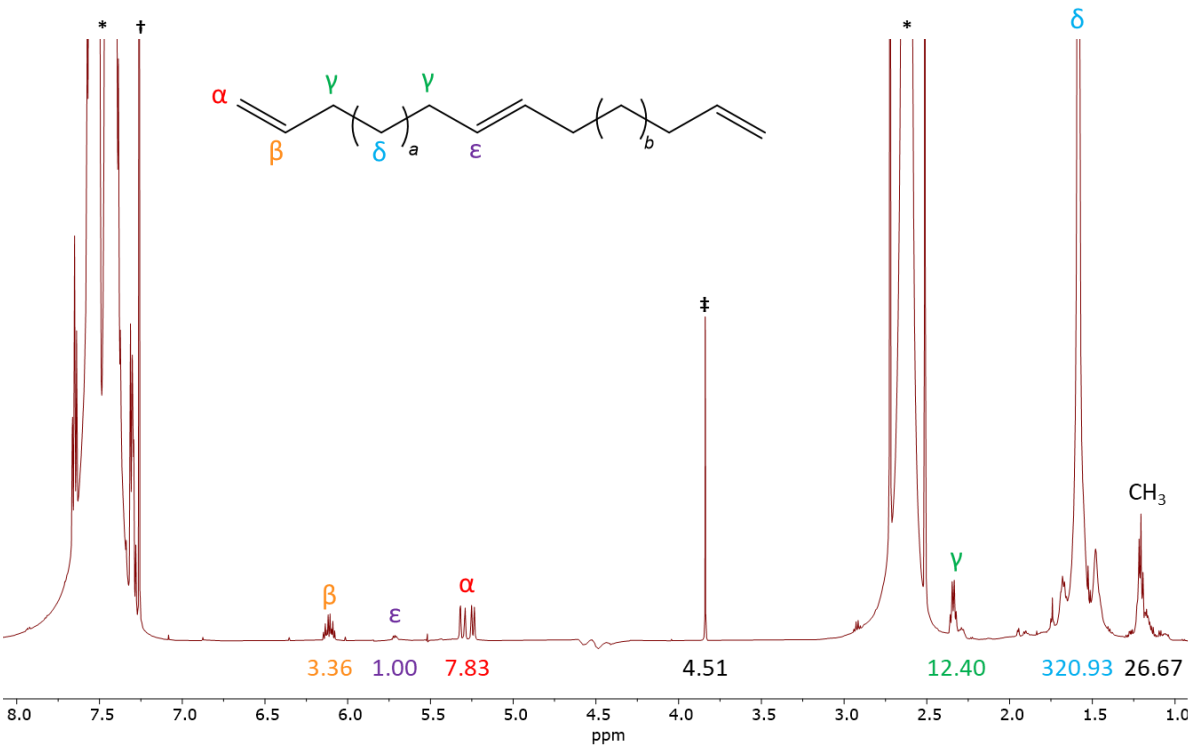

Figure B.13 ^{1}H NMR analysis of olefins in the reaction mixture after ethenolysis of VPE (Table 3.3, Entry 4). *Toluene from reaction mixture. †From $CDCl_3$ solvent. ‡Dichloroethane internal standard.

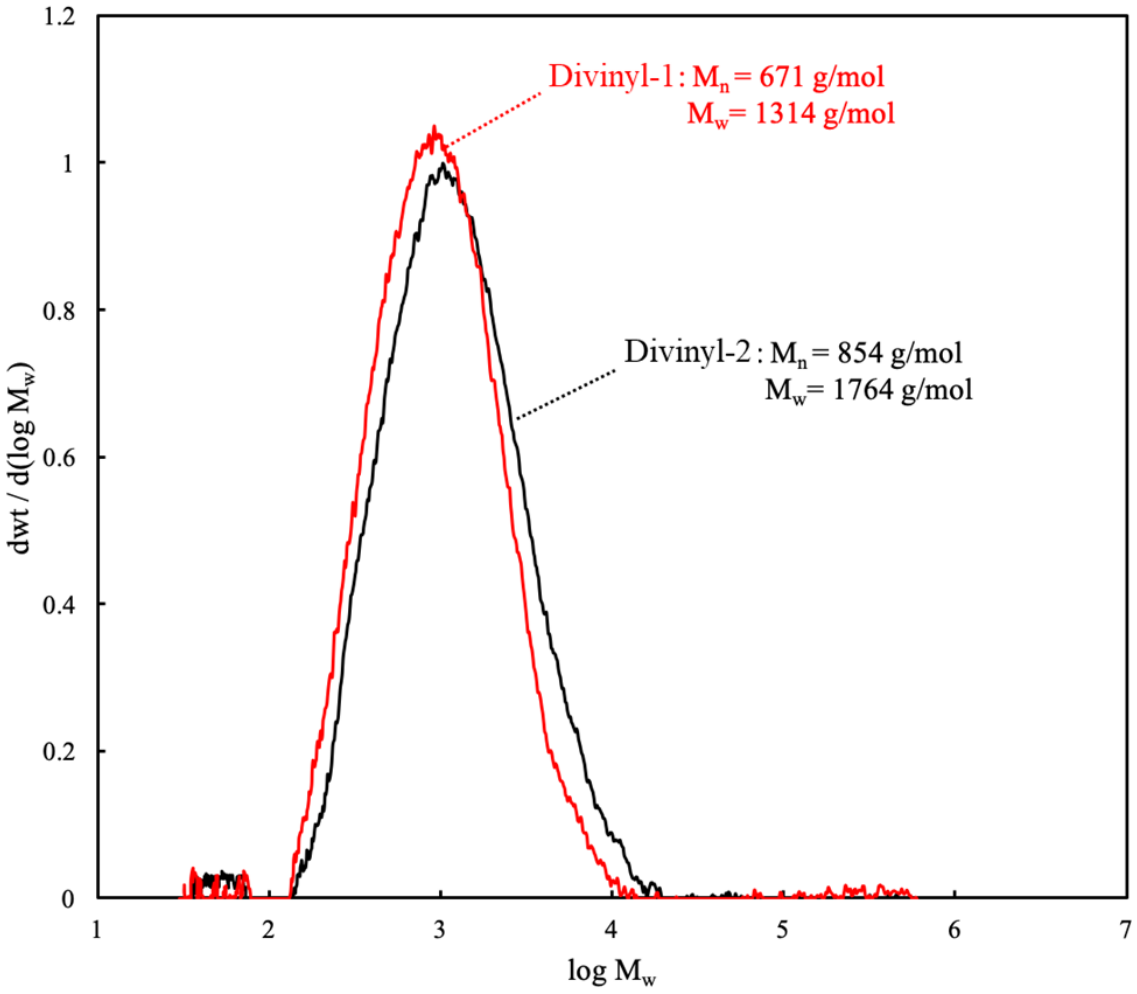

Figure B.14 GPC chromatograms of α,ω-divinyl-functionalized oligomers obtained by ethenolysis, performed in 1,2,4-trichlorobenzene at 150 °C.

Preliminary Techno-Economic Assessments

Process Simulation

HYSYS V10 (Aspen Technology, Inc.) was used to size unit operations and estimate utility costs for the PE-to-α,ω-divinyl-functionalized oligomer process shown in Figure B.15. The NRTL activity coefficient model was used. For compounds not in the Aspen database (including PE, BPE, VPE, *t*-BuOK, and α,ω-divinyl-functionalized oligomers), appropriate model compounds (specified below) or the hypothetical component function (when unspecified) were used. Species mass flow rates are summarized in Table B.1. Reactors were sized as continuously stirred tank reactors (CSTRs) using eq B.1.

$$V = \frac{F_{A0} X_A}{-r_A} \qquad \text{(eq B.1)}$$

Here, V is the reactor volume, F_{A0} is the molar reactant flow rate, X_A is conversion of A, and r_A is the reaction rate with respect to A. In the absence of kinetic data, reaction rates were estimated using eq B.2 with values from the laboratory scale demonstration.

$$-r_A = \frac{n_B}{\nu t} \qquad \text{(eq B.2)}$$

Here, n_B is moles of product formed, t is reaction time, and ν is solvent volume. For catalytic reactions, solvent volume is replaced by catalyst mass such that Eq B.1 yields needed catalyst mass.

For the base case, the process is initiated by mixing n-triacontane (a model compound for PE), stoichiometric Br_2, and benzene (recycled solvent) and heating to 85 °C. The heated mixture is fed to the bromination reactor, where complete conversion of Br_2 and PE to BPE is assumed. The mixture of BPE, HBr, and benzene exiting the bromination reactor is heated to 150 °C before entering a flash drum designed to separate BPE from benzene and HBr. Next,

the mixture of HBr and benzene is cooled to 35 °C before separation in a second flash drum. The purified benzene is recycled as solvent to the bromination reactor.

The HBr is mixed with stoichiometric, pure O_2 and allowed to react over a RuO_2/TiO_2 catalyst at 157 °C to form H_2O and Br_2.[2] Br_2 is separated from H_2O via distillation and recycled to the bromination reactor, while H_2O is discharged with >99 wt% purity. BPE is combined with recycled THF and a stoichiometric amount of *t*-BuOK, and heated to 66 °C, before being fed to the dehydrobromination reactor. THF, KBr, *t*-BuOH, and VPE leaving the reactor are filtered in a drum filter. Insoluble KBr is recovered to be sold. The filtrate is heated to 150 °C, then sent to a flash drum designed to separate THF and *t*-BuOH from VPE. After cooling to 65 °C, THF and *t*-BuOH are sent to a distillation column designed to separate THF for recycle and *t*-BuOH for sale.

VPE is mixed with recycled toluene and ethylene and heated to 100 °C before entering an ethenolysis reactor A heterogeneous ethenolysis catalyst with similar activity and cost to Grubbs Catalyst® M202 was chosen, for ease of separation from products. 1,15-hexadecadiene (a model compound for the α,ω-divinyl-functionalized oligomers), ethylene, and toluene leave the reactor and enter a flash drum at 108 °C to separate ethylene and toluene vapors from the liquid stream containing 1,15-hexadecadiene and toluene. A distillation column separates toluene and 1,15-hexadecadiene such that the latter is 99.99% pure and the toluene, combined with the gaseous toluene and ethylene from the preceding flash drum, is recycled back into the ethenolysis reactor.

A preliminary TEA was also undertaken for a process involving thermal dehydrobromination (see Figure B.16). The process design is very similar to the base case described above. However, since no THF, KBr, *t*-BuOH, and *t*-BuOK are involved in the

process, the KBr filter, THF/ *t*-BuOH column, and some heat exchangers are not needed. BPE is heated to 190 °C prior to entering the dehydrobromination reactor, and only VPE and HBr exit the reactor. These components are separated by a flash drum operating at 190 °C. The recovered HBr is then mixed with HBr from the bromination reactor and converted to Br_2 thermally.

Table B.1 Mass flow rates of species leaving/entering reactors to convert 300 kta waste PE to α,ω-divinyl-functionalized oligomers.

Raw Material/Product	Base Case (kg/s)	Thermal Dehydrobromination Case (kg/s)
Br_2	2.6	2.6
Waste PE	8.8[a]	8.8[a]
Benzene	44	44
HBr	1.3	2.6
BPE	10	10
^{t}BuOK	1.8	N/A
^{t}BuOH	1.2	N/A
THF	44	N/A
KBr	1.9	N/A
VPE	8.7	8.7
Toluene	44	44
Ethylene	43	43
α,ω-divinyl-functionalized oligomers	9.8	9.8
O_2	0.51	1.0
H_2O	0.29	0.58
Ru-based ethenolysis catalyst	360[b]	360[b]
RuO_2/TiO_2	1600[b]	3200[b]

[a] Accounts for 98% process operating time. [b] kg of catalysts replaced annually

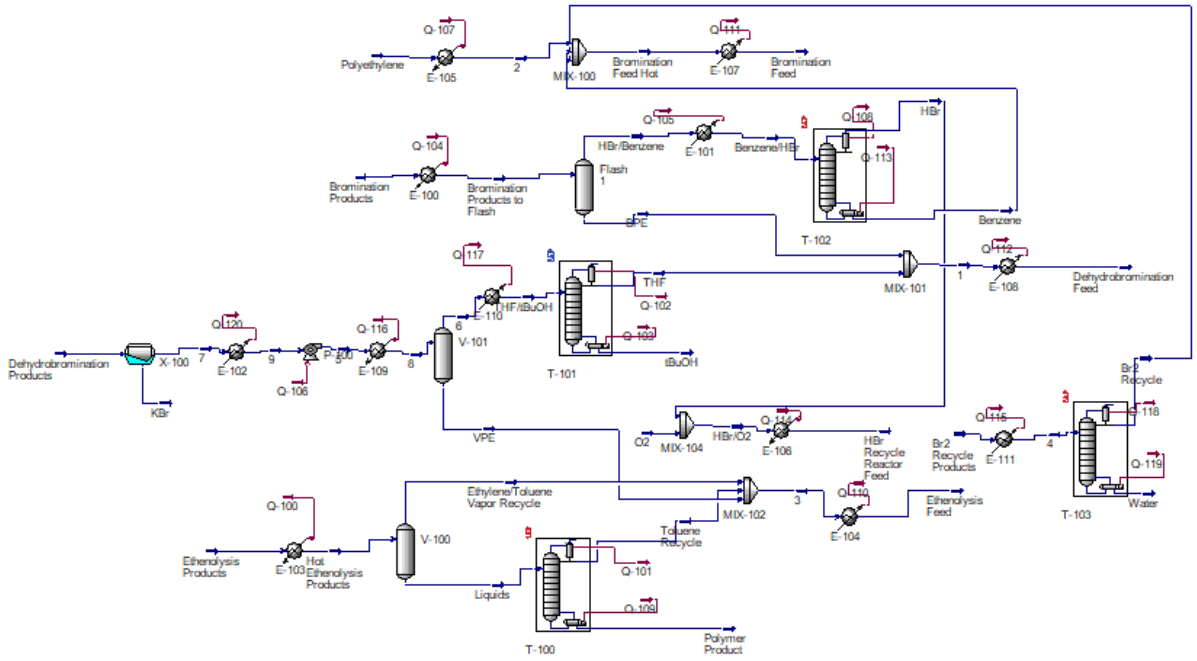

Figure B.15 Process flow diagram for base case of a PE-to-α,ω-divinyl-functionalized oligomers process, designed in HYSYS.

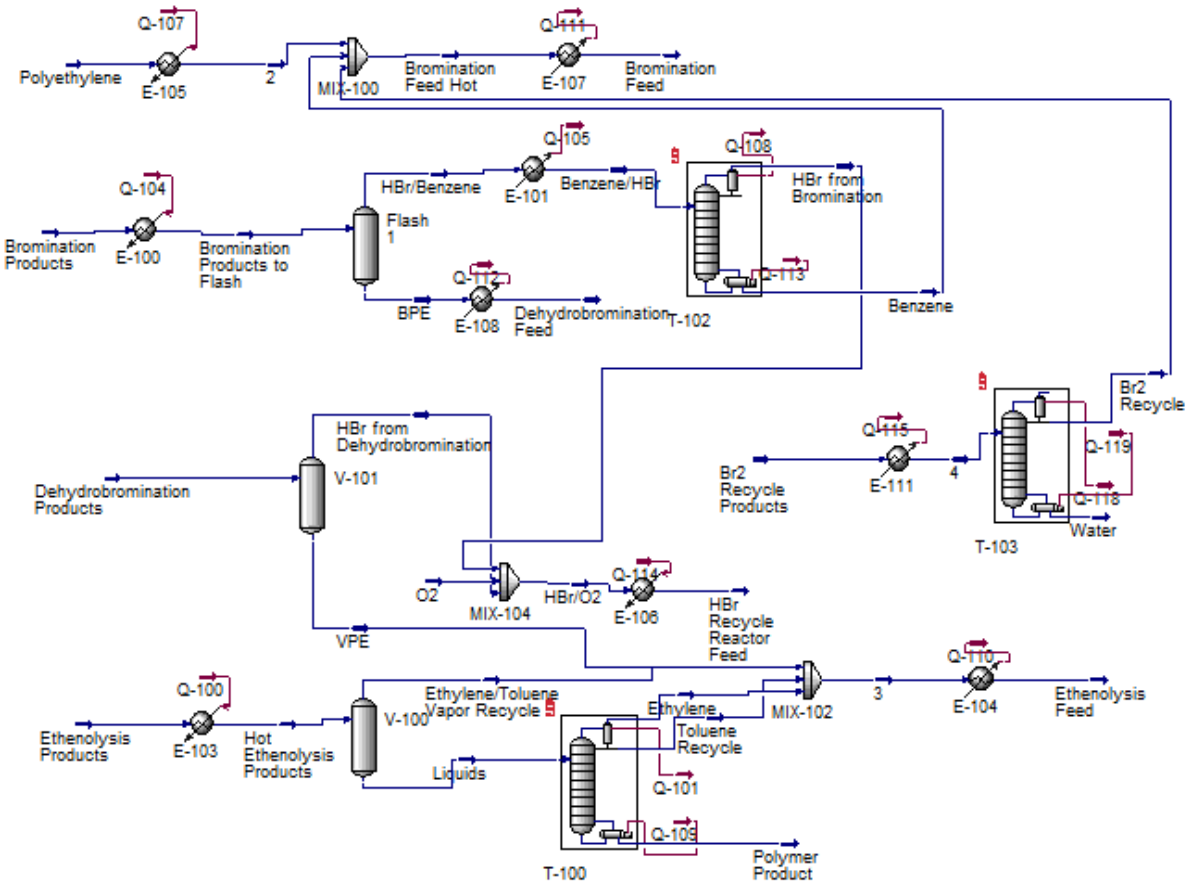

Figure B.16 Process flow diagram for PE-to-α,ω-divinyl-functionalized oligomers process with thermal dehydrobromination, designed in HYSYS.

Fixed Capital Investment Estimation

Total process equipment cost (TPEC) was estimated using the open-source Microsoft Excel file CAPCOST_2017_rev2.[1] The average chemical engineering plant cost index (CEPCI) for 2020 was used to scale equipment costs to USD in 2020. Unit operation sizes estimated in HYSYS were used to calculate the purchased equipment cost (PEC) for each unit operation. For equipment that handles compounds containing bromine, the construction material is nickel. Other equipment is made of carbon steel. All distillation columns use sieve trays with 2-ft spacing, and all heat exchangers are floating head shell and tube heat exchangers. The filter

was designed as a drum filter. Flash drums are oriented vertically. Sizing and PEC results are summarized in Tables B.2 and B.3, respectively. TPEC is the sum of PECs. It is used to estimate the fixed capital investment (FCI), based on the assumptions given in Table B.4.[3]

Discounted Cash Flow Analysis

A discounted cash flow analysis was conducted to estimate the net present value (NPV) and internal rate of return (IRR), based on the method reported in Turton *et al*.[1] Table B.5 summarizes the assumptions used in this analysis.

Table B.2 Purchased equipment costs and sizes for base case scenario shown in Figure B.15.

Equipment	Purchased Equipment Cost, USD	Size Parameters
Bromination Reactor	2,260,000	621 m^3
Dehydrobromination Reactor	1,490,000	404 m^3
Ethenolysis Reactor	12,400,000	3420 m^3
HBr Recycle Reactor	47,400	38 m^3
Bromination Products Flash Drum	1,410,000	Diameter 4.3 m, Height 15.0 m
HBr/Benzene Flash Drum	2,750,000	Diameter 5.2 m, Height 18.1 m
KBr Filter	1,420,000	368 m^2
THF/VPE/^{t}BuOH Flash Drum	3,000,000	Diameter 5.3 m, Height 18.7 m
THF/^{t}BuOH Distillation Column	5,650,000	Trays 30, Diameter 4.7 m
Ethenolysis Products Flash Drum	2,470,000	Diameter 9.9 m, Height 34.7 m
Toluene/Product Distillation Column	680,000	Trays 8, Diameter 2.6 m
Br_2/H_2O Column	235,000	Trays 20, Diameter 0.82
Heat Exchanger E-100	266,000	456 m^2
Heat Exchanger E-101	462,000	2480 m^2
Heat Exchanger E-102	2,330,000	4170 m^2
Heat Exchanger E-103	251,000	423 m^2
Heat Exchanger E-104	147,000	203 m^2
Heat Exchanger E-105	142,000	190 m^2
Heat Exchanger E-106	74,000	26 m^2
Heat Exchanger E-107	418,000	1490 m^2
Heat Exchanger E-108	474,000	1690 m^2
Heat Exchanger E-109	537,000	3820 m^2
Heat Exchanger E-110	393,000	2100 m^2
Heat Exchanger E-111	80,000	4 m^2

Table B.3 Purchased equipment costs and sizes for scenario with thermal dehydrobromination, shown in Figure B.16.

Equipment	Purchased Equipment Cost, USD	Size Parameters
Bromination Reactor	2,260,000	621 m^3
Dehydrobromination Reactor	1,490,000	404 m^3
Ethenolysis Reactor	12,400,000	3420 m^3
HBr Recycle Reactor	47,400	38 m^3
Bromination Products Flash Drum	1,410,000	Diameter 4.3 m, Height 15.0 m
HBr/Benzene Flash Drum	2,310,000	Diameter 4.9 m, Height 17.1 m
HBr/VPE Flash Drum	93,800	Diameter 1.1 m, Height 5.9 m
Ethenolysis Products Flash Drum	2,470,000	Diameter 9.9 m, Height 34.7 m
Toluene/Product Distillation Column	680,000	Trays 8, Diameter 2.6 m
Br_2/H_2O Column	235,000	Trays 20, Diameter 0.82 m
Heat Exchanger E-100	113,000	125 m^2
Heat Exchanger E-101	518,000	2770 m^2
Heat Exchanger E-103	251,000	423 m^2
Heat Exchanger E-104	173,000	259 m^2
Heat Exchanger E-105	142,000	190 m^2
Heat Exchanger E-106	75,200	15 m^2
Heat Exchanger E-107	418,000	1490 m^2
Heat Exchanger E-108	150,000	208 m^2
Heat Exchanger E-111	80,000	4 m^2

Table B.4 Assumptions for Fixed Capital Investment calculation from TPEC[1]

Parameter	Estimation Factor
Service Facilities	55% of TPEC
Purchased equipment installation	39% of TPEC
Piping	31% of TPEC
Building (including services)	29% of TPEC
Instrumentation and controls	26% of TPEC
Yard Improvements	12% of TPEC
Electrical Systems	10% of TPEC
Total Installed Costs (TIC)	302% of TPEC
Project Contingency	34% of TPEC
Construction	34% of TPEC
Engineering	32% of TPEC
Legal and Contractors Fees	23% of TPEC
Total Indirect Costs (TI)	123% of TPEC
Land	6% of TPEC
Fixed Capital Investment (FCI)	TIC + TI + Land
Working Capital (WC)	15% of TIC + TI

Table B.5 Assumptions Used for Discounted Cash Flow Analysis

Parameter	Value[a]
Minimum acceptable rate of return (%)	15
Project economic life (years)	20
Depreciation Method	5-year MACRS
Tax Rate (%)	35
Base Year	2020
Operating Days per Year (%)	98
Investment Year 1	50% FCI
Investment Year 2	50% FCI
Investment Year 3	WC

[a] MACRS: modified accelerated cost recovery system. FCI: fixed capital investment. WC: working capital.

Figures B.17 and B.18 show discounted cash flow diagrams for each process design. The diagrams result from plotting the cumulative cash flow at each iteration of eq B.3, while including land sale and WC recovery at the end of the project's economic life.

$$\text{NPV} = -FCI - WC + \sum_{i=0}^{20} \frac{(100-TR)(R-COM-d)+d}{(1+MARR)^i} \qquad \text{(eq B.3)}$$

Here, NPV is net present value, FCI is fixed capital investment, WC is working capital, TR is the tax rate percentage, R is annual revenue, COM is annual cost of manufacturing, d is depreciation allowance based on MACRS depreciation with a 9.5-year equipment life, 5-year recovery, and the half-year convention, and MARR is the minimal acceptable rate of return. Revenue from sales of KBr, ^{t}BuOH, and α,ω-divinyl-functionalized oligomers and COM were calculated using the prices listed in Table B.6. COM was estimated using eq B.4.[2]

$$\text{COM} = 0.28\text{FCI} + 821989(6.29 + 0.23N_{np})^{0.5} + 1.23(C_{RM}+C_U) \qquad \text{(eq B.4)}$$

Here, C_{RM} is the annual raw material cost, C_U is the annual utility cost estimated in Aspen HYSYS, and N_{np} is the number of process units. The second term in the equation accounts for the cost of operating labor, assuming a salary for each operator of $66,910. The raw material cost includes reactants needed to convert 300 kta PE into α,ω-divinyl-functionalized oligomers and byproducts, annual catalyst replacement for the ethenolysis and HBr recycle operations, and replacement of lost solvent. IRR is calculated by setting NPV to 0 in Eq B.3, replacing MARR with IRR, and solving for IRR.

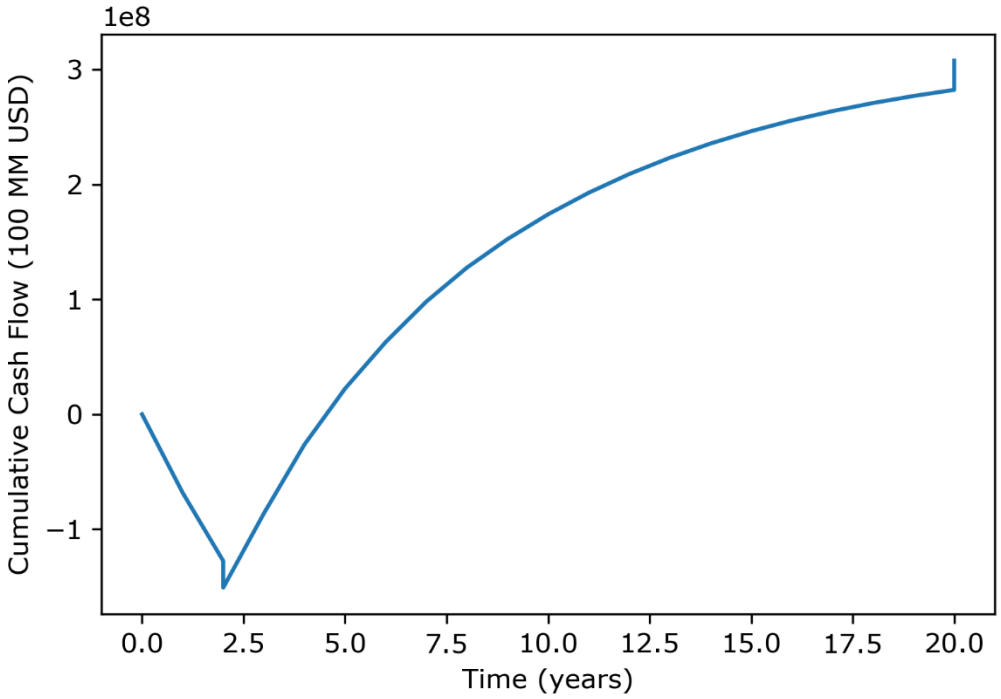

Figure B.17 Discounted cash flow diagram for process to convert PE to α,ω-divinyl-functionalized oligomers (base case scenario)

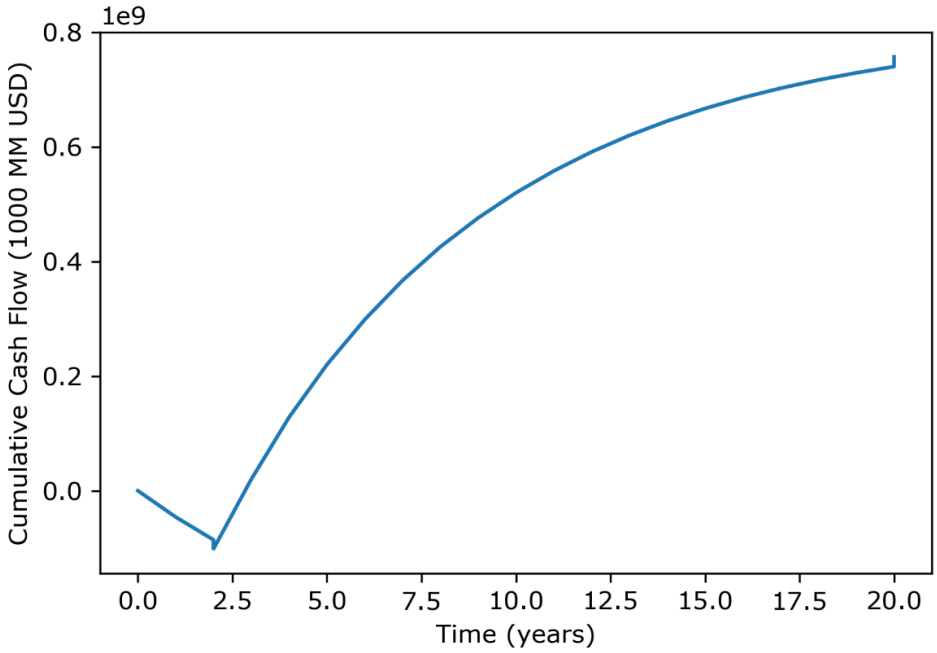

Figure B.18 Discounted cash flow diagram for process to convert PE to α,ω-divinyl-functionalized oligomers (thermal dehydrobromination scenario)

Table B.6 Assumptions Used in Discounted Cash Flow Analysis

Raw Material/Product	Price (USD/kg)
Br_2[4]	5.8
Waste PE[5]	0
KBr[6]	3.7
^{t}BuOK[7]	1.4
^{t}BuOH[8]	1.00
HBr[9]	3
THF[10]	1.5
Benzene[11]	0.83
Toluene[12]	0.73
Ethylene[13]	1.03
O_2[14]	0.077
Ru-based metathesis catalyst[15]	14,400
α,ω-divinyl-functionalized oligomers[a]	1.45

[a] Based on current polyalphaolefin (PAO) price.[16]

References

(1) *Analysis, Synthesis, and Design of Chemical Processes*, 4th ed.; Turton, R., Ed.; Prentice Hall: Upper Saddle River, NJ, 2012.

(2) Moser, M.; Rodríguez-García, L.; Amrute, A. P.; Pérez-Ramírez, J. Catalytic Bromine Recovery: An Enabling Technology for Emerging Alkane Functionalization Processes. *ChemCatChem* **2013**, *5* (12), 3520–3523. https://doi.org/10.1002/cctc.201300609.

(3) Winjobi, O.; Shonnard, D. R.; Zhou, W. Production of Hydrocarbon Fuel Using Two-Step Torrefaction and Fast Pyrolysis of Pine. Part 1: Techno-Economic Analysis. *ACS Sustainable Chem. Eng.* **2017**, *5* (6), 4529–4540. https://doi.org/10.1021/acssuschemeng.7b00372.

(4) AWS. Bromine. Https://S3-Us-West-2.Amazonaws.Com/Prd-Wret/Assets/Palladium/Production/Mineral-Pubs/Bromine/Mcs-2016-Bromi.Pdf (Accessed June 9, 2021).

(5) Gracida-Alvarez, U. R.; Winjobi, O.; Sacramento-Rivero, J. C.; Shonnard, D. R. System Analyses of High-Value Chemicals and Fuels from a Waste High-Density Polyethylene Refinery. Part 1: Conceptual Design and Techno-Economic Assessment. *ACS Sustainable Chem. Eng.* **2019**, *7* (22), 18254–18266. https://doi.org/10.1021/acssuschemeng.9b04763.

(6) Alibaba Group. Potassium Bromide. Https://Www.Alibaba.Com/Product-Detail/Potassium-Bromide-KBr-Potassium-Bromide-KBr_1600248481946.Html?Spm=a2700.7724857.Normal_offer.D_title.55ef4e84ljwsXz&s=p (Accessed June 9, 2021).

(7) OKCHEM. Tert-Butoxide. Https://Www.Okchem.Com/Showroom/Tert-Butoxide.Html (Accessed June 9, 2021).

(8) Alibaba Group. Tert-Butyl Alcohol. Https://Www.Alibaba.Com/Showroom/Tert-Butyl-Alcohol.Html (Accessed June 9, 2021).

(9) Alibaba Group. Hydrobromic Acid. Https://Www.Alibaba.Com/Product-Detail/Hydrobromic-Acid-HBr-10035-10-6_60822228643.Html?Spm=a2700.7724857.Normal_offer.D_title.1c8a6722LdXtr1A (Accessed June 9, 2021).

(10) Alibaba Group. Tetrahydrofuran Price. Https://Www.Alibaba.Com/Showroom/Tetrahydrofuran-Price.Html (Accessed June 9, 2021).

(11) ECHEMI. Benzene. Https://Www.Echemi.Com/ProductsInformation/Pid_Seven2868-Benzene.Html (Accessed June 9, 2021).

(12) Intratec. Toluene Price. Https://Www.Intratec.Us/Chemical-Markets/Toluene-Price (Accessed June 9, 2021).

(13) Statista. Price Ethylene Forecast Globally. Https://Www.Statista.Com/Statistics/1170573/Price-Ethylene-Forecast-Globally/ (Accessed June 9, 2021).

(14) Alibaba Group. Oxygen. Https://Www.Alibaba.Com/Trade/Search?Fsb=y&IndexArea=product_en&CatId=&SearchText=oxygen (Accessed July 16, 2021).

(15) BASF. EIB Prices Https://Apps.Catalysts.Basf.Com/Apps/Eibprices/Mp/ (Accessed June 9, 2021).

(16) Alibaba Group. Polyalphaolefins. Https://Www.Alibaba.Com/Product-Detail/Polyalphaolefins-Pao-6_50013671726.Html?Spm=a2700.Galleryofferlist.Normal_offer.D_title.14e9255aNgG8PB (Accessed July 26, 2021).

Appendix C

Appendix to Chapter 5

***** *Sections of this chapter were reproduced from the following publication with permission from Dr. Benjamin Harvey, the principal investigator of the project at the Naval Air Weapons Station China Lake (Ridgecrest, CA). The author of this Ph. D. thesis, Manhao Zeng, is a coauthor of this publication who contributed to experimental design, performed reactions, and analyzed research data relevant to this work.*

Siirila, M. J.; **Zeng, M.**; Woodroffe, J.-D.; Askew, R. L.; Harvey, B. G. Synthesis and Characterization of High-Performance Renewable Diesel Fuel from Bioderived 1-Octen-3-Ol. *Energy Fuels* **2020**, *34* (7), 8325–8331. https://doi.org/10.1021/acs.energyfuels.0c00120.

Experimental Section

Materials and Methods. 1-Octen-3-ol (98%), *p*-toluenesulfonic acid monohydrate (PTSA), and PtO_2 were all purchased from Millipore Sigma and used as received. Dehydration and cycloaddition reactions were performed under a nitrogen atmosphere. NMR spectra were collected with a Bruker AVANCE II 500 MHz NMR spectrometer. ^{1}H and ^{13}C NMR chemical shifts are reported versus the deuterated solvent peak [$CDCl_3$: δ 7.27 ppm (^{1}H), 77.23 ppm (^{13}C)]. Products were further characterized via GC–MS (electron-impact ionization). The GC–MS system was equipped with an RTX-5MS 30-meter column and the analysis was conducted under the following conditions: inlet temperature, 250 °C; initial column temperature, 40 °C; temperature ramp, 4 °C/min to 100 °C; 2nd temperature ramp, 20 °C/min to 300 °C. The

kinematic viscosity and density of hydrogenated octadiene dimer (HOD**)** and fuel blends were measured with a Stabinger Viscometer, SVM 3001 connected to a TC-502 circulation cooler. A 5 mL disposable syringe was used to inject 3–4 mL of the sample into the viscometer. NHOC measurements were conducted by the Southwest Research Institute (SwRI) in accordance with ASTM D4809. IQT measurements were conducted by SwRI (ASTM D6890). The flash point of HOD was measured with a Grabner Instruments/Ametek Miniflash FLP Touch according to ASTM D7094. For each measurement, 2 mL of fuel were transferred via an auto pipette to a 7 mL stainless steel sample cup. Elemental analysis was performed by Atlantic Microlabs, Inc. Norcross, GA.

Dehydration of 1-Octen-3-ol. 1-Octen-3-ol was dehydrated as depicted in Scheme C.1. 1-Octen-3-ol (220 g, 1.72 mol) and PTSA (3.82 g, 20.1 mmol, 1.17 mol%) were added to a 500 mL round bottom flask with a stir bar, and the flask was placed in a silicone oil bath. A vacuum-jacketed simple distillation apparatus and a 500 mL round bottom receiving flask were connected, and the apparatus was wrapped in glass wool and aluminum foil to reduce heat loss. The entire system was placed under positive N_2 pressure, and the receiving flask was lowered into an ice bath. The oil bath was slowly heated while stirring the reaction flask. The distillate was collected at oil bath temperatures of 140–161 °C and distillate temperatures of 117–119 °C. The crude product was transferred to a separatory funnel to remove the aqueous layer, and then washed with a 10% $NaHCO_3$ solution and brine, followed by drying over magnesium sulfate. The residual starting material was removed from the product using the same distillation apparatus as before, except the simple distillation column was replaced with a 16″ vacuum-jacketed Vigreux column. Analysis of the distilled product by GC–MS showed that isomerization of the 1,3-octadiene occurred during the synthesis and purification procedure,

resulting in a 46:54 ratio of 1,3:2,4 octadienes. Yield: 58%. The ^{1}H and ^{13}C NMR spectra for the blend of octadienes can be found in Figures C.1 and C.2, respectively. ^{1}H NMR (500 MHz, $CDCl_3$) δ 6.71–6.63 (m), 6.38–6.29 (m), 6.10–5.95 (m), 5.76–5.65 (m), 5.63–5.54 (m), 5.51–5.44 (m), 5.35–5.29 (m), 5.26 (t, J = 1.5 Hz), 5.22 (t, J = 1.4 Hz), 5.21 (d, J = 2.0 Hz), 5.18 (d, J = 2.1 Hz)), 5.13 (t, J = 1.4 Hz), 5.12–5.08 (m), 4.98 (bs), 4.96 (bs), 2.24-2.03 (m), 1.80 (d, J = 6.7 Hz), 1.75 (d, J = 7.3 Hz), 1.47-1.32 (m), 1.06-1.01 (m), 0.96-0.91 (m). ^{13}C NMR (125 MHz, $CDCl_3$) 137.58, 136.31, 135.72, 134.50, 134.08, 133.18, 132.55, 132.12, 131.97, 131.92, 131.87, 131.11, 130.64, 129.81, 129.79, 129.63, 129.36, 129.11, 128.89, 128.25, 127.33, 126.84, 126.04, 125.72, 124.84, 124.80, 124.02, 123.69, 116.82, 114.7, 35.21, 34.89, 32.46, 31.99, 31.57, 29.94, 29.76, 27.65, 26.10, 25.81, 25.25, 23.13, 23.04, 22.81, 22.51, 22.47, 21.22, 18.45, 18.17, 14.50, 13.96, 13.92, 13.88, 13.86, 13.43.

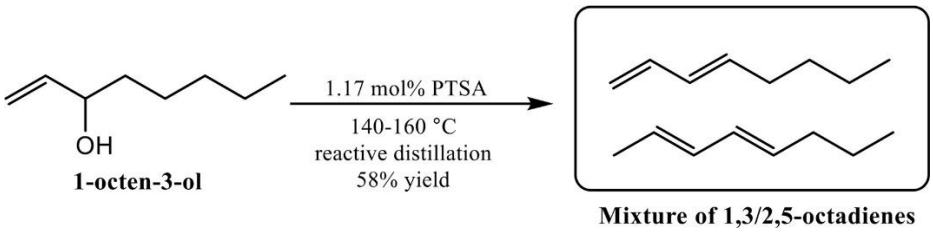

Scheme C.1 Dehydration of 1-Octen-3-ol

Cycloaddition of Conjugated Octadienes. Octadienes prepared as described above were cyclodimerized as depicted in Scheme C.2. In a typical preparation, a mixture of 1,3/2,4-octadienes (72 mL) was added to a 200 mL, PTFE lined Parr bomb under nitrogen, and the reaction vessel was then placed in an oven at 240 °C for 22 h. GC analysis showed 92% conversion to oligomers, with 81.2% dimers and 10.4% higher oligomers. Carrying out the Diels–Alder reaction with a 50:50 ratio of pentane:octadienes to increase the pressure did not

improve the selectivity to, or yield of, the dimer. The ^{1}H NMR spectrum of the dimer mixture can be found in Figure C.3.

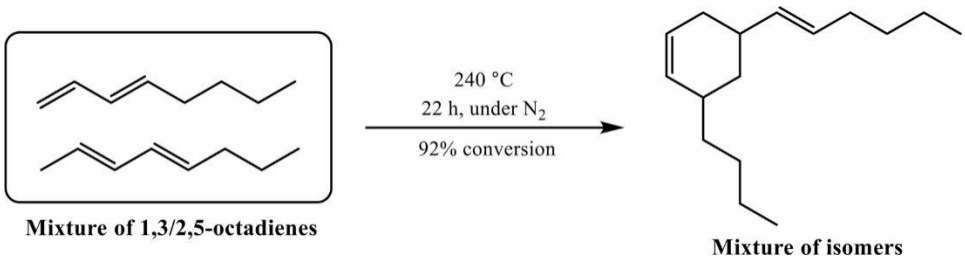

Scheme C.2 Diels–Alder Cyclodimerization of Octadienes

Synthesis of Hydrogenated Octadiene Dimers (HOD). Cyclodimerized octadienes were hydrogenated as depicted in Scheme C.3. Crude octadiene oligomers (359 g) were added to a 1000 mL round bottom flask fitted with a short path distillation column, and octadienes were removed under reduced pressure (30 Torr) at oil bath temperatures of 107–114 °C and distillate temperatures of 43–54 °C. Octadiene oligomers (339 g), consisting of 86% dimers, 11% higher oligomers, and 3% octadienes remained in the distillation flask. This material was transferred to a 2.5 L glass Parr bomb, and the reaction vessel was charged with glacial acetic acid (105 mL), hexanes (100 mL), and PtO_2 (2.21 g). The bomb was evacuated and back-filled with hydrogen three times and then shaken for 18 h at a hydrogen pressure of 50 psi. At the conclusion of the reaction, the mixture was filtered through Celite, transferred to a separatory funnel, and the acetic acid was removed by washing the organic phase with water, a 10% $NaHCO_3$ solution, and brine. The organic layer was then dried over magnesium sulfate and filtered. The hexanes were removed under reduced pressure to yield 329 g of hydrogenated oligomers (95% yield). The oligomers were then distilled under reduced pressure (~0.01 Torr) at oil bath temperatures of 120–185 °C, and distillate temperatures of 70–95 °C, to yield 186 g of HOD. A ^{1}H NMR spectrum (Figure C.4) and gas chromatogram of the product (Figure

C.5) can be found in this chapter. Anal. Calcd for $C_{16}H_{32}$: C, 85.63; H, 14.37. Found: C, 85.65; H, 14.34.

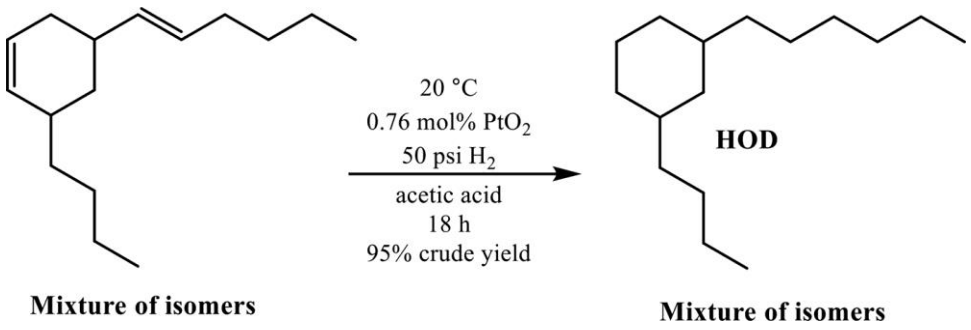

Scheme C.3 Hydrogenation of Octadiene Dimers to Generate HOD

Supplemental Figures and Tables

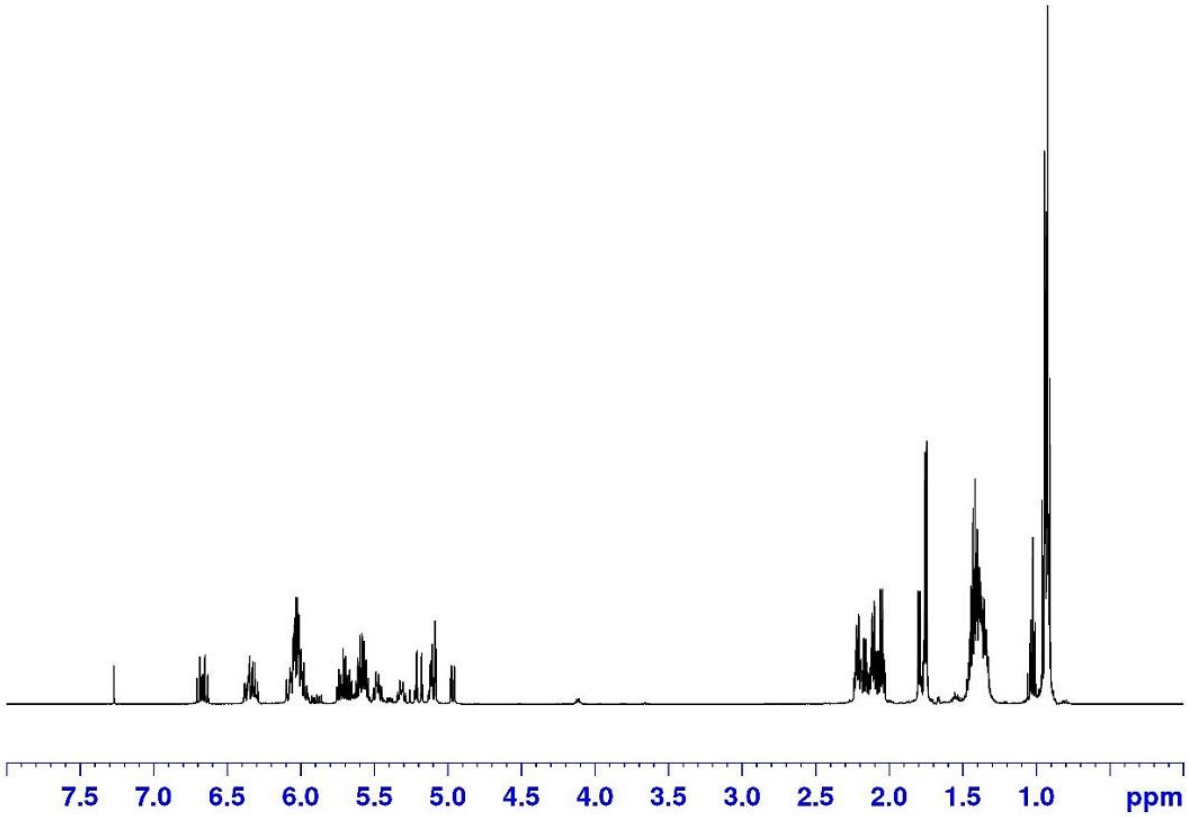

Figure C.1 ^{1}H NMR spectrum ($CDCl_3$) of 1,3/2,4-octadienes prepared by acid catalyzed dehydration of 1-octen-3-ol.

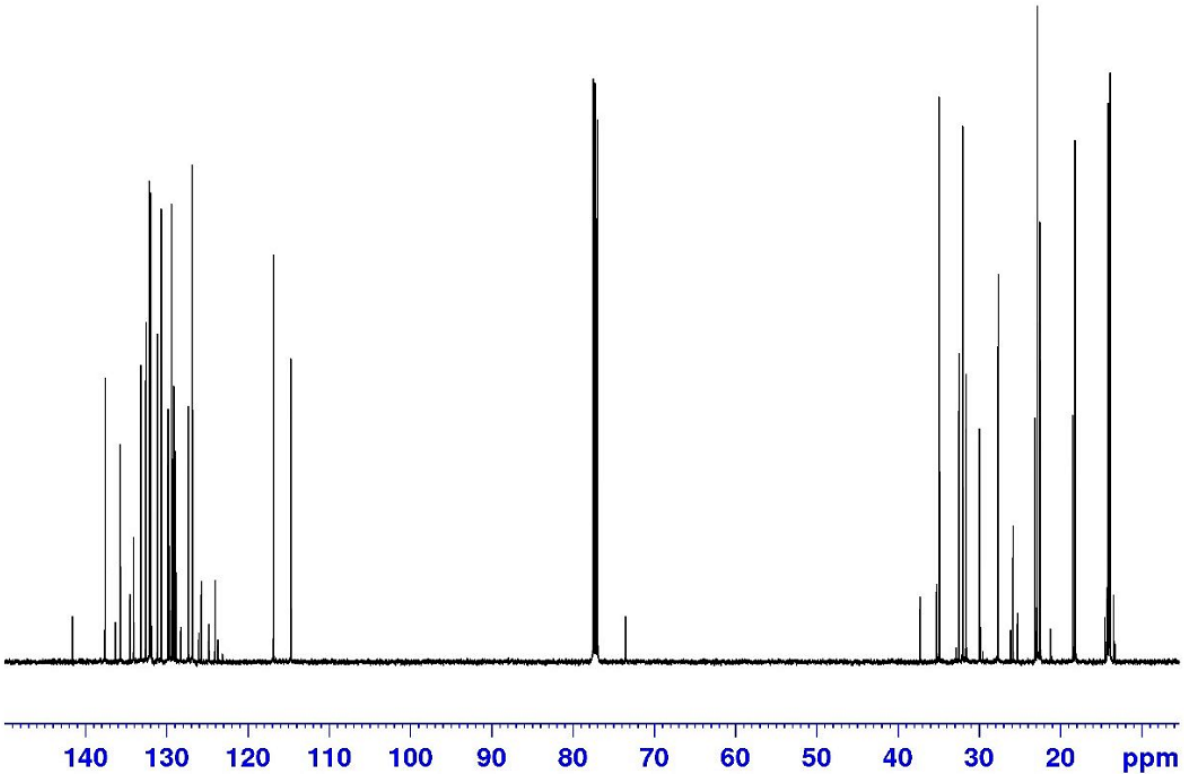

Figure C.2 $^{13}C\{^{1}H\}$ NMR spectrum ($CDCl_3$) of 1,3/2,4-octadienes prepared by acid catalyzed dehydration of 1-octen-3-ol.

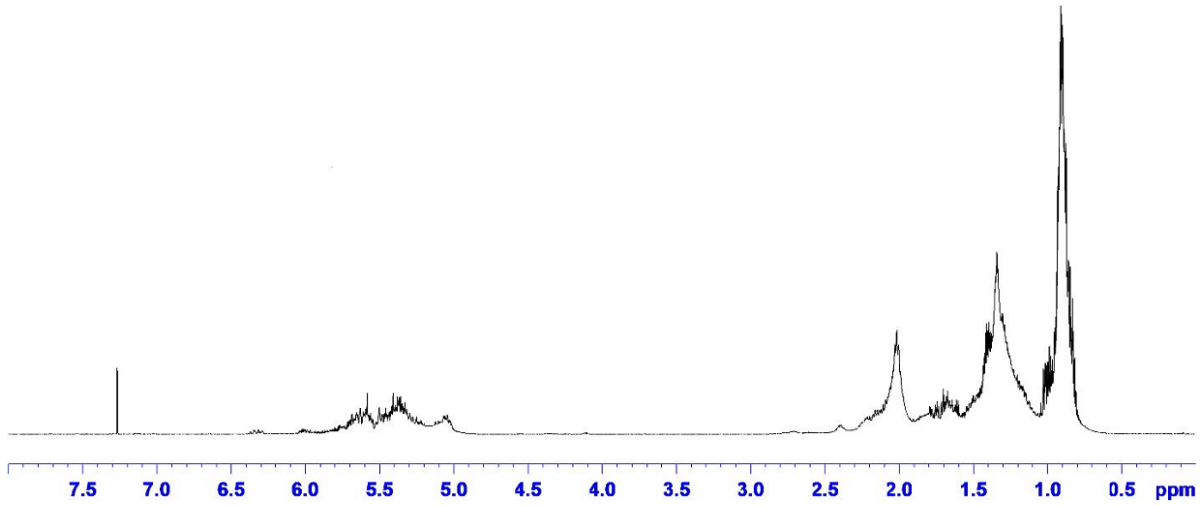

Figure C.3 ^{1}H NMR spectrum ($CDCl_3$) of thermally dimerized octadienes.

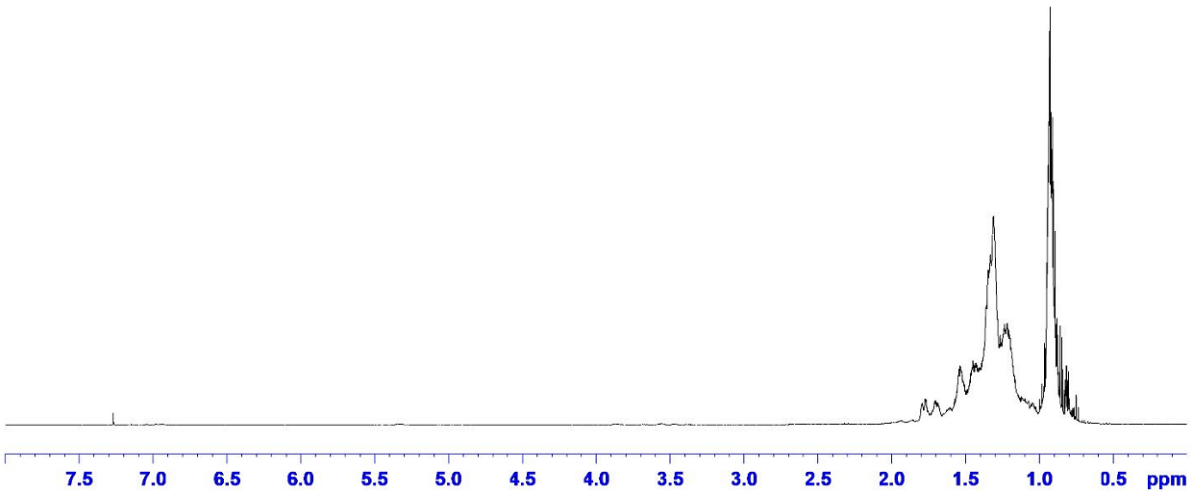

Figure C.4 ^{1}H NMR spectrum ($CDCl_3$) of hydrogenated octadiene dimers.

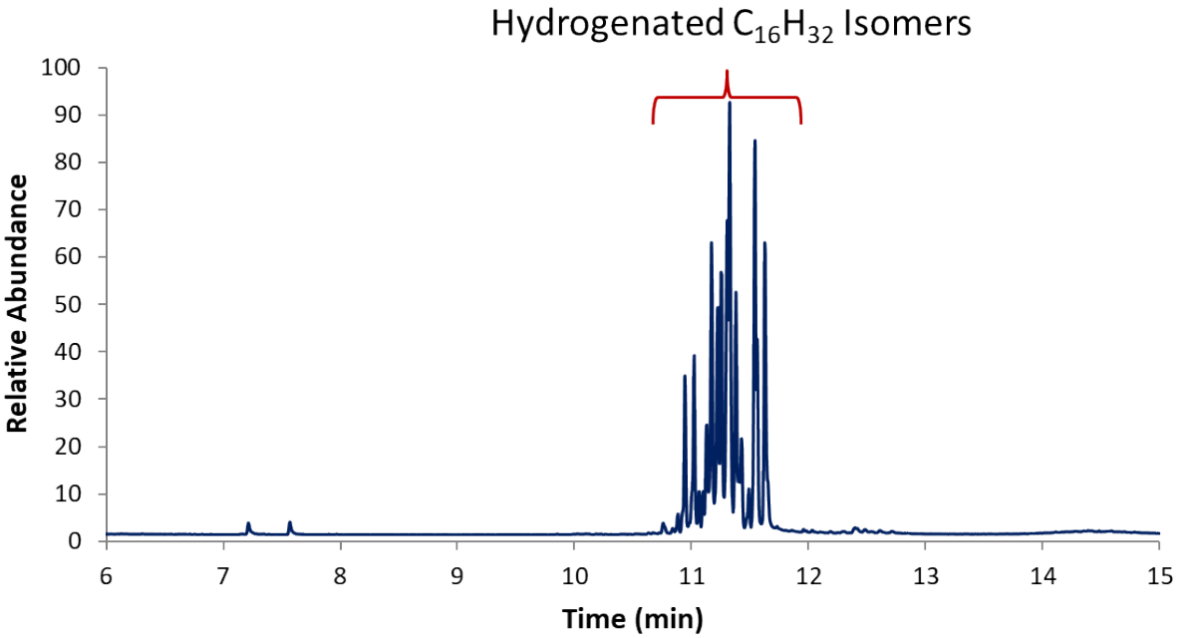

Figure C.5 Gas chromatogram of hydrogenated octadiene dimers.

Table C.1 Kinematic Viscosity and Density of 10% HOD: JET-A Blend.

Cell Temp (°C)	Kinematic Viscosity (mm²/s)	Density (g/mL)
20.002	1.902	0.8024
15.002	2.069	0.8063
10.001	2.273	0.8100
5.000	2.518	0.8138
0.000	2.811	0.8174
-5.002	3.208	0.8210
-10.001	3.651	0.8246
-15.002	4.192	0.8282
-20.001	4.864	0.8319
-25.001	5.712	0.8355
-30.002	6.806	0.8391
-35.002	8.259	0.8427
-39.999	10.352	0.8463

Table C.2 Kinematic Viscosity and Density of 15% HOD: JET-A Blend.

Cell Temp (°C)	Kinematic Viscosity (mm²/s)	Density (g/mL)
19.997	2.027	0.8046
14.999	2.224	0.8085
10.000	2.458	0.8122
5.000	2.738	0.8158
0.000	3.072	0.8194
-5.001	3.525	0.8229
-10.002	4.037	0.8264
-15.001	4.672	0.8300
-20.001	5.467	0.8336
-25.002	6.485	0.8372
-30.002	7.814	0.8408
-35.001	9.603	0.8443
-40.000	12.273	0.8478

Table C.3 Kinematic Viscosity and Density of 20% HOD: JET-A Blend.

Cell Temp (°C)	Kinematic Viscosity (mm^2/s)	Density (g/mL)
20.000	2.094	0.8057
14.999	2.302	0.8096
10.000	2.550	0.8133
4.998	2.847	0.8170
0.000	3.204	0.8206
-5.001	3.682	0.8241
-10.001	4.231	0.8277
-15.002	4.911	0.8313
-20.001	5.781	0.8349
-25.002	6.874	0.8385
-30.002	8.332	0.8420
-35.001	10.300	0.8456
-40.000	13.248	0.8491

Table C.4 Kinematic Viscosity and Density of 30% HOD: JET-A Blend.

Cell Temp (°C)	Kinematic Viscosity (mm^2/s)	Density (g/mL)
20.000	2.3418	0.8091
14.999	2.5906	0.8129
10.000	2.8903	0.8166
5.000	3.2517	0.8203
-0.001	3.6921	0.8239
-5.001	4.2765	0.8274
-10.001	4.9639	0.8310
-15.002	5.8318	0.8346
-20.002	6.9584	0.8381
-25.002	8.4075	0.8418
-30.001	10.3730	0.8453
-35.001	13.0930	0.8489
-40.000	17.2490	0.8524

Table C.5 Kinematic Viscosity and Density of 40% HOD: JET-A Blend.

Cell Temp (^{o}C)	Kinematic Viscosity (mm^2/s)	Density (g/mL)
20.000	2.647	0.8123
15.000	2.949	0.8162
10.000	3.317	0.8199
4.998	3.771	0.8235
-0.002	4.327	0.8271
-5.001	5.055	0.8306
-10.001	5.940	0.8342
-15.001	7.077	0.8378
-20.000	8.594	0.8413
-25.000	10.607	0.8448